

Syracuse University

**SURFACE**

---

Earth Sciences - Dissertations

College of Arts and Sciences

---

5-2012

## The Role of Magmatism in the Catalina Metamorphic Core Complex, Arizona: Insights from Integrated Thermochronology, Gravity and Aeromagnetic Data

Jessica Terrien  
*Syracuse University*

Follow this and additional works at: [https://surface.syr.edu/ear\\_etd](https://surface.syr.edu/ear_etd)



Part of the [Earth Sciences Commons](#)

---

### Recommended Citation

Terrien, Jessica, "The Role of Magmatism in the Catalina Metamorphic Core Complex, Arizona: Insights from Integrated Thermochronology, Gravity and Aeromagnetic Data" (2012). *Earth Sciences - Dissertations*. 28.

[https://surface.syr.edu/ear\\_etd/28](https://surface.syr.edu/ear_etd/28)

This Dissertation is brought to you for free and open access by the College of Arts and Sciences at SURFACE. It has been accepted for inclusion in Earth Sciences - Dissertations by an authorized administrator of SURFACE. For more information, please contact [surface@syr.edu](mailto:surface@syr.edu).

## ABSTRACT

The footwall of the Catalina MCC located within the Basin and Range Province has been intruded by several magmatic suites. Samples were collected from the Wilderness suite sills, the most voluminous suite. U/Pb data from zircon indicate that the Wilderness suite sills were emplaced during two separate phases of magmatism, the first at ~55 Ma and the second at ~45 Ma with additional evidence of zircon growth at <40 Ma.

$^{40}\text{Ar}/^{39}\text{Ar}$  data from the Wilderness suite sills indicate that the majority of the older  $^{40}\text{Ar}/^{39}\text{Ar}$  apparent ages from both potassium feldspar and mica were obtained from the structurally higher sills in the main range, and the younger  $^{40}\text{Ar}/^{39}\text{Ar}$  apparent ages were obtained on samples from structurally lower sills. The potassium feldspar samples yield  $^{40}\text{Ar}/^{39}\text{Ar}$  age gradients which may be the result of cooling for ~5 million years or thermal resetting by the Catalina pluton prior to exhumation along the Catalina detachment fault.  $^{40}\text{Ar}/^{39}\text{Ar}$  lower intercepts from potassium feldspar in the main range suggest that exhumation of the main range occurred ~25 to 23 million years ago. In the forerange, concordant AFT and ZFT data and  $^{40}\text{Ar}/^{39}\text{Ar}$  potassium feldspar lower age intercepts suggest rapid cooling due to exhumation ~23 to 22 million years ago. The muscovite and biotite samples from the Wilderness suite sills yield relatively flat  $^{40}\text{Ar}/^{39}\text{Ar}$  age spectra with ages ranging from ~28 to 23 Ma representing recrystallization below the closure temperature for muscovite and biotite.

Forward modeling of aeromagnetic and gravity data from the Catalina MCC region indicates a shallow, felsic to intermediate subsurface pluton in sharp contact with the Wilderness suite sills. The age of the subsurface pluton is unknown. However, on the basis of the gravity and aeromagnetic properties of intrusions in the region, a Tertiary or

Mesozoic age subsurface pluton is preferred. The age of the pluton relative to detachment faulting can help distinguish between differing models for MCC formation. A Mesozoic pluton suggests that crustal thickening influenced MCC development, and a preexisting zone of weakness may have controlled the emplacement of this body as well as the Wilderness suite sills. A Tertiary pluton suggests magmatism may have initiated low-angle faulting and MCC formation.

**THE ROLE OF MAGMATISM IN THE CATALINA METAMORPHIC CORE  
COMPLEX, ARIZONA: INSIGHTS FROM INTEGRATED  
THERMOCHRONOLOGY, GRAVITY AND AEROMAGNETIC DATA**

by

Jessica J. Terrien

A.B. Augustana College, 2001  
M.S. University of Missouri-Rolla, 2003

Dissertation

Submitted in partial fulfillment of the requirements for the degree of  
Doctor of Philosophy in Geology

Syracuse University  
May 2012

Copyright © Jessica J. Terrien 2012

All Rights Reserved

## TABLE OF CONTENTS

|   |          |
|---|----------|
| Preface.....  | 1        |
| <b>Chapter 1: <i>The Wilderness suite sills of the Catalina Metamorphic Core Complex, Arizona: Evidence for zircon inheritance and multiple phases of magmatism</i></b> ..... | <b>2</b> |
| Abstract.....   | 3        |
| Introduction.....   | 4        |
| Field and Microstructural Observations.....   | 6        |
| <i>Field observations</i> .....   | 6        |
| <i>Petrographic observations</i> .....  | 7        |
| Sample Preparation and Analysis.....  | 10       |
| Methods.....  | 10       |
| LA-ICPMS Results.....   | 12       |
| Discussion.....   | 15       |
| <i>Inherited zircon cores</i> .....   | 15       |
| <i>Intrusion at ~55 Ma and ~45 Ma</i> .....   | 16       |
| <i>Igneous or metamorphic zircon growth at &lt;40 Ma?</i> .....   | 17       |
| <i>&lt;40 Ma zircon rims</i> .....  | 18       |
| <i>Emplacement of the Wilderness suite sills</i> .....  | 19       |
| <i>Basin and Range magmatism</i> .....  | 20       |
| Conclusions.....  | 21       |
| References .....  | 23       |
| Figures.....  | 30       |
| Tables.....   | 46       |

|   |     |
|---|-----|
| <b>Chapter 2: <math>^{40}\text{Ar}/^{39}\text{Ar}</math> data from the Wilderness sills of the Catalina MCC: reheating vs. monotonic cooling of the footwall</b> .....  | 49  |
| Abstract.....   | 49  |
| Introduction and Nature of the Problem.....   | 51  |
| Geology of the Catalina MCC.....  | 52  |
| <i>Previous Data</i> .....  | 53  |
| Wilderness suite sills.....   | 55  |
| $^{40}\text{Ar}/^{39}\text{Ar}$ Method .....  | 58  |
| Results .....   | 59  |
| $^{40}\text{Ar}/^{39}\text{Ar}$ data.....   | 59  |
| <i>MDD modeling</i> .....   | 63  |
| Discussion.....   | 63  |
| $^{40}\text{Ar}/^{39}\text{Ar}$ potassium feldspar data and the timing of exhumation.....   | 63  |
| $^{40}\text{Ar}/^{39}\text{Ar}$ Muscovite and Biotite data.....   | 65  |
| $^{40}\text{Ar}/^{39}\text{Ar}$ and deformation of the Wilderness sills.....  | 66  |
| <i>Fission track data</i> .....   | 67  |
| Conclusions.....  | 68  |
| References.....   | 69  |
| Figures.....  | 74  |
| Tables.....   | 97  |
| <b>Chapter 3: Aeromagnetic and Bouguer Gravity modeling of the Catalina Metamorphic Core Complex: the Role of Magmatism in Metamorphic Core Complex Formation</b> ..... | 100 |
| Abstract.....   | 101 |
| Introduction.....   | 103 |
| Geology of the Catalina MCC.....  | 104 |
| Models for MCC Formation.....   | 105 |

|                                     |            |
|-------------------------------------|------------|
| Geophysical Data .....              | 107        |
| <i>Aeromagnetic Data</i> .....      | 107        |
| <i>Gravity Data</i> .....           | 108        |
| Geophysical Anomalies.....          | 109        |
| <i>Aeromagnetic Anomalies</i> ..... | 109        |
| <i>Gravity Anomalies</i> .....      | 112        |
| Modeling Results.....               | 112        |
| Discussion.....                     | 114        |
| <i>Thermochronologic Data</i> ..... | 114        |
| <i>Age of the Pluton</i> .....      | 116        |
| Conclusions.....                    | 118        |
| References.....                     | 120        |
| Figures.....                        | 132        |
| Tables.....                         | 144        |
| <b>Appendices</b> .....             | <b>149</b> |
| <b>Vita</b> .....                   | <b>232</b> |



## LIST OF FIGURES

### CHAPTER 1

|           |  |    |
|-----------|--|----|
| Figure 1  | Simplified geologic map of the Catalina MCC, Arizona.....  | 33 |
| Figure 2  | Geologic map of the forerange of the Catalina MCC, Arizona showing detailed mapping of the Wilderness suite sills.....   | 34 |
| Figure 3  | Cross-section from A-A' as shown in Figure 1 indicating the structural positions of the seven Wilderness sills.....  | 35 |
| Figure 4  | Representative CL images of zircon grains from the Wilderness suite sills.....   | 36 |
| Figure 5  | Concordia plots and weighted mean plots of LA-ICPMS zircon analyses for the Spencer, Wilderness and Shreve Pass sills.....   | 37 |
| Figure 6  | Concordia plots and weighted mean plots of LA-ICPMS zircon analyses for the Gibbon Mountain sill.....  | 38 |
| Figure 7  | Concordia plots and weighted mean plots of LA-ICPMS zircon analyses for the Seven Falls sill. ....   | 39 |
| Figure 8  | Probability density plots with zircon $^{206}\text{Pb}/^{238}\text{U}$ age populations for a) Gibbon Mountain sill and b) Seven Falls sill.....  | 40 |
| Figure 9  | Precambrian LA-ICPMS zircon analyses. a) Concordia plots and weighted mean plots for the Oracle Granite. b) Weighted mean plots of Precambrian LA-ICPMS zircon analyses from the Wilderness suite sills..... | 41 |
| Figure 10 | Weighted mean LA-ICPMS $^{208}\text{Pb}/^{232}\text{Th}$ monazite analyses from the Catnip Canyon sill.....  | 42 |
| Figure 11 | The Precambrian provinces including the location of the Catalina MCC.  | 43 |
| Figure 12 | Schematic diagram showing the intrusive sequence of the Wilderness suite sills.....  | 44 |
| Figure 13 | Location of migratory magmatism from ~60 to 30 Ma in the western United States.....  | 45 |

### CHAPTER 2

|          |  |    |
|----------|--|----|
| Figure 1 | Location of metamorphic core complexes across western North America..... | 77 |
|----------|--|----|

|              |  |       |
|--------------|--|-------|
| Figure 2     | a) Simplified geologic map of the Catalina MCC Arizona, b) Geologic map of the forerange of the Catalina MCC, Arizona showing detailed mapping of the Wilderness suite sills .....   | 78-79 |
| Figure 3     | Cross-section from A-A' as shown in Figure 2a indicating the structural positions of the seven Wilderness sills.....   | 80    |
| Figure 4     | $^{40}\text{Ar}/^{39}\text{Ar}$ spectra and inverse isochron plots for potassium feldspar and muscovite from Spencer sill of the Wilderness suite sills.....   | 81    |
| Figure 5     | $^{40}\text{Ar}/^{39}\text{Ar}$ spectra and inverse isochron plots for potassium feldspar and muscovite from the Wilderness sill (Windy Point locality) of the Wilderness suite sills.....   | 82    |
| Figure 6     | $^{40}\text{Ar}/^{39}\text{Ar}$ spectra and inverse isochron plots for potassium feldspar and muscovite from the Wilderness sill (General Hitchcock locality) of the Wilderness suite sills.....   | 83    |
| Figure 7     | $^{40}\text{Ar}/^{39}\text{Ar}$ spectra and inverse isochron plots for potassium feldspar and biotite from Catnip Canyon sill of the Wilderness suite sills.....   | 84    |
| Figure 8     | $^{40}\text{Ar}/^{39}\text{Ar}$ spectra and inverse isochron plots for potassium feldspar and biotite from Shreve Pass sill of the Wilderness suite sills.....   | 85    |
| Figure 9     | $^{40}\text{Ar}/^{39}\text{Ar}$ spectra and inverse isochron plots from potassium feldspar and muscovite from the Gibbon Mountain sill of the Wilderness suite sills...  | 86    |
| Figure 10    | $^{40}\text{Ar}/^{39}\text{Ar}$ spectra and inverse isochron plots for potassium feldspar and biotite from the Seven Falls sill of the Wilderness suite sills.....   | 87    |
| Figure 11-17 | a) Experimental, Free (black) and Monotonic (brown) modeled age spectra for the potassium feldspar samples from the Wilderness suite sills. b) Potassium feldspar MDD free (solid) and monotonic (outlined) thermal models for the Wilderness suite sill samples. c) Arrhenius plot for the potassium feldspar experimental and modeled data. d) $r/r_0$ plot for the Wilderness suite sill samples..... | 88-94 |
| Figure 18    | Thermal history of the Catalina MCC forerange (black) and main range (red).....  | 95    |
| Figure 19    | One dimensional transient thermal model of an intrusion with a radius of 5 kilometers.....   | 96    |

### CHAPTER 3

|          |  |         |
|----------|--|---------|
| Figure 1 | Generalized geologic map of the Santa Catalina, Rincon, Tortolita, Tucson and Galiuro Mountains..... | 134-135 |
| Figure 2 | Simplified geologic map of the Catalina MCC, Arizona.....  | 136     |
| Figure 3 | Generalized geologic history of the Catalina MCC region.....   | 137     |
| Figure 4 | Topography of the Catalina MCC region.....   | 138     |
| Figure 5 | Aeromagnetic map of the Catalina MCC region.....   | 139     |
| Figure 6 | Bouguer gravity anomaly map of the Catalina MCC region.....  | 140     |
| Figure 7 | Basement gravity anomaly map of the Catalina MCC region.....   | 141     |
| Figure 8 | Cross-section of the northern profile (A-A').....  | 142     |
| Figure 9 | Cross-section of the southern profile (B-B').....  | 143     |

## LIST OF TABLES

### CHAPTER 1

|         |  |       |
|---------|--|-------|
| Table 1 | Sample description and mineral(s) dated from the Wilderness suite sills..... | 47-48 |
|---------|--|-------|

### CHAPTER 2

|         |  |       |
|---------|--|-------|
| Table 1 | Summary table of Wilderness suite sill samples, description, and $^{40}\text{Ar}/^{39}\text{Ar}$ data..... | 98-99 |
|---------|--|-------|

### CHAPTER 3

|         |   |     |
|---------|---|-----|
| Table 1 | Aeromagnetic Surveys from the Tucson Basin and Catalina MCC region, AZ.....   | 145 |
| Table 2 | Susceptibilities of igneous and metamorphic rocks from the Catalina MCC region.....   | 146 |
| Table 3 | Susceptibility and density contrast values and ranges for the rock units modeled in Figures 8 and 9.....                          | 147 |
| Table 4 | Possible ages for the subsurface pluton and the possible relationship to MCC Formation and Wilderness sill thermochronology ..... | 148 |

## LIST OF APPENDICES

### CHAPTER 1

|  |     |
|--|-----|
| Appendix 1.1 Selected Photomicrographs from the Wilderness suite sills.....                                      | 150 |
| Appendix 1.2 CL zircon images from the Wilderness suite sills .....  | 154 |
| Appendix 1.3 LA-ICPMS Zircon U/Pb Data .....   | 191 |
| Appendix 1.4 Statistical Discussion of Zircon Populations from the Gibbon Mountain<br>and Seven Falls sills..... | 215 |

### CHAPTER 2

|  |     |
|--|-----|
| Appendix 2.1 $^{40}\text{Ar}/^{39}\text{Ar}$ Data from the Wilderness suite sills..... | 217 |
|--|-----|

## **PREFACE**

This dissertation includes three chapters written in the form of independent journal articles. Chapter one has been submitted to the Journal of Geophysical Research. This project focuses on understanding the role of magmatism within the Catalina metamorphic core complex (MCC). The Catalina MCC is located within the Basin and Range Province and is considered by many to be the type locality for MCC's. Chapters one and two address the crystallization history and the cooling history of the Wilderness suite sills which intrude the footwall of the Catalina MCC. Chapter three addresses aeromagnetic and gravity data from the Catalina MCC region; these data were modeled to study the subsurface geology in order to distinguish between models for forming MCC's.

The Catalina MCC has been the subject of numerous scientific studies. This project adds to that body of work, as it provides new details related to the timing and conditions of magmatism and formation of the MCC.

*The Wilderness suite sills of the Catalina Metamorphic Core Complex, Arizona:  
Evidence for zircon inheritance and multiple phases of magmatism*

Jessica J. Terrien

Syracuse University

Department of Earth Sciences

204 Heroy Geology Laboratory

Syracuse, New York 13244, USA

Suzanne L. Baldwin

Syracuse University

Department of Earth Sciences

204 Heroy Geology Laboratory

Syracuse, New York 13244, USA

George E. Gehrels

Department of Geosciences

Gould-Simpson Building #77

University of Arizona

1040 E. 4<sup>th</sup> Street

Tucson, Arizona 85721, USA

## **ABSTRACT**

The Catalina metamorphic core complex (MCC) in southeastern Arizona is intruded by several magmatic suites. The most voluminous is the Wilderness suite, a series of mylonitic to slightly deformed peraluminous sills that have sequentially intruded and inflated the footwall of the Catalina MCC. Zircon samples and one monazite sample from the Wilderness suite sills were analyzed by Laser Ablation Inductively Coupled Plasma Mass Spectrometry (LA-ICPMS) to gain insight into the timing of magmatic intrusion into the footwall of the Catalina MCC and the age of source material. A sample of the Precambrian Oracle Granite, the country rock, was also analyzed to determine if Tertiary zircon growth occurred during intrusion and deformation of the Wilderness suite sills. U/Pb data from zircon and Th/Pb data from monazite indicate that the Wilderness sills were emplaced during two separate phases of magmatism, the first at ~55–57 Ma and the second at ~45 Ma. A limited number of analyses from the structurally lowest sills indicated zircon growth as rims on preexisting zircon grains also occurred < 40 Ma. Inherited cores in several of the Tertiary age Wilderness suite sills range in age from ~1.7 to 1.4 Ga. No evidence for Tertiary zircon growth was found in the Oracle Granite sample. Results suggest the Precambrian Oracle Granite was partially melted to form the peraluminous Wilderness suite sills. Intrusion of the Wilderness sills modified the crustal thermal structure, elevating isotherms in the footwall prior to MCC formation thereby weakening the crust prior to extension.



## INTRODUCTION

Metamorphic core complexes (MCCs) are common features of extended terranes such as the Basin and Range Province of western North America. A MCC is an isolated topographic high in which crystalline basement has been overprinted by a mylonitic fabric and is structurally overlain by a faulted unmetamorphosed cover [Coney, 1980a]. In a MCC a low-angle detachment fault separates the footwall, comprised of ductilely deformed crystalline rocks, from brittlely deformed cover rocks of the hanging wall [Davis and Lister, 1988]. Normal-sense motion along the detachment fault exhumes deep-seated crystalline rocks [Davis and Lister, 1988].

MCCs form a linear trend within the Basin and Range Province from southern Canada to northern Mexico. Extension within the Basin and Range Province can be divided into two general categories on the basis of the type and timing of extension. Early extension dominated by low-angle detachment faulting and the development of MCC's began in the Eocene in the northern Basin and Range Province, and during Oligocene time in the southern Basin and Range Province. Detachment faulting in the Basin and Range Province was followed by a second stage of deformation dominated by high-angle faulting known as Basin and Range faulting. Detachment faults have accommodated most of the extension in the Basin and Range Province during the Tertiary [Spencer and Reynolds, 1989]. Magmatism, which is often accompanied by extension, is attributed to an increased geothermal gradient and weakening of the lithosphere [Armstrong and Ward, 1991]. A recent reconstruction of magmatism during Basin and Range faulting indicates that the majority of high-angle faulting occurred prior to magmatism within the Basin and Range Province [McQuarrie and Oskin, 2010].

The Catalina MCC of southeastern Arizona has long been considered to be a type locality for MCC's [e.g., *Coney*, 1980]. From the Late Mesozoic to early Cenozoic three magmatic suites intruded the Precambrian country rocks in the lower plate of the Catalina MCC. The country rock consists of the 1.4 Ga Oracle Granite, a porphyritic biotite granite that is variably deformed within the Catalina MCC.

The oldest suite, the Leatherwood suite, consists of quartz diorite and granodiorite plutons that, on the basis of cross-cutting relationships, were emplaced ~75-60 Ma [*Keith et al.*, 1980]. Generally, the timing of intrusion of the Leatherwood granodiorite corresponds to the Laramide orogeny in southern Arizona [*Dickinson*, 1991]. The youngest suite, the Catalina magmatic suite consists of biotite and hornblende-bearing granite and quartz monzonite emplaced at ~26 Ma [*Fornash et al.*, in prep].

The most voluminous magmatic suite within the footwall of the Catalina MCC is the peraluminous Wilderness magmatic suite sills. On the basis of geologic mapping seven Wilderness sills have been inferred to have inflated the crust by over 4 kilometers [*Force*, 1997]. The timing of emplacement of each of these sills into the footwall of the Catalina MCC has not been previously determined. Important remaining questions regarding the evolution of the Catalina MCC include: (1) What is the timing of magmatism relative to extension? (2) What was the duration of magma intrusion? (3) Did heat and deformation lead to new growth of zircons on rims of pre-existing zircons in the Precambrian country rocks? (4) What is the degree of zircon inheritance in the Wilderness suite sills? (5) Is there evidence of new zircon growth and/or metamorphic zircon in the Wilderness suite sills? (6) What was the source of the Wilderness sills? (7) When did the Catalina MCC form relative to magmatic intrusion?

This study addresses the timing of Wilderness sill emplacement within the footwall of the Catalina MCC and the temporal relationship between sill emplacement, detachment faulting and high-angle faulting. U/Pb analyses of zircon from the Wilderness sills (Figures 1 and 2) were undertaken in order to determine their crystallization age, which is necessary to interpret the thermal history of the Catalina MCC. Previous U/Pb TIMS (Thermal Ionization Mass Spectrometry) ages on zircons from the Wilderness sill at the Windy Point locality yielded an age of ~50 Ma [*Catanzaro and Kulp*, 1964]. K-Ar ages from potassium feldspar, biotite, and muscovite from the Wilderness suite range from ~35–20 Ma [*Keith et al.*, 1980; and references therein]. Cathodoluminescence (CL) images show that many of the zircons from the Wilderness suite sills are complexly zoned, and hence are targets for in-situ analyses to determine zircon age variations. In this study LA-ICPMS (Laser Ablation-Inductively Coupled Plasma Mass Spectrometry), was used to determine ages of zoned zircons, from the Wilderness suite sills and the Precambrian country rock, the Oracle granite. LA-ICPMS monazite data was also obtained for one of the Wilderness suite sills.

## **FIELD AND MICROSTRUCTURAL OBSERVATIONS**

### ***Field Observations***

The Catalina MCC comprises a forerange and a main range with rock exhumation generally attributed to motion along the MCC bounding normal fault [e.g., *Dickinson*, 1991; *Force*, 1997; Figure 3]. The main range and forerange are separated by the Romeo Basin fault and the Molino Basin fault. The forerange, which forms an anticline or arch with a northwest-southeast trending axis, is located on the southern flank of the Catalina MCC. Mylonites on the southwest side of the forerange arch have a top-to-the-SW sense

of shear whereas those on the north side of the arch have a primarily top-to-the-NE sense of shear. However, top-to-the-SW indicators are also present on the north side of the forerange [Force, 1997; Spencer, 2005]. Mylonites with top-to-the-SW shear sense are also observed at Windy Point within the main range [Force, 1997]. The basic description of the sills, including the degree of deformation and the minerals dated, is given in Table 1.

### ***Petrographic observations***

The microstructures observed within the Wilderness suite sills can be used to estimate temperatures reached during deformation [Passchier and Trouw, 2005]. For example, undulose extinction and bulging recrystallization of quartz occurs at temperatures of ~300–400°C, subgrain rotation of quartz occurs at temperatures of ~400–500°C, recrystallization of quartz due to grain-boundary migration occurs at ~500–700°C, and ductile deformation in mica occurs above 250°C [Passchier and Trouw, 2005]. All of the Wilderness suite samples are variably deformed and exhibit both ductile and brittle fabrics. Examples of the observed fabrics are shown in photomicrographs in Appendix 1.1 and the microstructures observed in each sill are described below.

### ***Spencer sill***

The Spencer sill is the structurally highest sill that consists of two lens that vary in thickness. It is a weakly foliated medium-grained granite that contains abundant biotite, large porphyroclasts of potassium feldspar and minor amounts of muscovite. Quartz has undergone grain-size reduction by subgrain rotation. Quartz ribbons are present, but rare, and show undulose extinction within the ribbons.

### *Wilderness sill*

The Wilderness sill is over 2000 meters thick [Force, 1997] and exhibits variable deformation throughout. Peraluminous granite at the General Hitchcock locality is slightly deformed whereas at the Windy Point location it is mylonitic. The Wilderness sill, in both localities, contains abundant muscovite and garnet. At the General Hitchcock locality, the sill contains brittlely deformed mica grains, whereas at the Windy Point locality the sill contains ductilely deformed mica grains. In samples from both locations petrographic observations indicate quartz has undergone subgrain rotation recrystallization and the Windy point locality also exhibits bulging recrystallization of quartz.

### *Catnip Canyon sill*

The ~300 meter thick Catnip Canyon sill consists of leucogranite and is subdivided into a felsic portion and a mafic portion [Force, 1997]. The mafic portion contains abundant biotite that is stained with iron oxide, brittlely deformed plagioclase feldspar, and recrystallized quartz. The felsic portion is biotite-poor, but contains muscovite, and also contains abundant quartz that exhibits subgrain rotation, bulging, and regions of extreme grain-size reduction.

### *Shreve Pass sill*

The Shreve Pass sill is about 60 meters thick and intrudes the Oracle Granite [Force, 1997]. The Romero Pass fault (Figure 3) has offset the Shreve Pass sill from the Gibbon Mountain and Seven Falls sills (described below). The Shreve Pass sill contains iron-stained biotite, is recrystallized to form ribbons that wrap around porphyroclasts of potassium feldspar and plagioclase feldspar, and contains little to no muscovite.

Fracturing of plagioclase feldspar and potassium feldspar is common. Quartz grains show evidence of subgrain rotation and bulging recrystallization.

#### *Gibbon Mountain sill*

The ~240 meter thick Gibbon Mountain sill intrudes both Oracle Granite and Leatherwood granodiorite [Force, 1997]. Force [1997] suggested that its emplacement followed an old Leatherwood sill because Leatherwood granodiorite is found above and below the Gibbon Mountain sill. Biotite is more abundant than muscovite within the Gibbon Mountain sill. Large porphyroclasts of plagioclase feldspar with deformation (taper) twins are present; subgrain rotation in quartz is observed and mantles plagioclase feldspar grains.

#### *Seven Falls sill*

The Seven Falls granite sill intrudes the Oracle Granite. Approximately 150 meters of the Seven Falls sill is exposed; however, the base of the Seven Falls sill is not exposed and thus its total thickness remains unknown [Force, 1997]. Biotite is abundant and defines a lineation. The sample studied displays deformation twins in potassium feldspar and myrmekite. Fractures are common in quartz, plagioclase, and potassium feldspar. The quartz has undergone subgrain rotation and bulging recrystallization.

#### *Oracle granite*

The mylonitized Oracle Granite was sampled in the forerange where the Wilderness suite and the Oracle Granite were in contact with one another. Undeformed, the Oracle Granite is a porphyritic biotite granite, but where found deformed it contains large augen of potassium feldspar.

## **SAMPLE PREPARATION AND ANALYSES**

Seven samples were collected from the Wilderness sills and one sample from Oracle Granite. Zircon and monazite were selected for analyses from the 100–300  $\mu\text{m}$  size fraction and then separated following conventional heavy liquid and magnetic separation techniques. Zircons were mounted in epoxy and polished to reveal their cross-sections. Prior to analysis, cathodoluminescent (CL) images of zircons were obtained using a SEM (Scanning Electron Microscope) in order to evaluate zoning; these images were used as a guide for the laser ablation analyses. Variations in CL intensity are commonly interpreted to represent different growth regions in the zircon [Corfu *et al.*, 2003]. Zircon zoning revealed in CL images is influenced largely by the distribution of trivalent rare earth elements; however, factors such as the amount of radiation damage to the grain can also influence CL intensity [Nasdala *et al.*, 2003]. CL images were also taken after LA-ICPMS analyses; in order to document the portions of the zircons ablated (Figure 4). The CL images for each grain analyzed are shown in Appendix 1.2.

## **METHODS**

Ablation of zircon was accomplished with a New Wave/Lambda Physik DUV193 Excimer laser (operating at a wavelength of 193 nm) in the LaserChron Center at the University of Arizona [Gehrels *et al.*, 2008]. Each analysis had a spot diameter of 10 to 15 microns. The laser spot was aimed at the zircon surface, away from epoxy or cracks within the grains. The ablated material from the zircon is carried with helium gas into the plasma source of a GV Instruments Isoprobe, equipped with a flight tube of sufficient width such that U, Th, and Pb isotopes can be measured simultaneously. All measurements were made in static mode, using Faraday detectors for  $^{238}\text{U}$  and  $^{232}\text{Th}$ , ion-

counting channeltron detectors for  $^{204}\text{Pb}$ , and either Faraday collectors or ion counting channeltron detectors for  $^{208-206}\text{Pb}$ . Ion yields are ~1 mv per ppm. Each analysis consists of one 20-second integration on peaks with the laser off (to determine backgrounds), 20 one-second integrations with the laser firing, and a 30 second delay to purge the previous sample and prepare for the next analysis. Zircon cores and rims were analyzed in each sample, however younger zircon growth (rims) were the primary targets for analysis.

The data are reported using the  $^{206}\text{Pb}/^{238}\text{U}$  age for samples < 1200 Ma and the  $^{206}\text{Pb}/^{207}\text{Pb}$  age for samples > 1200 Ma. The  $^{206}\text{Pb}/^{207}\text{Pb}$  age is more appropriate for >1200 Ma samples because the  $^{207}\text{Pb}$  can be measured with sufficient precision, whereas in samples <1200 Ma, the  $^{206}\text{Pb}/^{238}\text{U}$  ages are more precise because younger samples typically contain less Pb [Gehrels *et al.*, 2008; Ludwig, 1998; Parrish and Noble, 2003].  $^{204}\text{Pb}$  was used to correct for common Pb by assuming the initial Pb composition as determined by the growth model of Stacey and Kramers [1975].

The zircon analyses are plotted on a Concordia diagram and presented as a weighted mean for each sample with the random error associated with the individual analyses plus the systematic error (Figures 5–10). All plots were generated using Isoplot 3.00 software [Ludwig, 2003]. Many of the individual analyses had an error greater than 10%, possibly due to zoning within the zircons. Given the complicated zoning of the zircon grains, it was likely that material was ablated from more than one “zone”, resulting in a mixed age with very high error (> 10%). The raw analytical data illustrate how the isotopic measurements change over the course of a single analysis. The raw analytical data with high error, up to 50% in some cases, show that the isotopic values, and thus



calculated ages, of the zircons changed drastically over the course of the analysis. All zircon analyses are presented in Appendix 1.3.

Monazite analyses for the Catnip Canyon sample are presented as a weighted mean with the random error associated with the individual analyses plus the systematic error. Monazite standard 44069 was used to correct for fractionation and has a TIMS  $^{206}\text{U}/^{238}\text{Pb}$  age of 424.9 +/- 0.4 Ma [Aleinikoff *et al.*, 2006]. All of the analyses on monazite are presented in Appendix 1.3.

## **LA-ICPMS RESULTS**

Zircons were analyzed from the Oracle Granite and the following Wilderness suite sills [Force 1997]: Seven Falls sill, Gibbon Mountain sill, Shreve Pass sill, Wilderness sill (General Hitchcock and Windy Point localities), and Spencer sill. Many of the zircons from the Wilderness suite sills contained inherited Precambrian cores. However, many of the core analyses were also determined to be coeval with those on zircon rims. The weighted averages of the Phanerozoic samples include both rim and core determinations. All uncertainties are reported at 2-sigma level.

Zircon U/Pb age populations from both the Seven Falls and Gibbon Mountain sills contain a small proportion of grains that yielded ages < 40 Ma. These were the only sills that contained ages this young and the data visually contained multiple distinct populations. A statistical discussion of the age components within the Gibbon Mountain and Seven Falls sills is found in the description of the particular sill. These rims evidently were either formed, or altered (i.e. hydrothermal fluids) during an event subsequent to crystallization of the sills. Data from these analyses were calculated

separately and the age reported where appropriate. Primary crystallization ages were calculated after excluding data from the  $\leq 40$  Ma grains.

#### *Spencer sill*

Zircons from the Spencer sill are subtly zoned in CL images and several appear to be grain-fragments. The weighted mean  $^{206}\text{Pb}/^{238}\text{U}$  zircon age for the Spencer sill is  $57 \pm 2$  Ma based on 27 analyses from 19 zircon grains (Figure 5a). One zircon from the Spencer sill yielded an age of  $1713 \pm 12$  Ma.

#### *Wilderness sill*

Samples from both the General Hitchcock and Windy Point localities contain zircons that are zoned in CL, and both contain zircons with Precambrian cores. The weighted mean  $^{206}\text{Pb}/^{238}\text{U}$  zircon age for General Hitchcock is  $45 \pm 3$  Ma on the basis of 9 analyses from 6 zircon grains with less than 10% error, and the weighted mean zircon age for Windy Point is  $46 \pm 3$  Ma on the basis of 16 analyses from 12 zircon grains with less than 10% error (Figure 5b and 5c). These ages are indistinguishable within analytical error.

#### *Shreve Pass sill*

Zircons from the Shreve Pass sill are zoned in CL images and Precambrian cores were identified in this sample. The weighted mean  $^{206}\text{Pb}/^{238}\text{U}$  zircon age from the Shreve Pass sill is  $53 \pm 3$  Ma on the basis of 22 analyses from 14 zircon grains (Figure 5d).

#### *Catnip Canyon sill*

Monazite samples from the Catnip Canyon sill have been used as a monazite standard in previous studies [Harrison *et al.*, 1999]. LA-ICPMS analyses of monazite from Catnip Canyon yielded a  $^{232}\text{Th}/^{208}\text{Pb}$  age of  $43 \pm 2$  Ma (Figure 10).

### *Gibbon Mountain sill*

Zircons from the Gibbon Mountain sill are zoned in CL images. Precambrian age cores were identified in several grains. Paleocene-Eocene  $^{206}\text{Pb}/^{238}\text{U}$  zircon ages were obtained from 33 zircon grains separated from the Gibbon Mountain sill (Figure 6a and 6b). Using the mixing model described in *Sambridge and Compston* [1994] these analyses were separated into age components representing two separate periods of zircon growth:  $54 \pm 1$  Ma and  $38 \pm 1$  Ma. The probability density plot of the Gibbon Mountain sill data illustrates two populations (Figure 8a).

The relative misfit of the Gibbon Mountain sill analyses is low and increases if three age components are calculated. The relative misfit represents how the relative improvement in the data fit relates to the number of components [*Sambridge and Compston*, 1994]. If the number of age components increase it is predicted that the misfit will decrease. If there is no reduction in misfit, for example, when the number of components is increased from two to three, then only two distinct age components exist [*Sambridge and Compston*, 1994].

### *Seven Falls sill*

Zircons from the Seven Falls sill are zoned in CL images and Precambrian age cores were present in several grains. The Paleocene-Eocene  $^{206}\text{Pb}/^{238}\text{U}$  zircon ages from the Seven Falls sill were obtained from 46 zircon grains, and are separated into three populations:  $57 \pm 1$  Ma,  $46 \pm 1$  Ma, and  $38 \pm 1$  Ma using the mixing model described in *Sambridge and Compston* [1994; Figure 7a-c]. The probability density plot of the Seven Falls sill data reveals three age populations (Figure 8b). Regardless of the number of components chosen for the Seven Falls zircon population, the relative misfit remains

high. As predicted, the relative misfit is lower with three components than with two age components.

### *Oracle granite*

Zircons separated from the Oracle Granite are zoned in CL and yielded a  $^{206}\text{Pb}/^{207}\text{Pb}$  weighted mean age of  $1455 \pm 11$  Ma (Figure 9a), in agreement with previously published data [Shakel *et al.*, 1977]. The weighted mean age of the zircons from the Oracle granite included the cores and rims of the grains. No Phanerozoic zircon grains or zircon growth along older grains were present in the sample analyzed.

## **DISCUSSION**

### *Inherited zircon cores*

Precambrian age zircon cores were identified in all of the Wilderness sills. We infer that they were inherited from Paleoproterozoic basement rocks in the region that are subdivided into three provinces: Mojave, Yavapai and Mazatzal provinces (Figure 11). With the exception of the Spencer sill, ~ 1.4 Ga zircon cores, corresponding to the age of the Oracle Granite, were identified in all of the Wilderness sills. Precambrian cores were typically distinct from their corresponding rims in the CL images. Cores that range from ~1.6–1.7 Ga are also present (Figure 9b). The ~1.7 Ga cores are less abundant in the Wilderness sill samples. These zircons are interpreted to be inherited from the Yavapai terrane which contains 1.75 Ga volcanic-arc crust and is exposed to the northwest of the Catalina MCC [Karlstrom and Humphreys, 1998]. The 1.65 Ga grains are interpreted to be derived from the Mazatzal province, which comprise the basement terrane in the region [Karlstrom and Humphreys, 1998]. More zircon core analyses are required to further assess the significance of inheritance from the Yavapai and Mazatzal provinces in the

region. It is possible that a portion of the Yavapai province underlies the study area. For example, a portion of Paleoproterozoic basement equivalent in age and isotopic composition to the Mojave Province in the southwestern United States has been identified in northern Mexico [Farmer *et al.*, 2005].

Prior to emplacement of the Wilderness sills during the Laramide orogeny (~65–70 Ma), the crust in southeastern Arizona was thickened by the addition of primarily metaluminous intrusive and extrusive rocks and local volcanoclastic synorogenic strata [Dickinson, 1991]. The 1.4 Ga zircon cores found with the Wilderness sills indicate that xenocrystic grains were inherited from the country rock, and thus the Oracle Granite was partially melted to form the Wilderness suite sills. We did not identify any ~70 Ma zircon cores in the Wilderness sills, suggesting that these sills were not derived by partial melting of the Laramide age Leatherwood suite.

#### ***Intrusion at ~55 Ma and ~45 Ma***

The U/Pb zircon ages for the Wilderness sills indicate two intrusive events. The first occurred at ~55–57 Ma (Figure 12) and included the Spencer, Shreve Pass, and Gibbon Mountain sills. The second intrusive event took place at ~45 Ma (Figure 12) and included the Wilderness, Catnip Canyon, and Seven Falls sills. The Seven Falls sill contains age populations at ~57 Ma, ~46 Ma and ~38 Ma, and the Gibbon Mountain sill contains age populations at ~55 Ma, and ~38 Ma. The ~57 Ma ages from the Seven Falls sill is interpreted to represent inherited xenocrysts. The Catnip Canyon sill  $^{232}\text{Th}/^{208}\text{Pb}$  monazite age was within error of the Wilderness sill  $^{206}\text{Pb}/^{238}\text{U}$  zircon age; however it is possible that the Catnip Canyon sill is slightly older given the differences in closure temperature between the two systems [Harley *et al.*, 2007; Smith and Gilotti, 1997]. A

closure temperature between ~700 to 740°C is modeled for monazite grains that cooled at a rate of 10°C/my and have a diameter between 150 and 200 μm, the size of the Catnip Canyon sill monazite grains [Smith and Giletti, 1997]. A faster cooling rate would yield a higher closure temperature [Dodson, 1973].

The Thimble peak sill was not analyzed during this study, therefore its emplacement age is unknown. The Thimble Peak sill occurs above the Gibbon Mountain sill and structurally below the Shreve Pass sill, thus we would predict intrusion occurred at ~55–57 Ma. Holt *et al.*, [1986] concluded that the Wilderness suite sills likely extend to 7–12 km below the surface, thus it is possible that Wilderness material was intruded during events that are not recorded by samples exposed at the surface.

#### ***Igneous or metamorphic zircon growth at <40 Ma?***

The Wilderness sills were metamorphosed under greenschist-facies conditions, and thus the question of metamorphic zircon growth during deformation and metamorphism must be addressed. A minimum temperature of 300°C is estimated for the temperature of deformation within the Wilderness sills on the basis of microstructures in quartz. Metamorphic zircons have been determined to form under several conditions, including breakdown of silicate and accessory phases [Pan, 1997], recrystallization of protolith zircon [Bowring and Williams, 1999], and low temperature hydrothermal alteration [Schaltegger, 2007].

Zoning and morphology of zircon grains has also been used to infer the origin of the zircon or subsolidus modification [Corfu *et al.*, 2003]. The zircons from all of the Wilderness sills, including the Gibbon Mountain and Seven Falls sills, are generally euhedral. Euhedral zircon grains are not restricted to magmatic zircons, but subrounded

or resorbed zircon grains are a common distinguishing feature of grains formed under metamorphic conditions [Corfu *et al.*, 2003]. The inclusion-rich and spongy texture associated with zircon grown in the presence of hydrothermal fluids [Schaltegger, 2007] were not observed in any of the Wilderness sills. The majority of zircons from this study exhibit oscillatory zoning, typical of magmatic zircons [Corfu *et al.*, 2003]. Oscillatory zoning is not observed in several studies where subsolidus zircon growth was documented or inferred [Roberts and Finger, 1997; Wayne and Sinha, 1992].

Low Th/U (<0.1) is commonly used to infer growth of zircon in the presence of metamorphic fluids [Harley *et al.*, 2007]. However, there is no clear relationship between the Th/U ratio from the Wilderness sill zircon grains and  $^{206}\text{Pb}/^{238}\text{U}$  age, and low Th/U values are not observed. The average Th/U for each sample is listed in Table 1. The Gibbon Mountain sample plots as two clusters of analyses and all zircons greater than 40 Ma have a Th/U ratio that ranges from 0.2 to 1.0 whereas all zircons less than 40 Ma have a Th/U ratio <0.5. The Seven Falls sill, which also contains zircons less than 40 Ma, plots in a large cluster with the majority of samples having a Th/U ratio < 0.5 irrespective of  $^{206}\text{Pb}/^{238}\text{U}$  age.

#### ***<40 Ma zircon rims***

Primary crystallization of the Gibbon Mountain occurred at ~55 Ma and primary crystallization of the Seven Falls sill occurred at ~45 Ma. We propose that partial melting of the Gibbon Mountain and Seven Falls sills allowed for new magmatic zircon growth at < 40 my. This explains the euhedral grains and common oscillatory zoning observed in the < 40 Ma rims in these sills. The partial melting event at ~38 my affected the structurally lower sills; zircon ages less than 40 Ma are not observed in the

structurally higher sills. This could be due to a sampling bias, or because no zircon growth occurred after 40 Ma in the sills emplaced at shallower crustal levels. In addition, there is some evidence for ~40 Ma zircons present in other intrusions within the Catalina MCC region [Dickinson, 1991].

Gravity modeling by Holt *et al.* [1986] was interpreted to indicate that the Wilderness suite is responsible for the 20 mGal low over the center of the Catalina-Rincon MCC and that granitic rock likely extends to a depth of 7-12 km below the surface. Heat from intrusion of subsurface Wilderness material may be responsible for partially melting the Seven Falls and Gibbon Mountain sills. Furthermore, peraluminous magmatism is also observed in the Little Rincon Mountains, located east of the Catalina MCC [Gehrels and Smith, 1991]. This granite is not known to be related to the development of the MCC, but it supports our interpretation that partial melting and magmatism occurred at ~40 Ma in the region. Gehrels and Smith, [1991] analyzed zircon and monazite and report a lower-intercept age of  $24 \pm 12$  Ma for zircon, and a lower-intercept age of  $30 \pm 6$  Ma for monazite, which are interpreted to be the crystallization ages. The upper-intercept ages for the zircon and the monazite were ~1.4 Ga, which were interpreted to represent xenocrysts inherited from the country rocks [Gehrels and Smith, 1991]. The zircon ages from the Little Rincon Mountains are within error of the <40 Ma zircon  $^{206}\text{Pb}/^{238}\text{U}$  age data presented for the Gibbon Mountain and Seven Falls sills indicating zircon growth prior to extensional movement along the detachment fault.

#### ***Emplacement of the Wilderness suite sills***

The nature (e.g., timing, composition and thickness) of sill emplacement is important for understanding MCC evolution [Lister and Baldwin, 1993; Parsons and



*Thompson, 1993*]. The emplacement of the Wilderness suite sills predates low-angle normal faulting and uplift of the Catalina MCC and post-dates high-angle Basin and Range faulting. The emplacement mechanism of granite intrusions into the crust, as well as the corresponding rate of emplacement, continues to be a controversial topic. A model involving transport of granitic magma via dikes has replaced the traditional “blob” model for pluton formation [*Petford et al., 2000*]. It is likely that dikes have played a role in the emplacement of the Wilderness sills, but the dikes or conduits that supplied the magma for sill emplacement have not been observed in the field. Varying abundances of biotite and muscovite within the Wilderness sills is likely a function of variations in source material.

Peraluminous granites, in which  $Al_2O_3 / (CaO + Na_2O + K_2O) > 1$ , are thought to form via three mechanisms: by partial melting, by differentiation of metaluminous magma, and by late-stage super-solidus metasomatic loss of alkali through vapor phase transport [*Zen, 1988*]. Partial melting is the preferred method in the case of the Wilderness suite sills, where a large volume of muscovite-bearing peraluminous granites was generated. “Wet” anatexis occurs due to overthickening, and partial melting of sedimentary and igneous rocks, and by the addition of water via pathways such as shear zones or thrust faults [*Barbarin, 1996*]. Pegmatites are evidence that water was present [*Barbarin, 1996*]. Small pegmatite zones are observed within Wilderness sills; the largest pegmatite, known as the Mt. Lemmon pegmatite-aplite is found at high elevations within the Catalina MCC main range [e.g., *Force, 1997*].

### ***Basin and Range magmatism***

Post-Laramide magmatism within the Basin and Range is related to subduction

along the western margin of North America [Atwater and Stock, 1998]. Early in the Cenozoic, shortly following the Laramide orogeny, numerous batholiths produced by crustal melting were emplaced in the Basin and Range Province, including those in southern Arizona [Dickinson, 1991]. This magmatism, attributed to the subducted slab, occurred north and south of the Laramide gap in a region of little to no magmatism (Figure 13). The lack of magmatism in the Laramide gap is assumed to be the result of the low angle of that part of the subducted slab; magmatism occurred farther east in the Rocky Mountain region [Armstrong and Ward, 1991]. Magmatism north of the Laramide gap declined until approximately 60 Ma when increasing magmatism and extension dominated between 60 and 55 Ma [Parson, 1995]. In the late Oligocene and early Miocene, extension and magmatism migrated northward from Mexico and closed the Laramide gap [Parsons, 1995].

To assess the role of mantle involvement in the genesis of the Wilderness sills Farmer *et al.*, [1989] analyzed several peraluminous granites samples ranging in age from Late Cretaceous to mid-Tertiary from Arizona, including one sample from the Santa Catalina Mountains. The  $\epsilon_{Nd}$  values from the Wilderness sill sample and other peraluminous granites from southern Arizona range from -10 to -12 and indicate that the source material was felsic Precambrian basement rock and there was no mantle component [Farmer *et al.*, 1989].

## CONCLUSIONS

The Wilderness sills were intruded into the footwall of the Catalina MCC during two separate stages, the first at ~55–57 Ma and the second at ~45 Ma with additional zircon growth at <40 Ma. All of the Wilderness sills contain zircons with Precambrian

age inherited cores, which are derived from the 1.4 Ga Oracle Granite or from Paleoproterozoic crystalline basement rocks. There is no strong evidence (i.e. from Th/U or CL zoning patterns) for zircon growth during metamorphism, and thus the Wilderness sill zircons are interpreted to be magmatic in origin. The source of the Wilderness sills is likely crustal material that was partially melted.

The intrusion of the Wilderness suite sills predates extension and uplift of the Catalina MCC. Emplacement of the Wilderness suite sills at ~55–57 and ~45 Ma and partial melting at ~40 Ma elevated the local geothermal gradient, thereby weakening the crust for extension, which on the basis of fission track data [*Fayon et al.*, 2000], sedimentary assemblages associated with faulting [*Dickinson*, 1991], and  $^{40}\text{Ar}/^{39}\text{Ar}$  data from potassium feldspar and micas [*Terrien and Baldwin*, in prep.] occurred between ~30 and ~20 Ma.

## REFERENCES

- Aleinikoff, J. N., et al. (2006), Deciphering igneous and metamorphic events in high-grade rocks of the Wilmington Complex, Delaware: Morphology, cathodoluminescence and backscattered electron zoning, and SHRIMP U-Pb geochronology of zircon and monazite, *Geological Society of America Bulletin*, 118(1/2), 39-64.
- Armstrong, R. L., and P. Ward (1991), Evolving Geographic Patterns of Cenozoic Magmatism in the North American Cordillera: The Temporal and Spatial Association of Magmatism and Metamorphic Core Complexes, *Journal of Geophysical Research*, 96(B8), 13201-13224.
- Atwater, T., and J. Stock (1998), Pacific-North America Plate Tectonics of the Neogene Southwestern United States: An Update, *International Geology Review*, 40, 375-402.
- Barbarin, B. (1996), Genesis of the two main types of peraluminous granitoid, *Geology*, 24(4), 295-298.
- Bird, P. (1998), Kinematic history of the Laramide orogeny in latitudes 35 degrees- 49 degrees N, western United States, *Tectonics*, 17, 780-801.
- Bowring, S. A., and I. S. Williams (1999), Priscoan (4.00-4.03 Ga) orthogneisses from northwestern Canada, *Contributions to Mineralogy and Petrology*, 134, 3-16.
- Bykerk-Kauffman, A. (2008), Geologic map of the northeastern Santa Catalina Mountains, Pima County, Arizona.

- Catanzaro, E. J., and J. L. Kulp (1964), Discordant zircons from the Little Belt (Montana), Beartooth (Montana) and Santa Catalina (Arizona) Mountains, *Geochimica et Cosmochimica Acta*, 28, 87-124.
- Coney, P. J. (1980), Cordilleran metamorphic core complexes: An overview, in *Cordilleran Metamorphic Core Complexes*, edited by M. D. Crittenden Jr., et al., pp. 7-34, The Geological Society of America, Inc. Memoir 153.
- Corfu, F., et al. (2003), Atlas of zircon textures, in *Zircon*, edited by J. M. Hancher and P. W. O. Hosking, Mineralogical Society of America Geochemical Society.
- Davis, G. A., and G. S. Lister (1988), Detachment faulting in continental extension: Perspectives from the southwestern U.S. Cordillera, in *Processes in continental lithospheric deformation*, edited by S. P. Clark Jr., pp. 133-159.
- Dickinson, W. R. (1991), *Tectonic setting of faulted Tertiary strata associated with the Catalina core complex in southern Arizona*, 106 pp.
- Dickinson, W. R. (1999), Geologic framework of the Catalina foothills, outskirts of Tucson (Pima County, Arizona), scale 1:24,000, 031 p.
- Dodson, M. H. (1973), Closure temperature in cooling geochronological and petrological systems, *Contributions to Mineralogy and Petrology*, 40, 259-274.
- Farmer, G. F., et al. (2005), Paleoproterozoic Mojave province in northwestern Mexico? Isotopic and U-Pb zircon geochronologic studies of Precambrian and Cambrian

crystalline and sedimentary rocks, Caborca, Sonora, *Geological Society of America Bulletin Special Paper 393*, 183-1998.

Farmer, G. L., et al. (1989), Isotopic Evidence on the Structure and Origin of Subcontinental Lithospheric Mantle in Southern Nevada, *Journal of Geophysical Research*, 94(B6), 7885-7898.

Fayon, A. K., et al. (2000), Fission track analysis of the footwall of the Catalina detachment fault, Arizona: Tectonic denudation, magmatism and erosion, *Journal of Geophysical Research*, 105(B5), 11047-11062.

Force, E. R. (1997), Geology and Mineral Resources of the Santa Catalina Mountains, Southeastern Arizona, *Monographs in Mineral Resource Science No. 1*, 135.

Fornash, K.F., Patchett, J. P., Gehrels, G.E., and Spencer, J.E. (2012), Evolution of granitoids in the Catalina metamorphic core complex, southeastern Arizona: U-Pb, Nd, and Hf isotopic constraints, in preparation.

Gehrels, G. E., and C. H. Smith (1991), U-Pb geochronologic constraints on the age of thrusting, crustal extension, and peraluminous plutonism in the Little Rincon Mountains, southern Arizona, *Geology*, 19, 238-241.

Gehrels, G. E., et al. (2008), Enhanced precision, accuracy, efficiency, and spatial resolution of U-Pb ages by laser ablation--multicollector--inductively coupled plasma--mass spectrometry, *Geochemistry Geophysics Geosystems*, 9(3), 1-13.

Harley, S. L., et al. (2007a), Zircon Behaviour and the Thermal Histories of Mountain Chains, in *Elements*, edited, pp. 25-30.

Harley, S. L., et al. (2007b), Zircon Behaviour and the Thermal Histories of Mountain Chains, edited by Elements, pp. 25-30.

Harrison, T. M., et al. (1999), Origin and Episodic Emplacement of the Manaslu Intrusive Complex, Central Himalaya, *Journal of Petrology*, 40(1), 3-19.

Karlstrom, K. E., and E. D. Humphreys (1998), Persistent influence of Proterozoic accretionary boundaries in the tectonic evolution of southwestern North America; interaction of cratonic grain and mantle modification events, *Rocky Mountain Geology*, 33(2), 161-179.

Lister, G. S., and S. L. Baldwin (1993), Plutonism and the origin of metamorphic core complexes, *Geology*, 21, 607-610.

Ludwig, K. R. (1998), On the treatment of concordant uranium-lead ages, *Geochimica et Cosmochimica Acta*, 62(4), 665-676.

Ludwig, K. R. (2003), Users Manual for Isoplot/Ex version 3.0, A Geochronological Toolkit for Microsoft Excel, *Berkeley Geochronology Special Publication No. 4*, 1-70.

McQuarrie, N., and M. Oskin (2010), Palinspastic restoration of NAVDat and implications for the origin of magmatism in southwestern North America, *Journal of Geophysical Research*, 115, 1-16.

Nasdala, L., et al. (2003), Spectroscopic methods applied to zircon, in *Zircon*, edited by J. M. Hanchar and P. W. O. Hosking, pp. 427-467, Mineralogical Society of America and Geochemical Society.

Pan, Y. (1997), Zircon and Monazite forming Metamorphic Reactions at Manitouwadge, Ontario, *The Canadian Mineralogist*, 35, 105-118.

Parrish, R. R., and S. R. Noble (2003), Zircon U-Th-Pb geochronology by isotope dilution--thermal ionization mass spectrometry (ID-TIMS), in *Zircon: Reviews in Mineralogy and Geochemistry*, edited by J. M. Hanchar and P. W. O. Hoskin, Mineralogical Society of America and Geochemical Society, Washington, D.C.

Parson, T. (1995), The Basin and Range Province, in *Continental Rifts: Evolution, Structure, Tectonics*, edited by K. H. Olsen, pp. 277-316, Elsevier, New York.

Parsons, T., and G. A. Thompson (1993), Does magmatism influence low-angle normal faulting?, *Geology*, 21, 247-250.

Passchier, C. W., and R. A. J. Trouw (2005), *Microtectonics*, 2nd ed., Springer, New York.

Petford, N., et al. (2000), Granite magma formation, transport and emplacement in the Earth's crust, *Nature*, 408(7), 669-673.

Roberts, M. P., and F. Finger (1997), Do U-Pb zircon ages from granulites reflect peak metamorphic conditions?, *Geology*, 25(4), 319-322.



Sambridge, M. S., and W. Compston (1994), Mixture modeling of multi-component data sets with application to ion-probe zircon ages, *Earth and Planetary Science Letters*, 128, 373-390.

Schaltegger, U. (2007), Hydrothermal Zircon, in *Elements*, edited, p. 51.

Shakel, D. W., et al. (1977), Observations on the history of the gneissic core complex, Santa Catalina Mts, southern Arizona, *Geological Society of America Abstracts with Programs*, 9, 1169-1170.

Smith, H. A., and B. J. Giletti (1997), Lead diffusion in monazite, *Geochimica et Cosmochimica Acta*, 61(5), 1047-1055.

Spencer, J. E., and S. J. Reynolds (1989), Middle Tertiary Tectonics of Arizona and Adjacent Areas, *Geologica evolution of Arizona, Arizona Geological Society Digest*, 17, 539-574.

Spencer, J. E., et al. (2000), Compilation geologic map of the Oracle 7.5 Quadrangle, Pinal and Pima Counties, Arizona, scale 1:24,000 (001 sheet), 030 p.

Spencer, J. E., and P. A. Pearthree (2004), Geologic map of the Oro Valley 7.5 Quadrangle, Pima County, Arizona, version 2.0, scale 1:24,000.

Terrien, J.J., and S.L. Baldwin (2012),  $^{40}\text{Ar}/^{39}\text{Ar}$  data from the Wilderness sills of the Catalina Metamorphic Core Complex: reheating vs. monotonic cooling of the footwall, in preparation.

Wayne, D. M., and A. K. Sinha (1992), Stability of Zircon U-Pb Systematics in a Greenschist-Grade Mylonite: An Example from the Rockfish Valley Fault Zone, Central Virginia, USA, *The Journal of Geology*, 100, 593-603.

Zen, E. (1988), Phase relations of peraluminous granitic rocks and their petrogenetic implications, *Annual Review of Earth and Planetary Science*, 16, 21-51.

## FIGURES

Figure 1. Simplified geologic map of the Catalina MCC, Arizona [from *Fornash et al.*, in prep.,]. Mapping based on [*Bykerk-Kauffman*, 2008; *Dickinson*, 1999; *Force*, 1997; *Spencer et al.*, 2000; *Spencer and Pearthree*, 2004]. Sampling locations are indicated.

Figure 2. Geologic map of the forerange of the Catalina MCC, Arizona showing detailed mapping of the Wilderness suite sills [from *Fornash et al.*, in prep.,]. Mapping based on [*Bykerk-Kauffman*, 2008; *Dickinson*, 1999; *Force*, 1997; *Spencer et al.*, 2000; *Spencer and Pearthree*, 2004]. Sampling locations are indicated.

Figure 3. Cross-section from A-A' as shown in Figure 1 indicating the structural positions of the seven Wilderness sills. The cross-sectional relationships are diagrammatic. Thicknesses are not to scale. [After *Force*, 1997].

Figure 4. Representative CL images of zircon grains from the Wilderness suite sills. Spencer (CAT 93-8), Wilderness, General Hitchcock (CAT 0704), Wilderness, Windy Point (CAT 0705), Shreve Pass, (CAT 0703), Gibbon Mountain, (CAT 93-8), Seven Falls, (CAT 93-9) and Oracle Granite, (CAT 0701). LA-ICPMS ages are indicated in white and the analyses locations are outlined in white circles.

Figure 5. Concordia plots and weighted mean plots of LA-ICPMS zircon analyses for the Spencer, Wilderness and Shreve Pass sills. The box heights for the weighted mean and the concordia error ellipse represent 2-sigma errors a) Spencer sill has a weighted mean age of  $57 \pm 2$  Ma, MSWD=8, b) Wilderness sill, Windy Point locality has a weighted

mean age of  $46 \pm 3$  Ma, MSWD=0.7, c) Wilderness sill, General Hitchcock locality has a weighted mean age of  $45 \pm 3$  Ma, MSWD=0.1, d) Shreve Pass sill has a weighted mean age of  $53 \pm 2$  Ma, MSWD=6.6.

Figure 6. Concordia plots and weighted mean plots of LA-ICPMS zircon analyses for the Gobbon Mountain sill. The box heights for the weighted mean and the concordia error ellipses represent 2-sigma errors. a) Gibbon Mountain sill–55 Ma age component has a weighted mean age of  $55 \pm 2$  Ma, MSWD = 0.8, b) Gibbon Mountain sill–38 age component has a weighted mean age of  $38 \pm 2$  Ma, MSWD = 1.4.

Figure 7. Concordia plots and weighted mean plots of LA-ICPMS zircon analyses for the Seven Falls sill. The box heights represent 2-sigma errors and the error ellipse are 2-sigma errors a) Seven Falls sill–57 Ma age component has a weighted mean age of  $57 \pm 2$  Ma, MSWD = 2.7, b) Seven Falls sill–46 age component has a weighted mean age of  $46 \pm 2$  Ma, MSWD = 1.3 c) Seven Falls–38 age component has a weighted mean of  $37 \pm 3$  Ma, MSWD = 1.8.

Figure 8. Probability density plots with zircon  $^{206}\text{Pb}/^{238}\text{U}$  age populations for a) Gibbon Mountain sill and b) Seven Falls sill [*Sambridge and Compston, 1994*].

Figure 9. Precambrian LA-ICPMS zircon analyses. a) Concordia plots and weighted mean plots for the Oracle Granite. The Oracle Granite has a weighted mean of  $1455 \pm 11$  Ma, WSWD = 1.9. The box heights represent 2-sigma errors and the error ellipse are

2-sigma errors. b) Weighted mean plots of Precambrian LA-ICPMS zircon analyses from the Wilderness suite sills. The data point error ellipses are 2-sigma.

Figure 10. Weighted mean LA-ICPMS  $^{208}\text{Pb}/^{232}\text{Th}$  monazite analyses from the Catnip Canyon sill.

Figure 11. The Precambrian provinces including the location of the Catalina MCC [after Karlstrom and Humphreys, 1998].

Figure 12. Schematic diagram showing the intrusive sequence of the Wilderness suite sills. a) cross-section of the crust prior to intrusion, b) cross-section of the crust after intrusion at ~57 Ma, c) cross-section of the crust after intrusion at ~45 Ma and zircon growth at ~40 Ma occurs on zircon rims within the Seven Falls and Gibbon Mountain sills.

Figure 13. Location of migratory magmatism from ~60 to 30 Ma in the western United States. Magmatism is indicated by the gray zones. The dark gray zones indicate where magmatism was most intense [Bird, 1998].

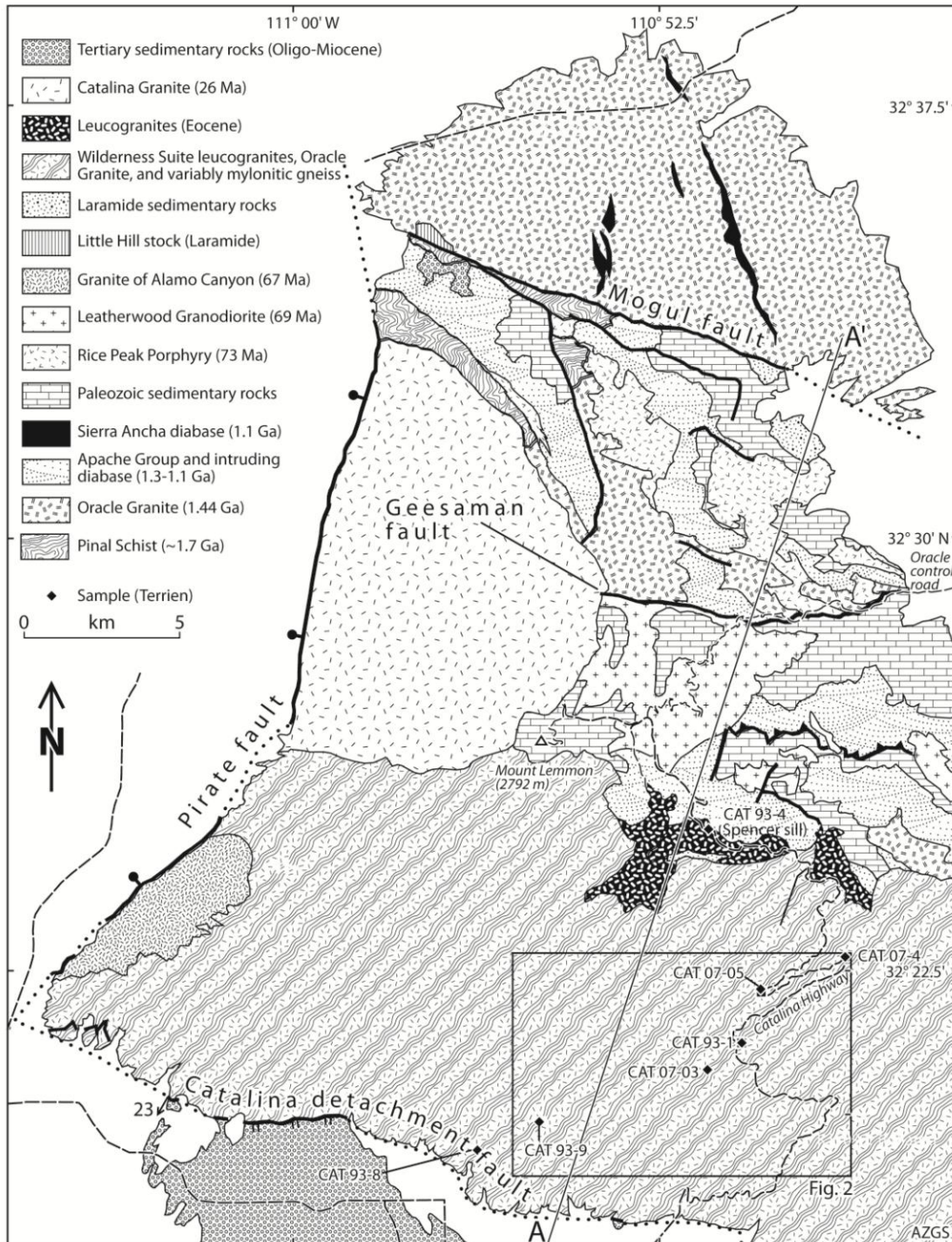


Figure 1.

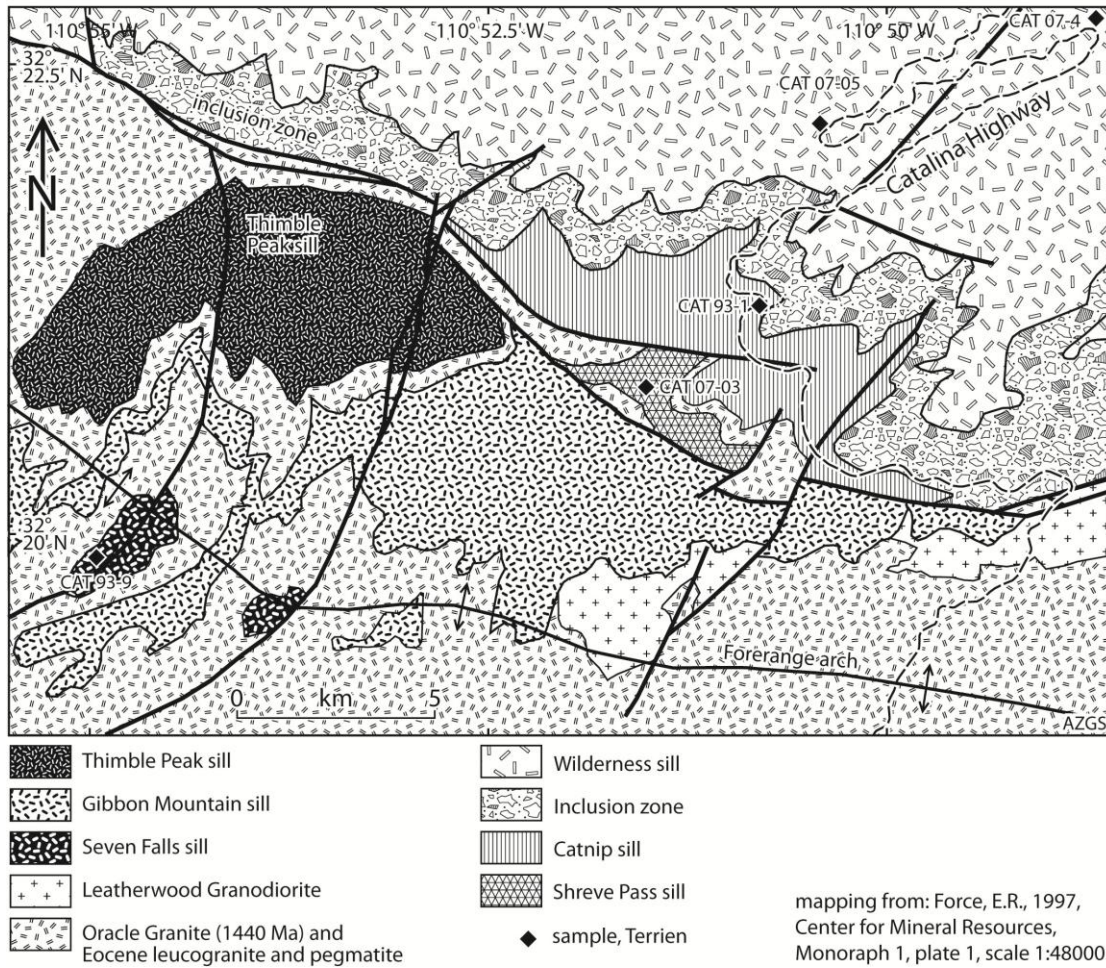
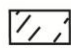




Figure 2.

Wilderness suite sills:

- I. Spencer sill
- II. Wilderness sill (Windy Pt. and Gen. Hitchcock)
- III. Catnip Canyon sill
- IV. Shreve Pass sill
- V. Thimble Peak sill
- VI. Gibbon Mountain sill
- VII. Seven Falls sills

 mylonites

Screens:

-  Apache Group
-  Oracle Granite

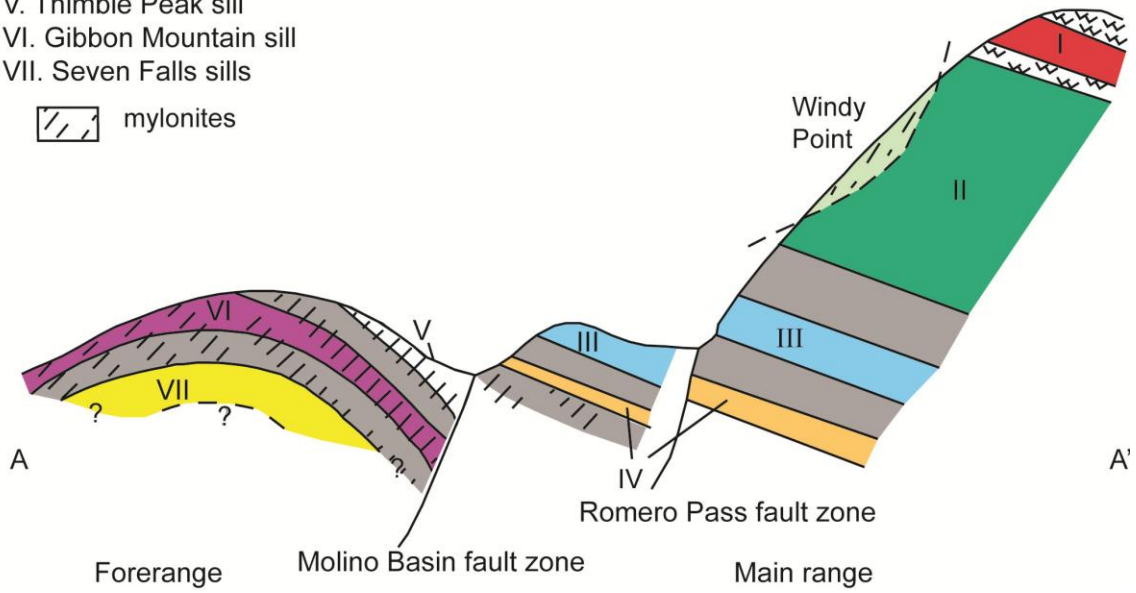


Figure 3.



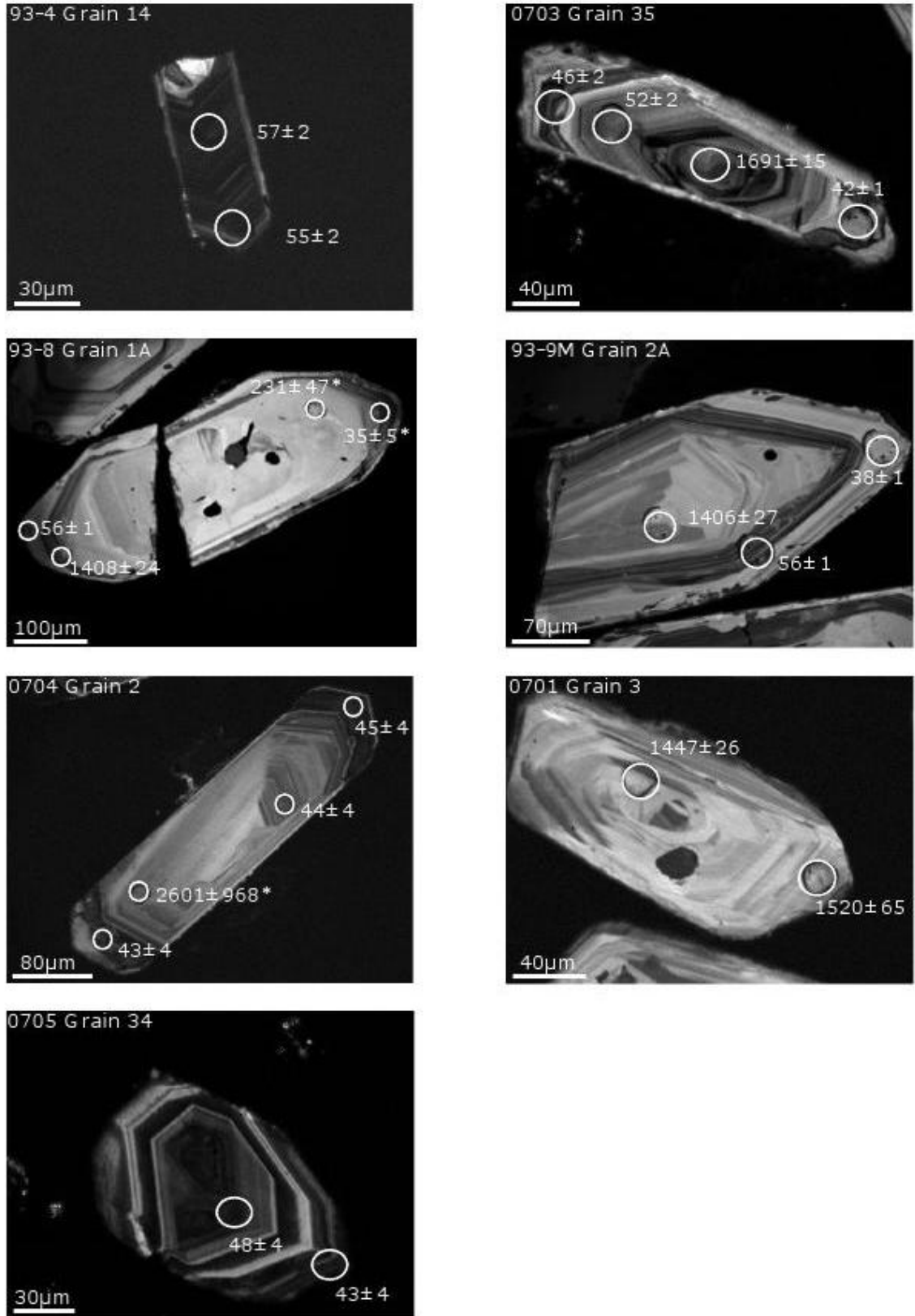


Figure 4.

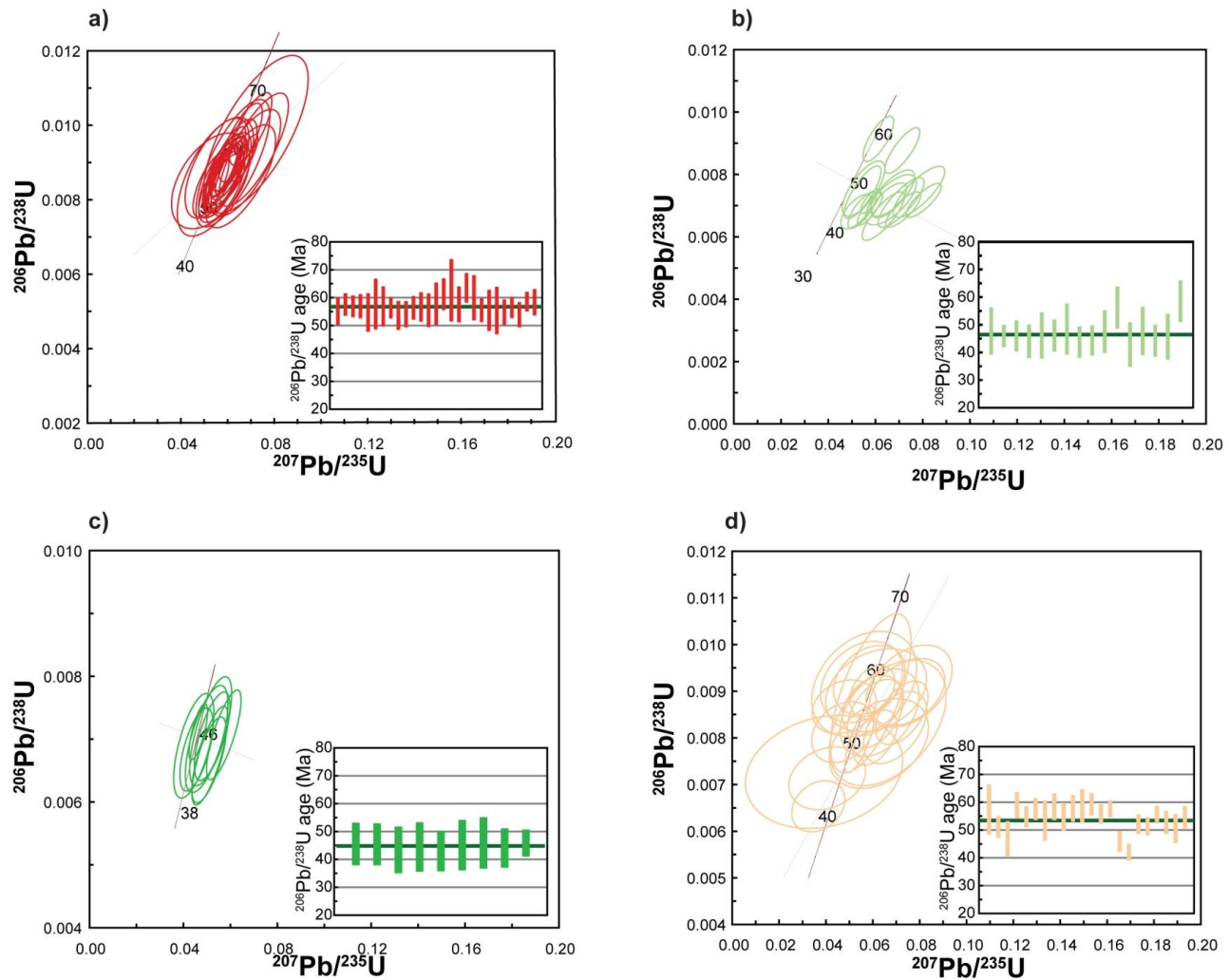


Figure 5.

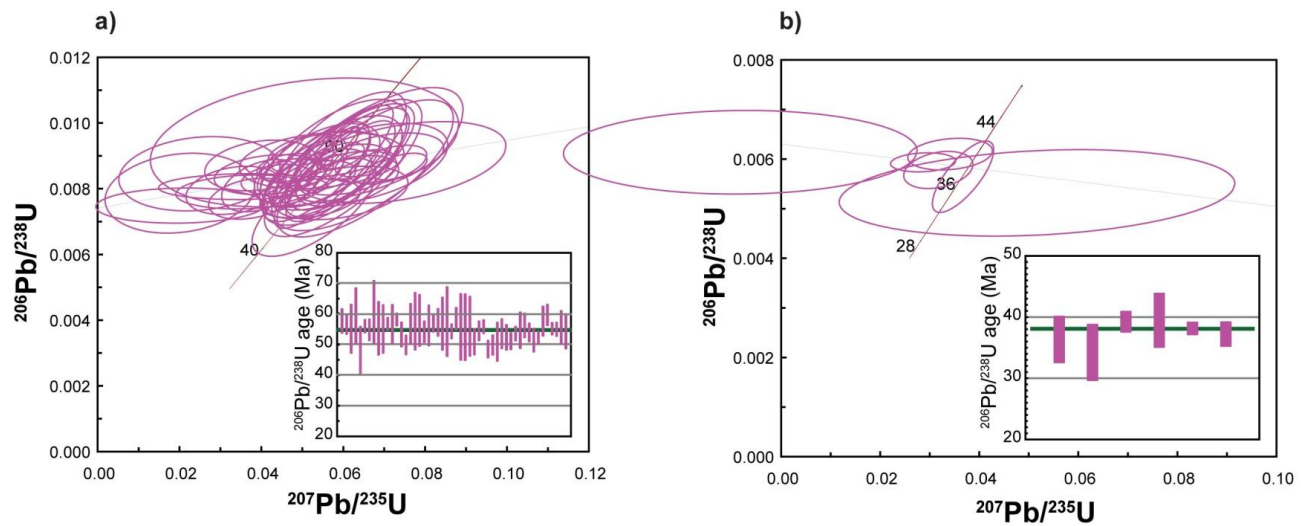


Figure 6.

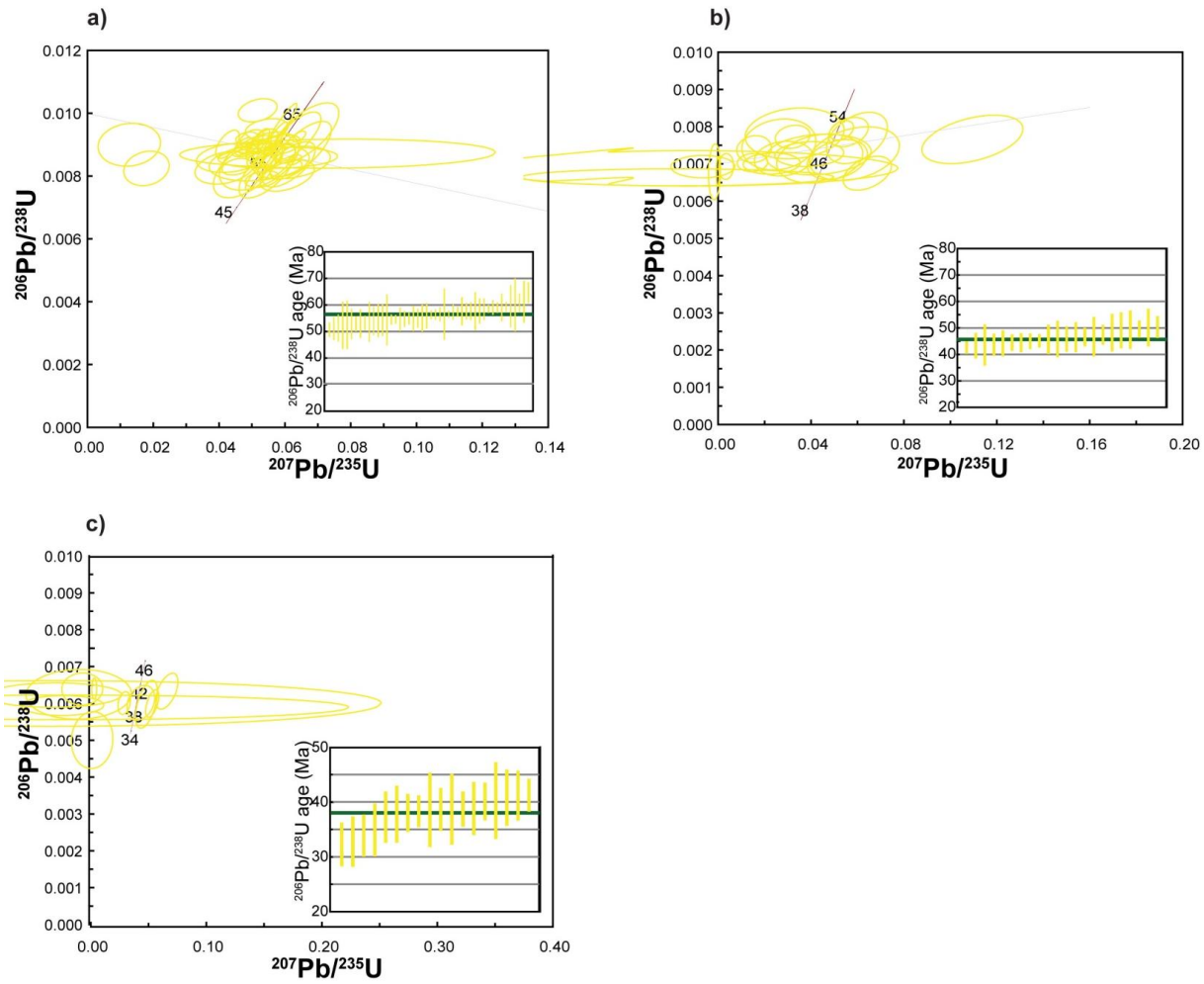


Figure 7.

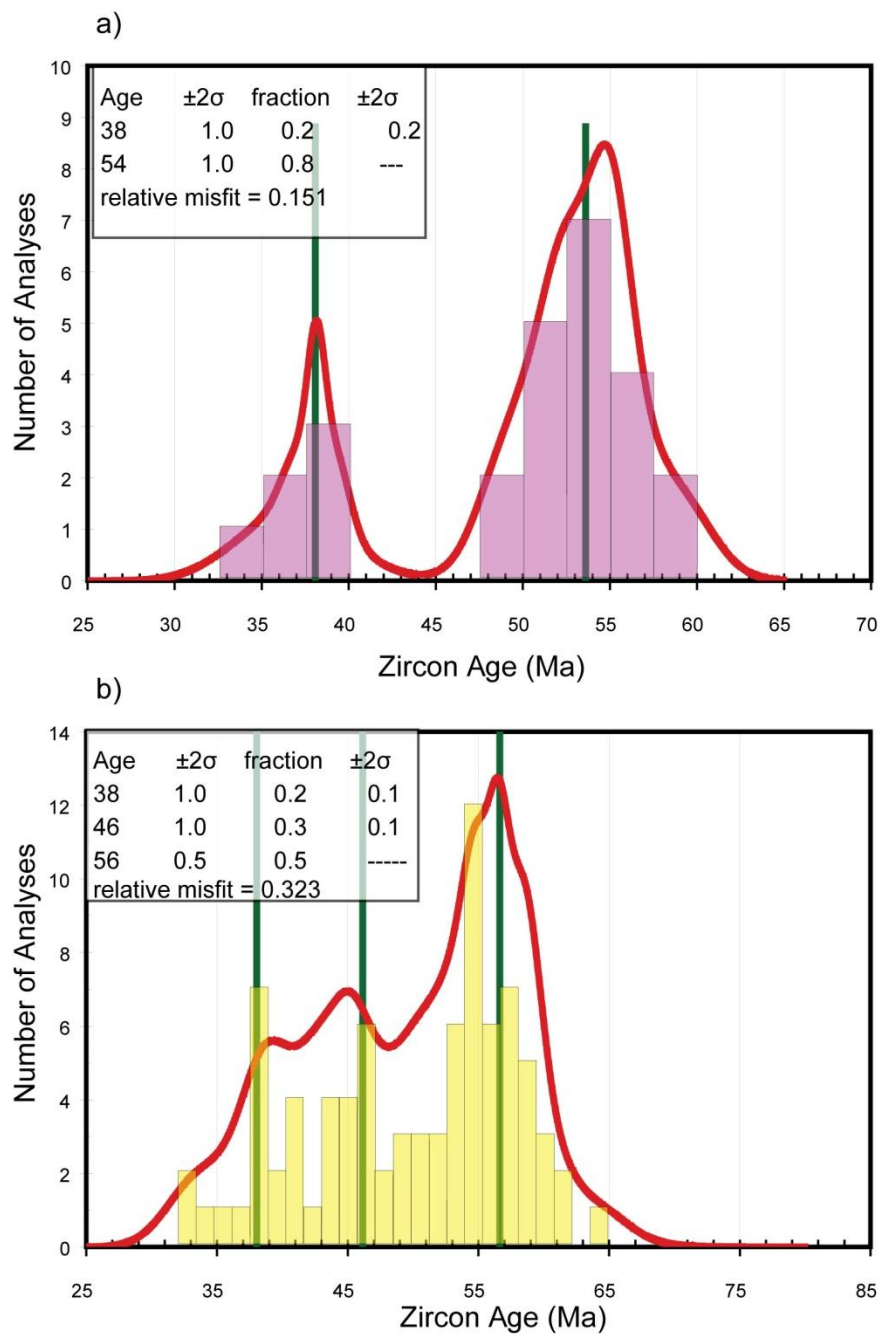


Figure 8.

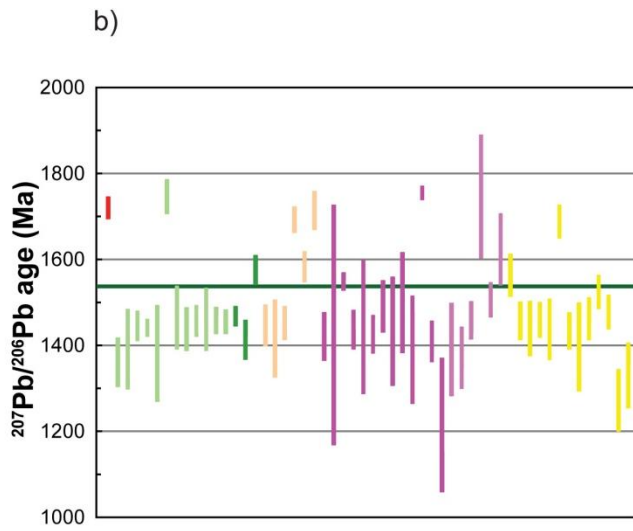
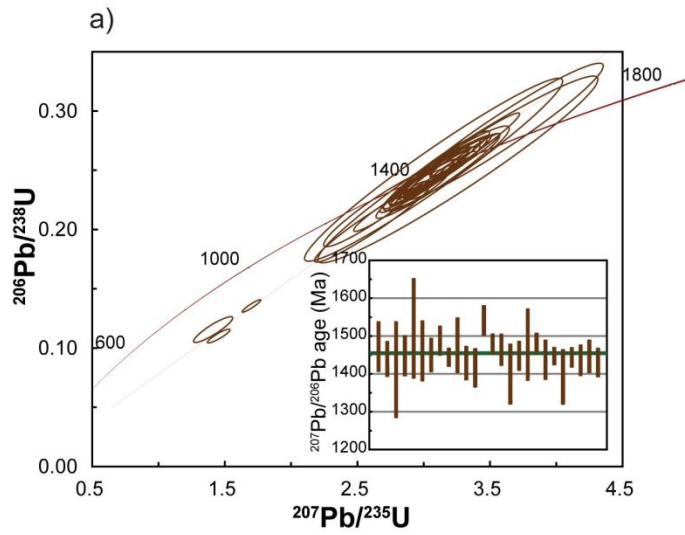


Figure 9.

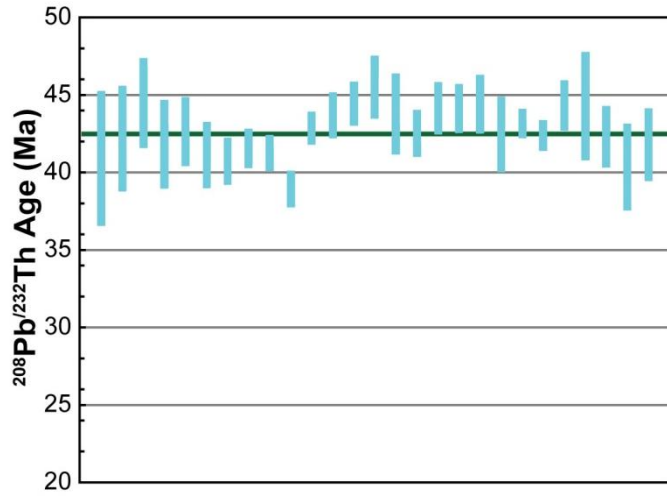


Figure 10.



Figure 11.



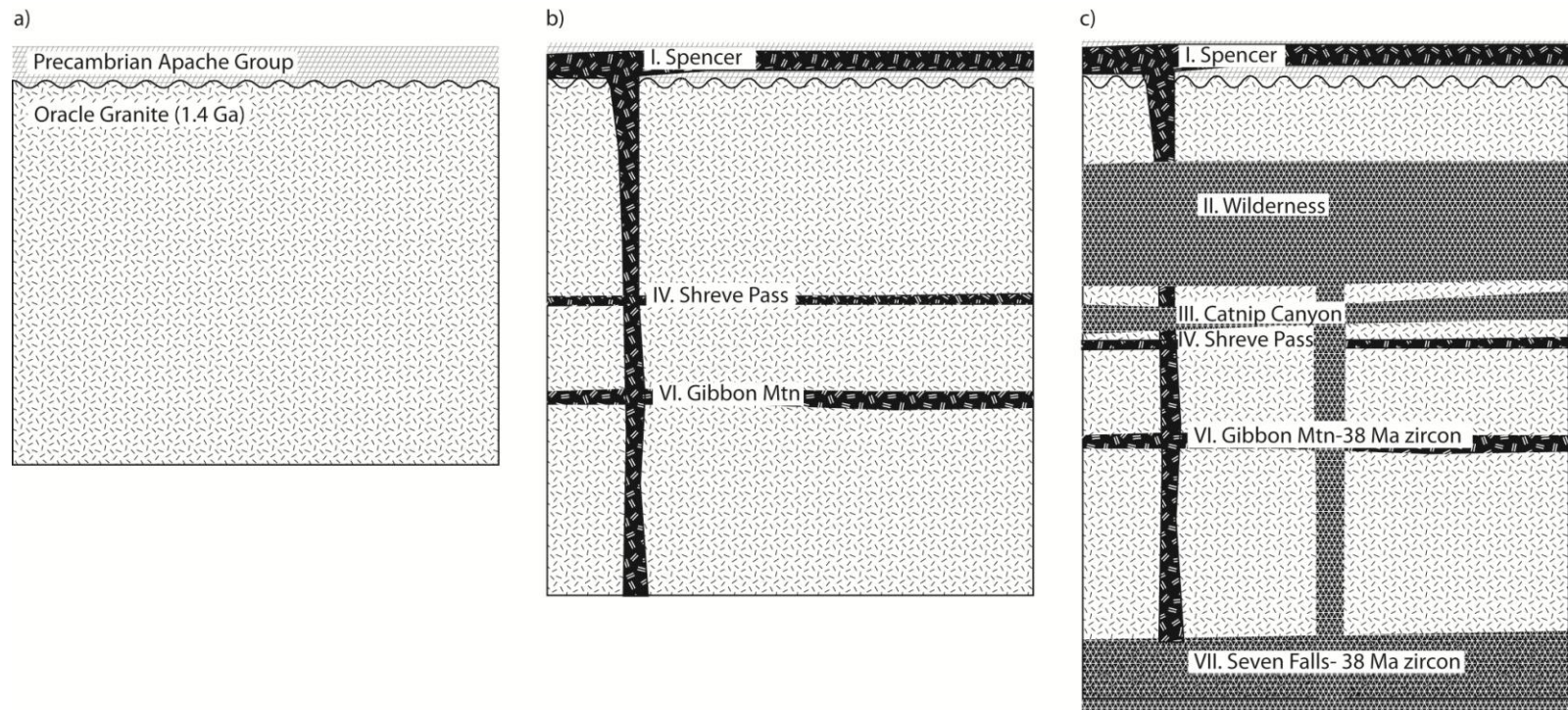


Figure 12.

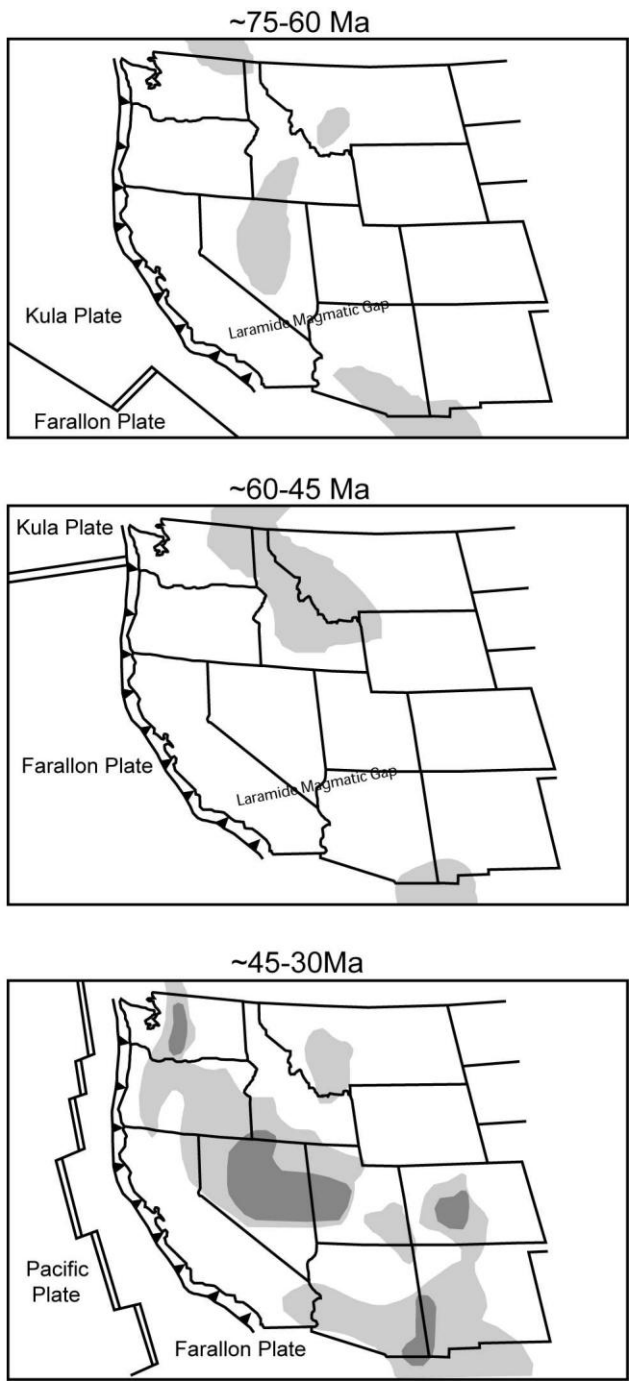


Figure 13.

## **TABLES**

Table 1. Sample description and mineral(s) dated from the Wilderness suite sills.

Table 1.

| <b>Wilderness Suite Sills</b>         | <b>Description (After Force, 1997)</b>                               | <b>Petrographic observations</b>   | <b>Mineral Dated</b> | <b>Mean age* (+/- random and systematic error)</b> | <b>Avg Th/U ratio</b> |
|---------------------------------------|--|--|----------------------|--|-----------------------|
| Spencer (93-4)                        | medium-grained biotite granite, biotite<< muscovite, weakly foliated | Large porphyroclasts of potassium feldspar are observed. Grain size reduction of quartz is observed. Quartz ribbons are present.   | Zircon               | 57 +/- 2   | 0.3                   |
| Wilderness - Windy Point (0705)       | equigranular, mylonitic  | The primary minerals in the Windy Point locality of the Wilderness sill are potassium feldspar, quartz and plagioclase feldspar. The sample is mylonitic. The Windy Point sample contains ductile deformation of mica (mica fish). The quartz has undergone grain size reduction   | Zircon               | 46 +/- 3   | 0.3                   |
| Wilderness - General Hitchcock (0704) | equigranular, mildly deformed, garnet visible in hand sample         | Large grains of quartz, potassium feldspar and plagioclase are observed in this sample. Quartz contains undulose extinction and grain size reduction. Muscovite is present and muscovite grains have undergone brittle deformation.  | Zircon               | 45 +/- 3   | 1.0                   |
| Catnip Canyon (93-1)                  | banded granite   | The primary minerals in the Catnip Canyon sill are potassium feldspar, quartz and plagioclase feldspar. CAT 93-1M, Biotite and muscovite are present. The biotite has iron oxide staining. The plagioclase contains fractures. Recrystallized quartz is common.<br>CAT 93-1F, The thin section is dominated by quartz, which exhibits subgrain migration and bulging. There are regions of extreme grain size reduction. | Monazite             | 43 +/- 2<br>[208Pb/232Th age]                      | _____                 |

Table 1, continued.

|                       |  |   |        |  |                   |
|-----------------------|--|---|--------|--|-------------------|
| Shreve Pass<br>(0703) | medium-grained biotite<br>granite, mildly deformed         | Iron stained biotite has recrystallized<br>forming ribbons that wrap around<br>porphyroclasts. Plagioclase and<br>potassium feldspar is fractured. Quartz<br>has undergone grain size reduction and<br>bulging. | Zircon | 53 +/- 2   | 0.3               |
| Gibbon Mtn<br>(93-8)  | porphyroclastic;<br>biotite<<muscovite,<br>mylonitic       | Recrystallized quartz is observed. Large<br>phyroclasts of plagioclase are present.<br>Iron oxide staining in fractures is visible.<br>Deformation (taper) twins present in<br>plagioclase.                     | Zircon | 55 +/- 2 (< 40 Ma)<br>38 +/- 2 (< 40 Ma)                       | 0.2<br>0.2        |
| Seven Falls<br>(93-9) | equigranular,<br>biotite>>>muscovite,<br>biotite lineation | Deformation twins in potassium feldspar.<br>Myrmekite is observed. Fracturing in<br>quartz, plagioclase, and potassium<br>feldspar is observed. Quartz has<br>undergone grain size reduction and<br>bulging.    | Zircon | 57 +/- 2 (> 40 Ma)<br>46 +/- 2 (> 40 Ma)<br>38 +/- 2 (< 40 Ma) | 0.2<br>0.2<br>0.1 |

\*all samples indicate zircon  $^{206}\text{Pb}/^{238}\text{U}$  age, unless indicated

***<sup>40</sup>Ar/<sup>39</sup>Ar data from the Wilderness sills of the Catalina MCC: reheating vs. monotonic cooling of the footwall***

Jessica J. Terrien

Syracuse University

Department of Earth Sciences

204 Heroy Geology Laboratory

Syracuse, New York 13244, USA

Suzanne L. Baldwin

Syracuse University

Department of Earth Sciences

204 Heroy Geology Laboratory

Syracuse, New York 13244, USA

**ABSTRACT**

The footwall of the Catalina metamorphic core complex (MCC) located in southeastern Arizona within the Basin and Range Province is intruded by three magmatic suites. The magmatic suites represent pre-extensional magmatism and syn-extensional magmatism. New biotite, muscovite and potassium feldspar <sup>40</sup>Ar/<sup>39</sup>Ar data from the Tertiary age Wilderness suite sills that intruded the footwall of the Catalina metamorphic core complex are presented in order to gain insight regarding the thermal history of the Catalina MCC and its relationship to detachment faulting and MCC formation.

Seven samples from the Wilderness sills were analyzed. The majority of the older  $^{40}\text{Ar}/^{39}\text{Ar}$  apparent ages from both feldspar and mica were obtained from the structurally higher sills in the main range, and the younger  $^{40}\text{Ar}/^{39}\text{Ar}$  apparent ages were obtained on samples from structurally lower samples, indicating that the structurally highest sills cooled first followed by sills at structurally lower depths in the forerange. The potassium feldspar samples from the Wilderness suite sills yield  $^{40}\text{Ar}/^{39}\text{Ar}$  age gradients with upper intercepts ranging from ~31 to 28 in the main range and ~28 to 26 Ma in the forerange, and lower intercepts ranging from ~25 to 23 Ma in the main range, and ~23 to 22 Ma in the forerange.

The potassium feldspar age gradients may be the result of cooling within the potassium feldspar partial retention zones for ~ 5 million years, or thermal resetting by the Catalina pluton prior to exhumation along the Catalina detachment fault.  $^{40}\text{Ar}/^{39}\text{Ar}$  lower intercepts from potassium feldspar in the main range suggest that exhumation of the main range occurred ~25 to 23 million years ago. In the forerange, concordant AFT and ZFT data and  $^{40}\text{Ar}/^{39}\text{Ar}$  potassium feldspar lower age intercepts suggest rapid cooling due to exhumation ~23 to 22 million years ago.

Generally, the muscovite and biotite samples from the Wilderness sills in both the main range and forerange yield flat  $^{40}\text{Ar}/^{39}\text{Ar}$  age spectra with  $^{40}\text{Ar}/^{39}\text{Ar}$  apparent ages of ranging from ~28 to 23 Ma representing recrystallization below the closure temperature for muscovite and biotite. Textures indicative of ductile deformation such as fine-grain muscovite and biotite wrapping porphyroclasts are observed.

## INTRODUCTION AND NATURE OF THE PROBLEM

A metamorphic core complex (MCC) consists of a low-angle detachment fault that separates the ductilely deformed crystalline rocks of the footwall, from the brittlely deformed cover rocks of the hanging wall [Coney, 1980b; Davis and Lister, 1988]. Motion along the detachment fault exhumes deep-seated crystalline rocks, including mylonitic rocks [Davis and Lister, 1989]. MCC's are common features of highly extended terranes such as the Aegean, Papua New Guinea, and Basin and Range Province of North America [Coney, 1980a; Forster and Lister, 1999; Hill et al., 1992]. In North America, MCC's are found from southern Canada to Mexico (Figure 1).

The association between magmatism and MCC formation is well established [Armstrong and Ward, 1991]. However, the role of magmatism in MCC formation and evolution is controversial [Lister and Baldwin, 1993; Parsons and Thompson, 1993]. The type of magma generated and the timing of magmatism relative to low-angle normal faulting is variable across extensional regimes [Parsons, 1995]. The modes of intrusion include dikes, plutons, and/or sills, and the composition of the magmas is commonly granitic or mafic, but intermediate and multiple rock types are also reported [Parsons, 1995 and references therein]. This compositional variability makes defining the role of magmatism in MCC evolution difficult and necessitates dating magmatic rocks to establish temporal and spatial relationships. Magmatism in MCC's is attributed to an increased geothermal gradient and weakening of the lithosphere. In the case of the Basin and Range Province, extensional forces accompanied these factors and promoted extension along low-angle detachment faults [Coney, 1980a].



The Catalina MCC is an ideal location to learn more about MCC evolution, particularly its thermal history; the Catalina MCC is easily accessible and the tectonic setting is well characterized [Dickinson, 1991]. This study focuses on the Paleocene-Eocene Wilderness suite that intrudes the Precambrian Oracle Granite and the Leatherwood suite. The Wilderness suite consists of leucocratic muscovite-bearing peraluminous granites that were emplaced as a series of sills. The following questions will be addressed: (1) How does the cooling history of the sills vary? (2) What is the relationship between Catalina MCC formation and the thermal history of the Wilderness sills?

We present  $^{40}\text{Ar}/^{39}\text{Ar}$  data from biotite, muscovite, and potassium feldspar from the Wilderness suite sills that intruded the footwall of the Catalina MCC, and interpret the cooling history of the Catalina MCC using our data and previously reported apatite and zircon fission track data, as well as higher temperature thermochronology data from the footwall of the Catalina MCC. Potassium feldspar  $^{40}\text{Ar}/^{39}\text{Ar}$  data yields information from  $\sim 150^\circ\text{C}$  to  $350^\circ\text{C}$  and the muscovite and biotite  $^{40}\text{Ar}/^{39}\text{Ar}$  data yield thermal information from  $\sim 300^\circ\text{C}$  to  $350^\circ\text{C}$  [Harrison *et al.*, 2009; Lovera *et al.*, 1997; McDougall and Harrison, 1999].  $^{40}\text{Ar}/^{39}\text{Ar}$  data from potassium feldspar generated during laboratory step heat experiments can be modeled to produce a thermal history of the sample.

## **GEOLOGY OF THE CATALINA MCC**

Igneous rocks intruded Precambrian country rocks in the lower plate of the Catalina MCC in southeastern Arizona from the Late Mesozoic to early Cenozoic. The most voluminous intrusive rocks, the peraluminous Wilderness suite sills, which are the

focus of this study, inflated the crust by over 4 kilometers as a result of their intrusion [Force, 1997].

The Catalina MCC is divided into the forerange and the main range. The forerange forms an anticline or arch with a northwest-southeast trending axis located on the southern flank of the Catalina MCC (Figure 2). Mylonites on the southwest side of the forerange arch have a top-to-the-SW sense of shear. The north side of the arch have a primarily top-to-the-NE sense of shear; however, top-to-the-SW indicators are also present [Force, 1997; Spencer, 2005]. The NE sense of shear indicators are interpreted to represent either folding of the mylonitic front or a distinct period of shearing, which could represent re-activation of the Catalina detachment fault. The Catalina detachment fault trends NW-SE and is located along the southwest side of the Catalina MCC.

### ***Previous Data***

Previous thermochronologic and geochronologic studies of the Catalina MCC include K-Ar studies on biotite, muscovite and potassium feldspar from the Wilderness and Leatherwood suites of the Catalina MCC that primarily yielded ages from ~20 to 37 Ma [Damon *et al.*, 1963; Mauger *et al.*, 1968]. Mauger *et al.* [1968] and Damon *et al.* [1963] interpreted these to be “anomalous” mid-Tertiary ages obtained on minerals from Precambrian rocks that were reheated by mid-Tertiary intrusions.

A subsequent compilation and reinterpretation of the K-Ar data concluded that the ages were not “anomalous” and thus the magmatic suites are not Precambrian [Davy *et al.*, 1989b; Keith *et al.*, 1980]. Davy *et al.* [1989] examined the thermal history of the MCC by compiling available U-Pb zircon data, Rb-Sr muscovite data, Rb-Sr biotite data, K-Ar biotite data, K-Ar muscovite data, K-Ar hornblende data, and titanite, apatite and

zircon fission track data, and concluded that the three magmatic suites that intrude the Catalina MCC cooled rapidly after emplacement, and that the region generally cooled rapidly between 35 and 22 Ma from 530°C to 100°C.

U/Pb data from zircon and Th/Pb data from monazite indicate that the Wilderness sills were emplaced during two separate phases of magmatism, the first at ~55 Ma and the second at ~45 Ma. A limited number of analyses from the structurally lowest Gibbon Mountain and Seven Falls sills indicated zircon growth as rims on preexisting zircon grains also occurred < 40 Ma (see Chapter 1).

*Fayon et al.* [2000] used apatite fission track (AFT) and zircon fission track (ZFT) ages, from samples collected along a southwest-northeast trending profile, to determine the lower temperature cooling history parallel to the Catalina detachment fault. This study determined that the low temperature history was not a one-stage cooling history, but was more complicated. A period of rapid cooling from ~20 Ma to 24 Ma is recorded by the concordant ZFT and AFT ages in the forerange and concordant higher temperature thermochronometers [*Davy et al.*, 1989b], and ZFT ages in the main range. This period of rapid cooling was followed by a period of slower cooling, suggested by shortened confined apatite fission track lengths (<14µm). The weighted mean zircon fission track ages decrease in the direction of slip on the detachment fault from ~31 Ma to 20 Ma and the apatite fission track ages increase in the direction of slip; this unusual trend is interpreted by *Fayon et al.* [2000] to indicate that the main range remained at higher temperatures and cooled slowly during the later stages of detachment faulting possibly due to intrusion of the Catalina pluton, which also may have affected the AFT ages. Low-angle detachment faulting did not bring the Catalina MCC to its current topography;

isostatic uplift, associated with post-middle Miocene high-angle Basin and Range faulting, created the regional topographic high observed today [Davis *et al.*, 2004].

## **WILDERNESS SUITE SILLS**

The peraluminous Wilderness suite granites range from mylonitic to slightly deformed. Microstructures observed within the Wilderness suite sills can be used to estimate the temperature reached during deformation. Undulose extinction and bulging recrystallization of quartz occurs at ~300–400°C, subgrain rotation of quartz occurs at ~400–500°C, recrystallization of quartz due to grain-boundary migration occurs at ~500–700°C, and ductile deformation in mica occurs above 250°C [Passchier and Trouw, 2005]. All of the Wilderness suite samples show both brittle and ductile deformation to varying degrees. Examples of these fabrics are shown in photomicrographs in Appendix 1.1. The structures observed in each sill are described below. The most intensely deformed mylonitic rocks formed at depths of 8–10 km [Force, 1997]. A minimum temperature of 300°C is estimated for the temperature of deformation within the Wilderness sills based on the microstructures found within the sills [Passchier and Trouw, 2005].

### *Spencer sill*

The Spencer sill (Figure 3) is the structurally highest sill that consists of two lens that vary in thickness from ~150 meters to 400 meters [Force, 1997]. It is weakly foliated, medium-grained, biotite rich, poor in muscovite, and contains large porphyroclasts of potassium feldspar. Quartz has undergone grain-size reduction by subgrain rotation. Quartz ribbons are present, but are rare, and show undulose extinction

and evidence of grain boundary migration within the ribbon. Temperatures of deformation based on observed microstructures are estimated at  $\sim 500^{\circ}\text{C}$ – $700^{\circ}\text{C}$ .

#### *Wilderness sill*

The Wilderness sill is over 2000 meters thick [Force, 1997] and exhibits variable deformation throughout. Peraluminous granite from the General Hitchcock locality is slightly deformed whereas at the Windy Point location it is mylonitic. The Wilderness sill, in both localities, contains abundant muscovite and garnet. At the General Hitchcock locality, the sill contains brittlely deformed mica grains, whereas at the Windy Point locality, the sill contains ductilely deformed mica grains. In samples from both locations petrographic observations indicate quartz has undergone subgrain rotation and the Windy point locality also exhibits bulging recrystallization of quartz. Temperatures of deformation based on observed microstructures are estimated at  $\sim 300$  to  $400^{\circ}\text{C}$ .

#### *Catnip Canyon sill*

The Catnip Canyon sill is about 300 meters thick and is subdivided into felsic portions and mafic portions [Force, 1997]. The mafic portion contains abundant biotite, stained with iron oxide, brittlely deformed plagioclase feldspar and potassium feldspar, and recrystallized quartz. The felsic portion is biotite-poor, but contains muscovite. The felsic portion also contains abundant quartz which exhibits subgrain rotation, bulging, and regions of extreme grain-size reduction. Temperatures of deformation based on observed microstructures are estimated at  $\sim 300$  to  $400^{\circ}\text{C}$ .

#### *Shreve Pass sill*

The Shreve Pass sill is about 60 meters thick and intrudes Oracle Granite [Force, 1997]. The Romero Pass fault (see Figure 3) has offset the Shreve Pass sill from the

Gibbon Mountain and Seven Falls sills (described below); these sills were intruded during the first phase of magmatism and faulting is post-intrusion. The Shreve Pass sill contains iron-stained biotite, is recrystallized to form ribbons that wrap around porphyroclasts of potassium feldspar and plagioclase feldspar, and contains little to no muscovite. Fracturing of plagioclase feldspar and potassium feldspar is common. The quartz shows evidence of subgrain rotation and bulging recrystallization. Temperatures of deformation based on observed microstructures are estimated at ~300 to 400°C.

#### *Gibbon Mountain sill*

The ~240 meter thick Gibbon Mountain sill intrudes both Oracle Granite and Leatherwood granodiorite [Force, 1997]. Force [1997] suggested its emplacement followed an old Leatherwood sill because Leatherwood granodiorite is found above and below the Gibbon Mountain sill. Biotite is more abundant than muscovite, and large porphyroclasts of plagioclase feldspar with deformation (taper) twins are present; subgrain rotation in quartz is observed and mantles plagioclase feldspar grains. Temperatures of deformation based on observed microstructures are estimated at ~300 to 400°C.

#### *Seven Falls sill*

The Seven Falls granite sill intrudes the Oracle Granite. Approximately 150 meters of the Seven Falls sill is exposed; however, the base of the Seven Falls sill is not exposed and thus its thickness is not known [Force, 1997]. Biotite is abundant and defines a lineation. The sample studied displays deformation twins in potassium feldspar and myrmekite. Fractures are common in quartz, plagioclase, and potassium feldspar.

The quartz has undergone subgrain rotation and bulging recrystallization. Temperatures of deformation based on observed microstructures are estimated at ~300 to 400°C.

#### **<sup>40</sup>Ar/<sup>39</sup>Ar METHOD**

Standard methods for mineral separation, sample preparation, and irradiation were used. Samples were wrapped individually in Cu foil, along with biotite standard GA1550 [97.9 Ma, *McDougall and Harrison*, 1999], Alder Creek sanidine standard [*Turrin et al.*, 1994], and salts used to monitor the neutron dose of three separate irradiation, referred to as Irradiation I, II and III. Prior to analysis, samples were vacuum-sealed in super silica quartz tubes and irradiated 0.5 (I and III) or 10 (II) hours in the Cadmium-Lined In-Core Irradiation Tube (CLICIT) of the 1 MW TRIGA type reactor at the Oregon State University Radiation Center.

Argon analyses were performed in the Syracuse University Noble Gas Isotopic Research Laboratory. Extraction of gas from flux monitors and salts was accomplished using a Synrad 48-2 CO<sub>2</sub> laser, tunable from 0 to 25 W. Step-heat experiments were performed on samples using a double-vacuum resistance furnace with a thermocouple in contact with the crucible to monitor the temperature. Two SAES getters were used for purification of the extracted gas. Pumping was through either a turbomolecular pump or a Varian ion pump. Isotopic analyses were performed using a Micromass 5400 mass spectrometer with an ion-counting electron multiplier. Machine mass discrimination and sensitivity were determined from repeated analysis of atmospheric argon. Data reduction was completed on a computer using in-house programs. Samples were corrected for blanks, neutron-induced interfering isotopes, decay of <sup>37</sup>Ar and <sup>39</sup>Ar, mass discrimination, and atmospheric argon. Correction factors used to account for interfering nuclear

reactions were determined by analyzing argon extracted from irradiated CaF<sub>2</sub> and K glass and are: (<sup>36</sup>Ar/<sup>37</sup>Ar)<sub>Ca</sub> = 2.71447E-04 (I), 2.62232E-04, (II) 2.78410E-04 (III)

(<sup>39</sup>Ar/<sup>37</sup>Ar)<sub>Ca</sub> = 7.30406E-04 (I), 7.11194E-04, (II) 7.12865E-04 (III)

(<sup>40</sup>Ar/<sup>39</sup>Ar)<sub>K</sub> = 1.99720E-02 (I), 2.12809E-02, (II) 2.23237E-02 (III)

All ages are calculated using the decay constants recommended by Steiger and Jager [1977]. Stated precisions for <sup>40</sup>Ar/<sup>39</sup>Ar ages include all uncertainties in the measurement of isotope ratios and are quoted at the 1σ level.

There are several advantages of the <sup>40</sup>Ar/<sup>39</sup>Ar method over the K-Ar method, including: the daughter and parent can be determined in a single smaller aliquot of sample, measuring absolute abundances is not necessary, and the <sup>40</sup>Ar/<sup>39</sup>Ar yields additional information when the incremental heating method is used [McDougall and Harrison, 1999]. Step-heating or incremental-heating is a method of heating the sample in small increasing temperature increments rather than total fusion in which the sample is heated and the gas is released in one step [Merrihue and Turner, 1966]. The ratio of <sup>40</sup>Ar\*/<sup>39</sup>Ar<sub>K</sub> is measured for each step and yields an apparent age. The <sup>40</sup>Ar/<sup>39</sup>Ar method yields information regarding the cooling rate of the mineral sample as well as whether a sample has been partially or completely reset [McDougall and Harrison, 1999].

## RESULTS

### *<sup>40</sup>Ar/<sup>39</sup>Ar data*

The <sup>40</sup>Ar/<sup>39</sup>Ar age spectra and inverse isochron plots were generated using Isoplot 3.00 software [Ludwig, 2003] and are shown in Figures 4–10. The first order observations of the data (Table 1) are: (1) The majority of the <sup>40</sup>Ar/<sup>39</sup>Ar age spectra of potassium feldspar from the Wilderness sills show variable apparent age gradients, (2)



the  $^{40}\text{Ar}/^{39}\text{Ar}$  age spectra for the mica samples, with the exception of the Spencer Lens sample, are relatively flat with apparent ages between ~28 and 23 Ma, (3) the oldest muscovite and biotite apparent ages were obtained from the structurally higher samples, and (4) inverse isochron plots indicate that several of the samples contain excess argon.

#### *Excess Argon*

Excess argon is defined as  $^{40}\text{Ar}$  that is not atmospheric, or  $^{40}\text{Ar}$  that has been incorporated into a sample by processes other than radioactive decay [McDougall and Harrison, 1999]. The blanks corrected  $^{40}\text{Ar}/^{36}\text{Ar}$  ratio is used when discussing or comparing atmospheric argon and excess argon. Several Wilderness suite samples have a  $^{40}\text{Ar}/^{36}\text{Ar}$  ratio greater than  $298.56 + 0.31$  [Lee et al., 2006], the present atmospheric ratio of  $^{40}\text{Ar}/^{36}\text{Ar}$  and thus excess argon is present [Kelley, 2002]. As a default the ratio 298.56 is used to correct for atmospheric argon prior to calculation of the  $^{40}\text{Ar}/^{39}\text{Ar}$  apparent ages for each step in a step heat experiment. However when excess argon is present erroneously old  $^{40}\text{Ar}/^{39}\text{Ar}$  apparent ages are calculated because the additional  $^{40}\text{Ar}$  is assumed to be radiogenic.

For each sample that contained excess argon it was possible to recalculate the  $^{40}\text{Ar}/^{39}\text{Ar}$  apparent ages, using the  $^{40}\text{Ar}/^{36}\text{Ar}$  ratio determined by the intercept on an inverse isochron plot. Recalculating the  $^{40}\text{Ar}/^{39}\text{Ar}$  apparent ages for the main range and forerange samples that contain excess argon decreases the apparent ages by ~1-3 million years and the apparent ages are within error of the ages obtained from the other main range samples or forerange respectively. The excess argon present in the Wilderness suite samples is interpreted to have been contributed from heating of the Precambrian age Oracle Granite as the Wilderness sills intruded.

### *Spencer sill*

The Spencer sill muscovite sample yielded the oldest  $^{40}\text{Ar}/^{39}\text{Ar}$  ages from the Wilderness suite sills (Figure 4). The  $^{40}\text{Ar}/^{39}\text{Ar}$  muscovite data yielded an age gradient from ~40 Ma to ~30 Ma, unlike the other Wilderness sill mica samples which yielded flat age spectra. The  $^{40}\text{Ar}/^{39}\text{Ar}$  potassium feldspar data yielded an age gradient ranging from ~23 to ~29 Ma, which is comparable in age to the muscovite and biotite data obtained from other samples within the main range and the forerange. The Spencer sill has a  $^{206}\text{Pb}/^{238}\text{U}$  zircon age of  $57 \pm 2$  Ma (Chapter 1).

### *Windy Point Locality*

The potassium feldspar sample from the Windy Point (Figure 5) locality of the Wilderness sill yields a slight age gradient from ~31 Ma to ~24 Ma.  $^{40}\text{Ar}/^{39}\text{Ar}$  muscovite data from the Windy Point locality within the Wilderness sill has a plateau age  $26.3 \pm 3$  Ma (includes 94.4% of  $^{39}\text{Ar}$ ). The Windy Point locality has a  $^{206}\text{Pb}/^{238}\text{U}$  zircon age of  $46 \pm 3$  (Chapter 1).

### *General Hitchcock Locality*

The potassium feldspar sample from the General Hitchcock locality (Figure 6) of the Wilderness sill yields a  $^{40}\text{Ar}/^{39}\text{Ar}$  age gradient from ~25 Ma to 28 Ma.  $^{40}\text{Ar}/^{39}\text{Ar}$  muscovite data from the General Hitchcock locality within the Wilderness sill ranged from ~28 to 26 Ma. It was not possible to fit a plateau to the General Hitchcock data. The General Hitchcock locality has a  $^{206}\text{Pb}/^{238}\text{U}$  zircon age of  $45 \pm 3$  Ma (Chapter 1).

### *Catnip Canyon*

The potassium feldspar sample from the Catnip Canyon sill yielded an age gradient from ~26 Ma to ~28 Ma, and the inverse isochron plot indicates the sample

contains excess argon. The  $^{40}\text{Ar}/^{36}\text{Ar}$  ratio is  $417 \pm 96$  and the MSWD = 6 (Figure 7). The biotite sample from the Catnip Canyon sill has a relatively flat age spectrum with apparent ages ranging from ~25 to 26 Ma, which is within error of the low temperature portion of the potassium feldspar step heat experiment (Figure 7). The Catnip Canyon sill has a monazite  $^{208}\text{Pb}/^{232}\text{Th}$  age of  $43 \pm 2$  Ma (Chapter 1).

#### *Shreve Pass*

The Shreve Pass samples of potassium feldspar and biotite yielded overlapping  $^{40}\text{Ar}/^{39}\text{Ar}$  spectra (Figure 8). The potassium feldspar yielded a slight age gradient from ~23 Ma to ~28 Ma. The biotite sample from the Shreve Pass sill has a relatively flat spectrum with apparent ages that range from ~23 to 24 Ma. The Shreve Pass sill has a  $^{206}\text{Pb}/^{238}\text{U}$  zircon age of  $53 \pm 2$  Ma (Chapter 1).

#### *Gibbon Mountain*

The potassium feldspar sample from the Gibbon Mountain sill yielded an age gradient from ~23 Ma to ~26 Ma and the inverse isochron plot indicates the sample contains excess argon. The  $^{40}\text{Ar}/^{36}\text{Ar}$  ratio is  $366 \pm 14$  and the MSWD = 3.2 (Figure 9). The muscovite sample from the Gibbon Mountain sill has a plateau age of  $24 \pm 0.3$  Ma (includes 94.4% of the  $^{39}\text{Ar}$ ). The  $^{206}\text{Pb}/^{238}\text{U}$  zircon data from the Gibbon Mountain sill indicates two populations of zircon ages; the oldest is  $54 \pm 1$  Ma and the youngest is  $38 \pm 1$  Ma (Chapter 1).

#### *Seven Falls*

The potassium feldspar from the Seven Falls sill locality yielded a slight age gradient from ~22 Ma to ~28 Ma. The biotite sample from the Seven Falls sills yielded apparent ages that range from ~ 23 to 24 Ma (Figure 10). The  $^{206}\text{Pb}/^{238}\text{U}$  zircon data from

the Seven Falls sill indicates three populations of zircon ages at:  $57 \pm 1$  Ma,  $46 \pm 1$  Ma, and  $38 \pm 1$  Ma (Chapter 1).

### ***MDD Modeling***

$^{40}\text{Ar}/^{39}\text{Ar}$  data for potassium feldspar samples from the Wilderness suite sills were modeled using multi-diffusion domain (MDD) models to constrain the thermal history between  $150^\circ\text{C}$  and  $350^\circ\text{C}$  [Lovera *et al.*, 1989; Lovera, 1992, Lovera *et al.*, 2002; <http://sims.ess.ucla.edu/argon.htm>; Figures 11-17]. Both monotonic models, models that do not allow reheating, and free models, models that allow reheating were run. For the Spencer, Wilderness (Windy Point), and Shreve Pass sills the monotonic and free spectra were very similar and both fit the experimental spectrum. Visually, the free spectra were a better fit for the Catnip Canyon, Gibbon Mountain and Seven Falls experimental data and the monotonic spectrum was a better fit for the Wilderness (General Hitchcock) experimental data.

## **DISCUSSION**

### ***$^{40}\text{Ar}/^{39}\text{Ar}$ potassium feldspar data and the timing of exhumation***

The potassium feldspar  $^{40}\text{Ar}/^{39}\text{Ar}$  data from the Wilderness suite sills yielded age gradients that can be interpreted as the result of slow cooling, or resetting due to a thermal event. During slow cooling, the rock passes through the argon partial retention zone slowly [Baldwin and Lister, 1998], and therefore  $^{40}\text{Ar}^*$  diffusion of the least retentive sites, or sites closer to the crystal boundary, continue to diffuse, resulting in a  $^{40}\text{Ar}/^{39}\text{Ar}$  age gradient. In the case of a thermal event that partially resets feldspar, heat allows diffusion of argon from the least retentive sites. Either scenario may be possible with regards to the Wilderness sills potassium feldspar samples.

Generally, the older  $^{40}\text{Ar}/^{39}\text{Ar}$  apparent ages are found within the main range and the younger ages are found within the forerange, although there is considerable overlap in ages from the forerange and the main range. In the main range all of the potassium feldspar samples yielded  $^{40}\text{Ar}/^{39}\text{Ar}$  age gradients. The upper intercept from potassium feldspar from the main range samples range from ~31 to 28 Ma and the lower intercept of the potassium feldspar samples range from ~25 to 23 Ma. In the forerange the potassium feldspar also yielded  $^{40}\text{Ar}/^{39}\text{Ar}$  age gradients with oldest ages ranging from ~28 to 26 Ma and youngest apparent ages ranging from ~23 to 22 Ma. In both scenarios the older ages for each sample are interpreted to reflect initial cooling after crystallization. However, the younger apparent ages are the result of slow cooling or partial reheating by a thermal event. In the first scenario the potassium feldspars from both the main range and the forerange cooled for approximately 5 million years until extension along the Catalina detachment fault exhumed the samples toward the surface and the samples cooled below 150°C between ~25 and 23 Ma. This scenario is supported by a detailed study of the Catnip Canyon sill where  $^{40}\text{Ar}/^{39}\text{Ar}$  data from potassium feldspar, biotite, muscovite and (U-Th)/He from monazite were analyzed [Peterman *et al.*, 2011]. The results indicated rapid cooling from ~450°C to 150°C from ~27 to 23 Ma with no evidence of reheating [Peterman *et al.*, 2011].

In the second scenario the potassium feldspars were reheated following the intrusion of the Catalina pluton, which has a U/Pb age of ~26 Ma [Fornash *et al.*, in prep] and then exhumed toward the surface between ~25 and 23 Ma. The main range was exhumed to the surface first and thus several of the main range potassium feldspars cooled below 150°C before the forerange potassium feldspars. Many of the apparent ages

from the lower intercept of the age gradients in both the forerange and main range are within error of each other, and are interpreted to indicate the samples were exhumed very quickly.

As mentioned, MDD modeling of potassium feldspars was performed using the free model, which allows reheating in the thermal history, and also the monotonic model [Lovera *et al.*, 1989; Lovera, 1992, Lovera *et al.*, 2002; <http://sims.ess.ucla.edu/argon.htm>]. In general, both types of models resulted in a reasonable fit to the experimental spectra. The age gradients observed within the majority of the potassium feldspar leaves only a few million years for reheating or slow cooling to occur. Heat from the Catalina pluton may have been responsible for keeping the temperature elevated above 150°C or resetting the potassium feldspar  $^{40}\text{Ar}/^{39}\text{Ar}$  age spectra, which is indicated in the free MDD models. A simple cooling model for a 10 km wide pluton emplaced at 700°C, after Ehlers [2005; Figure 19], illustrates that after one million years ~ 10 km from the center of the intrusion the country rock would be at ~200°C. Detailed thermal modeling, beyond the scope of this research, is needed to fully assess the possible role of heat from the Catalina pluton. It is also possible that detachment faulting led to upwarping of the isotherms and thus an increased geothermal gradient which kept the temperature within the partial retention zone of potassium feldspar [Ketchum, 1996].

#### **$^{40}\text{Ar}/^{39}\text{Ar}$ Muscovite and Biotite data**

The Spencer sill  $^{40}\text{Ar}/^{39}\text{Ar}$  muscovite data yielded the oldest mica ages and an age gradient from ~ 40 to 30 Ma. This sample is interpreted to represent cooling of muscovite following crystallization from the magma. However, the muscovite and

biotite data from the main range, excluding the Spencer Lens sill, yield flat  $^{40}\text{Ar}/^{39}\text{Ar}$  apparent age spectra between ~27 and 25 Ma. In the forerange, the Seven Falls biotite sample yielded ages from ~24 to 23 Ma and the Gibbon Mountain muscovite sample yielded a plateau age of  $24 \pm 0.3$  Ma. In several samples the muscovite and biotite ages correspond to the youngest ages obtained for the potassium feldspars for the same sample. Muscovite and biotite are interpreted to have undergone recrystallization below the partial retention zone for biotite and muscovite, but above the closure temperature for potassium feldspar. The temperature remained less than ~300°C but above 150°C during recrystallization.

#### *$^{40}\text{Ar} / ^{39}\text{Ar}$ and deformation of the Wilderness sills*

As previously discussed, the Wilderness sills vary from slightly deformed to mylonitic. The Windy Point samples were taken from a mylonitic zone in the main range, and the General Hitchcock samples from a slightly deformed region in the main range; these samples yielded similar muscovite  $^{40}\text{Ar}/^{39}\text{Ar}$  apparent ages of ~26 Ma and 27 Ma, and concordant potassium feldspar apparent ages.

Deformation of muscovite and biotite in shear zones at amphibolite to greenschist facies and deformation of muscovite at 600–650°C in laboratory experiments lead to argon loss due to the creation of defects or diffusion “pathways” which allow for argon transport [Bourgeix *et al.*, 2006; Mulch *et al.*, 2002]. If the deformation of the Windy Point samples had occurred after the muscovite was closed to argon diffusion, it would be expected that the Windy Point muscovite  $^{40}\text{Ar}/^{39}\text{Ar}$  apparent ages would be younger than the General Hitchcock sample. In the case of the Windy Point and General Hitchcock the ages are interpreted to reflect the timing of recrystallization between ~150°C and ~300°C.

This explains why the General Hitchcock and Windy Point samples have similar  $^{40}\text{Ar}/^{39}\text{Ar}$  ages. The proximity to the shear zone controlled the degree of deformation; the Windy Point locality was closer to the detachment fault and the shear zone.

### ***Fission track data***

The  $^{40}\text{Ar}/^{39}\text{Ar}$  data combined with ZFT and AFT data yield thermal information from ~350 to 60°C. The fission track study by Fayon et al. [2000] indicated that the main range and the forerange had different low temperature thermal histories. In the main range the AFT ages range from  $20.5 \pm 2.6$  to  $14.6 \pm 2.4$  Ma with a weighted mean  $17.8 \pm 0.4$  Ma and the ZFT ages ranged from  $24.5 \pm 3.8$  to  $31.0 \pm 3.8$  Ma with a weighted mean of  $28.7 \pm 2.0$  Ma. The ZFT closure temperature used in Fayon et al. [2000] was ~260°C and the AFT closure temperature was 60°C. It is worth noting that the ZFT closure temperature has been calculated to be 210–240°C for field studies and as high as 360°C for laboratory studies [Bernet et al., 2002]. Interestingly, the weighted mean ZFT age is within error of many older  $^{40}\text{Ar}/^{39}\text{Ar}$  ages observed in the upper intercepts of the age gradients observed in potassium feldspar. This is interpreted to mean the temperature rapidly decreased below the ZFT closure temperature as well as the upper extent of the potassium feldspar closure temperature window. Several of the ZFT ages are older than the muscovite and biotite  $^{40}\text{Ar}/^{39}\text{Ar}$  apparent ages, which are interpreted to be the result of recrystallization of muscovite and biotite below the closure temperature of ZFT.

Samples from the forerange yielded AFT ages that range from  $21.4 \pm 4.4$  to  $18.8 \pm 3.6$  Ma with a weighted mean average of  $20.1 \pm 1.0$  Ma, and ZFT ages that range from  $26.2 \pm 4.1$  to  $20.4 \pm 3.8$  Ma with a weighted mean average of  $23.6 \pm 3.9$  Ma which is within error of the apparent ages that define the lower intercept of the potassium feldspar



$^{40}\text{Ar}/^{39}\text{Ar}$  age gradients within the forerange [Fayon *et al.*, 2000]. Concordant  $^{40}\text{Ar}/^{39}\text{Ar}$  data, AFT, and ZFT data from the forerange indicate rapid cooling which was also suggested by Fayon *et al.* [2000]. In the main range, however, the period of rapid cooling was followed by slower cooling as indicated by the AFT data ( $\sim 60^\circ\text{C}$  to  $100^\circ\text{C}$ ) and described by Fayon *et al.*, [2000] to possibly be related to heat from the Catalina pluton.

## CONCLUSIONS

The Wilderness suite sills represent extensive pre-extensional magmatism in the Catalina MCC. Potassium feldspar  $^{40}\text{Ar}/^{39}\text{Ar}$  age gradients from the Wilderness suite sills are the result of cooling for  $\sim 5$  million years or partial resetting due to heat provided by the emplacement the Catalina pluton prior to exhumation along the Catalina detachment fault. Potassium feldspar  $^{40}\text{Ar}/^{39}\text{Ar}$  data from the main range and forerange indicate exhumation occurred between  $\sim 25$  and 22 million years ago, as indicated by the lower intercept ages. AFT data (weighted average of  $20.1 \pm 1.0$  Ma) and ZFT data (mean average of  $23.6 \pm 3.9$ ) are within error of the lower intercept of potassium feldspar  $^{40}\text{Ar}/^{39}\text{Ar}$  age gradients in the forerange, which indicates rapid cooling below  $60^\circ\text{C}$ .

Muscovite and biotite data from the Wilderness sills yielded flat age spectra with ages ranging from  $\sim 28$  to 23 Ma and are interpreted to represent recrystallization below their closure temperature. Ductilely deformed micas and fine-grained muscovite and biotite wrapping prophyroclasts are observed in thin section.

## REFERENCES

Armstrong, R. L., and P. Ward (1991), Evolving Geographic Patterns of Cenozoic Magmatism in the North American Cordillera: The Temporal and Spatial Association of Magmatism and Metamorphic Core Complexes, *Journal of Geophysical Research*, 96(B8), 13201-13224.

Bernet, M., et al. (2002), Determining the Zircon Fission-track Closure Temperature, *Geological Society of America Cordilleran Section Meeting*.

Bourgeix, A. L., et al. (2006), Argon loss in experimentally deformed muscovites, paper presented at Goldschmidt Conference Abstracts.

Coney, P. J. (1980a), Cordilleran metamorphic core complexes: An overview, in *Cordilleran Metamorphic Core Complexes*, edited by J. Crittenden, M.D., et al., pp. 7-34, Geological Society of America.

Coney, P. J. (1980b), Cordilleran metamorphic core complexes: An overview, in *Cordilleran Metamorphic Core Complexes*, edited by M. D. Crittenden Jr., et al., pp. 7-34, The Geological Society of America, Inc. Memoir 153.

Damon, P. E., et al. (1963), K-Ar dating of Basin and Range uplift, Catalina Mountains, Arizona, *Nuclear Geophysics, National Academy of Sciences/National Research Council Publication, 1075*, 113-121.

Davis, G. A., and G. S. Lister (1988), Detachment faulting in continental extension: Perspectives from the southwestern U.S. Cordillera, in *Processes in continental lithospheric deformation*, edited by S. P. Clark Jr., pp. 133-159.

Davis, G. A., et al. (2004), Fault and fault-rock characteristics associated with Cenozoic extension and core-complex evolution in the Catalina-Rincon region, southeastern Arizona, *GSA Bulletin*, 116(1/2), 128-141.

Davy, P., et al. (1989), Thermal constraints on the tectonic evolution of a metamorphic core complex (Santa Catalina Mountains, Arizona), *Earth and Planetary Science Letters*, 94, 425-440.

Dickinson, W. R. (1991), *Tectonic setting of faulted Tertiary strata associated with the Catalina core complex in southern Arizona*, 106 pp.

Ehlers, T. A. (2005), Crustal thermal processes and the interpretation of thermochronometer data, in *Low-Temperature Thermochronology: Techniques, Interpretations, and Applications*, edited by P. W. Reiners and T. A. Ehlers, pp. 315-349, Mineralogical Society of America and Geochemical Society.

Fayon, A. K., et al. (2000), Fission track analysis of the footwall of the Catalina detachment fault, Arizona: Tectonic denudation, magmatism and erosion, *Journal of Geophysical Research*, 105(B5), 11047-11062.

Force, E. R. (1997), Geology and Mineral Resources of the Santa Catalina Mountains, Southeastern Arizona, *Monographs in Mineral Resource Science No. 1*, 135.

Forster, M. A., and G. S. Lister (Eds.) (1999), *Detachment faults in the Aegean core complex of Ios, Cyclades, Greece*, Geological Society, London, Special Publications, London.

- Harrison, T. M., et al. (2009), Diffusion of  $^{40}\text{Ar}$  in muscovite, *Geochimica et Cosmochimica Acta*, 73, 1039-1051.
- Hill, E. J., et al. (1992), Unroofing of active metamorphic core complexes in the D'Entrecasteaux Islands, Papua New Guinea, *Geology*, 20(10), 907-910.
- Keith, S. B., et al. (1980), Evidence for multiple intrusion and deformation within the Santa Catalina-Rincon-Tortolita crystalline complex, southeastern Arizona, in *Cordilleran Metamorphic Core Complexes*, edited by M. D. Crittenden Jr., et al., pp. 217-268, The Geological Society of America, Inc. Memoir 153.
- Kelley, S. (2002), Excess argon in K-Ar and Ar-Ar geochronology, *Chemical Geology*, 188, 1-22.
- Lister, G. S., and S. L. Baldwin (1993), Plutonism and the origin of metamorphic core complexes, *Geology*, 21, 607-610.
- Lovera, O. M., et al. (1997), Systematic analysis of K-feldspar  $^{40}\text{Ar}/^{39}\text{Ar}$  step heating results: I. Significance of activation energy determinations, *Geochimica et Cosmochimica Acta*, 61(15), 3171-3192.
- Ludwig, K. R. (2003), Users Manual for Isoplot/Ex version 3.0, A Geochronological Toolkit for Microsoft Excel, *Berkeley Geochronology Special Publication No. 4*, 1-70.
- Mauger, R. L., et al. (1968), Cenozoic Argon Ages on Metamorphic Rocks From the Basin and Range Province, *American Journal of Science*, 266, 579-589.

McDougall, I., and T. M. Harrison (1999), *Geochronology and Thermochronology by the  $^{40}\text{Ar}/^{39}\text{Ar}$  Method*, Second ed., 269 pp., Oxford University Press, New York.

Mulch, A., et al. (2002), In-situ UV-laser  $^{40}\text{Ar}/^{39}\text{Ar}$  geochronology of a micaceous mylonite: an example of defect enhanced argon loss, *Contributions to Mineralogy and Petrology*, 142, 738-752.

Parsons, T., and G. A. Thompson (1993), Does magmatism influence low-angle normal faulting?, *Geology*, 21, 247-250.

Parsons, T. (1995), The Basin and Range Province, in *Continental rifts: evolution, structure, tectonics.*, edited by K. H. Olsen, pp. 277-324, Elsevier, Amsterdam.

Passchier, C. W., and R. A. J. Trouw (2005), *Microtectonics*, 2nd ed., Springer, New York.

Peterman, E. M., et al. (2011), Development and Intercalibration of Monazite (U-Th)/He Thermochronology: Catnip Sill, Catalina Core Complex, in *Geological Society of America Annual Meeting*, edited, p. 331, Minneapolis.

Spencer, J. E. (2005), Intersecting Mylonitic Shear Zones in the Footwall of the Catalina Detachment Fault, Santa Catalina Mountains, Southeastern Arizona, paper presented at Eos Trans.AGU, (86(52) Fall Meet. Suppl., Abstract T24C-03.

Steiger, R. H., and E. Jager (1977), Subcommision on geochronology: Convention on the use of decay constants in geo- and cosmochronology, *Earth and Planetary Science Letters*, 36, 359-362.

Turrin, B. D., et al. (1994),  $^{40}\text{Ar}/^{39}\text{Ar}$  ages from the rhyolite of Alder Creek, California:  
Age of the Cobb Mountain Normal-Polarity SUBchron revisited, *Geology*, 22(3), 251-  
254.

## FIGURES

Figure 1. Location of metamorphic core complexes across western North America. Gray line indicates the approximate boundary of the Basin and Range Province [After, *Dickinson, 1991*].

Figure 2. a) Simplified geologic map of the Catalina MCC, Arizona. b) Geologic map of the forerange of the Catalina MCC, Arizona showing detailed mapping of the Wilderness suite sills [from *Fornash et al.*, in prep.,]. Mapping based on [*Bykerk-Kauffman, 2008; Dickinson, 1999; Force, 1997; Spencer et al., 2000; Spencer and Pearthree, 2004*]. Sampling locations are indicated.

Figure 3. Cross-section from A-A' as shown in Figure 2a indicating the structural positions of the seven Wilderness sills. The cross-sectional relationships are diagrammatic. Thicknesses are not to scale. [After *Force, 1997*].

Figure 4.  $^{40}\text{Ar}/^{39}\text{Ar}$  spectra and inverse isochron plots for potassium feldspar and muscovite from Spencer sill of the Wilderness suite sills. The unfilled (outlined) ellipses on the inverse isochron plots indicate data that was not included in the regression.

Figure 5.  $^{40}\text{Ar}/^{39}\text{Ar}$  spectra and inverse isochron plots for potassium feldspar and muscovite from the Wilderness sill (Windy Point locality) of the Wilderness suite sills.

Figure 6.  $^{40}\text{Ar}/^{39}\text{Ar}$  spectra and inverse isochron plots for potassium feldspar and muscovite from the Wilderness sill (General Hitchcock locality) of the Wilderness suite sills. The muscovite sample was analyzed at the University of Arizona and provided by Baldwin (unpublished data).

Figure 7.  $^{40}\text{Ar}/^{39}\text{Ar}$  spectra and inverse isochron plots for potassium feldspar and biotite from Catnip Canyon sill of the Wilderness suite sills. The unfilled (outlined) ellipses on the inverse isochron plots indicate data that was not included in the regression.

Figure 8.  $^{40}\text{Ar}/^{39}\text{Ar}$  spectra and inverse isochron plots for potassium feldspar and biotite from Shreve Pass sill of the Wilderness suite sills. The unfilled (outlined) ellipses on the inverse isochron plots indicate data that was not included in the regression.

Figure 9.  $^{40}\text{Ar}/^{39}\text{Ar}$  spectra and inverse isochron plots from potassium feldspar and muscovite from the Gibbon Mountain sill of the Wilderness suite sills. The unfilled (outlined) ellipses on the inverse isochron plots indicate data that was not included in the regression.

Figure 10.  $^{40}\text{Ar}/^{39}\text{Ar}$  spectra and inverse isochron plots for potassium feldspar and biotite from the Seven Falls sill of the Wilderness suite sills.

Figure 11-17. a) Experimental, Free (black) and Monotonic (brown) modeled age spectra for the potassium feldspar samples from the Wilderness suite sills. b) Potassium feldspar



MDD free (solid) and monotonic (outlined) thermal models for the Wilderness suite sill samples. The colored histories represent 90% confidence interval of the median and the envelope (black line) surrounding the history represent 90% confidence of the solutions [Lovera *et al.*, 1989; Lovera, 1992, Lovera *et al.*, 2002]. c) Arrhenius plot for the potassium feldspar experimental and modeled data. The black data points represent data obtained during the step heat experiment and the colored data points represent model derived data. d)  $r/r_0$  plot for the Wilderness suite sill samples. The black data points represent data obtained during the step heat experiment and the colored data points represent model derived data.

Figure 18. Thermal history of the Catalina MCC forerange (black) and main range (red). Fission track data is from *Fayon et al.* [2000]. AFT = Apatite Fission Track, and ZFT = Zircon Fission Track.

Figure 19. One dimensional transient thermal model of an intrusion with a radius of 5 kilometers. The country rock has a background temperature of 50°C. The initial intrusion temperature was 700°C, and the thermal diffusivity of 32 km<sup>2</sup>/Ma. [Ehlers, 2005].

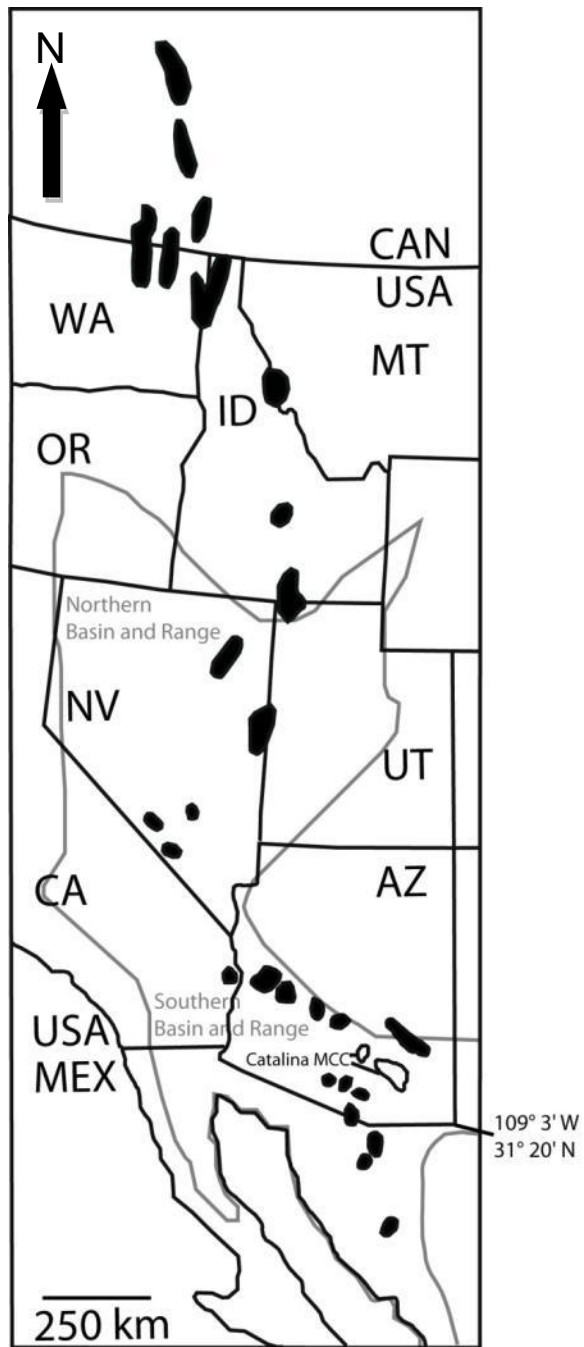


Figure 1.

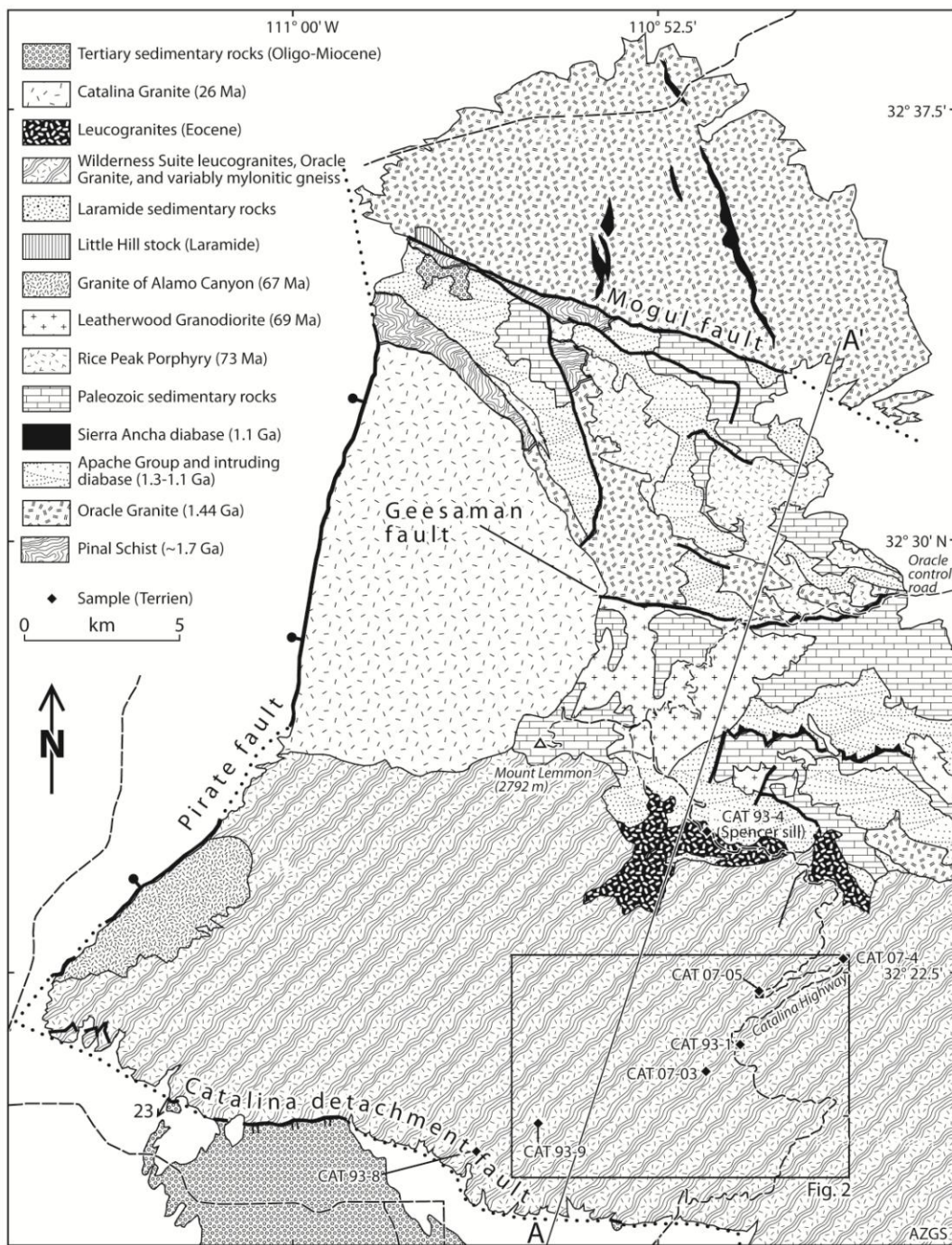


Figure 2a.

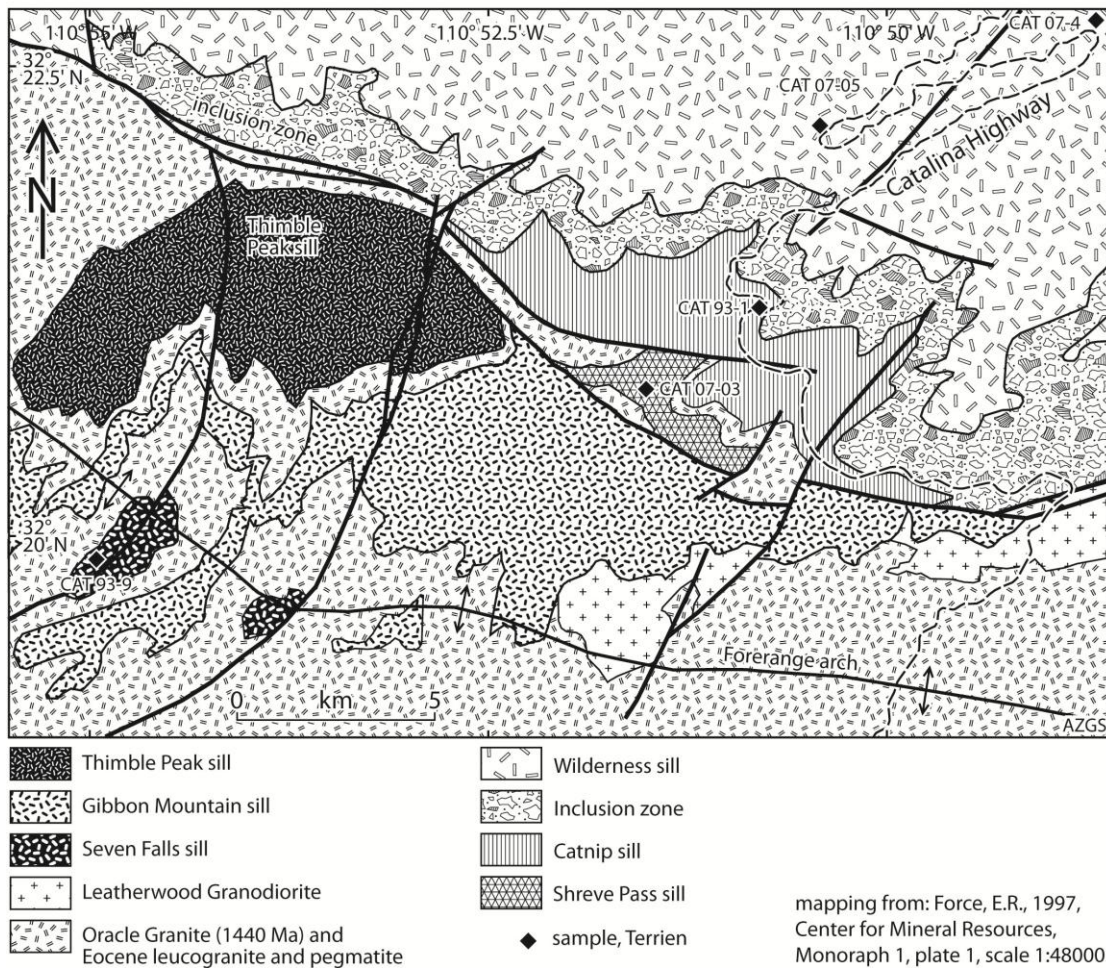
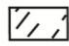


Figure 2b.

Wilderness suite sills:

- I. Spencer sill
- II. Wilderness sill (Windy Pt. and Gen. Hitchcock)
- III. Catnip Canyon sill
- IV. Shreve Pass sill
- V. Thimble Peak sill
- VI. Gibbon Mountain sill
- VII. Seven Falls sills

 mylonites

Screens:

-  Apache Group
-  Oracle Granite

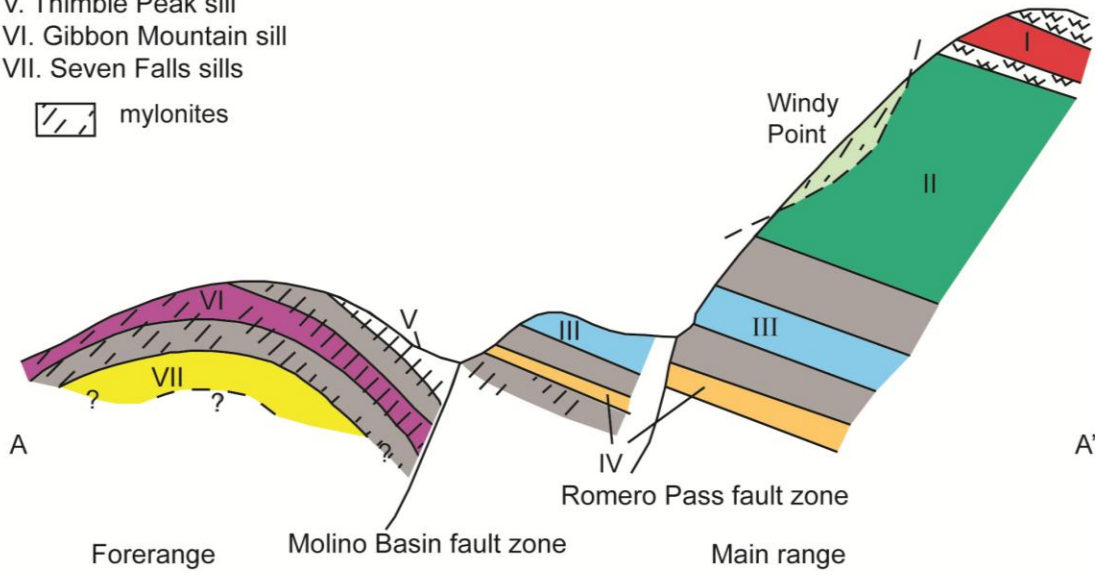


Figure 3.

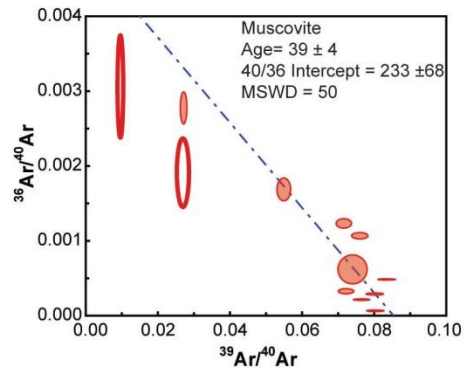
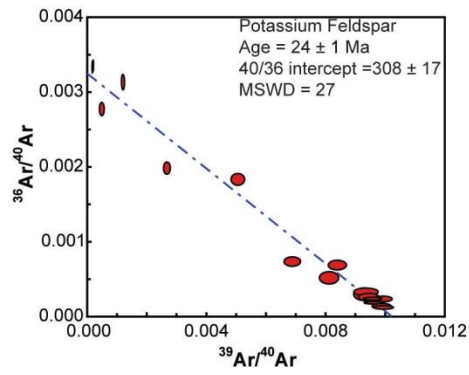
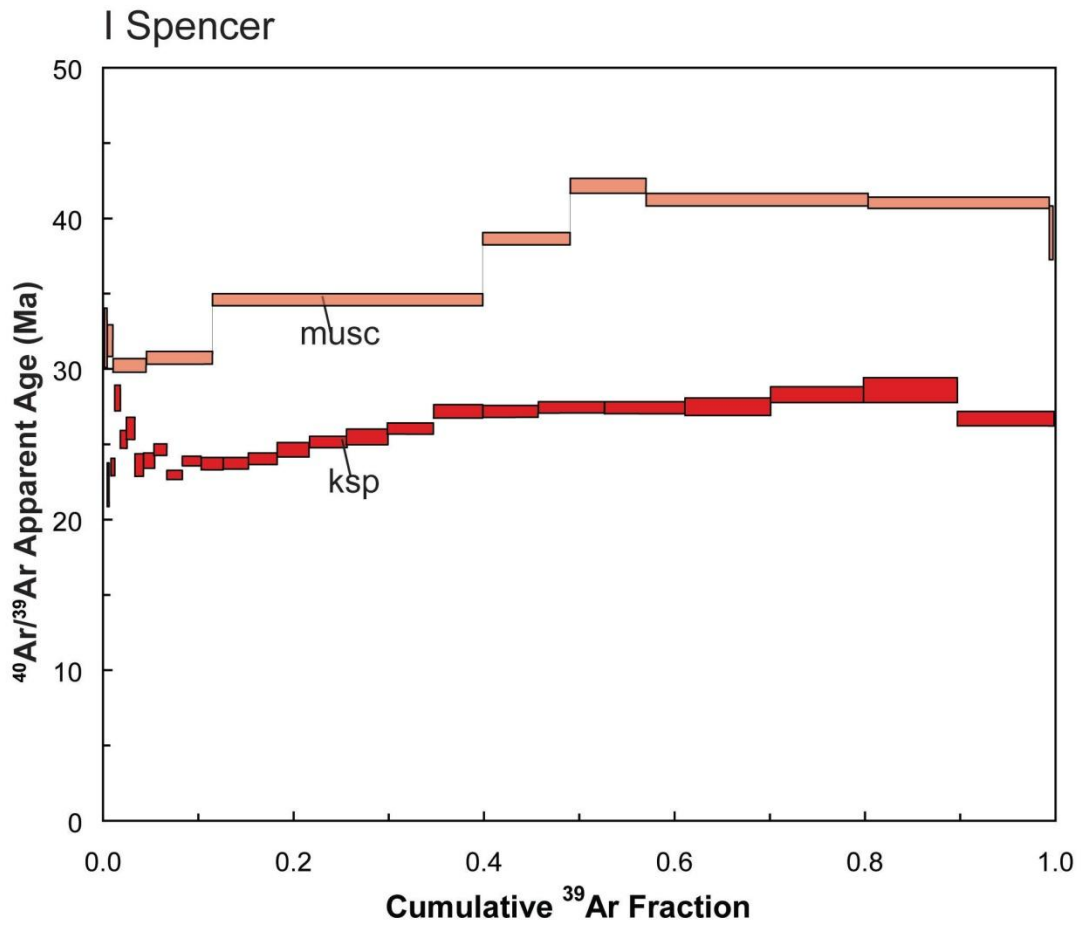


Figure 4.

## II Wilderness (Windy Point)

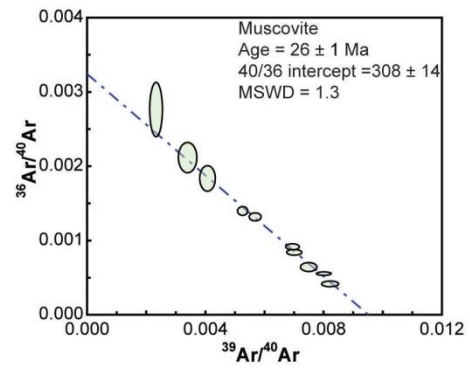
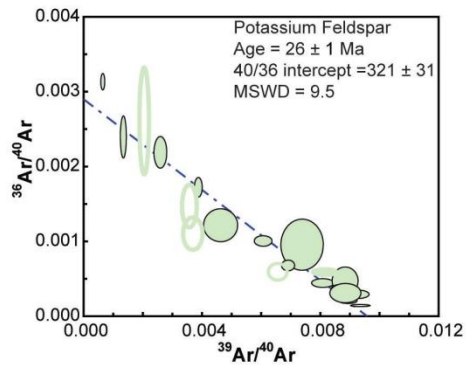
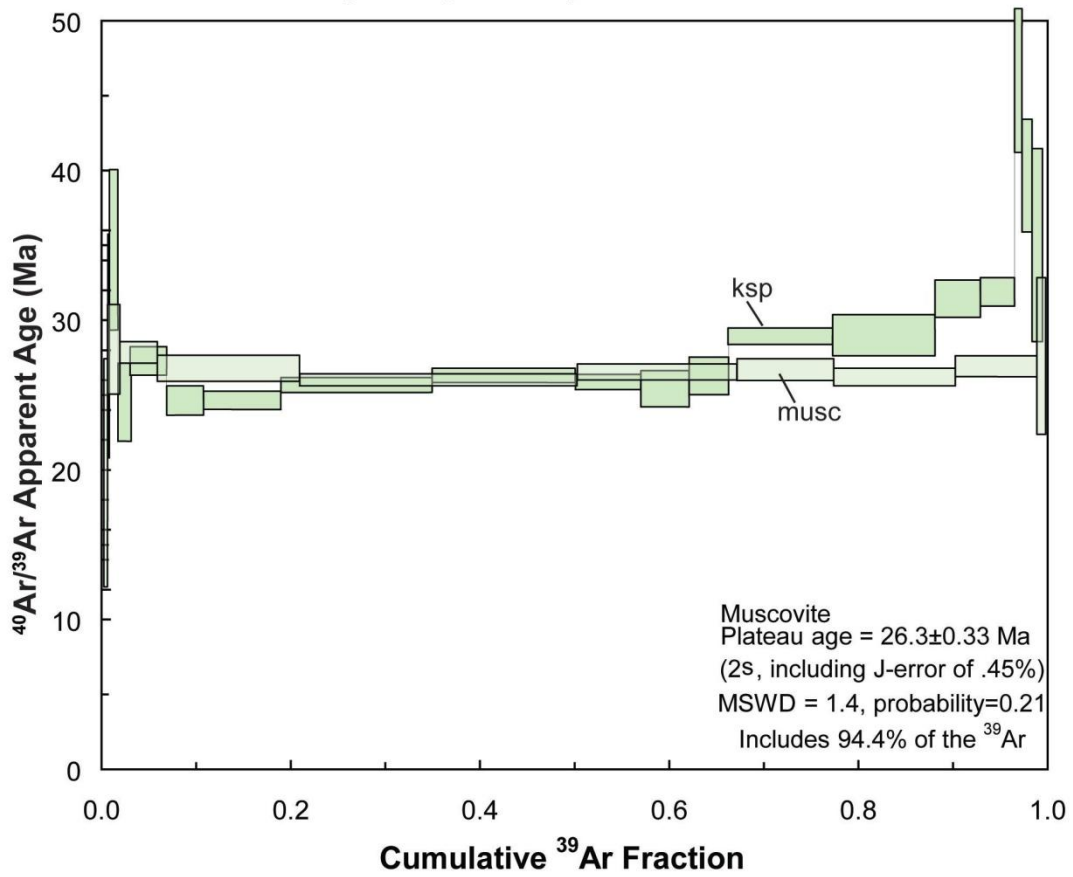


Figure 5.

## II Wilderness (General Hitchcock)

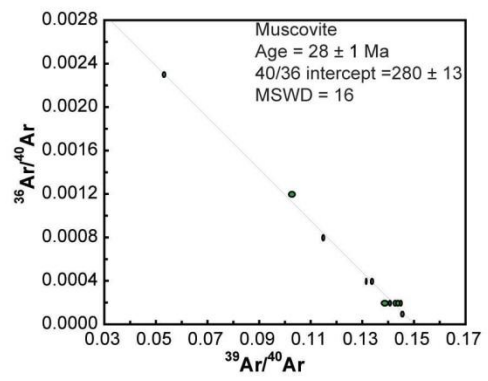
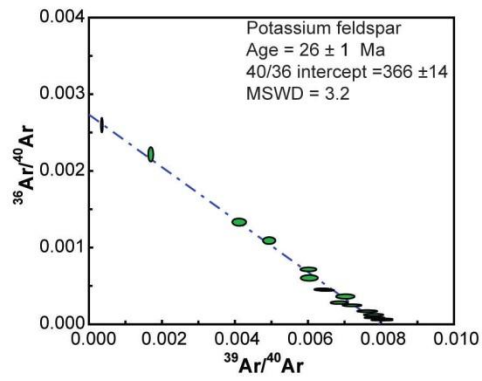
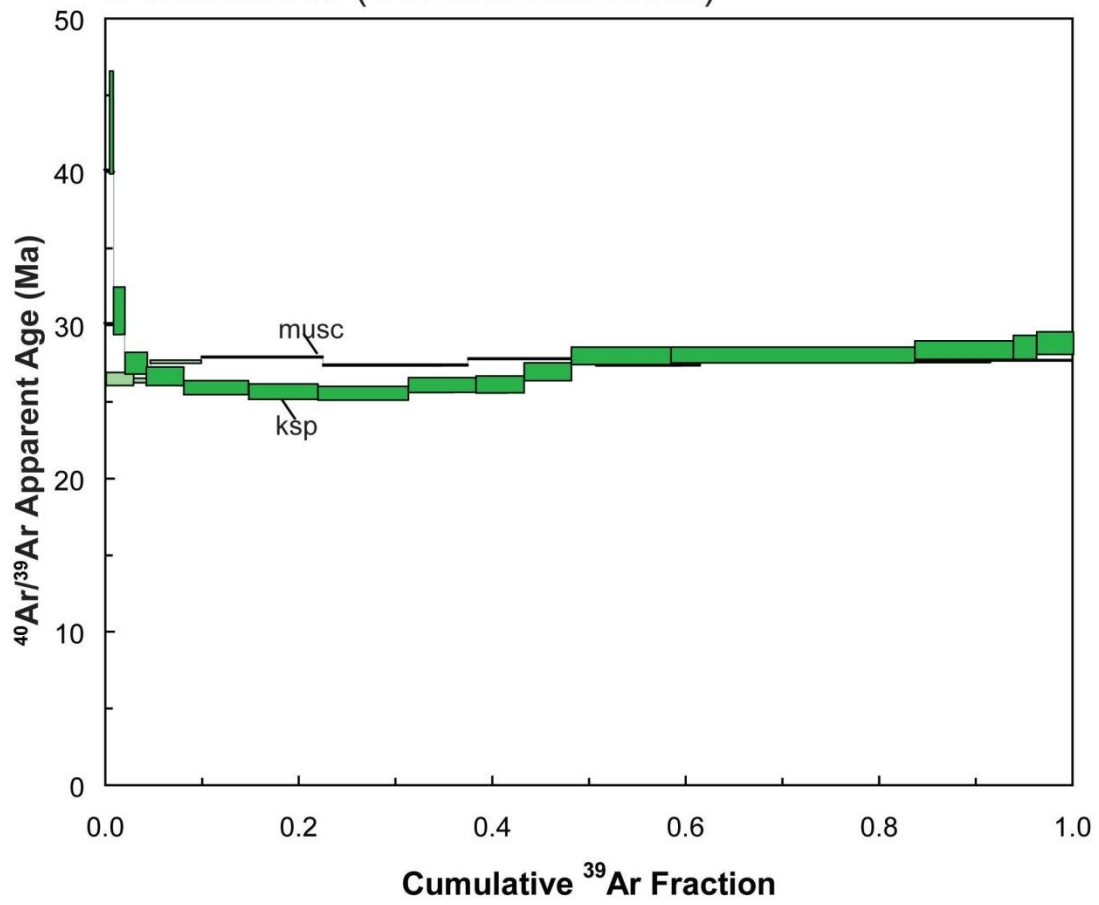


Figure 6.



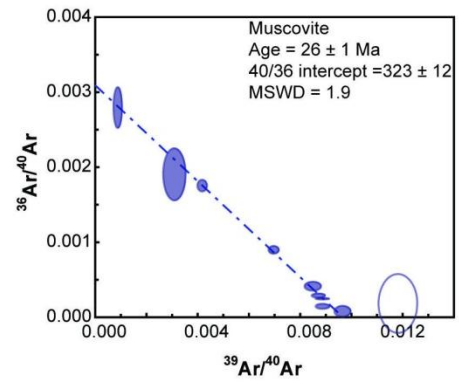
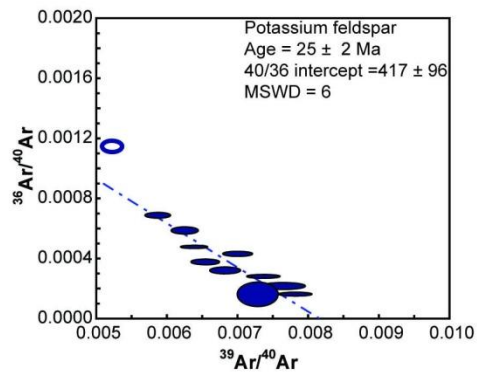
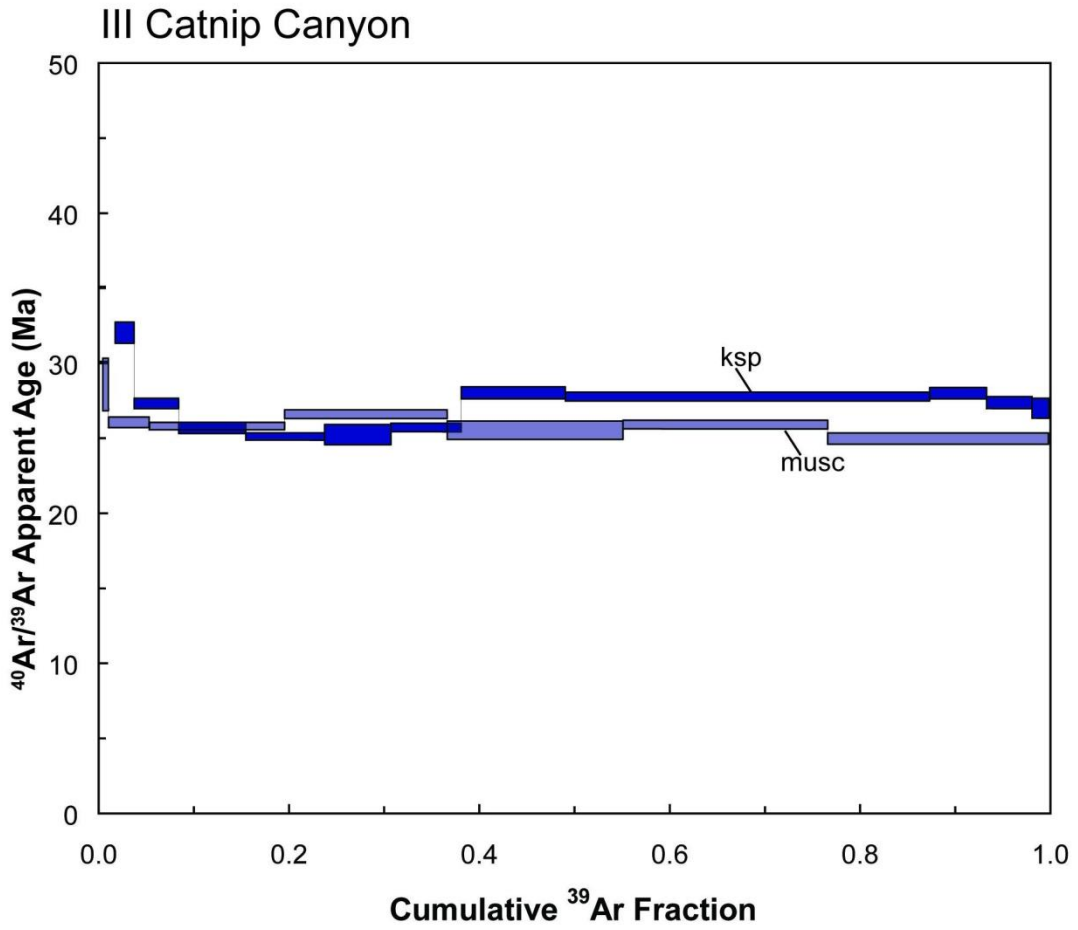


Figure 7.

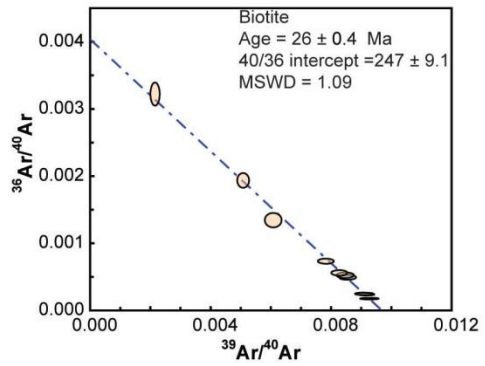
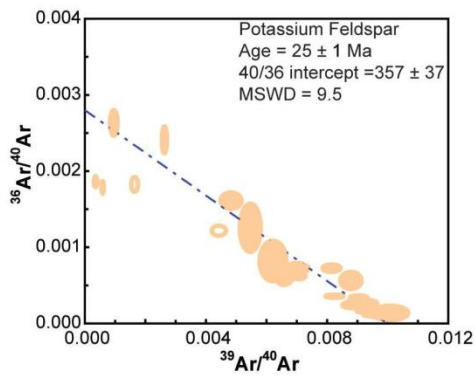
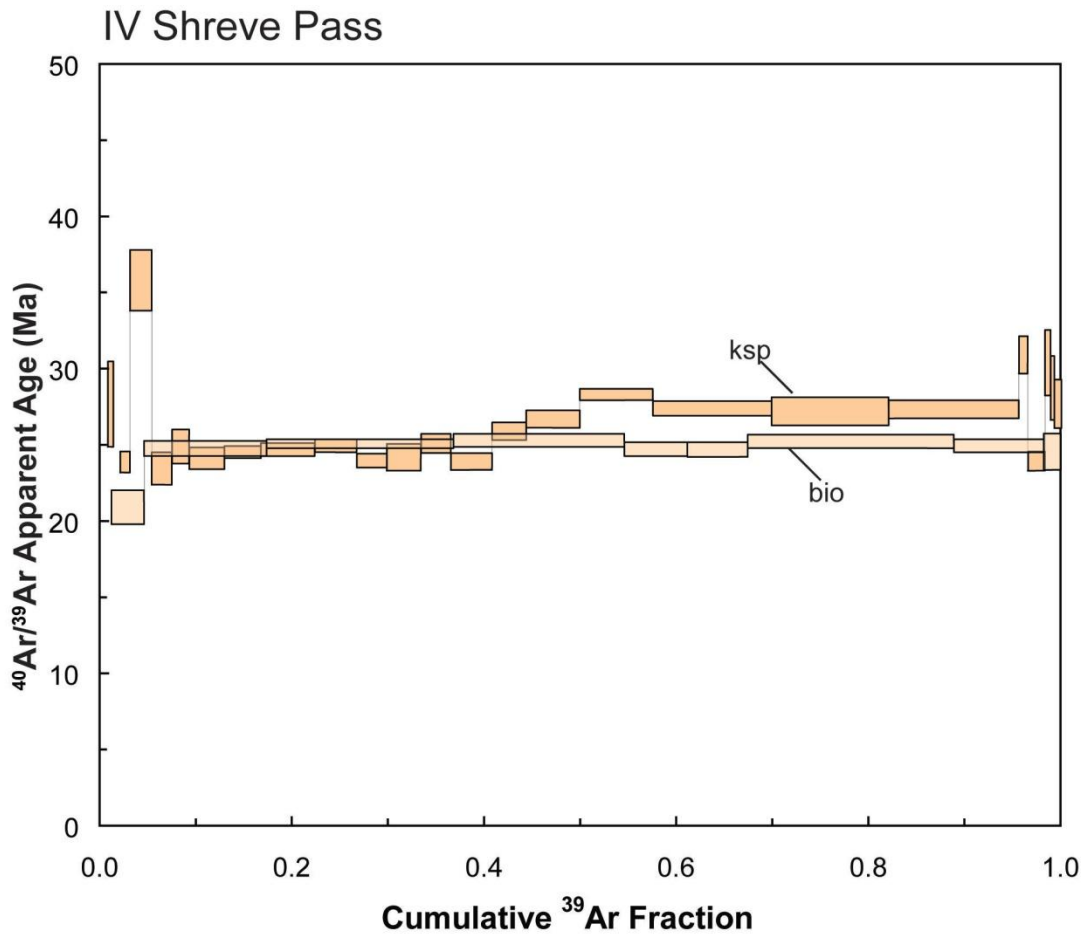


Figure 8.

# VI Gibbon Mountain

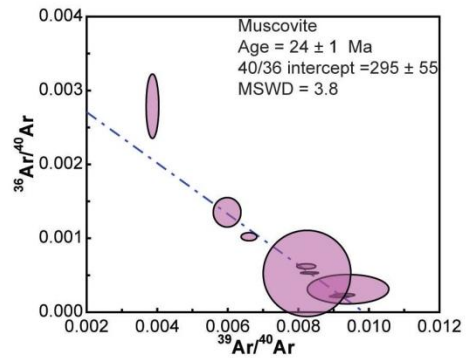
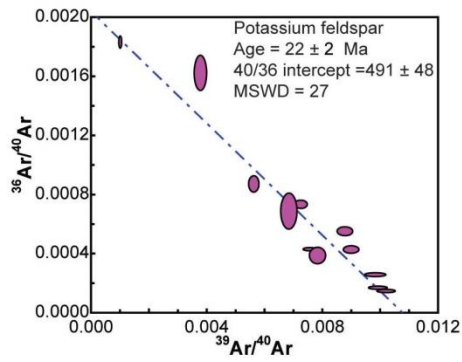
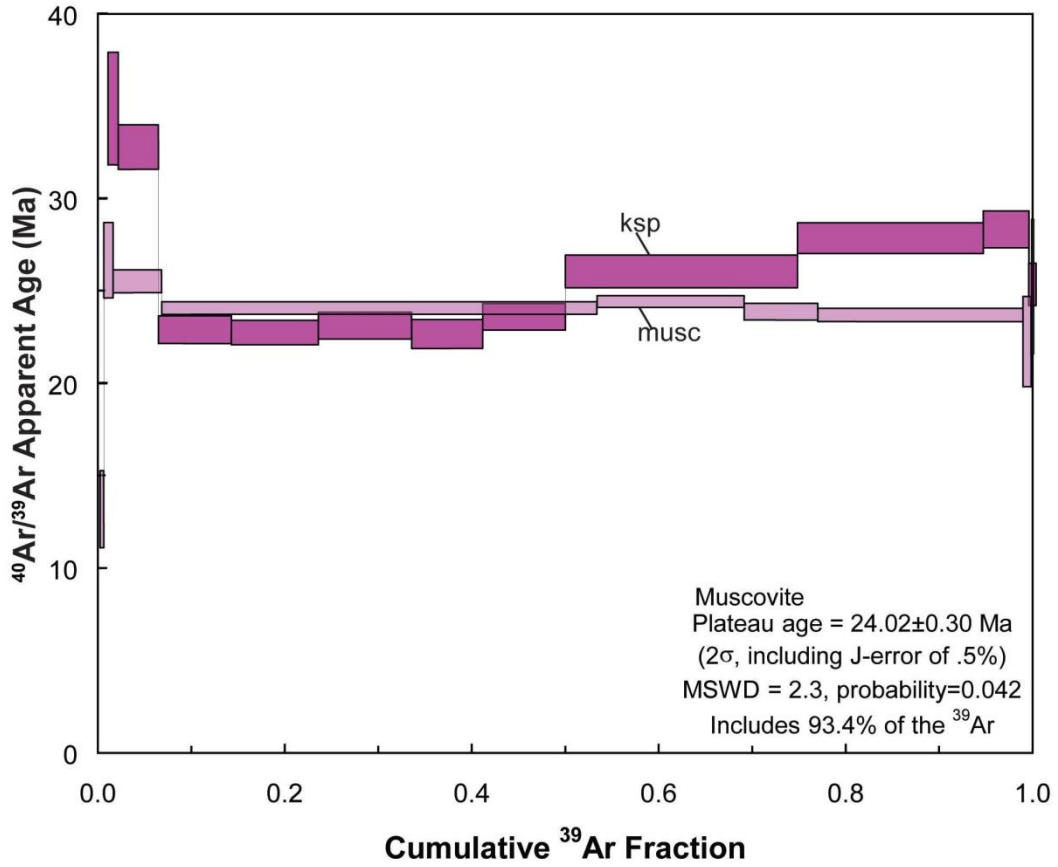


Figure 9.

# VII Seven Falls

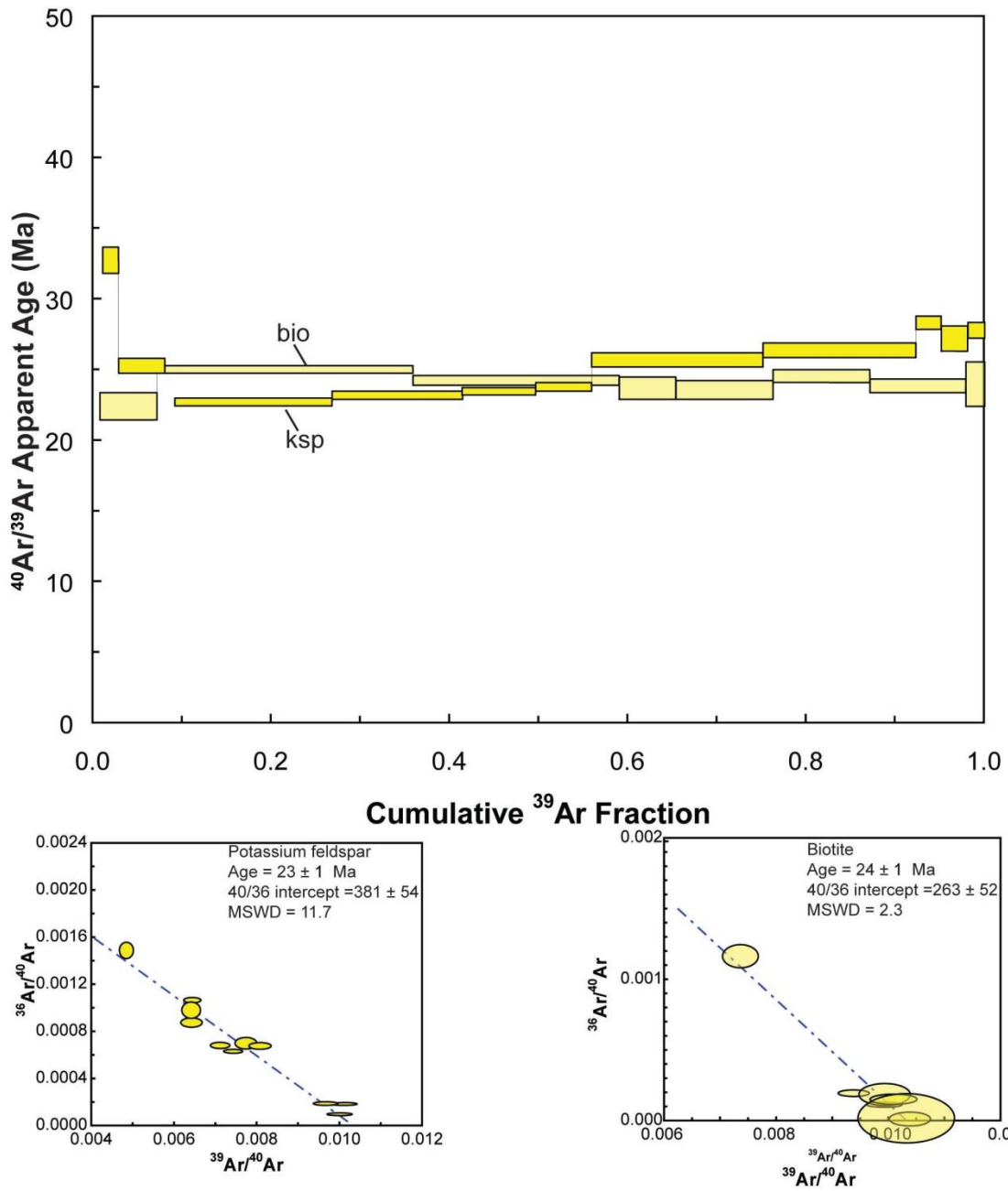


Figure 10.

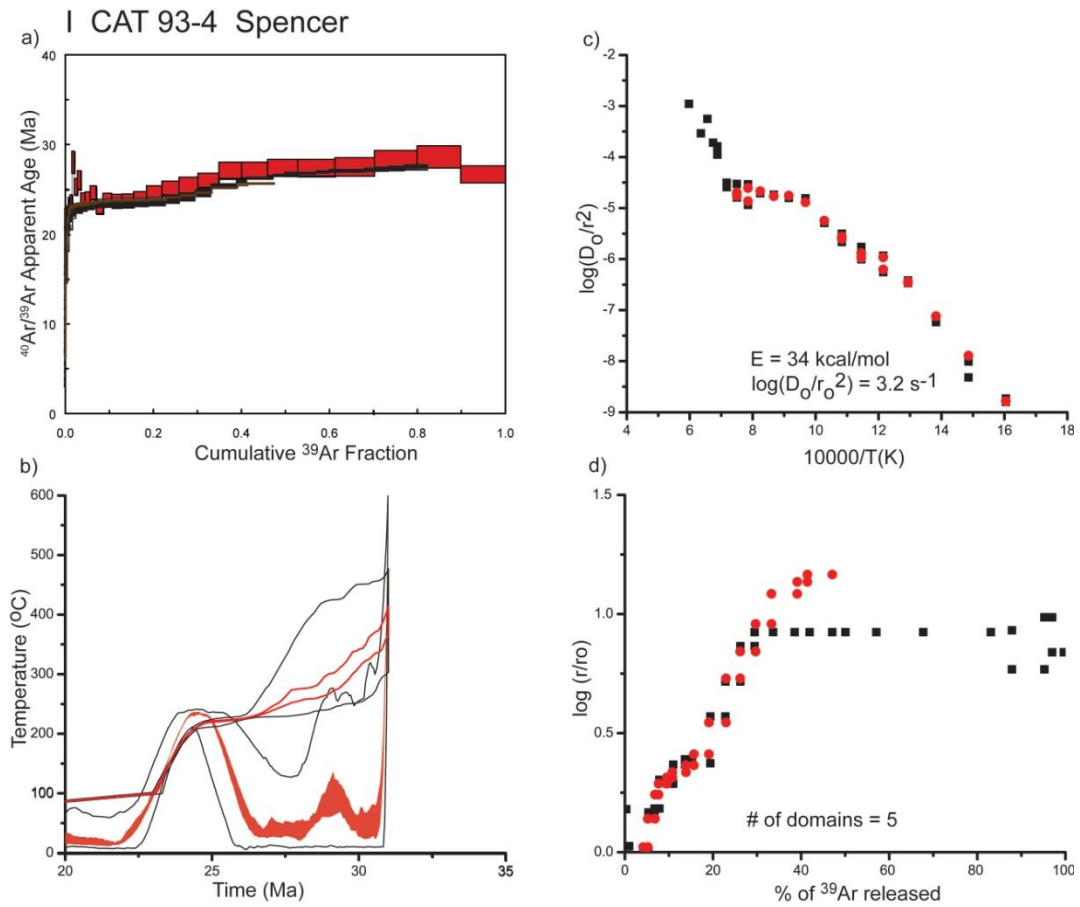


Figure 11.

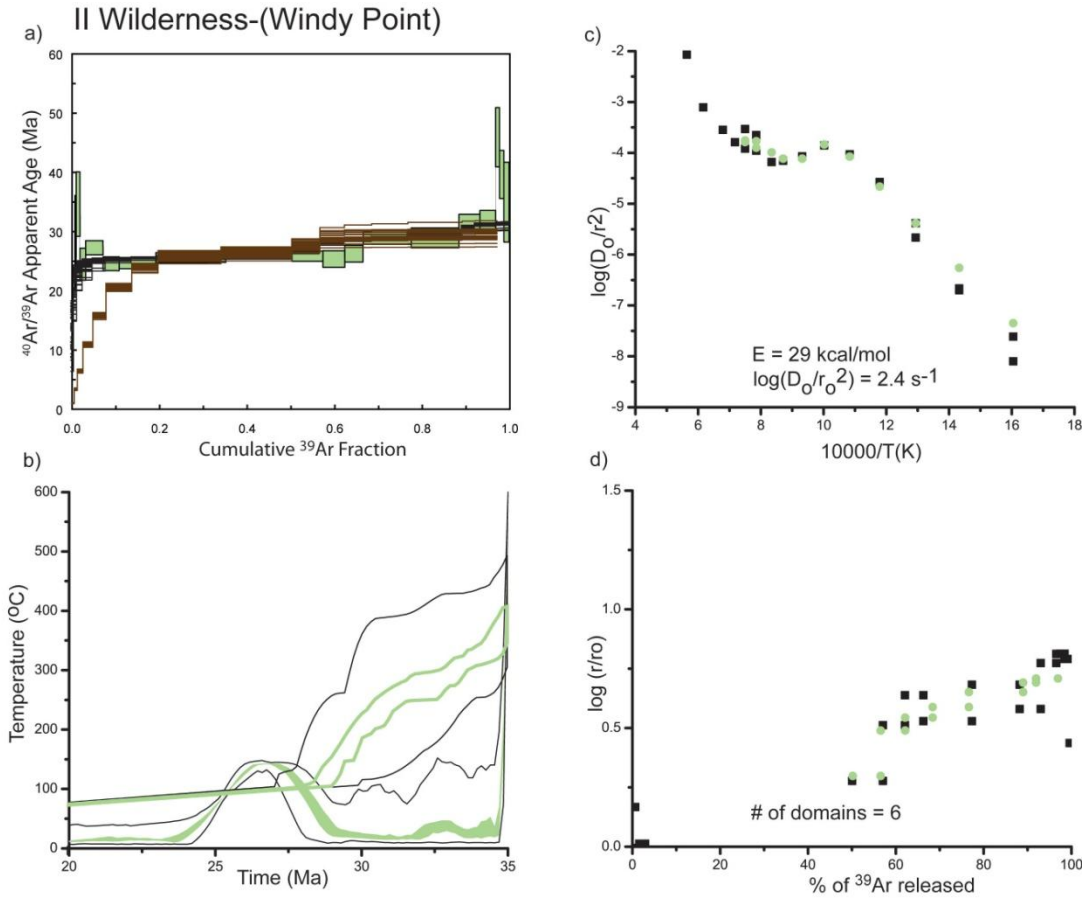


Figure 12

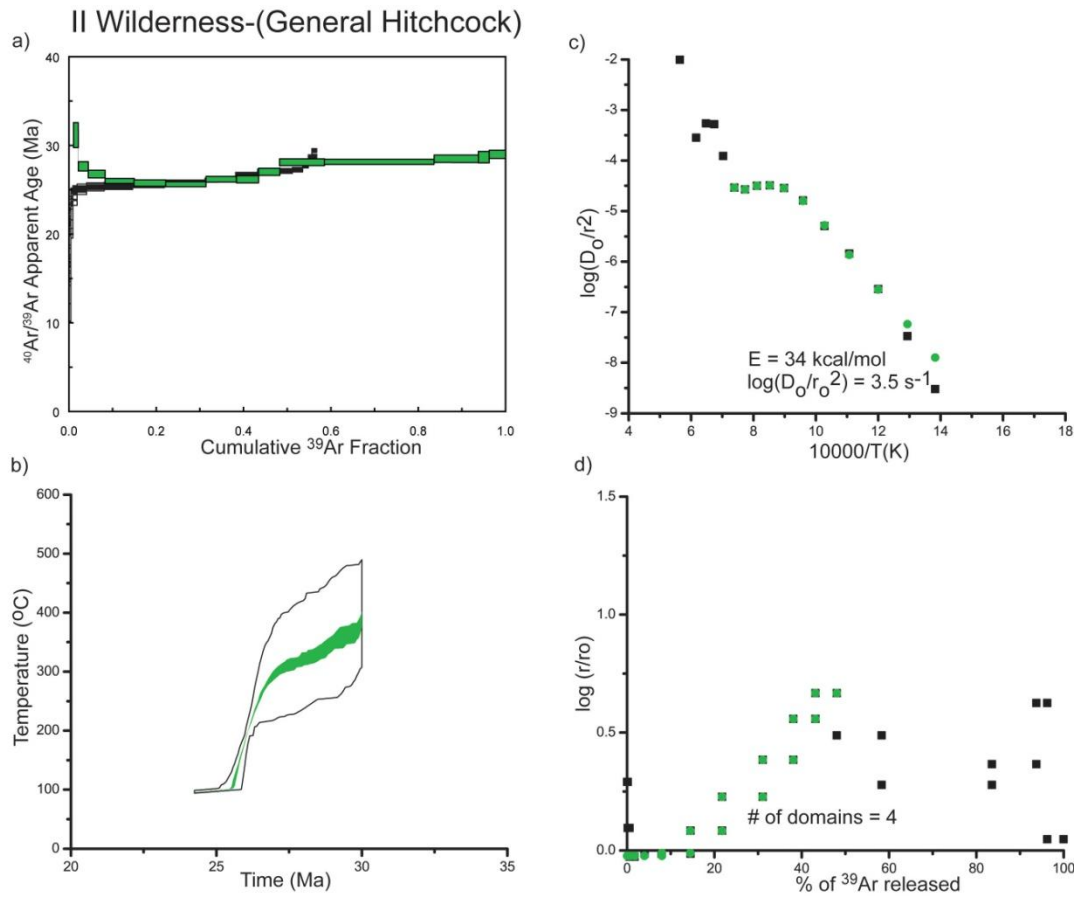


Figure 13.

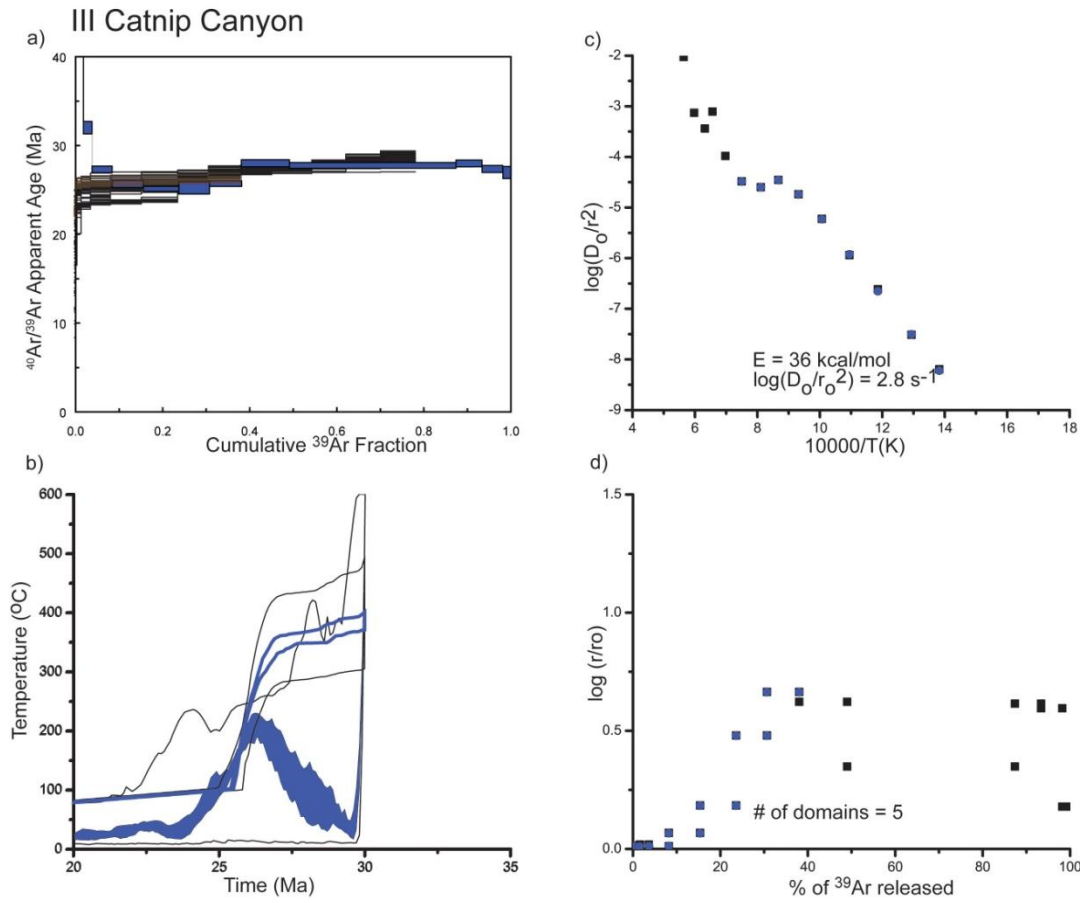


Figure 14.



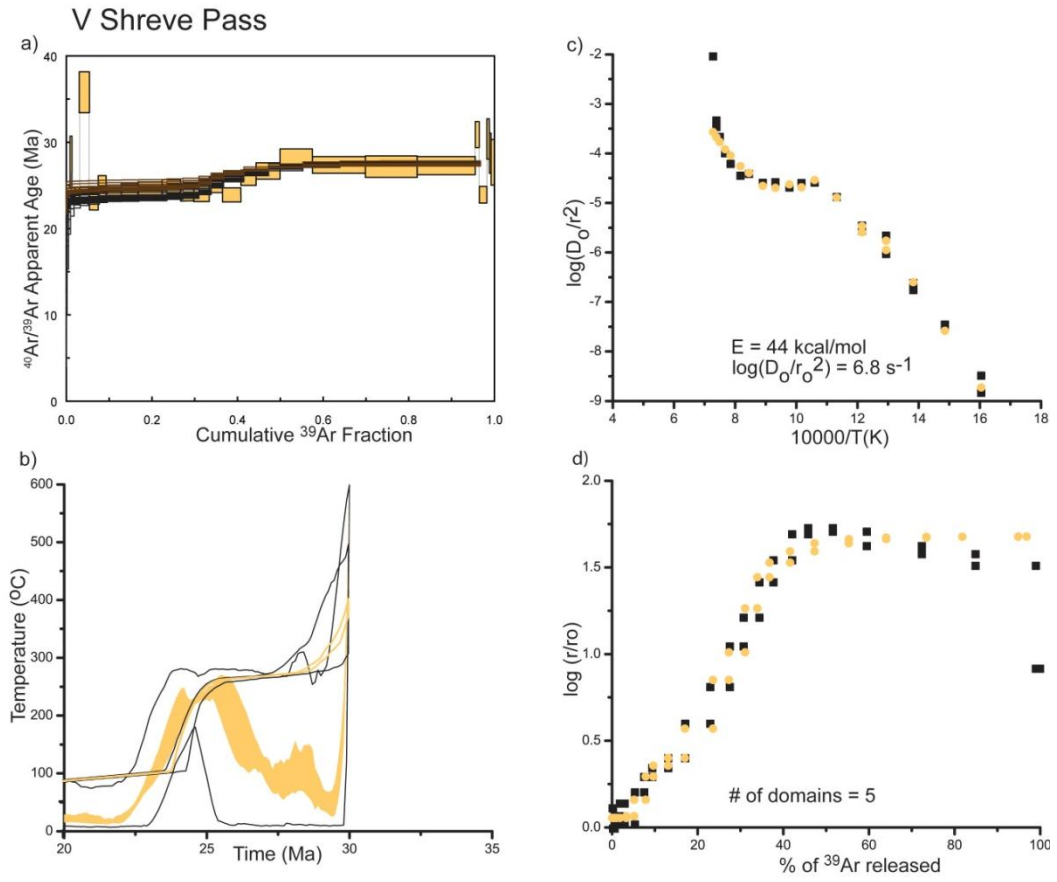


Figure 15.

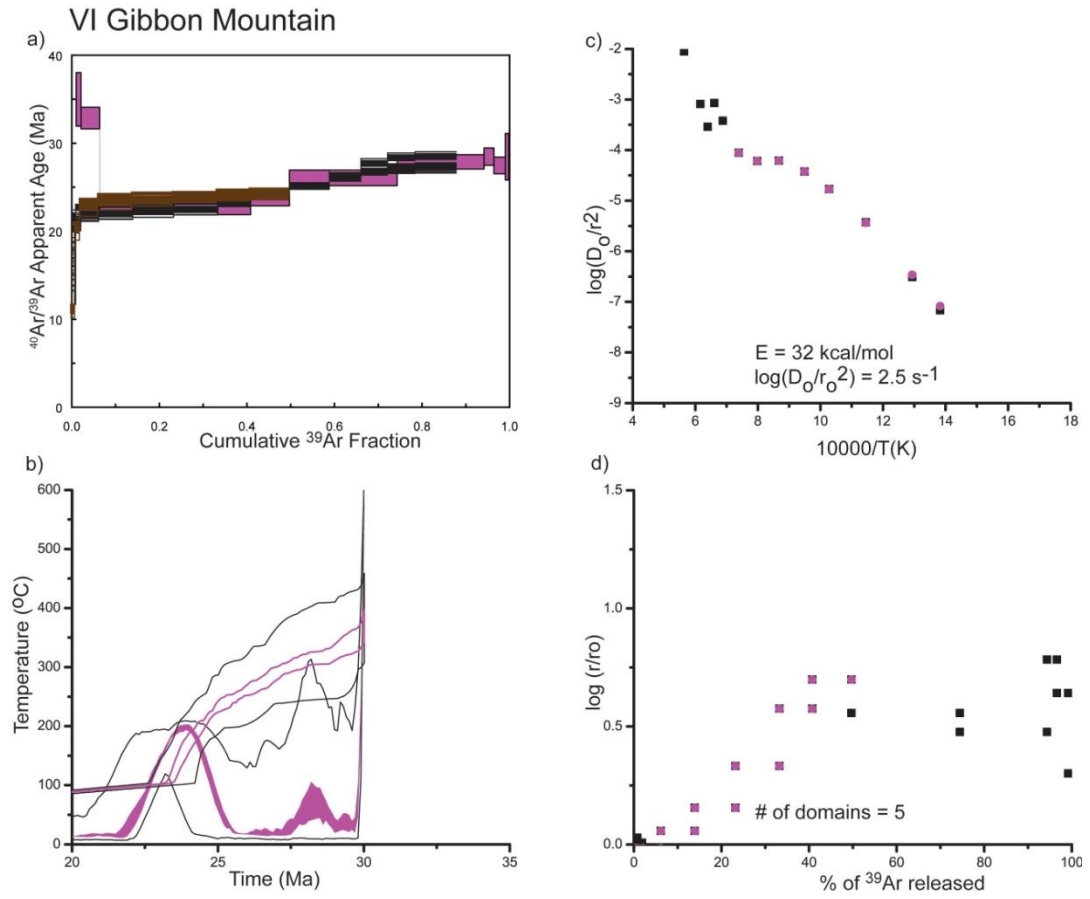


Figure 16.

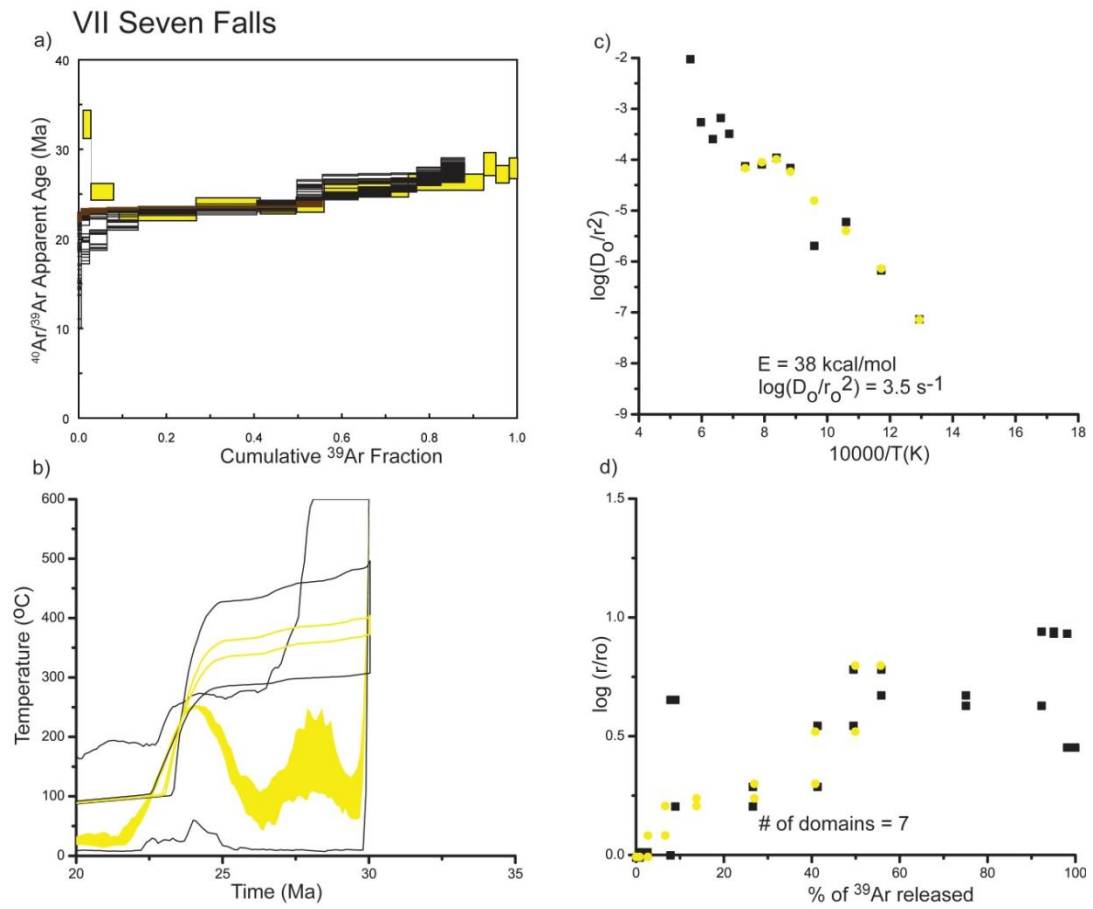
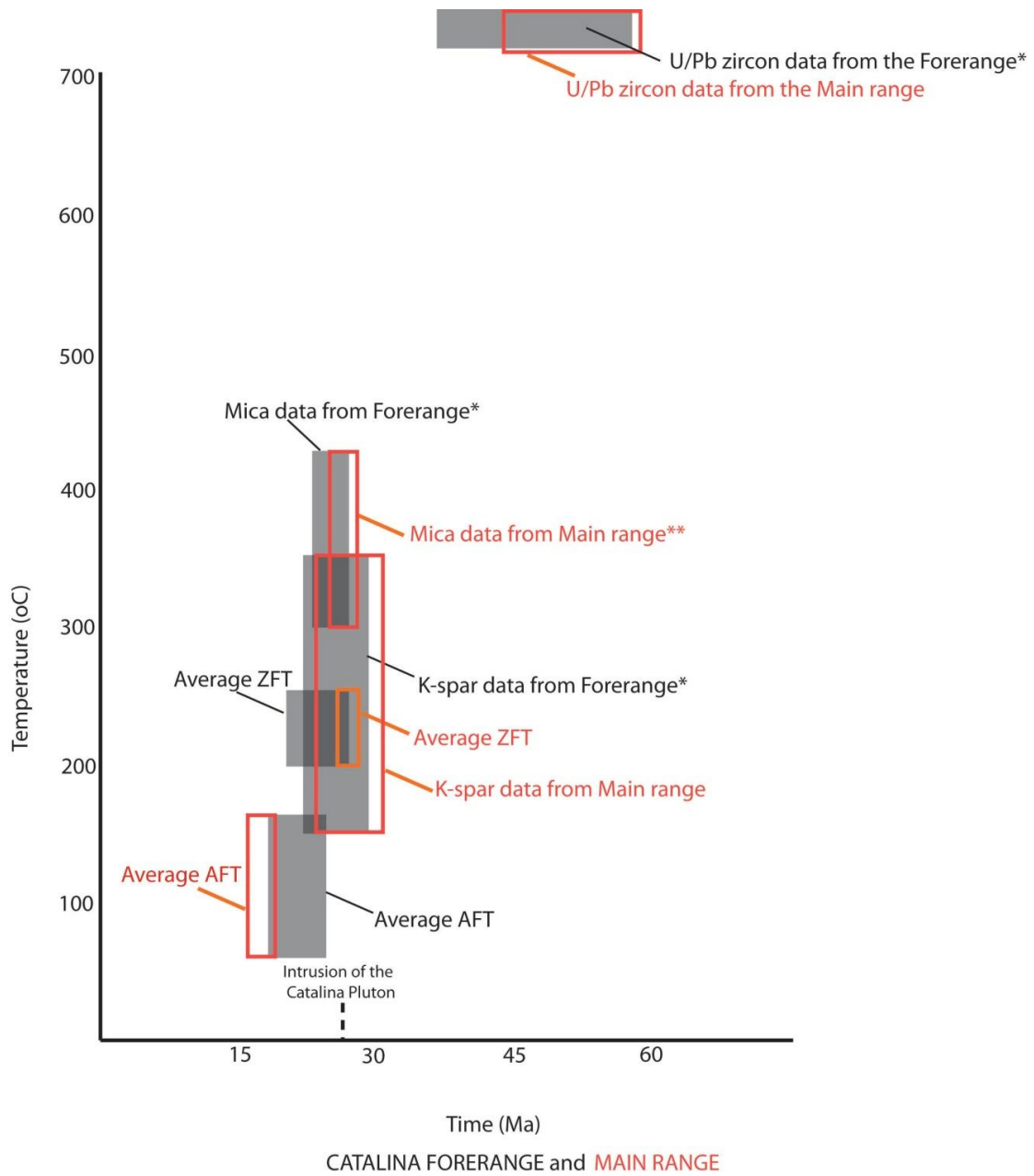


Figure 17.



\* includes Seven Falls and Gibbon Mountain sills

\*\*excluding Spencer sill that yielded an  $^{40}\text{Ar}/^{39}\text{Ar}$  age gradient from ~40 to 30 Ma

Figure 18.

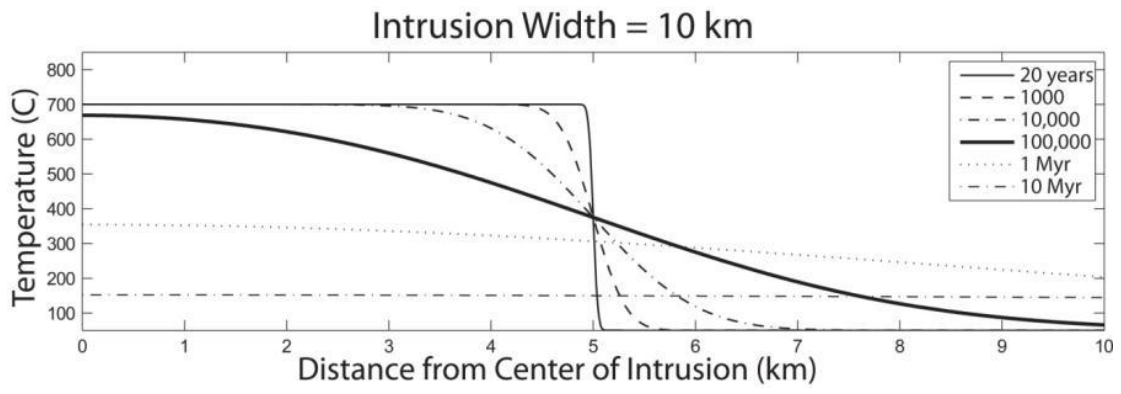


Figure 19.

## **TABLES**

Table 1. Summary table of Wilderness suite sill samples, description, and  $^{40}\text{Ar}/^{39}\text{Ar}$  data.

Table 1.

| <b>Sample No.</b>                    | <b>Wilderness Suite Sill</b>   | <b>Lat/Long coordinates</b> | <b>Description (after Force, 1997)</b>                                   | <b>Thin section description</b>   | <b>Biotite and Muscovite 40Ar/39Ar age data*</b>            | <b>Potassium Feldspar 40Ar/39Ar age data*</b> |
|--------------------------------------|--------------------------------|-----------------------------|--|---|---|---|
| CAT 93-4<br>(355-425 $\mu\text{m}$ ) | Spencer                        | 32°26'31" N<br>110°44'10"W  | medium-grained biotite granite, biotite<<muscovite, weakly foliated      | Large porphyroclasts of potassium feldspar, grain size reduction of quartz, rare quartz ribbons are present.  | Muscovite; age gradient from ~30 to 40 Ma                   | Age gradient from ~23 Ma to ~29 ma            |
| CAT 0705<br>(355-425 $\mu\text{m}$ ) | Wilderness - Windy Point       | 32°22'04" N<br>110°42'58"W  | equigranular, mylonitic  | Ductile deformation of mica (mica fish) is observed. The quartz has undergone grain size reduction  | Muscovite; Plateau age = 26 +/- 0.3 Ma                      | Age gradient from ~31 Ma to ~24 Ma            |
| CAT 0704<br>(355-425 $\mu\text{m}$ ) | Wilderness - General Hitchcock | 32°22'38" N<br>110°41'15"W  | equigranular, mildly deformed, garnet visible in hand sample             | Large quartz grains, potassium feldspar and plagioclase feldspar are present. Quartz contains undulose extinction and grain size reduction. Muscovite grains have undergone brittle deformation   | Muscovite; No plateau, steps range from ~27 Ma to 28 Ma     | Age gradient from ~ 25 Ma to ~28 Ma           |
| CAT 93-1<br>(250-425 $\mu\text{m}$ ) | Catnip Canyon                  | 32°21'08" N<br>110°43'44"W  | banded granite that contains a biotite rich band and a biotite poor zone | CAT 93-1M contains biotite, which has iron oxide staining. Fracture plagioclase. Recrystallized quartz and muscovite and biotite.<br>CAT 93-1F<br>No biotite present in this thin section. The thin section is dominated by quartz, which exhibits subgrain migration and bulging. There are regions of extreme grain size reduction. | Biotite; No Plateau age, steps range from ~25 Ma to ~ 26 Ma | Age gradient from ~28 Ma to ~26 Ma            |

Table 1, continued.

|                                    |             |                            |   |   |  |                                    |
|------------------------------------|-------------|----------------------------|---|---|--|------------------------------------|
| CAT 07-03 (355-425 $\mu\text{m}$ ) | Shreve Pass | 32°20'41" N<br>110°44'04"W | medium-grained biotite granite, mildly deformed     | Biotite has iron staining and is recrystallized forming ribbons that wrap around porphyroclasts. Fracturing of plagioclase feldspar and potassium feldspar is common.   | Biotite; No Plateau age, steps range from ~23 Ma to ~24 Ma | Age gradient from ~28 Ma to ~23 Ma |
| CAT 93-8 (355-425 $\mu\text{m}$ )  | Gibbon Mtn  | 32°19'18" N<br>110°48'45"W | porphyroclastic; biotite<<muscovite, mylonitic      | Recrystallized quartz with 120° grain intersections. A large porphyroclasts of plagioclase is present. Iron oxide staining in fractures is visible. Deformation (taper) twins present in plagioclase                      | Muscovite; Plateau age = 24.0 $\pm$ 0.3 Ma                 | Age gradient from ~26 Ma to ~23 Ma |
| CAT 93-9 (355-425)                 | Seven Falls | 32°19'47" N<br>110°47'30"W | equigranular, biotite>>muscovite, biotite lineation | Deformation twins are present in potassium feldspar Myrmekite is present. Large amounts of fractures in quartz, plagioclase and potassium feldspar. The quartz has undergone grain size reduction and bulging is present. | Biotite; No Plateau age, steps range from ~23 Ma to ~24 Ma | Age gradient from ~28 Ma to ~22 Ma |

\*ages were calculated using an atmospheric  $^{40}\text{Ar}/^{36}\text{Ar}$  ratio of 298.56



***Aeromagnetic and Bouguer Gravity modeling of the Catalina Metamorphic Core Complex: the Role of Magmatism in Metamorphic Core Complex Formation***

Jessica J. Terrien

Syracuse University

Department of Earth Sciences

204 Heroy Geology Laboratory

Syracuse, New York 13244, USA

Carol A. Finn

Unites States Geological Survey

P.O. Box 25046

20 Denver Federal Center

Denver, Colorado 80225, USA

Suzanne L. Baldwin

Syracuse University

Department of Earth Sciences

204 Heroy Geology Laboratory

Syracuse, New York 13244, USA

## **ABSTRACT**

Aeromagnetic and gravity data from the Catalina metamorphic core complex (MCC) and the surrounding region were used to study the subsurface geology in order to gain insight regarding MCC formation. The aeromagnetic anomalies over the Tucson Basin and Catalina MCC are dominated by a NW–SE trending, positive, ~100 km long and ~30 km wide magnetic anomaly that is bordered to both the NE and SW by NW–SE trending long-wavelength magnetic lows. The Bouguer gravity anomalies also indicate a NW–SE trending positive anomaly that is bordered to the NE and SW by a negative anomaly. Subsurface geology was correlated, when possible, with rocks exposed at the surface. The magnetic and density lows to the NE of the positive gravity anomaly are interpreted to represent Wilderness suite sills which are exposed at the surface and are inferred to continue at depth.

Forward modeling of the gravity and aeromagnetic data indicates the observed subsurface body responsible for the positive aeromagnetic and gravity anomalies represents a shallow (2 kilometers or less) felsic to intermediate pluton. Magmatic bodies in the region, including the Precambrian Oracle Granite, the Tertiary Wilderness suite sills, the Catalina pluton, and the less extensive Leatherwood suite, were considered as possible outcrops of this pluton. Thermochronology data from the Wilderness suite sills indicate the possibility of a thermal event that corresponds to emplacement of the Catalina pluton, but seem primarily to reflect the timing of exhumation along the detachment fault.

Based on the regional geology and the gravity and aeromagnetic properties of intrusions in the region, a Tertiary or Mesozoic age subsurface pluton is preferred; the age of the pluton can help distinguish between differing models for MCC formation. A Mesozoic pluton suggests that crustal thickening influenced MCC development, and a preexisting zone of weakness may have controlled the emplacement of this subsurface body as well as the Wilderness suite sills. A Tertiary pluton suggests magmatism may have initiated low-angle detachment faulting and MCC formation.

## INTRODUCTION

The Catalina metamorphic core complex (MCC) is considered a type locality for core complexes [eg. *Coney*, 1980], yet its origin is still debated. Like other MCCs, the basic structure of the Catalina MCC consists of a metamorphic basement terrane and unmetamorphosed cover, between which is a mylonitized decollement (Figure 1). Tectonic denudation occurs along low-angle faults with brittle over-prints onto already ductilely deformed rock [*Armstrong*, 1982]. MCC's are asymmetrically dome-like, and usually form the highest topography in the region [*Coney*, 1980].

Normal-sense motion along the detachment fault exhumes deep-seated crystalline rocks that are now exposed at the surface, and are thus subject to erosion [*Davis and Lister*, 1988]. Movement along a low-angle normal fault is nearly always accompanied by magmatism [*Axen*, 2007]. However, the development of low-angle normal faults and the role of magmatism in forming MCC's are controversial. It has been suggested that magmatism can change the local stress field, as well as weaken the crust, and thus the presence of magmatic rocks can be used to explain the development of low-angle normal faults which violate Andersonian theory [*Parsons and Thompson*, 1993]. Andersonian theory predicts the angle of normal faults will range from ~45–70 degrees [*Anderson*, 1972]. Many MCC's show evidence (e.g., paleomagnetic data or offset marker beds) that the low-angle fault has rotated from high angles [*Wong and Gans*, 2003]. Modern seismic evidence indicates that slip can occur along low-angle normal faults [*Abers et al.*, 1997] and seismic reflection data from the Santa Rita Mountains in southeastern Arizona provides evidence for seismogenic low-angle faulting in the Miocene [*Johnson and Loy*, 1992]. In order to understand the role of magmatism and the development of the Catalina

MCC, information on the subsurface composition, particularly, that of igneous bodies is necessary. The aim of this paper is to help constrain the subsurface lithology and structure of the Catalina MCC using aeromagnetic and gravity data. If possible, these data will be used to elucidate the processes that formed the MCC.

## **GEOLOGY OF THE CATALINA MCC**

The Tortolita, Santa Catalina, and Rincon Mountains of southern Arizona comprise the footwall of the Catalina MCC and are associated with the Catalina detachment fault that generally trends northwest-southeast (Figures 1 and 2). Movement along the Catalina detachment fault was top-to-the-southwest based on mylonitic lineations that trend S 60–65 W<sup>0</sup> [Dickinson, 1991]. The Catalina detachment fault extends from the southwest flank of the Catalina MCC and dips beneath the central basin of the Tucson Basin, which is within the hanging wall of the fault [Wagner III and Johnson, 2006]. The Catalina MCC is divided into the forerange and the main range. The forerange forms an anticline or arch with a northwest-southeast trending axis located on the southern flank of the Catalina MCC. High-angle Basin and Range faults that trend north and northwest cut the Catalina MCC.

Igneous rocks associated with the Catalina MCC have been studied extensively to attempt to understand the absolute and relative timing of the history of the region. The Precambrian country rock is intruded by three magmatic suites: the Leatherwood, the Wilderness, and the Catalina suites [Keith *et al.*, 1980]. The oldest suite, the Laramide-age Leatherwood suite, is comprised of three plutons that range in composition from quartz diorite to granodiorite: the Chirreon Wash granodiorite, located in the Tortolita Mountains, and the Rice Peak and Leatherwood plutons, located in the Santa Catalina

Mountains. The Wilderness suite that intrudes the Leatherwood suite and the Precambrian Oracle/Ruin granite consists of leucocratic muscovite-bearing peraluminous granites that have been emplaced as a series of sills [Force, 1997]. The sills inflated the crust by ~4 km during the Eocene [Keith *et al.*, 1980]. U-Pb zircon data indicates that the Wilderness sills were emplaced at ~57 Ma and ~45 Ma, with evidence of additional zircon rim growth <40 Ma in the structurally lowest sills (Chapter 1). The Catalina suite consists of biotite and hornblende-bearing granite and quartz monzonite plutons including the Catalina granite, which was emplaced at ~26 Ma [Fornash, *et al.*, in prep]. Portions of the Catalina and Wilderness suites and the Oracle/Ruin granite are highly sheared to form mylonites. The general temporal evolution of the Catalina MCC is closely related to the tectonic, magmatic and deformational history of the Basin and Range Province (Figure 3).

## **MODELS FOR MCC FORMATION**

Several models have been developed to explain the development of MCCs. MCC models must explain low-angle faulting, as well as the high topography of the lower plate. The Catalina MCC developed in two stages, as indicated by the depositional history of the Tucson Basin [Houser *et al.*, 2004; Wagner III and Johnson, 2006]. The first stage requires motion along the detachment fault that led to development of the Tucson Basin in the hanging wall and exhumation of the footwall. However, the mylonitic footwall is either not exposed at the surface during this stage, or it is exposed but does not form a topographic high based on the absence of deposition of mylonitic clasts. During the second stage, the Catalina MCC breached the surface and reached higher elevations due to footwall flexure in response to high-angle Basin and Range

faulting [*Wagner III and Johnson, 2006*]. Uplift of the footwall led to flow of ductile material from beneath the Tucson Basin to the Catalina MCC [*Wagner III and Johnson, 2006*]. This model does not address the role of magmatism in development of the Catalina MCC.

As described by *Wagner and Johnson [2006]* flexural uplift as a result of tectonic denudation explains the high topography of most MCC models. Flexural uplift requires thickening of the crust before the mid-Tertiary, followed by extension which results in regional uplift due to tectonic denudation, and complete isostatic uplift occurs during high-angle Basin and Range faulting. The crust in the Catalina MCC region may have been as thick as ~42 kilometers, the current crustal thickness of the Colorado plateau [*Parsons and McCarthy, 1995*] and thus the role of gravitational instability and spreading due to thickening of the crust (possibly by Laramide-related magmatism) as described by *Coney [1987]* may have played a role in MCC development. A seismic study suggests the presence of a felsic crustal root which is depressing the Moho by ~ 4.2 km [*Myers and Beck, 1994*]. However, the presence of a crustal root has been reinterpreted to represent local variation of the crustal Vp/Vs ratio; both seismic and gravity data imply the absence of a supporting root under the Catalina and other MCCs [*Frassetto et al., 2006*]. In the case of the Catalina MCC, the high elevation has been modeled to be the result of a lower density crust that is underlain by normal density mantle [*Frassetto et al., 2006*].

Magmatism has played a large role in MCC models with regard to differential uplift [*Lister and Baldwin, 1993*] and the formation of the low-angle normal fault [*Parsons and Thompson, 1993*]. Magmatic underplating or intrusions may change the greatest principal stress orientation and initiate low-angle faulting. If magmatic intrusion

occurs at a faster rate than extension, the extensional stress would be focused above the zone of intrusion [*Parsons and Thompson, 1993*].

## **GEOPHYSICAL DATA**

### ***Aeromagnetic Data***

Magnetic anomaly data provide a means of “seeing through” nonmagnetic rocks and cover to reveal lithologic variations and structural features such as faults, folds, and dikes. Magnetic anomalies are the result of variations in total rock magnetization [*Reynolds, 1987*], reflecting variations in the distribution and type of magnetic iron oxide minerals—primarily magnetite—in Earth’s crust. Total magnetization, the vector sum of induced magnetization and remanent magnetization, produces magnetic anomalies. Induced magnetization is induced by the current magnetic field and is proportional to magnetic susceptibility. Remanent magnetization is permanent magnetization related to the direction of the magnetic field at the time of rock formation. The shape and intensity of a magnetic anomaly is dependent upon the rock’s magnetic properties, the size, shape and depth of the rock body, and the topography. Magnetic highs are the result of strongly normally magnetized rocks, or rocks with high magnetizations such as basalt. In contrast, magnetic lows may be the result of reversely magnetized volcanic rocks, weakly magnetized rocks such as carbonates, or topographic lows.

Multiple aeromagnetic surveys (Table 1) were flown in the Catalina MCC region from 1964–1999 [*U.S.G.S., 1980; 1982; 2000*]. The data were collected at altitudes ranging from ~150–305 meters along parallel flight lines with crossing tie lines. The line spacing between flight lines ranged from 0.08–1.61 km. All of the data were obtained digitally with the exception of survey 0528 which was digitized after collection



[U.S.G.S., 2000]. The appropriate IGRF (International Geomagnetic Reference Field) was removed from all of data sets with the exception of survey 0528 where an arbitrary base value was removed and is not known. All data sets were continued to a common elevation of 305 meters above terrain, merged together and reduced to the pole in order to center anomalies over their sources [Baranov and Naudy, 1964; Blakely, 1995]

### ***Gravity Data***

Gravity anomalies are the result of lateral density variations in the crust and upper mantle. Like magnetic anomalies, the wavelength of gravity anomalies yields information regarding the depth of the source; long wavelength anomalies indicate deep or broad shallow sources and short wavelength anomalies are caused by near surface features. Gravity data from the Tucson Basin and the Catalina MCC were collected with random spacing. A grid was produced from the irregularly spaced gravity stations and standard data corrections were applied. The data were corrected for drift of the instrument, variation in the earth's gravity field due to tides, and latitude of the gravity station [Blakely, 1995]. The Bouguer gravity data have been corrected for the effects of mass between the gravity stations and a reference level; this brings out subsurface density contrasts (Figure 6). Isostatic compensation of a mountain range by a low density root results in a large negative Bouguer anomaly. Isostatic gravity data corrections remove the effects of isostatic roots calculated to be present under mountainous regions; this yields information regarding the near surface density differences [Simpson *et al.*, 1986].

The basement gravity map (Figure 7) was produced by Richard Saltus of the U.S.G.S. following the procedure described in [Saltus and Jachens, 1995]. The map was produced by using gravity stations that sit on basement rock to construct an estimate of

the basement gravity grid. An estimate of the gravity field produced by sedimentary and volcanic rocks is made by subtracting the basement gravity grid from the isostatic residual gravity grid. The gravity field produced by sedimentary and volcanic rocks is then inverted for basin depth. Corrections for the basin effects are predicted iteratively on the basis of the basin gravity anomaly and the depth model for the basin.

## **GEOPHYSICAL ANOMALIES**

### ***Aeromagnetic Anomalies***

In order to determine the sources of magnetic anomalies, polygons delineating geologic units with magnetizations high enough to produce magnetic anomalies at the height of the surveys are overlain on the reduced-to-the-pole magnetic map (Figure 5). Trends, wavelengths, and amplitudes of magnetic anomalies can help determine their sources. Positive magnetic anomalies ( $> \sim 50$  nT) represent normally magnetized sources, such as dikes, granitic intrusions, volcanic flows, tuffs, and volcano-clastic units; low anomalies ( $< \sim 50$  nT) characterize non-magnetic sedimentary and metamorphic rocks in the region, and reverse-polarity magnetic sources. When an anomaly cannot be correlated with topography or mapped geology, the possibility of buried sources arises. Magnetic susceptibility measurements from the region and values from the literature (Table 2) aid in the identification of magnetic units.

Aeromagnetic anomalies within the Catalina MCC and within the surrounding mountain ranges, including the Tucson Mountains, Santa Rita Mountains, Galiuro Mountains and Sierrita Mountains (Figure 5), are correlated with outcrops when possible. Outcrops of Cretaceous granodiorites in the Santa Rita Mountains, located south of the Catalina-Rincon Mountains, correspond to high-amplitude positive anomalies [*Rystrom,*

2003]. The mid-Tertiary intrusive rocks exposed in the Sierrita Mountains are not associated with the high-amplitude positive anomalies [Rystrom, 2003]. Similarly, the outcrops in the Tucson Mountains located southwest of the Catalina MCC do not correlate with observed magnetic anomalies.

Within the Catalina MCC, the Leatherwood, Chirreon Wash plutons and the Rice Peak Porphyry cannot be easily correlated to a magnetic anomaly. The Precambrian Oracle/Ruin granite seems to correlate with a positive magnetic anomaly north of the Santa Catalina Mountains and a magnetic low within the range and thus, it is interpreted to be variably magnetic. The outcrops of the Catalina granitic pluton near the Pirate fault and the Tortolita granite pluton located in the Tortolita Mountains correlate with positive anomalies and thus are interpreted to be the sources of these anomalies. The Tortolita granite pluton is of similar age to the Catalina granite and is part of the Catalina magmatic suite [Keith *et al.*, 1980]. The Wilderness granite, with an average susceptibility of 0.00032 SI, intrudes Oracle/Ruin granite and corresponds to a large magnetic low (Figure 5). The Wilderness and Oracle/Ruin granites have been deformed to form mylonites. The mylonites produce high frequency magnetic highs with high measured susceptibilities, which can be observed along the southwest side of the range (Figure 5). Volcanic rocks in the southern Galiuro Mountains also produce high frequency magnetic anomalies in regions with high resolution data coverage.

The aeromagnetic anomalies over the Tucson Basin and Catalina MCC region are dominated by a NW–SE trending positive (up to ~300 nT) ~100 km long and ~30 km wide magnetic anomaly that is bordered to both the NE and SW by NW–SE trending long wavelength magnetic lows. The contact between the magnetic high and the

magnetic low to the NE is sharp and in isolated areas corresponds to the location of the Catalina detachment fault, but mostly does not. The western edge of the positive anomaly is a steep gradient corresponding to the high angle Pirate fault, which cuts the NW side of the Santa Catalina Mountains (Figure 1). The east side of the range is cut by the Martinez high angle fault, which does not produce a clear magnetic signal, because the surficial rocks are not magnetic.

Interpretation of older aeromagnetic data over the Tucson Basin identified the NW–SE trending anomaly and NE trending structures within the aeromagnetic data and interpreted the positive magnetic anomaly to be a batholith. The age of the batholith was hypothesized to be either Late Cretaceous (not Laramide), Laramide or mid-Tertiary [Sauk *et al.*, 1971]. In a more recent study of the Tucson Basin and Rincon Mountains by Rystrom [2003] low susceptibility Precambrian granodiorites and gneiss that outcrop at the surface in the Rincon Mountains are interpreted to be partially responsible for the positive anomaly, but a pluton that is not exposed at the surface is needed to fully explain the anomaly. Rystrom [2003] modeled the pluton with a density contrast of zero and a susceptibility of 0.035 SI based on the properties of Cretaceous/Tertiary igneous rocks in the region. No Laramide age rocks outcrop in the surface in this region and thus cannot be correlated with the high [Rystrom, 2003]. This pluton or batholith extends from along the southwestern edge of Santa Catalina Mountains along the Rincon Mountains and terminates along the western edge of the Santa Rita Mountains.

The magnetic lows to the NE of the positive magnetic anomaly are attributed to the Wilderness granitic suite, and magnetic lows to the SW are attributed to over 3000 meters of fill and sedimentary rocks within the Tucson Basin [Rystrom, 2003].

### ***Gravity Anomalies***

In order to determine the sources of gravity anomalies, polygons delineating geologic units are overlain on the Bouguer gravity map (Figure 6). Similar to the aeromagnetic anomalies, the Bouguer gravity anomalies over the Tucson Basin and Catalina MCC region show a NW-SE trending gravity high (up to ~ -100 mGal ) that is bordered to the NE by a gravity low (~ -150 mGal). Previous gravity modeling concluded that the Wilderness suite is responsible for the gravity low over the center of the Catalina MCC and the granites likely extend to 7–12 km below the surface [*Holt et al.*, 1986]. The Catalina Granite also corresponds to a gravity low.

Southwest of the Catalina MCC a Bouguer gravity low corresponds to the location of the Tucson Basin. A Cretaceous quartz monzonite and a small Jurassic rhyolitic porphyry pluton were interpreted to be responsible for the positive gravity anomaly over the Tucson Mountains [*Rystrom*, 2003].

North of the Santa Catalina Mountains the mapped location of Precambrian Oracle/Ruin granite corresponds to a positive gravity anomaly. The Oracle Granite is intruded by the Wilderness suite within the Santa Catalina Mountains and does not correspond to a positive gravity anomaly. A high amplitude gravity high is present over both the Tortolita Mountains and the Tucson Mountains.

### **MODELING RESULTS**

Forward modeling of the aeromagnetic and isostatic gravity data was performed using GM-SYS software in order to: 1) constrain the nature of the contact between the magnetic/dense body and the Wilderness suite, 2) constrain the depth of the magnetic/dense body and 3) distinguish between mechanisms of MCC formation such as,

upwarping of the lower crust and pluton emplacement. Two NE-SW trending profiles (A-A' and B-B'), which transect the magnetic/gravity "high" and the magnetic/gravity "low" were modeled (Figures 8 and 9). For all models the background crustal density was  $2670 \text{ kg/m}^3$  based on the measured outcrops of granitoids in the region [Gettings, 1996]; the background susceptibility was 0 SI based on the susceptibilities measured from the Exxon well (32) drilled in the Tucson Basin. The susceptibilities and density contrasts used for the crustal sections are shown in Table 3.

Cross-section A-A' represents the northern most model. The southeast portion of the model intersects the Tucson Basin. The thickness and density contrasts of the Tucson Basin sediments are based on previous gravity and density models [Rystrom, 2003] and information obtained from Exxon well (32) [Houser *et al.*, 2004]. The Wilderness suite sills crop out at the surface and represent the -200 nT magnetic low and the -10 to -20 mGal gravity low over the Catalina MCC. The mylonitic rocks are modeled with susceptibilities 0.004 SI and density contrast ranging from  $-40$  to  $0 \text{ kg/m}^3$ . To the southwest the gravity and magnetic high can be modeled as an igneous pluton with an assigned susceptibility of 0.035 SI and a density contrast of  $37 \text{ kg/m}^3$ . The body is not exposed at the surface, it is as shallow as  $\sim 1$  km, and reaches a depth of  $\sim 11$  km to the northwest where it thickens rapidly and is in sharp, nearly vertical, contact with the Wilderness suite. Paleozoic sedimentary rocks on the northwest edge of the profile have an assigned density contrast of  $-310 \text{ kg/m}^3$  and a susceptibility of 0 SI.

Cross section B-B' was modeled along the main gravity and magnetic high and the gravity and magnetic low. The gravity and magnetic low is again represented by the Wilderness suite sills (density contrast =  $-64.2 \text{ kg/m}^3$ , susceptibility = 0.001 SI). An

igneous body is responsible for the positive gravity and positive magnetic anomalies, pluton thickens gradually towards the Wilderness suite sills and again the contact with the Wilderness suite is the steeply dipping pluton, (density contrast =  $38 \text{ kg/m}^3$ , susceptibility = 0.035 SI). One of the main differences between the southern model and the northern model is that the pluton is generally thicker and it is partially underneath the Wilderness suite sills exposed at the surface as mylonites in cross-section B-B'. Tucson Basin sediments are observed on the southwest edge of the model and are assigned a density contrast of  $-272.6 \text{ kg/m}^3$  and a susceptibility of 0 SI. Paleozoic sediments are observed on the northeast edge of the profile and have assigned density contrasts of  $-173 \text{ kg/m}^3$  and  $-44.5 \text{ kg/m}^3$  and susceptibilities of 0 SI and 0.022 SI.

The pluton observed in both cross-sections is not exposed, but is likely granite to granodiorite in composition based on the magnetic susceptibility. The highest reasonable value of magnetic susceptibility for a granodiorite is  $\sim 0.042 \text{ SI}$  [Hunt *et al.*, 1995]. However, with a lower magnetic susceptibility of zero and similar density contrast ( $40 \text{ kg/m}^3$ ) the pluton thickness was  $\sim 20 \text{ km}$ .

## **DISCUSSION**

### ***Thermochronologic Data***

$^{40}\text{Ar}/^{39}\text{Ar}$  data from potassium feldspar and either muscovite or biotite were obtained from seven samples from the Wilderness sills (Chapter 2). The majority of the older  $^{40}\text{Ar}/^{39}\text{Ar}$  apparent ages from feldspar, muscovite and biotite were obtained from the structurally higher sills in the main range, and the younger  $^{40}\text{Ar}/^{39}\text{Ar}$  apparent ages were obtained on samples from structurally lower sills indicating that the structurally highest sills cooled first followed by sills at structurally lower depths in the forerange.

The potassium feldspar samples from the Wilderness suite sills yield  $^{40}\text{Ar}/^{39}\text{Ar}$  age gradients with upper intercepts ranging from ~31 to 28 in the main range and ~28 to 26 Ma in the forerange, and lower intercepts ranging from ~25 to 23 Ma in the main range, and ~23 to 22 Ma in the forerange.

The potassium feldspar age gradients may be the result of cooling within the potassium feldspar closure temperature window for ~ 5 million years or thermal resetting by the Catalina pluton prior to exhumation along the Catalina detachment fault. The Catalina pluton has a U/Pb age of ~26 Ma [Fornash *et al.*, in prep].  $^{40}\text{Ar}/^{39}\text{Ar}$  lower intercepts from feldspar in the main range suggest that exhumation of the main range occurred ~25 to 23 million years ago. In the forerange, concordant AFT and ZFT data and  $^{40}\text{Ar}/^{39}\text{Ar}$  potassium feldspar lower age intercepts suggest rapid cooling due to exhumation ~23 to 22 million years ago.

*Fayon et al.* [2000] used apatite fission track (AFT) and zircon fission track (ZFT) ages, from samples collected along a southwest-northeast trending profile, to determine the lower temperature cooling history along the Catalina detachment fault. This study determined the low temperature history was not a one-stage cooling history, but was more complicated. A period of rapid cooling is recorded by the concordant ZFT and AFT ages in the forerange and concordant higher temperature thermochronometers [Davy *et al.*, 1989b] and ZFT ages in the main range. In the main range the AFT ages have a weighted mean of  $17.8 \pm 0.4$  Ma and the ZFT ages have a weighted mean of  $28.7 \pm 2.0$  Ma. Samples from the forerange yielded AFT ages have a weighted mean average of  $20.1 \pm 1.0$  Ma, and ZFT ages have a weighted mean average of  $23.6 \pm 3.9$  Ma [Fayon *et al.*, 2000].



The period of rapid cooling was followed by a period of slower cooling, suggested by shortened confined apatite fission track lengths (<14 $\mu$ m). The zircon fission track ages decrease in the direction of slip and the apatite fission track ages increase in the direction of slip; this unusual trend is interpreted by *Fayon et al.* [2000] to indicate that the main range remained at higher temperatures and cooled slowly during the later stages of detachment faulting possibly due to intrusion of the Catalina pluton which affected the AFT ages.

### ***Age of the pluton***

We interpret the subsurface body responsible for the positive gravity and magnetic anomalies to be a ~ 20 km wide and ~100 km long pluton. *Sauk et al.* [1971] suggested Cretaceous or mid-Tertiary as possible ages of the pluton or batholith. Given the extent of Precambrian plutons in the region, the possibility of a Precambrian pluton must also be considered. The age of the subsurface pluton is critical to understanding its role (if any) in MCC formation. The presence of a large subsurface pluton in an extended terrane requires reassessment of the importance of magmatism in forming MCCs. Thermochronology data from the footwall has the potential to record cooling and reheating events. A large igneous body that is not exposed at the surface has the potential to reset or partially reset thermochronometers at the surface. The majority of the footwall is composed of Wilderness suite granites and thus minerals within the Wilderness suite are appropriate to use to understand the thermal history of the footwall. The possible effect of a pluton on thermochronometers from the Wilderness suite depends on the timing of pluton emplacement relative to Wilderness emplacement and cooling (Table 4).

The subsurface pluton may be equivalent to the Precambrian Oracle/Ruin or the Continental Granodiorite pluton which outcrop in the Catalina MCC and the Santa Rita Mountains. A Precambrian pluton would have cooled prior to MCC exhumation and would have no thermal affect on younger intrusive rocks. However, the Oracle/Ruin granite is responsible for a positive magnetic anomaly located north of the Santa Catalina Mountains, and is intermingled with the Wilderness suite granites that are responsible for the NW-SE trending magnetic low and is interpreted to be variable magnetic. The subsurface pluton does not fit the observed trends for Precambrian plutons in the western United States; 1.4 Ga plutons trend NE-SW and 1.1 Ga plutons trend N-S [*Karlstrom and Humphreys, 1998*].

Exxon State (32)-1 well penetrated 169 meters of granitoid crystalline rock between 3,658 and 3,827 meters depth in the Tucson Basin [*Houser et al., 2004*]. Only rock cuttings of the granitoid rock, which is interpreted to represent basement rock, are available and the age is not known; it is assumed to be either Mesozoic or Precambrian in age based on the sediments found above the granitoid [*Houser et al., 2004*]. In a 2-dimensional model across the Tucson Basin, *Rystrom* [2003] connects the basement rock of the Tucson Basin with Precambrian granite that outcrops at the surface within the Rincon Mountain.

A Mesozoic pluton or pluton associated with Laramide deformation which lasted into the Tertiary in southern Arizona [~55 Ma; *Dickinson, 1991*] is also possible. Mesozoic plutons are represented by the Leatherwood suite in the Santa Catalina Mountains, the Amole pluton in the Tucson Mountains and Cretaceous granodiorites in the Santa Rita Mountains. Neither the Leatherwood suite, which is a minor intrusion in

comparison to the Wilderness suite or Oracle Granite, nor the Amole pluton, are clearly correlated with a positive magnetic or gravity anomaly. However, the Cretaceous granodiorites outcropping in the Santa Rita Mountains located south of the Santa Catalina-Rincon Mountains correspond to high-amplitude positive anomalies [Rystrom, 2003], which do not exhibit the same map pattern as the subsurface body. The granite of Alamo Canyon is exposed along the Pirate fault over a portion of the subsurface body; however field measurements indicate an average susceptibility of 0.008 SI. If the subsurface body is assumed to be Mesozoic in age a pre-existing zone of weakness may be responsible for the location and trend of this body, which is in sharp contact with the extensive Wilderness suite.

If the subsurface pluton was emplaced during the Tertiary, it may overlap the timing of emplacement of the Wilderness suite, Catalina suite and/or detachment faulting. Radiometric data from various minerals with specific closure temperature ranges have been used to constrain the cooling history of the magmatic suites that intrude the footwall of the Catalina MCC [Davy *et al.*, 1989a]. The Catalina pluton does not correspond to a positive gravity anomaly and thus the subsurface pluton cannot be equivalent in composition to the Catalina pluton, however it is possible that the subsurface pluton is Tertiary in age and related to exhumation of the Catalina MCC due to the proximity and parallel relationship with the detachment fault.

## **CONCLUSIONS**

Aeromagnetic data and gravity data indicate that a subsurface pluton is present beneath the northeast side of the Tucson Basin and along the southwest side of the Catalina MCC. Forward modeling of the data indicate that the subsurface pluton is felsic

to intermediate, shallow, and is in sharp contact with the peraluminous Wilderness suite sills.

Based on the intrusions in the region the age of the pluton may be equivalent in age to the Precambrian Oracle Granite, the Laramide Leatherwood suite, or the Catalina suite.  $^{40}\text{Ar}/^{39}\text{Ar}$  data from potassium feldspars indicate that Wilderness suite sills experienced slow cooling for ~5 million years or were partially reset due to a thermal event. Intrusion of the Catalina pluton correlates with the timing of resetting; however the relationship to the subsurface pluton is not clear.

We favor a Tertiary age or Mesozoic age pluton over a Precambrian age pluton because Precambrian rocks in the region are variably magnetic. In addition, the subsurface body does not follow NE-SW trend associated 1.4 Ga plutons or the N-S trend of 1.1 Ga plutons [*Karlstrom and Humphreys, 1998*].

A Mesozoic age intrusion suggests that crustal thickening may have played an important role in forming the Catalina MCC. The sub parallel relationship between the subsurface pluton and the Wilderness suite sills also suggests that a zone of weakness of unknown origin may be present and controlled the location of magmatism. However, a Tertiary age pluton suggests that syn-tectonic magmatism influenced the location of the Catalina detachment fault and the Catalina MCC.

## REFERENCES

Abers, G. A., et al. (1997), Earthquakes in the Woodlark-D'Entrecasteaux rift system, Papua New Guinea, *Journal of Geophysical Research*, 102(B7), 15,301-315,317.

Aleinikoff, J. N., et al. (2006), Deciphering igneous and metamorphic events in high-grade rocks of the Wilmington Complex, Delaware: Morphology, cathodoluminescence and backscattered electron zoning, and SHRIMP U-Pb geochronology of zircon and monazite, *Geological Society of America Bulletin*, 118(1/2), 39-64.

Anderson, E. M. (1972), *The Dynamics of Faulting and Dyke Formation with Application to Britain (reprint of the 1951 Edition)*, 206 pp., Hafner Publishing Company, New York

Armstrong, R. L., and P. Ward (1991), Evolving Geographic Patterns of Cenozoic Magmatism in the North American Cordillera: The Temporal and Spatial Association of Magmatism and Metamorphic Core Complexes, *Journal of Geophysical Research*, 96(B8), 13201-13224.

Atwater, T., and J. Stock (1998), Pacific-North America Plate Tectonics of the Neogene Southwestern United States: An Update, *International Geology Review*, 40, 375-402.

Axen, G. J. (2007), Research Focus: Significance of large-displacement, low-angle normal faults, *Geology*, 35(3), 287-288.

Baranov, V., and H. Naudy (1964), Numerical Calculation of the Formula of Reduction to the Magnetic Pole, *Geophysics*, 29(1).

Barbarin, B. (1996), Genesis of the two main types of peraluminous granitoid, *Geology*, 24(4), 295-298.

Bernet, M., et al. (2002), Determining the Zircon Fission-track Closure Temperature, *Geological Society of America Cordilleran Section Meeting*.

Bird, P. (1998), Kinematic history of the Laramide orogeny in latitudes 35 degrees- 49 degrees N, western United States, *Tectonics*, 17, 780-801.

Blakely, R. J. (1995), *Potential theory in gravity & magnetic applications*, 441 pp., Cambridge University Press.

Bourgeix, A. L., et al. (2006), Argon loss in experimentally deformed muscovites, paper presented at Goldschmidt Conference Abstracts.

Bowring, S. A., and I. S. Williams (1999), Priscoan (4.00-4.03 Ga) orthogneisses from northwestern Canada, *Contributions to Mineralogy and Petrology*, 134, 3-16.

Bykerk-Kauffman, A. (2008), Geologic map of the northeastern Santa Catalina Mountains, Pima County, Arizona.

Catanzaro, E. J., and J. L. Kulp (1964), Discordant zircons from the Little Belt (Montana), Beartooth (Montana) and Santa Catalina (Arizona) Mountains, *Geochimica et Cosmochimica Acta*, 28, 87-124.

Coney, P. J. (1980a), Cordilleran metamorphic core complexes: An overview, in *Cordilleran Metamorphic Core Complexes*, edited by M. D. Crittenden Jr., et al., pp. 7-34, The Geological Society of America, Inc. Memoir 153.

- Coney, P. J. (1980b), Cordilleran metamorphic core complexes: An overview, in *Cordilleran Metamorphic Core Complexes*, edited by J. Crittenden, M.D., et al., pp. 7-34, Geological Society of America.
- Corfu, F., et al. (2003), Atlas of zircon textures, in *Zircon*, edited by J. M. Hanchar and P. W. O. Hosking, Mineralogical Society of America Geochemical Society.
- Damon, P. E., et al. (1963), K-Ar dating of Basin and Range uplift, Catalina Mountains, Arizona, *Nuclear Geophysics, National Academy of Sciences/National Research Council Publication, 1075*, 113-121.
- Davis, G. A., and G. S. Lister (1988), Detachment faulting in continental extension: Perspectives from the southwestern U.S. Cordillera, in *Processes in continental lithospheric deformation*, edited by S. P. Clark Jr., pp. 133-159.
- Davis, G. A., et al. (2004), Fault and fault-rock characteristics associated with Cenozoic extension and core-complex evolution in the Catalina-Rincon region, southeastern Arizona, *GSA Bulletin, 116(1/2)*, 128-141.
- Davy, P., et al. (1989a), Thermal constraints on the tectonic evolution of a metamorphic core complex (Santa Catalina Mountains, Arizona), *Earth and Planetary Science Letters, 94*, 425-440.
- Davy, P., et al. (1989b), Thermal constraints on the tectonic evolution of a metamorphic core complex (Santa Catalina Mountains, Arizona), *Earth and Planetary Science Letters, 94*, 425-440.

- Dickinson, W. R. (1991), *Tectonic setting of faulted Tertiary strata associated with the Catalina core complex in southern Arizona*, 106 pp.
- Dickinson, W. R. (1999), Geologic framework of the Catalina foothills, outskirts of Tucson (Pima County, Arizona), scale 1:24,000, 031 p.
- Dodson, M. H. (1973), Closure temperature in cooling geochronological and petrological systems, *Contributions to Mineralogy and Petrology*, 40, 259-274.
- Ehlers, T. A. (2005), Crustal thermal processes and the interpretation of thermochronometer data, in *Low-Temperature Thermochronology: Techniques, Interpretations, and Applications*, edited by P. W. Reiners and T. A. Ehlers, pp. 315-349, Mineralogical Society of America and Geochemical Society.
- Farmer, G. F., et al. (2005), Paleoproterozoic Mojave province in northwestern Mexico? Isotopic and U-Pb zircon geochronologic studies of Precambrian and Cambrian crystalline and sedimentary rocks, Caborca, Sonora, *Geological Society of America Bulletin Special Paper 393*, 183-1998.
- Farmer, G. L., et al. (1989), Isotopic Evidence on the Structure and Origin of Subcontinental Lithospheric Mantle in Southern Nevada, *Journal of Geophysical Research*, 94(B6), 7885-7898.
- Fayon, A. K., et al. (2000), Fission track analysis of the footwall of the Catalina detachment fault, Arizona: Tectonic denudation, magmatism and erosion, *Journal of Geophysical Research*, 105(B5), 11047-11062.



Force, E. R. (1997), Geology and Mineral Resources of the Santa Catalina Mountains, Southeastern Arizona, *Monographs in Mineral Resource Science No. 1*, 135.

Forster, M. A., and G. S. Lister (Eds.) (1999), *Detachment faults in the Aegean core complex of Ios, Cyclades, Greece*, Geological Society, London, Special Publications, London.

Frassetto, A., et al. (2006), Support of high elevation in the southern Basin and Range based on the composition and architecture of the crust in the Basin and Range and Colorado Plateau, *Earth and Planetary Letters*, 249, 62-73.

Gehrels, G. E., and C. H. Smith (1991), U-Pb geochronologic constrains on the age of thrusting, crustal extension, and peraluminous plutonism in the Little Rincon Mountains, southern Arizona, *Geology*, 19, 238-241.

Gehrels, G. E., et al. (2008), Enhanced precision, accuracy, efficiency, and spatial resolution of U-Pb ages by laser ablation--multicollector--inductively coupled plasma--mass spectrometry, *Geochemistry Geophysics Geosystems*, 9(3), 1-13.

Gettings, M. (1996), An interpretation of the 1996 aeromagnetic data for the Santa Cruz basin, Tumacacori Mountains, Santa Rita Mountains, and Patagonia Mountains area, south-central Arizona, *US Geological Survey Open-File Report*, 97-676.

Harley, S. L., et al. (2007), Zircon Behaviour and the Thermal Histories of Mountain Chains, edited by Elements, pp. 25-30.

Harrison, T. M., et al. (1999), Origin and Episodic Emplacement of the Manaslu Intrusive Complex, Central Himalaya, *Journal of Petrology*, 40(1), 3-19.

Harrison, T. M., et al. (2009), Diffusion of  $^{40}\text{Ar}$  in muscovite, *Geochimica et Cosmochimica Acta*, 73, 1039-1051.

Hill, E. J., et al. (1992), Unroofing of active metamorphic core complexes in the D'Entrecasteaux Islands, Papua New Guinea, *Geology*, 20(10), 907-910.

Holt, W. E., et al. (1986), Crustal structure from three-dimensional gravity modeling of a metamorphic core complex: A model for uplift, Santa Catalina-Rincon mountains, Arizona, *Geology*, 14, 927-930.

Houser, B. B., et al. (2004), Stratigraphy and Tectonic History of the Tucson Basin, Pima County, Arizona, Based on the Exxon State (32)-1 Well, *Scientific Investigations Report 2004-5076*, 37.

Hunt, C. P., et al. (1995), Magnetic Properties of Rocks and Minerals, in *AGU Shelf Reference*, edited, pp. 189-204.

Johnson, R. A., and K. L. Loy (1992), Seismic reflection evidence for seismogenic low-angle faulting in southeastern Arizona, *Geology*, 20, 597-600.

Karlstrom, K. E., and E. D. Humphreys (1998), Persistent influence of Proterozoic accretionary boundaries in the tectonic evolution of southwestern North America; interaction of cratonic grain and mantle modification events, *Rocky Mountain Geology*, 33(2), 161-179.

Keith, S. B., et al. (1980), Evidence for multiple intrusion and deformation within the Santa Catalina-Rincon-Tortolita crystalline complex, southeastern Arizona, in *Cordilleran Metamorphic Core Complexes*, edited by M. D. Crittenden Jr., et al., pp. 217-268, The Geological Society of America, Inc. Memoir 153.

Kelley, S. (2002), Excess argon in K-Ar and Ar-Ar geochronology, *Chemical Geology*, 188, 1-22.

Lipman, P. W. (1993), Geologic Map of the Tucson Mountains Caldera, Southern Arizona, Map I-2205.

Lister, G. S., and S. L. Baldwin (1993), Plutonism and the origin of metamorphic core complexes, *Geology*, 21, 607-610.

Lovera, O. M., et al. (1997), Systematic analysis of K-feldspar  $^{40}\text{Ar}/^{39}\text{Ar}$  step heating results: I. Significance of activation energy determinations, *Geochimica et Cosmochimica Acta*, 61(15), 3171-3192.

Ludwig, K. R. (1998), On the treatment of concordant uranium-lead ages, *Geochimica et Cosmochimica Acta*, 62(4), 665-676.

Ludwig, K. R. (2000), Users Manual for Isoplot/Ex version 2.3, A Geochronological Toolkit for Microsoft Excel, *Berkeley Geochronology Special Publication No. 1a*, 1-54.

Ludwig, K. R. (2003), Users Manual for Isoplot/Ex version 3.0, A Geochronological Toolkit for Microsoft Excel, *Berkeley Geochronology Special Publication No. 4*, 1-70.

- Mauger, R. L., et al. (1968), Cenozoic Argon Ages on Metamorphic Rocks From the Basin and Range Province, *American Journal of Science*, 266, 579-589.
- McDougall, I., and T. M. Harrison (1999), *Geochronology and Thermochronology by the  $^{40}\text{Ar}/^{39}\text{Ar}$  Method*, Second ed., 269 pp., Oxford University Press, New York.
- McQuarrie, N., and M. Oskin (2010), Palinspastic restoration of NAVDat and implications for the origin of magmatism in southwestern North America, *Journal of Geophysical Research*, 115, 1-16.
- Mulch, A., et al. (2002), In-situ UV-laser  $^{40}\text{Ar}/^{39}\text{Ar}$  geochronology of a micaceous mylonite: an example of defect enhanced argon loss, *Contributions to Mineralogy and Petrology*, 142, 738-752.
- Myers, S. C., and S. Beck (1994), Evidence for a local crustal root beneath the Santa Catalina metamorphic core complex, Arizona, *Geology*, 22(3), 223-226.
- Nasdala, L., et al. (2003), Spectroscopic methods applied to zircon, in *Zircon*, edited by J. M. Hanchar and P. W. O. Hosking, pp. 427-467, Mineralogical Society of America Geochemical Society.
- Pan, Y. (1997), Zircon and Monazite forming Metamorphic Reactions at Manitouwadge, Ontario, *The Canadian Mineralogist*, 35, 105-118.
- Parrish, R. R., and S. R. Noble (2003), Zircon U-Th-Pb geochronology by isotope dilution--thermal ionization mass spectrometry (ID-TIMS), in *Zircon: Reviews in*

*Mineralogy and Geochemistry*, edited by J. M. Hanchar and P. W. O. Hoskin,  
Mineralogical Society of America and Geochemical Society, Washington, D.C.

Parson, T. (1995), The Basin and Range Province, in *Continental Rifts: Evolution, Structure, Tectonics*, edited by K. H. Olsen, pp. 277-316, Elsevier, New York.

Parsons, T., and G. A. Thompson (1993), Does magmatism influence low-angle normal faulting?, *Geology*, 21, 247-250.

Parsons, T. (1995), The Basin and Range Province, in *Continental rifts: evolution, structure, tectonics.*, edited by K. H. Olsen, pp. 277-324, Elsevier, Amsterdam.

Parsons, T., and J. McCarthy (1995), The active southwest margin of the Colorado Plateau: Uplift of mantle origin, *Geological Society of America Bulletin*, 107(2), 139-147.

Passchier, C. W., and R. A. J. Trouw (2005), *Microtectonics*, 2nd ed., Springer, New York.

Peterman, E. M., et al. (2011), Development and Intercalibration of Monazite (U-Th)/He Thermochronology: Catnip Sill, Catalina Core Complex, in *Geological Society of America Annual Meeting*, edited, p. 331, Minneapolis.

Petford, N., et al. (2000), Granite magma formation, transport and emplacement in the Earth's crust, *Nature*, 408(7), 669-673.

Reynolds, L. R., Rosenbaum, J.G., Hudson, M.R., and Fishman, N.S. (1987), Rock Magnetism, The Distribution of Magnetic Minerals in the Earth's Crust, and Aeromagnetic Anomalies, *Geologic Applications of Modern Aeromagnetic Surveys*.

Roberts, M. P., and F. Finger (1997), Do U-Pb zircon ages from granulites reflect peak metamorphic conditions?, *Geology*, 25(4), 319-322.

Rystrom, V. L. (2003), Structure of the Tucson Basin, Arizona from Gravity and Aeromagnetic data, *USGS Open-File Report 03-116*, 80 p.

Saltus, R. W., and R. C. Jachens (1995), Gravity and Basin-depth Maps of the Basin and Range Province, Western United States, U.S. Geological Survey.

Sambridge, M. S., and W. Compston (1994), Mixture modeling of multi-component data sets with application to ion-probe zircon ages, *Earth and Planetary Science Letters*, 128, 373-390.

Sauk, W. A., et al. (1971), Aeromagnetic map of the northern part of the Tucson Basin, Pima County, Arizona, *Arizona Geological Society Digest*, 9, 123-135.

Schaltegger, U. (2007), Hydrothermal Zircon, in *Elements*, edited, p. 51.

Shakel, D. W., et al. (1977), Observations on the history of the gneissic core complex, Santa Catalina Mts, southern Arizona, *Geological Society of America Abstracts with Programs*, 9, 1169-1170.

Simpson, R. W., et al. (1986), A New Isostatic Residual Gravity Map of the Conterminous United States With a Discussion on the Significance of Isostatic Residual Anomalies, *Journal of Geophysical Research*, 91(B8), 8348-8372.

Smith, H. A., and B. J. Giletti (1997), Lead diffusion in monazite, *Geochimica et Cosmochimica Acta*, 61(5), 1047-1055.

Spencer, J. E., and S. J. Reynolds (1989), Middle Tertiary Tectonics of Arizona and Adjacent Areas, *Geologica evolution of Arizona, Arizona Geological Society Digest*, 17, 539-574.

Spencer, J. E., et al. (2000), Compilation geologic map of the Oracle 7.5 Quadrangle, Pinal and Pima Counties, Arizona, scale 1:24,000 (001 sheet), 030 p.

Spencer, J. E., and P. A. Pearthree (2004), Geologic map of the Oro Valley 7.5 Quadrangle, Pima County, Arizona, version 2.0, scale 1:24,000.

Spencer, J. E. (2005), Intersecting Mylonitic Shear Zones in the Footwall of the Catalina Detachment Fault, Santa Catalina Mountains, Southeastern Arizona, paper presented at Eos Trans.AGU, (86(52) Fall Meet. Suppl., Abstract T24C-03.

Steiger, R. H., and E. Jager (1977), Subcommision on geochronology: Convention on the use of decay constants in geo- and cosmochronology, *Earth and Planetary Science Letters*, 36, 359-362.

Turrin, B. D., et al. (1994),  $^{40}\text{Ar}/^{39}\text{Ar}$  ages from the rhyolite of Alder Creek, California: Age of the Cobb Mountain Normal-Polarity Subchron revisited, *Geology*, 22(3), 251-254.

U.S.G.S. (1980), Aeromagnetic map of the Dragoons area, Arizona, edited, U.S. Geological Survey Open File Report. 80-998, scale 1:62,500.

U.S.G.S. (1982), Aeromagnetic map of the Rattlesnake area, Arizona, edited, U.S. Geological Survey Open File Report 82-658, 1 sheet, scale 1:62,500.

U.S.G.S. (2000), Three Aeromagnetic Surveys in south Central Arizona; A Web Site for Distribution of Data (on-line edition), edited, U.S. Geological Survey Open File Report 00-0155.

Wagner III, F. H., and R. A. Johnson (2006), Coupled basin evolution and late-stage metamorphic core complex exhumation in the southern Basin and Range Province, southeastern Arizona, *Tectonophysics*, 420(1-2, 26), 141-160.

Wayne, D. M., and A. K. Sinha (1992), Stability of Zircon U-Pb Systematics in a Greenschist-Grade Mylonite: An Example from the Rockfish Valley Fault Zone, Central Virginia, USA, *The Journal of Geology*, 100, 593-603.

Wong, M. S., and P. B. Gans (2003), Tectonic implications of early Miocene extensional unroofing of the Sierra Mazata'n metamorphic core complex, Sonora, Mexico, *Geology*, 31(11), 953-956.

Zen, E. (1988), Phase relations of peraluminous granitic rocks and their petrogenetic implications, *Annual Review of Earth and Planetary Science*, 16, 21-51.



## FIGURES

Figure 1. Generalized geologic map of the Santa Catalina, Rincon, Tortolita, Tucson and Galiuro Mountains [After *Dickinson*, 1991].

Figure 2. Simplified geologic map of the Catalina MCC, Arizona [from *Fornash et al.*, in prep.,]. Mapping based on [*Bykerk-Kauffman*, 2008; *Dickinson*, 1999; *Force*, 1997; *Spencer et al.*, 2000; *Spencer and Pearthree*, 2004].

Figure 3. Generalized geologic history of the Catalina MCC region. Time scale is logarithmic in Ma [After *Dickinson*, 1991 and references therein].

Figure 4. Topography of the Catalina MCC region. The colored outlined areas represent the geologic units shown in Figure 1. Black lines show locations of model cross-sections.

Figure 5. Aeromagnetic map of the Catalina MCC region. The colored outlined areas represent the geologic units shown in Figure 1. Black lines show locations of model cross-sections.

Figure 6. Bouguer gravity anomaly map of the Catalina MCC region. The colored outlined areas represent the geologic units shown in Figure 1. Black lines show locations of model cross-sections.

Figure 7. Basement gravity anomaly map of the Catalina MCC region [*Saltus*, personal communication, 2012]. The colored outlined areas represent the geologic units shown in Figure 1. Black lines show locations of model cross-sections

Figure 8. Cross-section of the northern profile (A-A'). The subsurface pluton is 2 km deep and ~7 km thick and ~18 km wide. The magnetic susceptibility is 0.028 SI and the density is 2730 kg/m<sup>3</sup>. Susceptibilities and densities are discussed in text.

Figure 9. Cross-section of the southern profile (B-B'). Susceptibilities and densities are discussed in text.

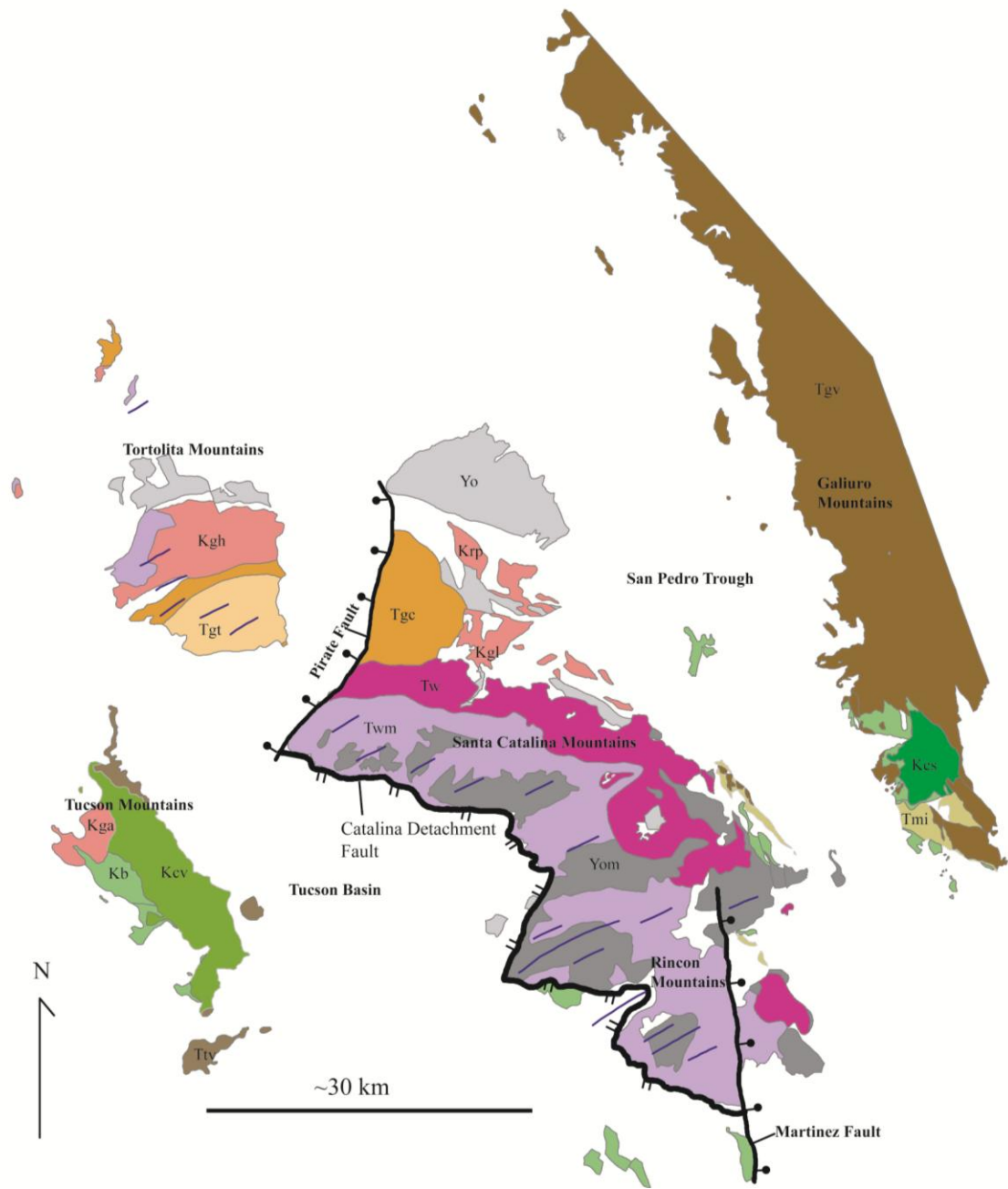


Figure 1.



Figure, 1 continued.

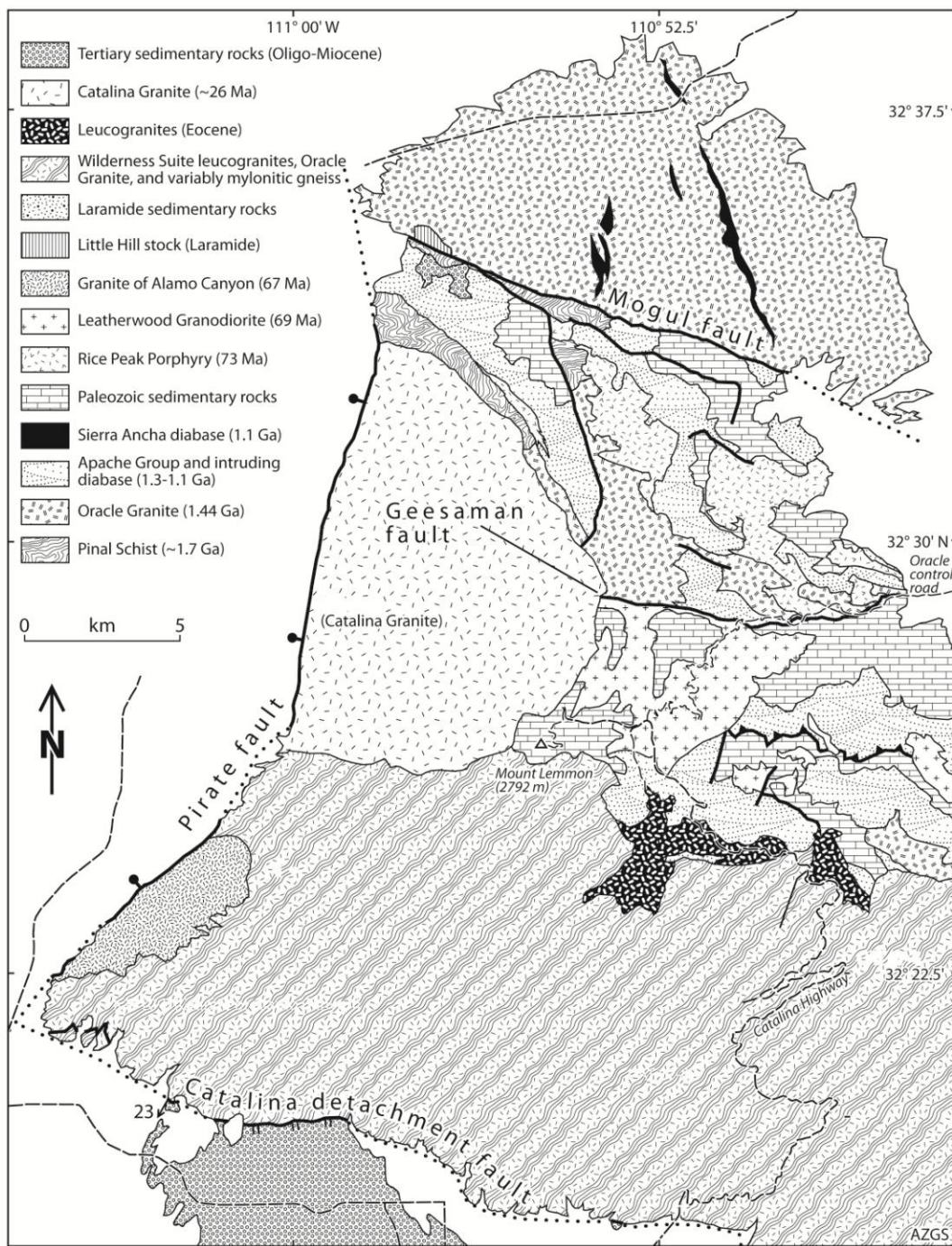


Figure 2.

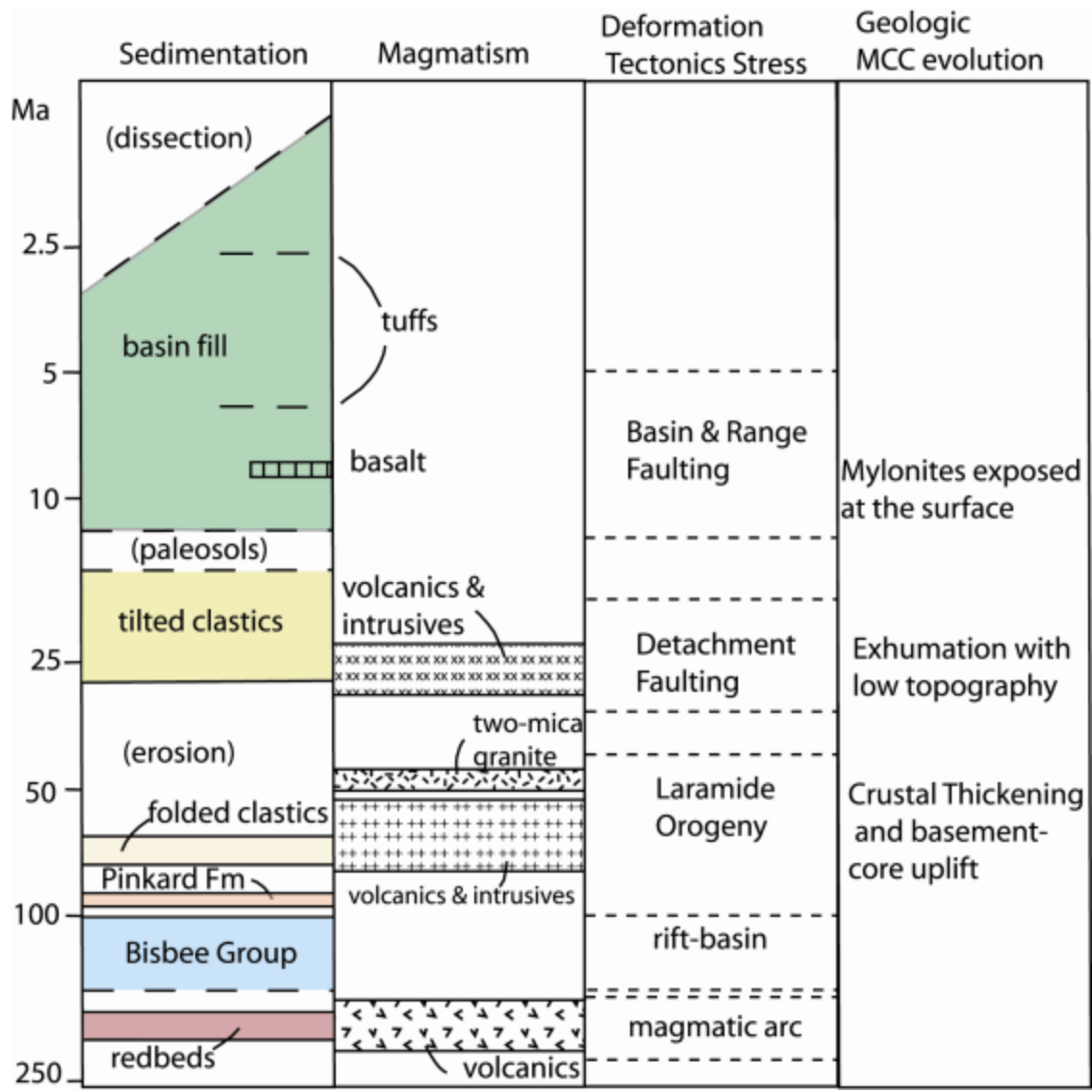


Figure 3.

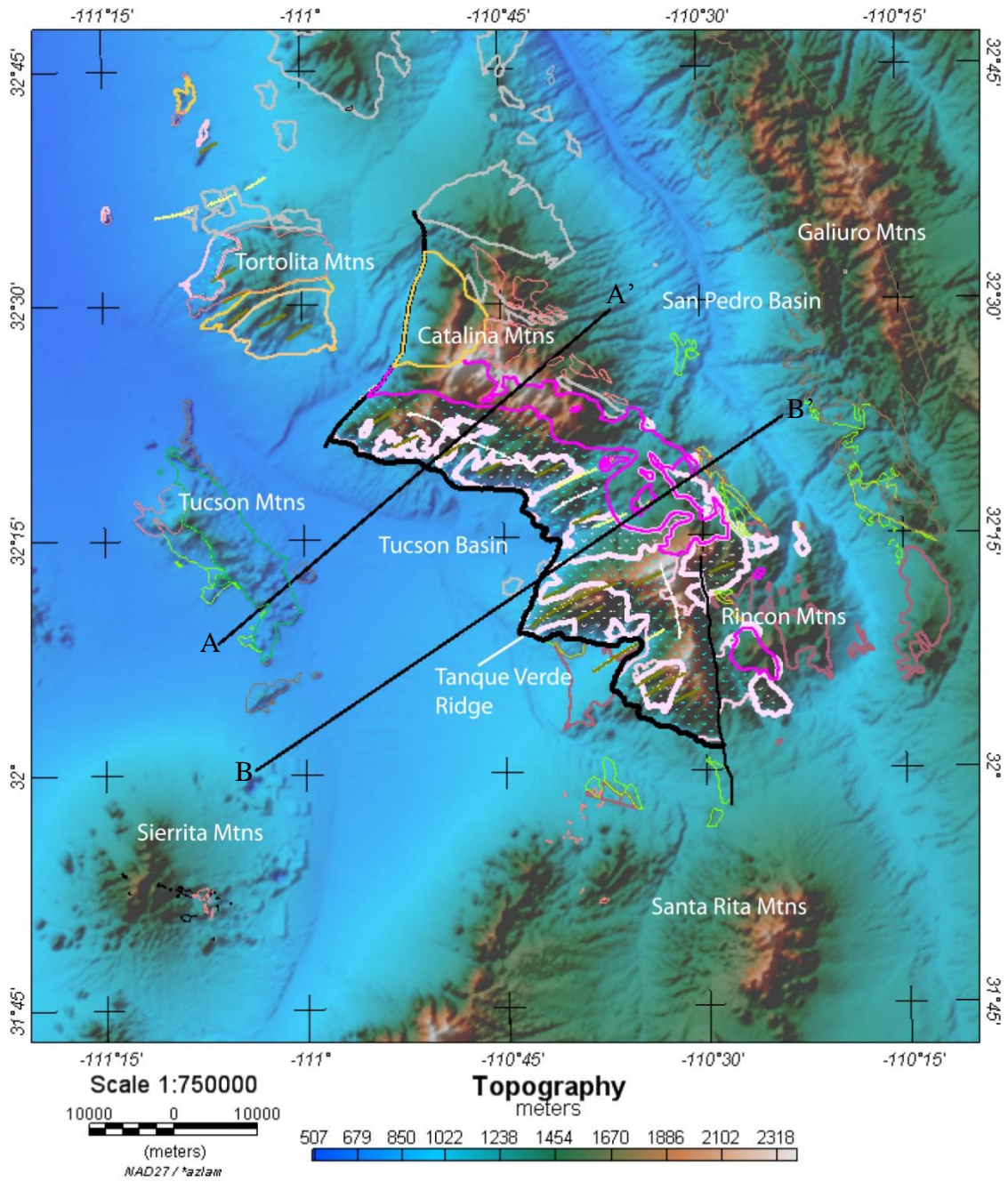


Figure 4.

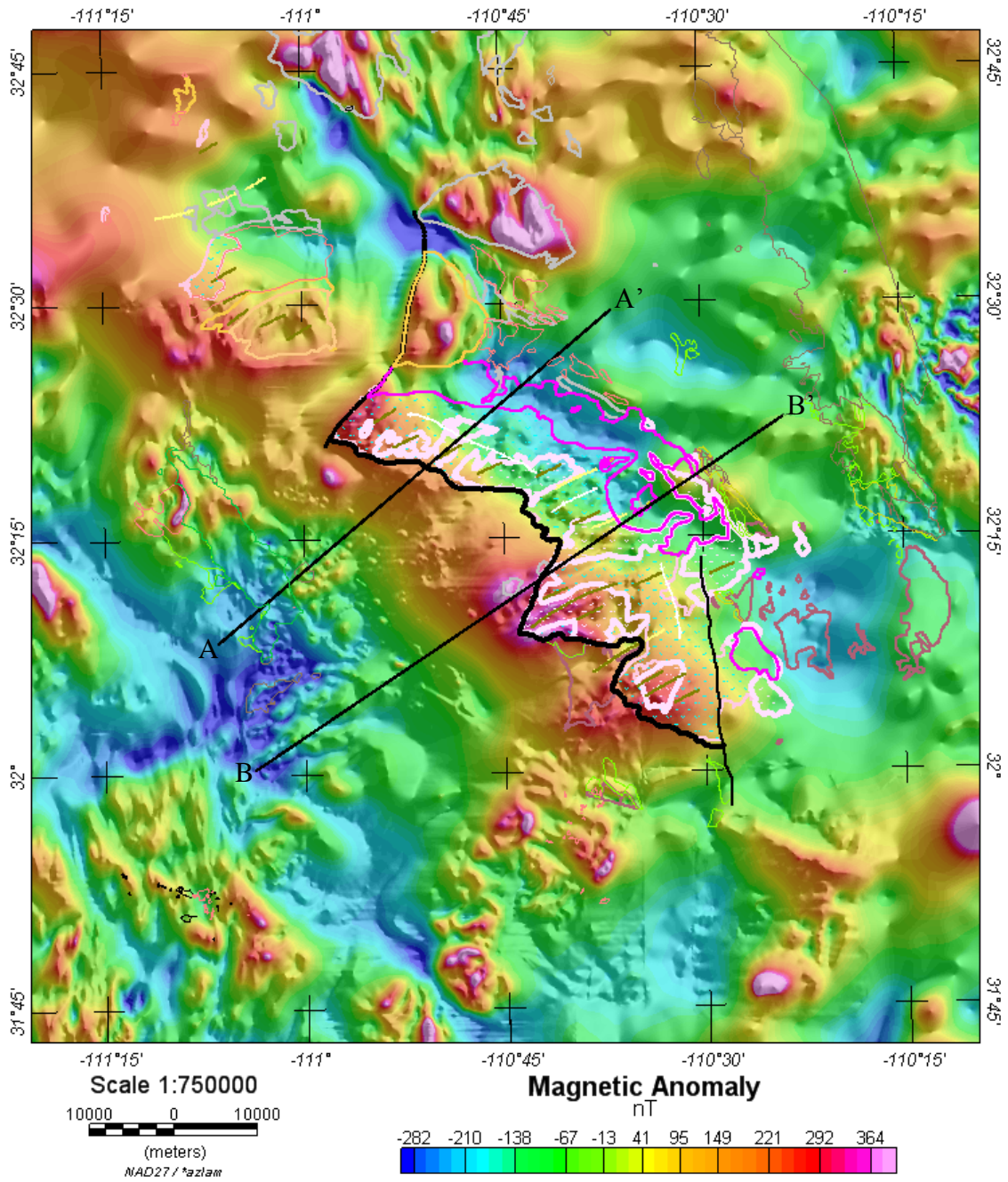


Figure 5.



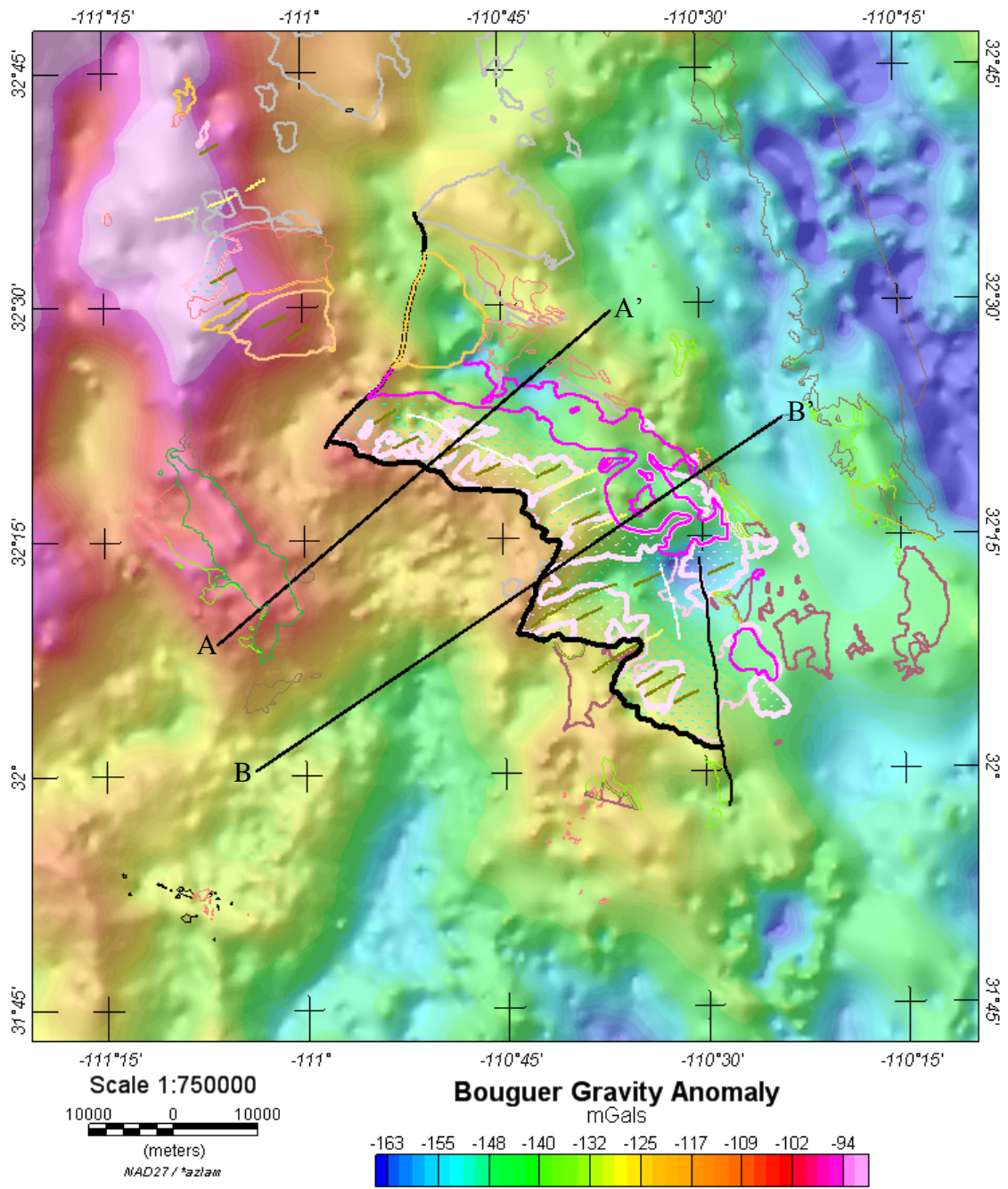


Figure 6.

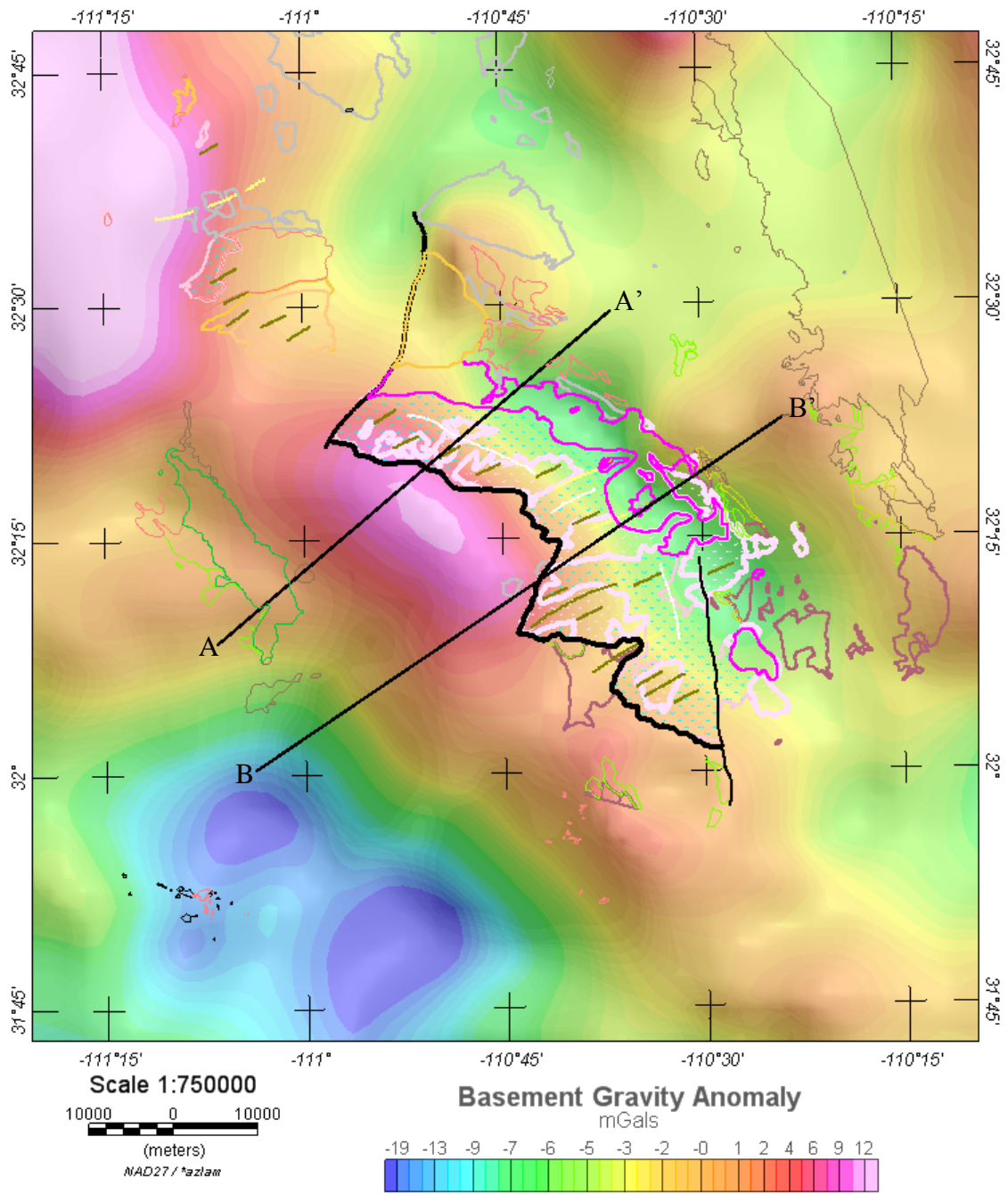


Figure 7.

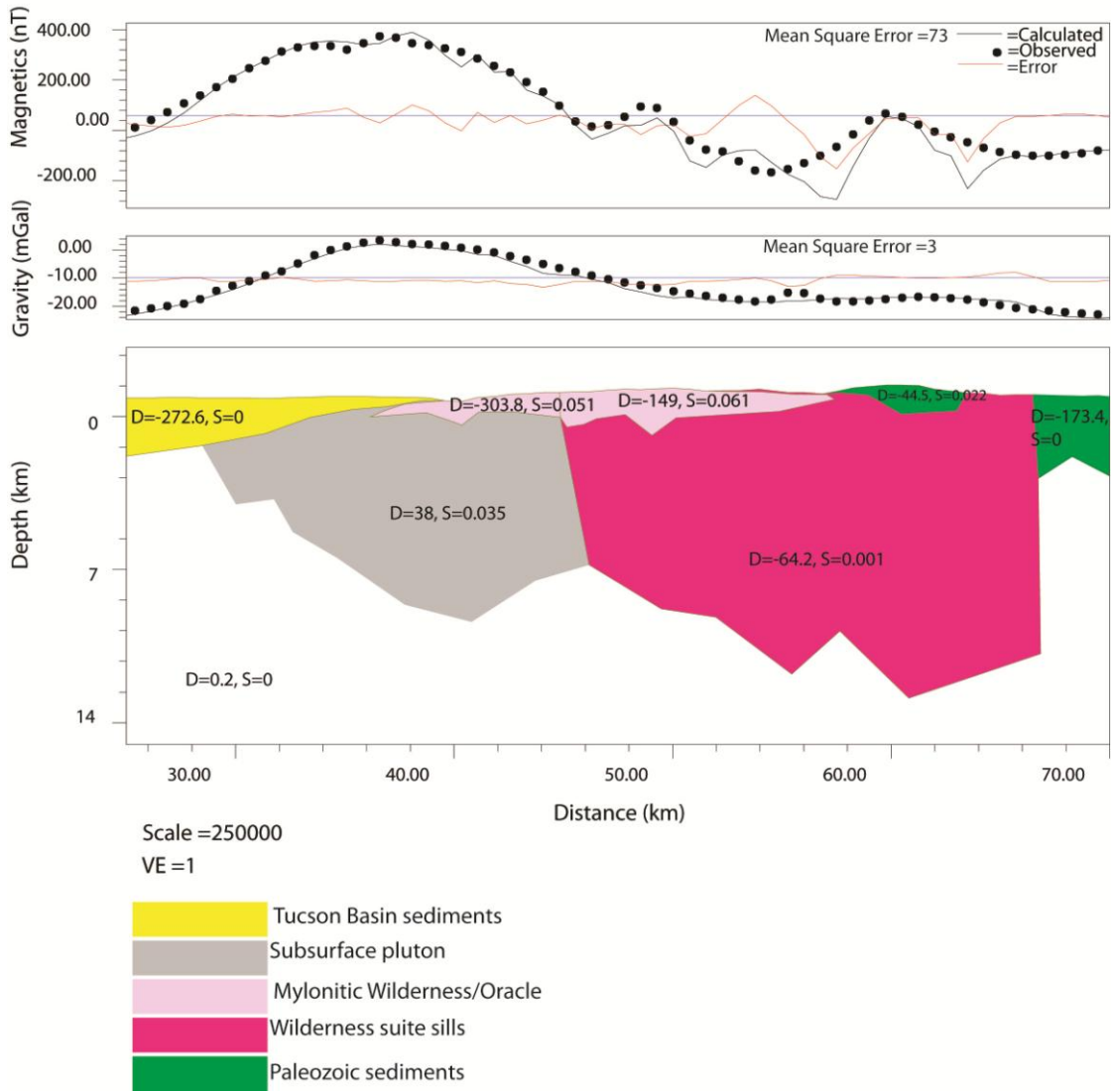


Figure 8.

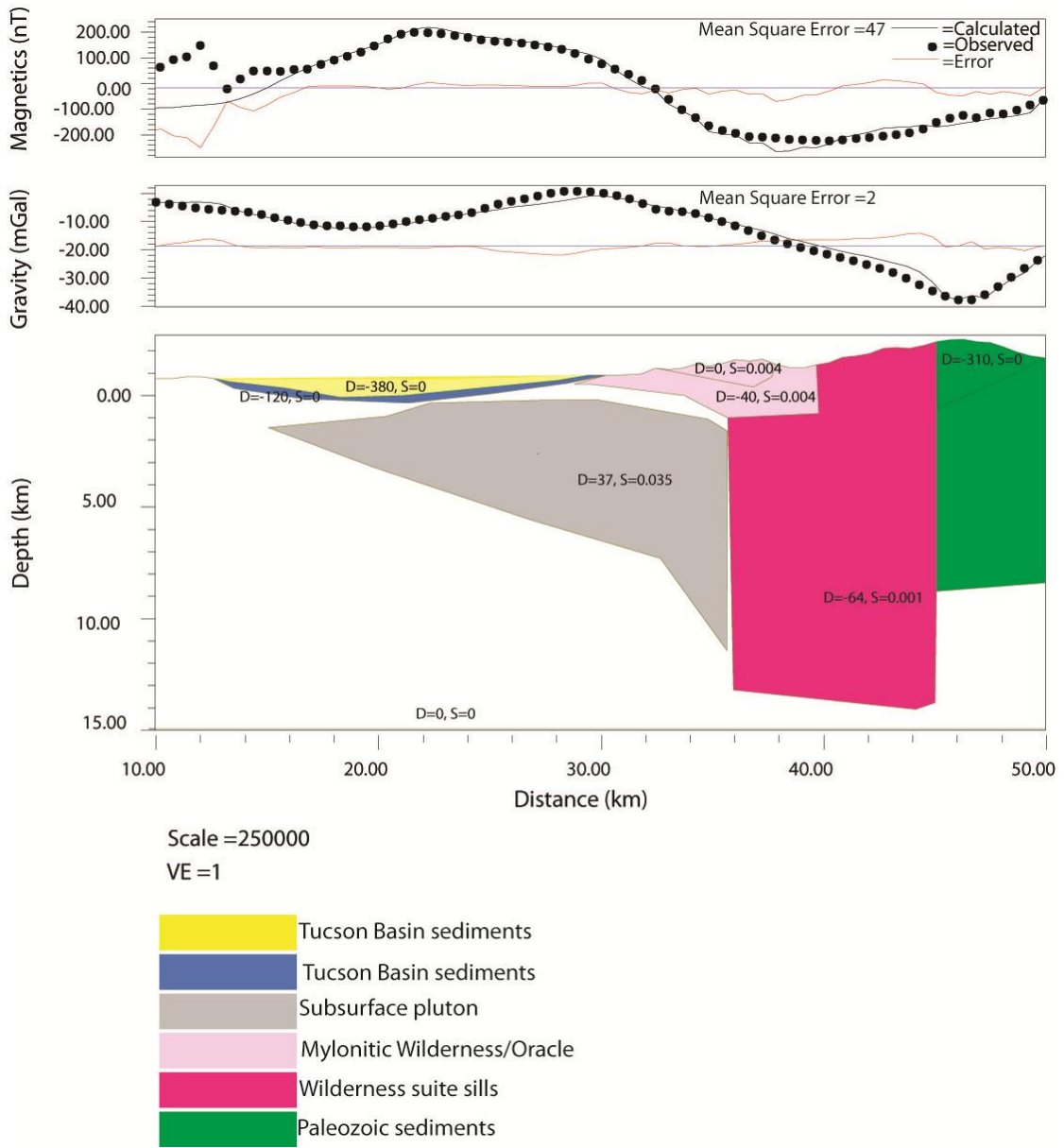


Figure 9.

## **TABLES**

Table 1. Aeromagnetic Surveys from the Tucson Basin and Catalina MCC region, AZ.

Table 2. Susceptibilities of igneous and metamorphic rocks from the Catalina MCC region. The units correspond to the geologic map (Figure 1).

Table 3. Susceptibility and density contrast values and ranges for the rock units modeled in Figures 8 and 9. See text for more detailed description of the rock unit.

Table 4. Possible ages for the subsurface pluton and the possible relationship to MCC Formation and Wilderness sill thermochronology.

Table 1.

| <u>Line</u><br><u>Number</u> | <u>Date</u> | <u>Line</u><br><u>Spacing</u><br><u>(miles)</u> | <u>Flight</u><br><u>Direction</u> | <u>Altitude</u><br><u>(feet</u><br><u>above</u><br><u>ground)</u> | <u>IGRF</u> | <u>USGS</u><br><u>Open-File</u><br><u>reports</u> | <u>References</u>        |
|------------------------------|-------------|---|-----------------------------------|---|-------------|---|--------------------------|
| 4325                         | 1999        | 0.25  | E-W                               | 500   | IGRF95      | OF00-155  | [U.S.G.S., 2000]         |
| 4211                         | 1997        | 0.093   | E-W                               | 500   | IGRF95      | OF00-155  | [U.S.G.S., 2000]         |
| 4191                         | 1996        | 0.155   | E-W                               | 750   | IGRF95      | OF00-155  | [U.S.G.S., 2000]         |
| 4052                         | 1981        | 0.55  | N-S                               | 1000  | IGRF75      | OF82-544  | [U.S.G.S., 1982]         |
| 4015                         | 1980        | 0.05  | E-W                               | 1000  | IGRF75      | OF80-998  | [U.S.G.S., 1980]         |
| 0528                         | 1964        | 1.00  | N-S                               | 9000*   | **          | OF65-004  | [Andreasen et al., 1965] |

\* barometric elevation

\*\*No regional field was removed. An arbitrary datum was removed

Table 2.

| Unit  | Lithology            | Susceptibility                       | Age   |
|---|----------------------|--------------------------------------|---|
| Wilderness granite (Tw, Twm)                                | Two-mica granite     | 0.00032 SI (SD:0.00023) <sup>4</sup> | ~45-55 Ma   |
| Oracle/Ruin Granite (Yo)                                    | Biotite Granite      | 0.00035 SI                           | 1.4 Ga <sup>7</sup>   |
| Leatherwood quartz diorite (Kgl)/Chirreon Wash pluton (Kgh) | Quartz Diorite       | 0.0012-0.0302 SI <sup>6</sup>        | ~75 Ma <sup>7</sup>   |
| Cat Mountain Tuff (Kcv)                                     | Rhyolite             |                                      | Upper Cretaceous/Laramide                                       |
| Amole Pluton (Kga)  | Granite/granodiorite | 0.0012-0.0302 SI <sup>6</sup>        | Upper Cretaceous/Laramide (73 Ma K-Ar biotite age) <sup>8</sup> |

<sup>4</sup>SD-Standard Deviation of 4 samples

<sup>6</sup> based on the range for the Josephine Canyon Diorite [Rystrom, 2003]

<sup>7</sup> age information from [Keith *et al.*, 1980]

<sup>8</sup> information from [Lipman, 1993]

Table 3.

| Unit  | Susceptibility | Density Contrast                |
|---|----------------|---------------------------------|
| Tucson Basin Upper fill                               | 0 SI           | -380 kg/m <sup>3</sup>          |
| Tucson Basin Lower fill                               | 0 SI           | -120 kg/m <sup>3</sup>          |
| Wilderness granitic sill                              | 0.001          | 64 kg/m <sup>3</sup>            |
| Mylonitic Wilderness sill                             | 0.004 SI       | -40-0 kg/m <sup>3</sup>         |
| Paleozoic sedimentary rocks<br>(outside Tucson Basin) | 0-0.22 SI      | -310 to -44.5 kg/m <sup>3</sup> |
| Granite to<br>GranodioritePluton                      | 0.035 SI       | 37-38 kg/m <sup>3</sup>         |



Table 4.

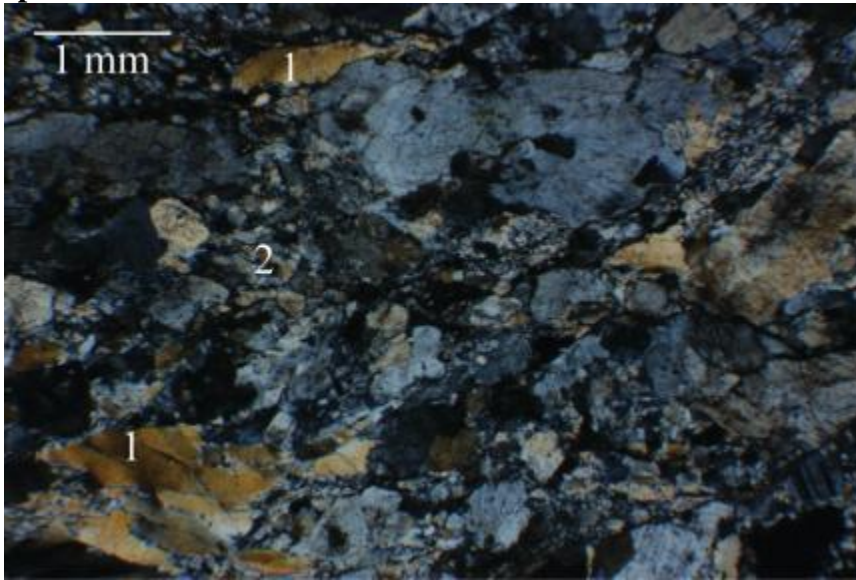
|                                | <i>Relationship to MCC Formation</i>              | <i>Affect on Wilderness suite thermochronology</i> |
|--------------------------------|---|--|
| Precambrian                    | No Role   | No effect  |
| Mesozoic                       | Heating the crust prior to extension              | No effect  |
| Tertiary<br>(Eocene/Oligocene) | Heating the crust prior to extension/Synkinematic | No effect/Variable effect                          |
| Tertiary (Miocene)             | Post-detachment faulting                          | Reset Wilderness thermochronometers                |

## APPENDICES

## **Appendix 1.1**

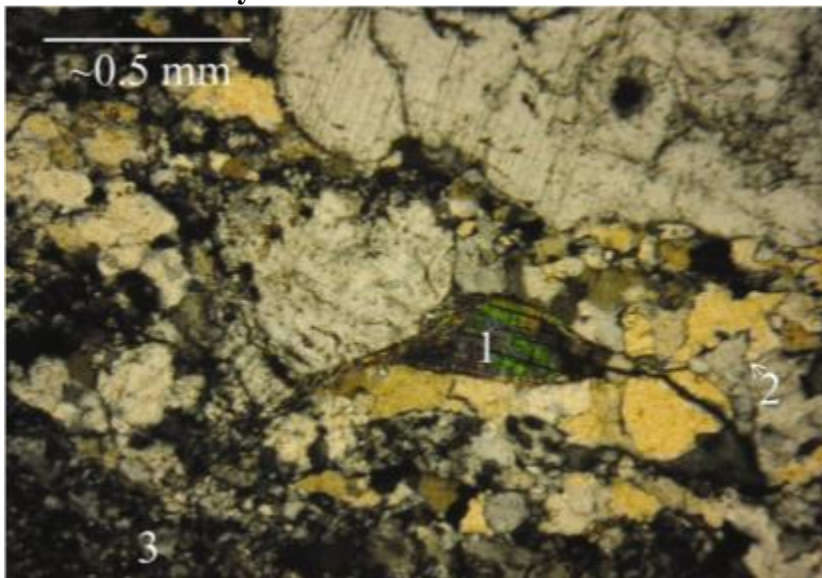
### **Select Photomicrographs from the Wilderness suite sills**

### Spencer Lens



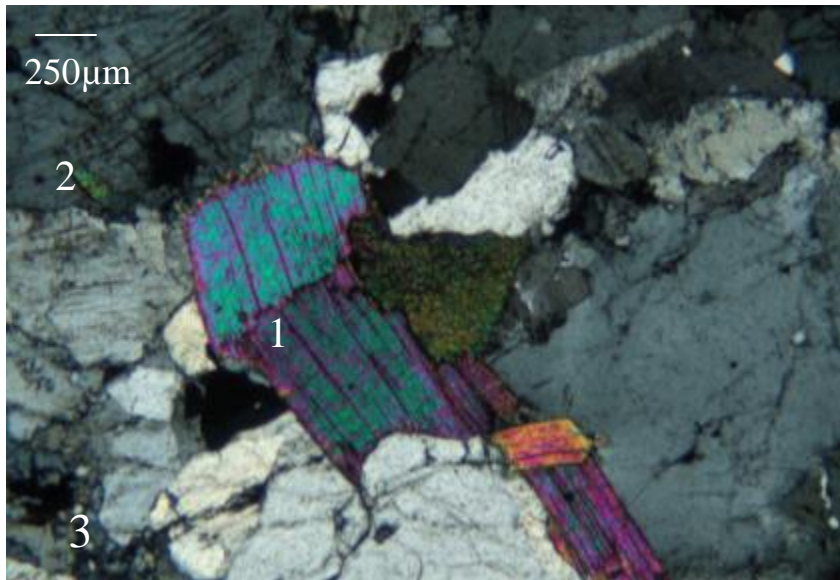
- 1= Recrystallized Quartz
- 2=Subgrain rotation of Quartz

### Wilderness Windy Point



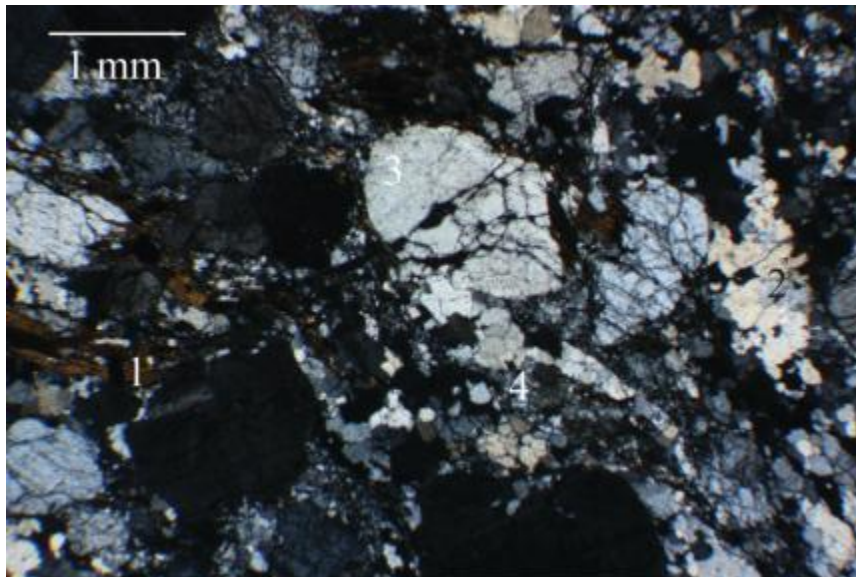
- 1= Ductile deformed Muscovite
- 2= Bulging recrystallization in Quartz
- 3= Subgrain rotation of Quartz

### Wilderness General Hitchcock



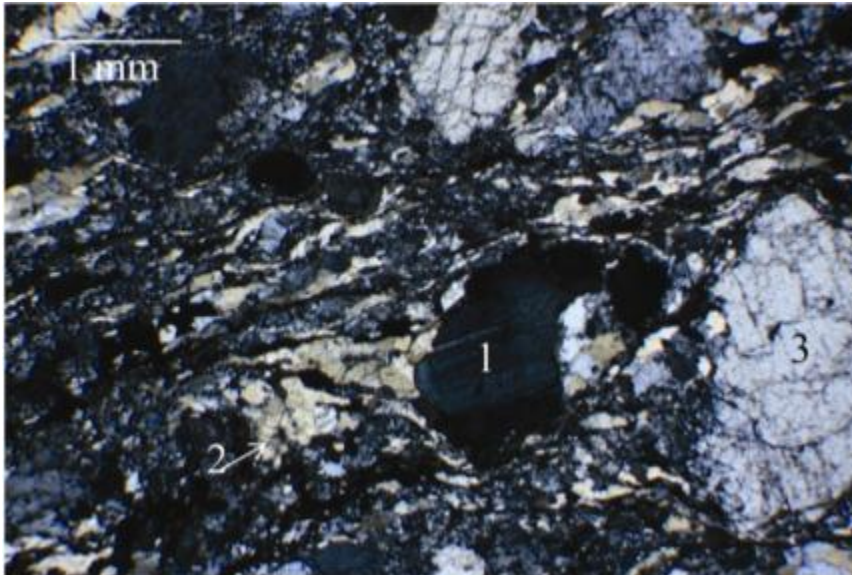
- 1=Fractured Potassium Feldspar
- 2=Fractured muscovite
- 3=Subgrain rotation in Quartz

### Shreve Pass



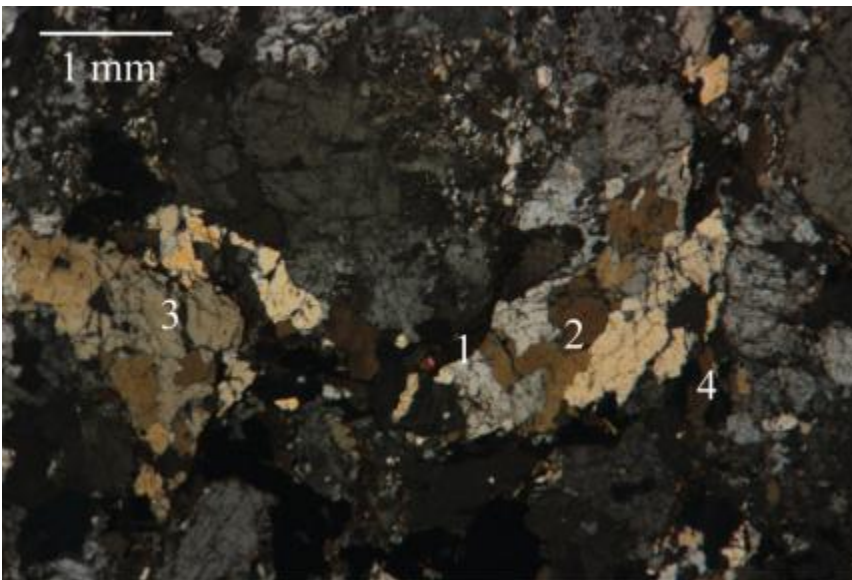
- 1 = Fine-grained iron oxide-stained Biotite
- 2 = Bulging recrystallization in Quartz
- 3 = Fractures in Plagioclase Feldspar
- 4 = Subgrain rotation in Quartz

### Gibbon Mountain



- 1 = Twinning in plagioclase feldspar
- 2 = Subgrain rotation in Quartz
- 3 = Fractured Feldspar

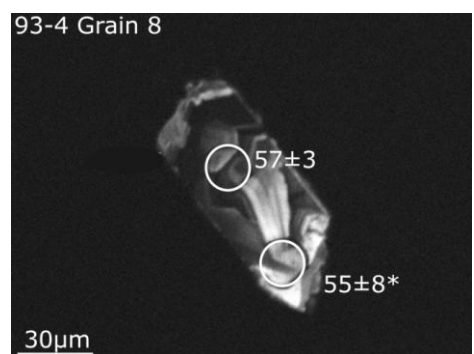
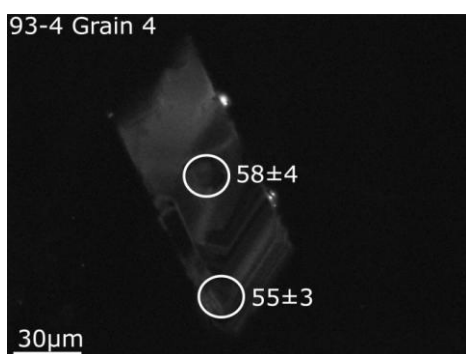
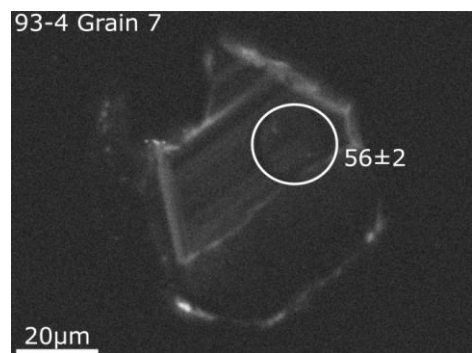
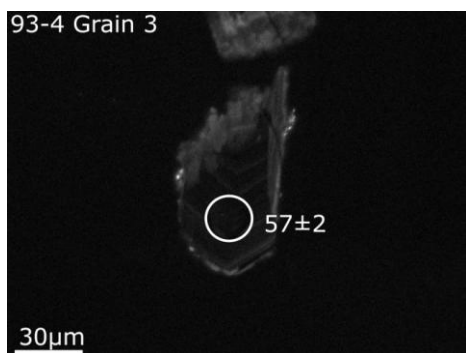
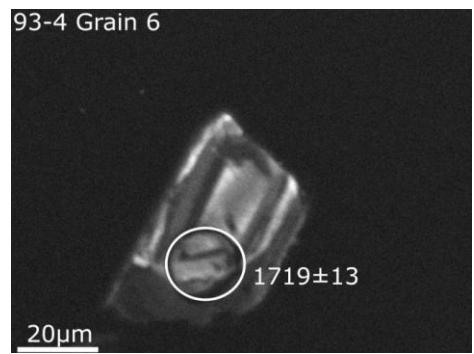
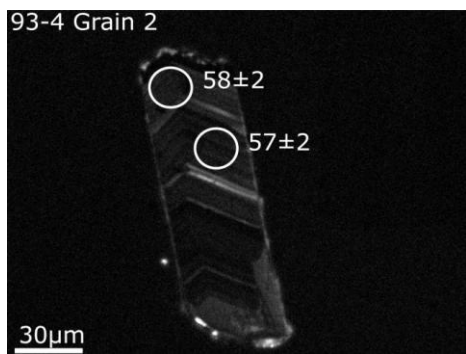
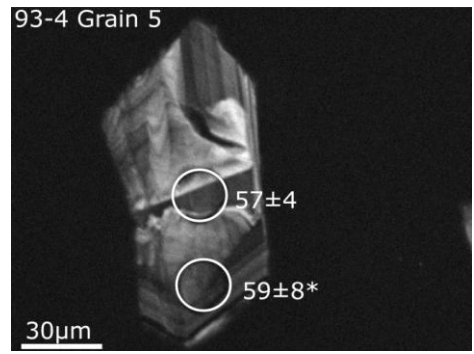
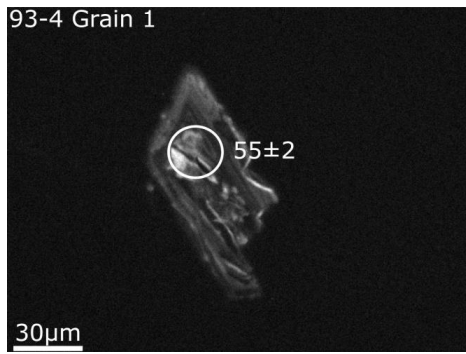
### Seven Falls



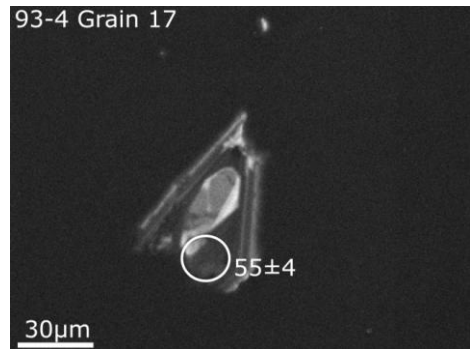
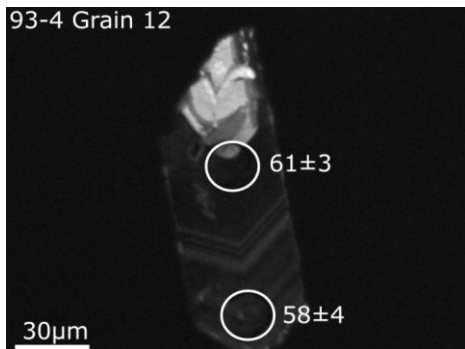
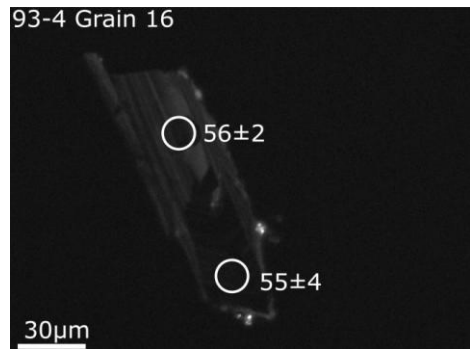
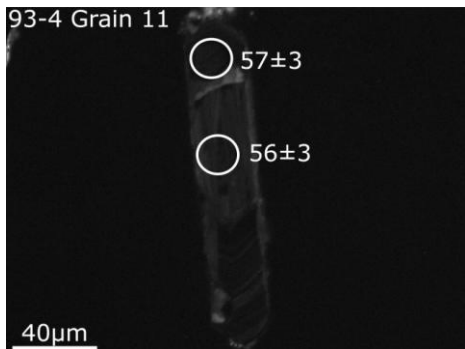
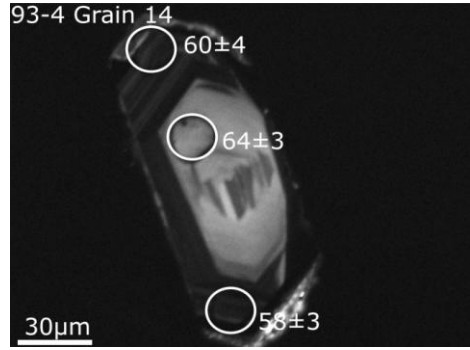
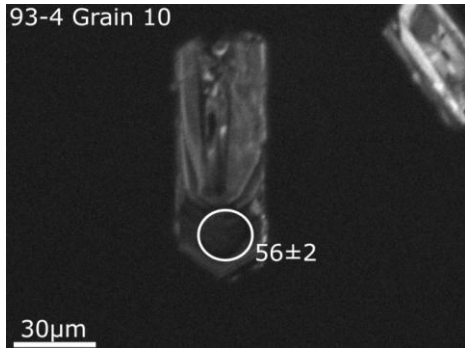
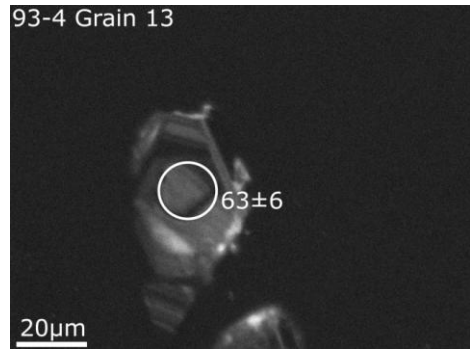
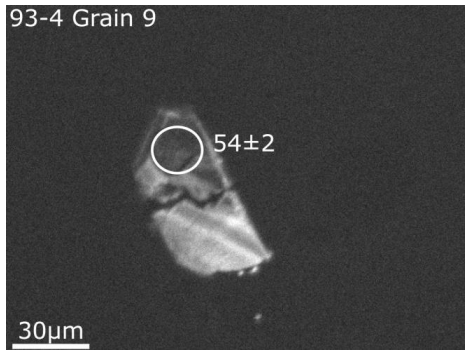
- 1 = Fine-grained iron oxide-stained Biotite
- 2 = Bulging recrystallization in Quartz
- 3 = Fractured Quartz
- 4 = Subgrain rotation in Quartz

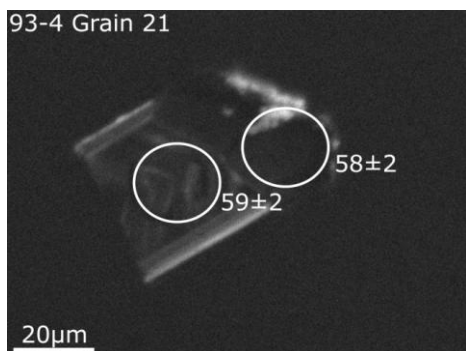
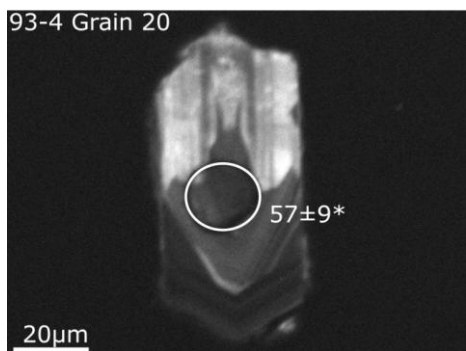
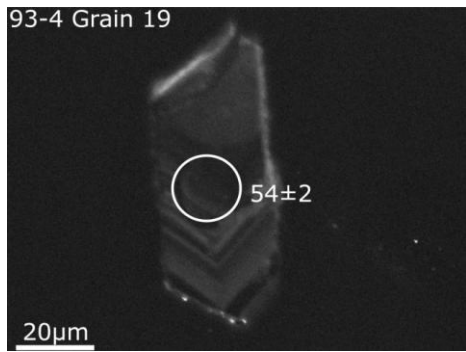
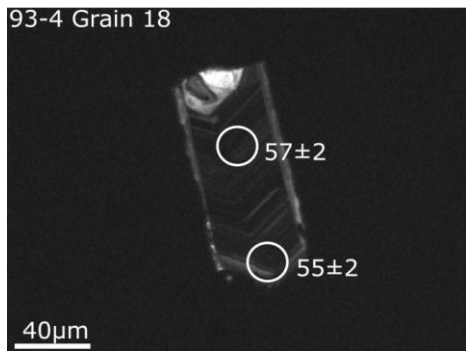
## **Appendix 1.2**

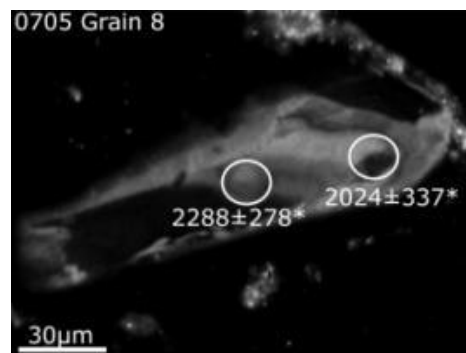
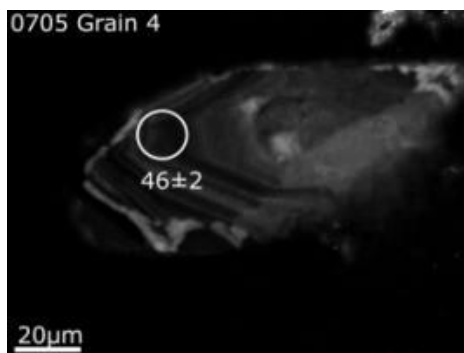
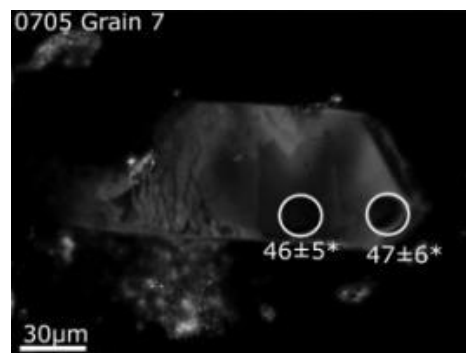
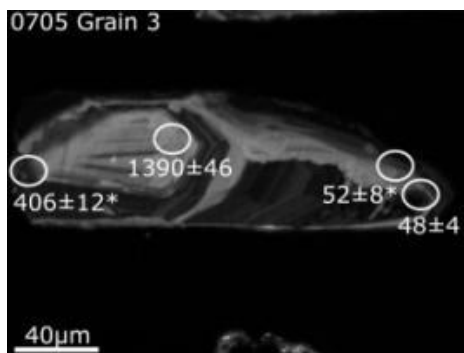
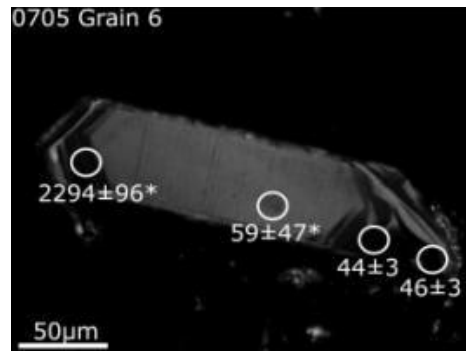
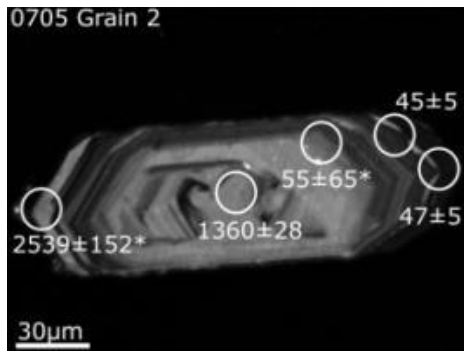
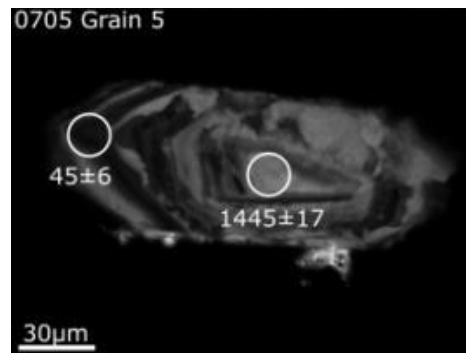
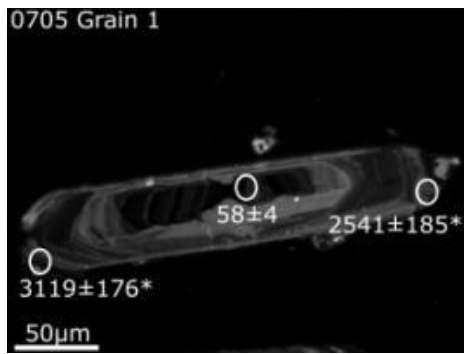
### **CL zircon images from the Wilderness suite sills**

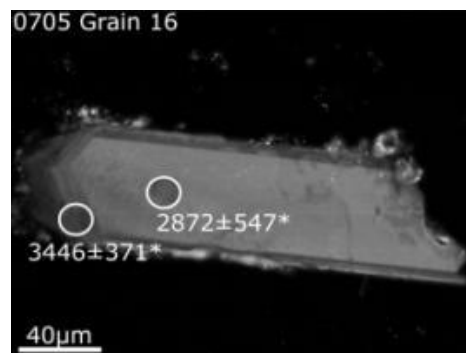
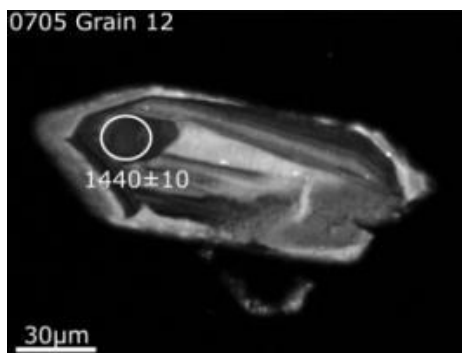
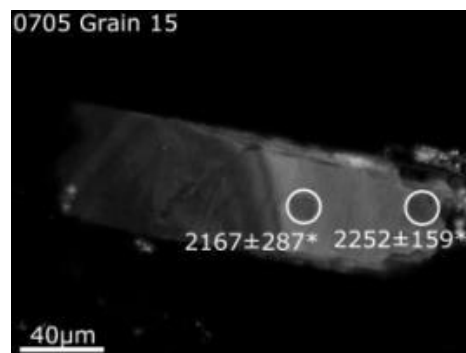
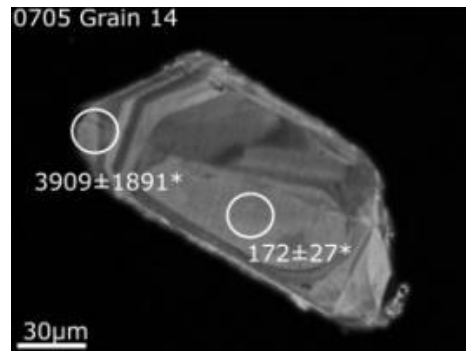
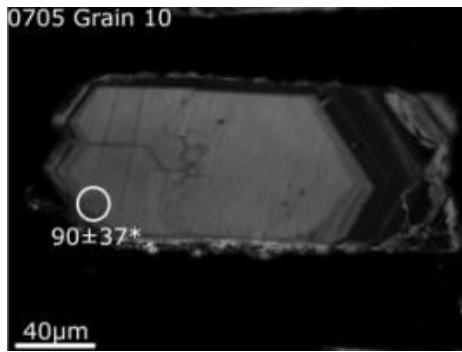
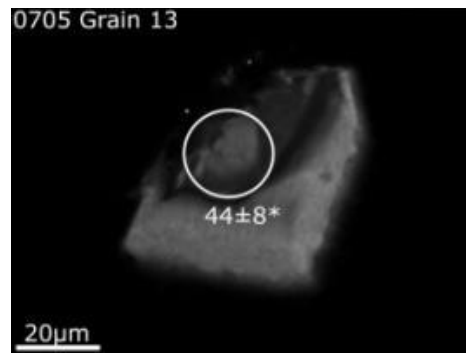
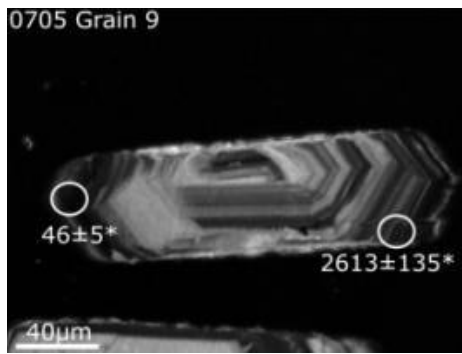


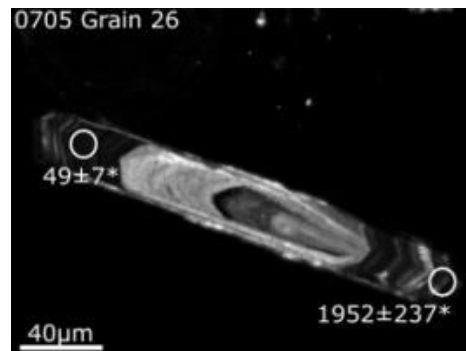
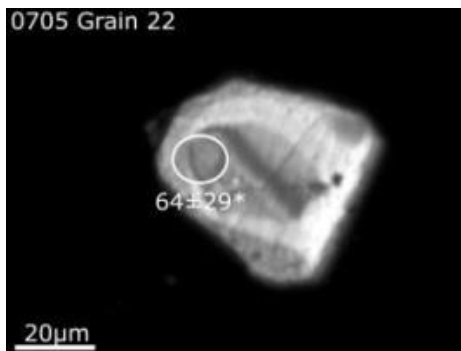
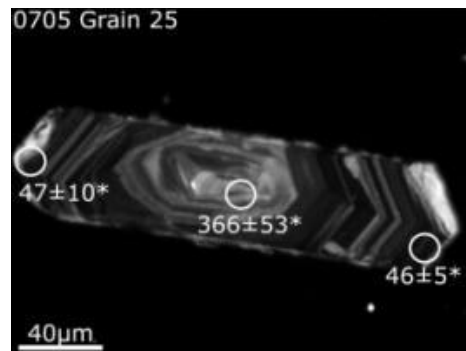
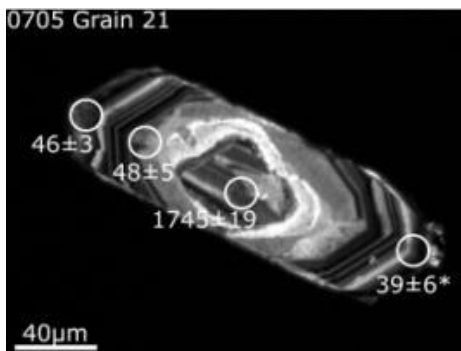
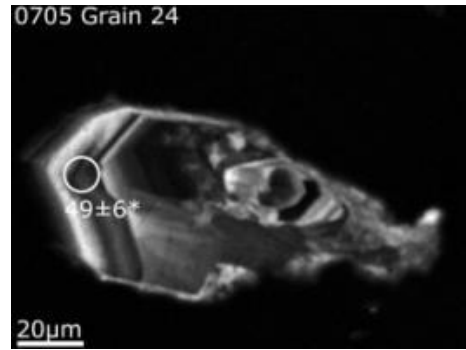
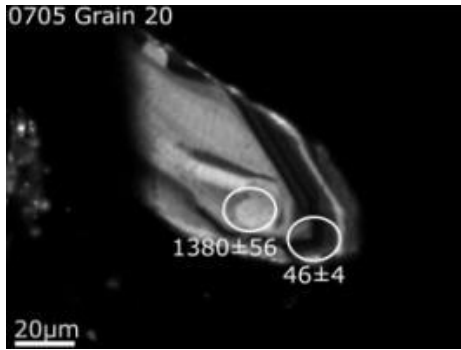
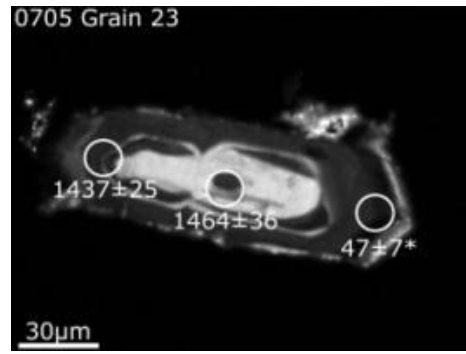
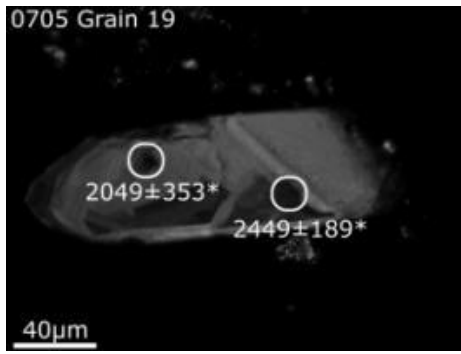


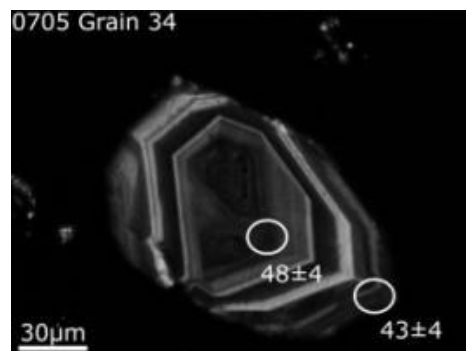
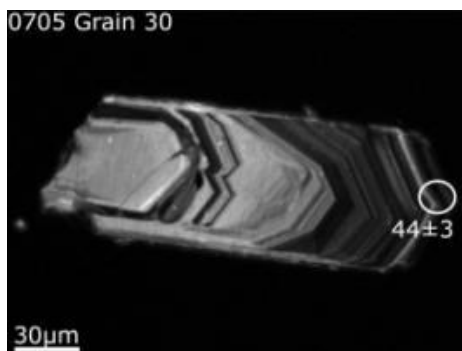
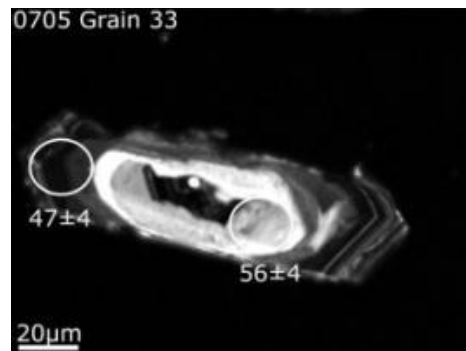
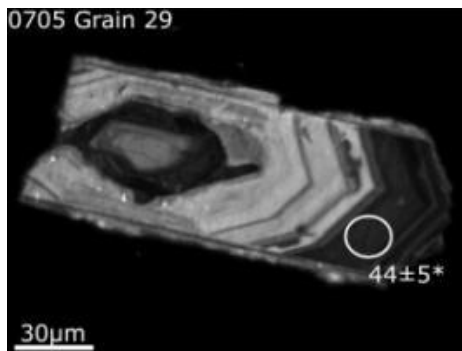
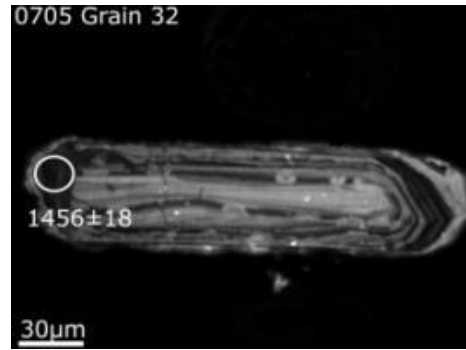
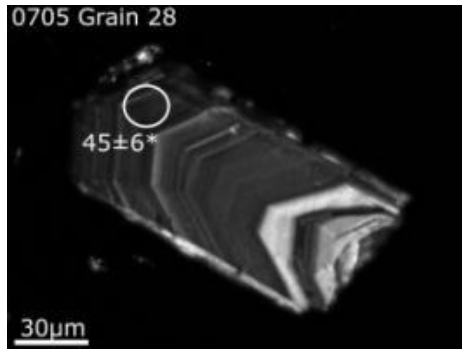
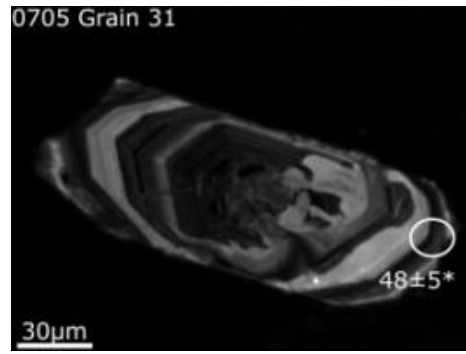
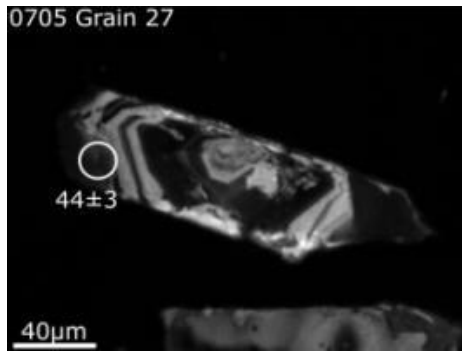


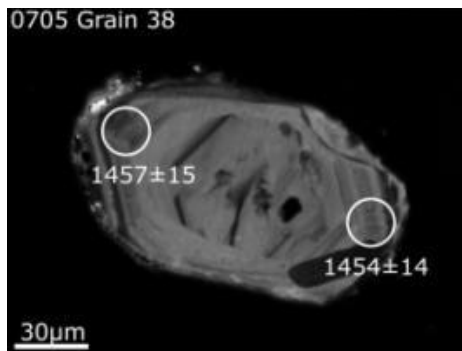
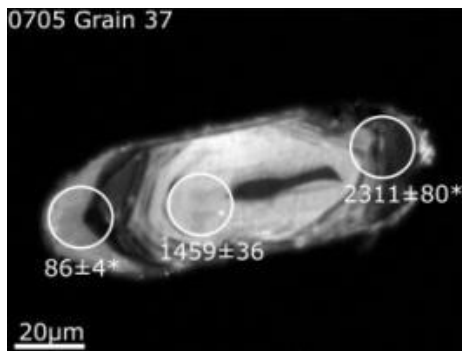
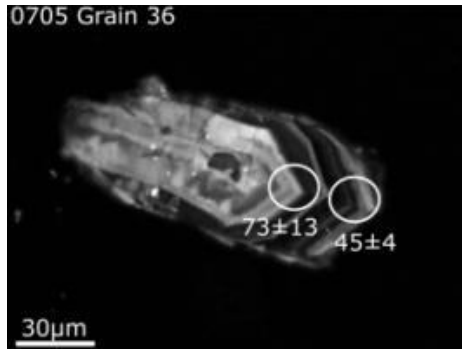
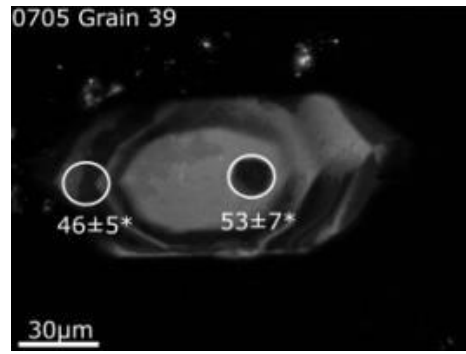
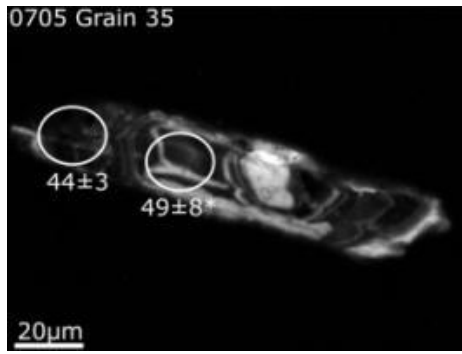


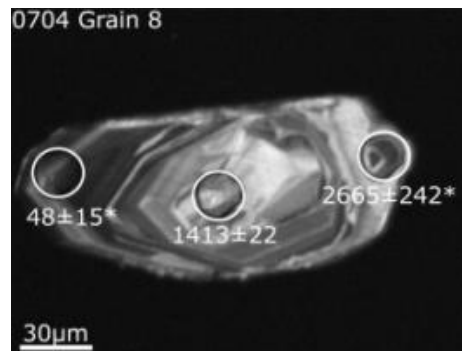
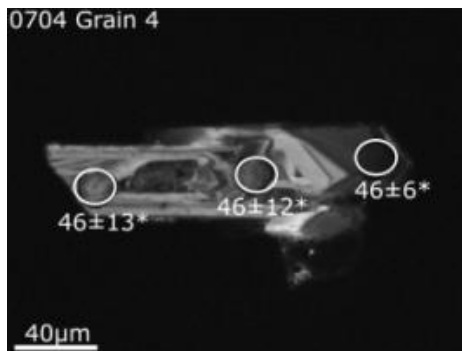
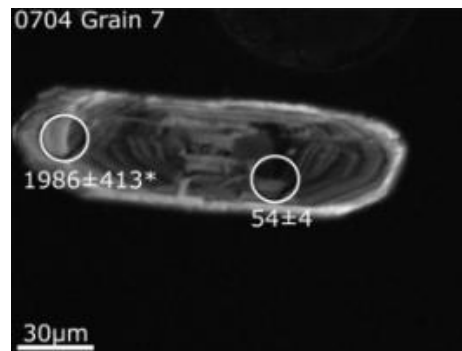
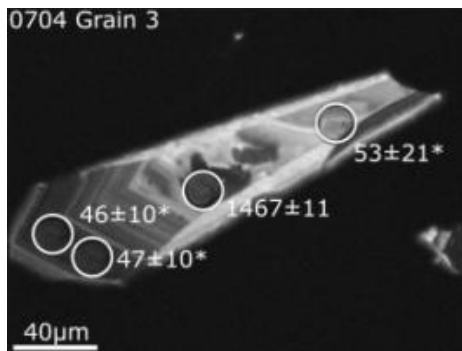
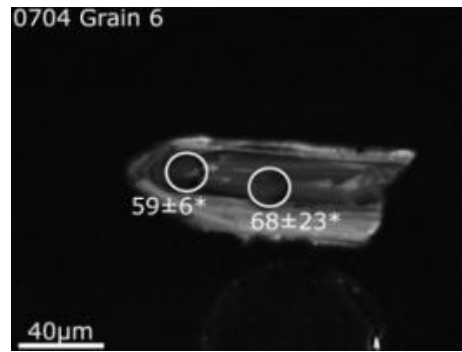
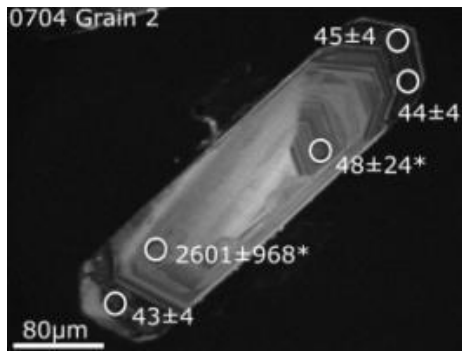
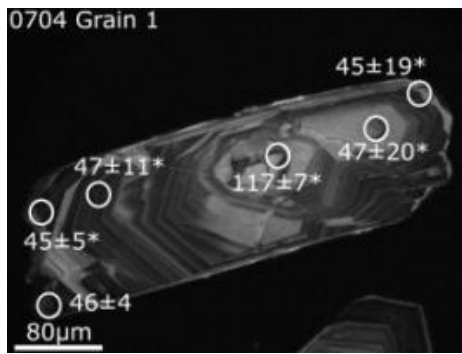




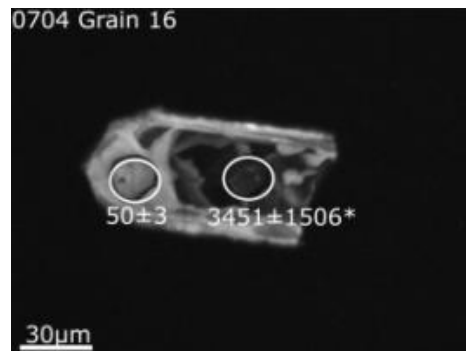
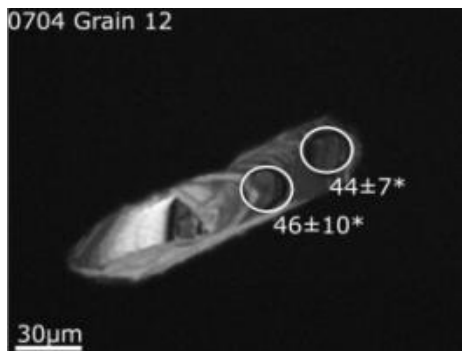
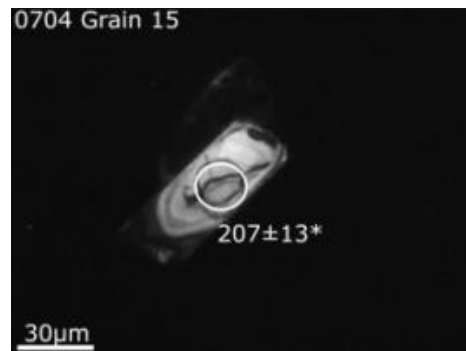
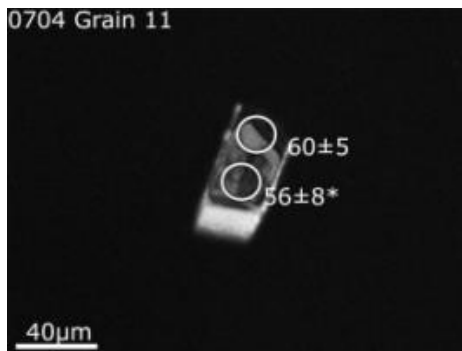
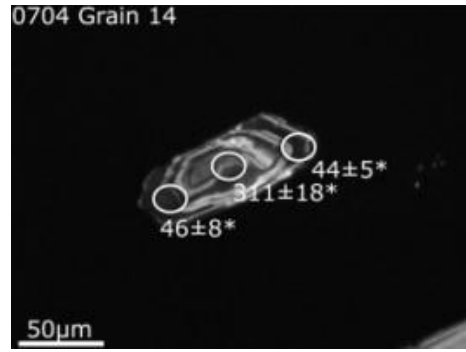
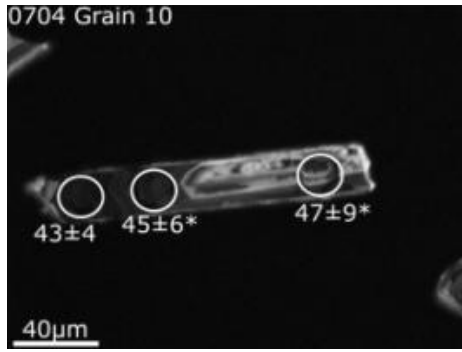
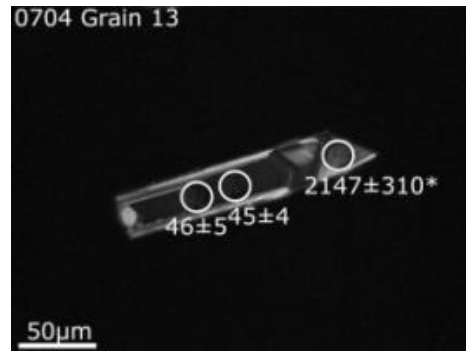
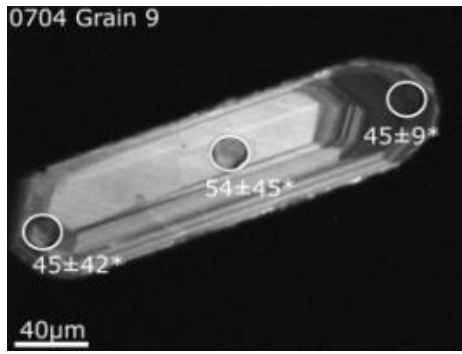


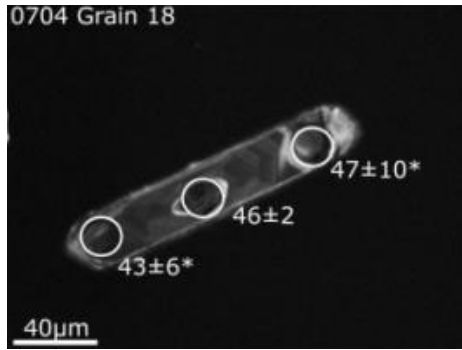
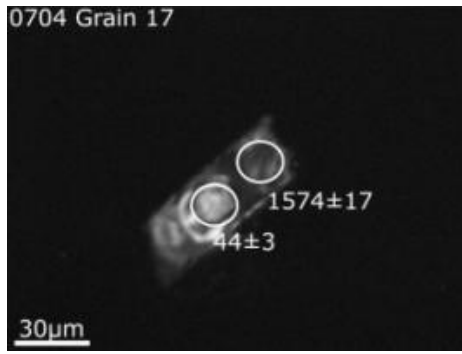


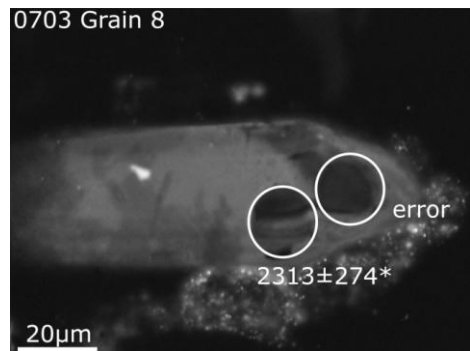
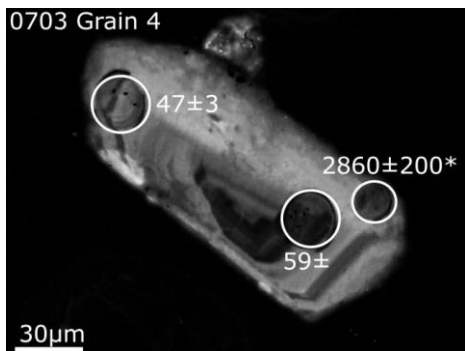
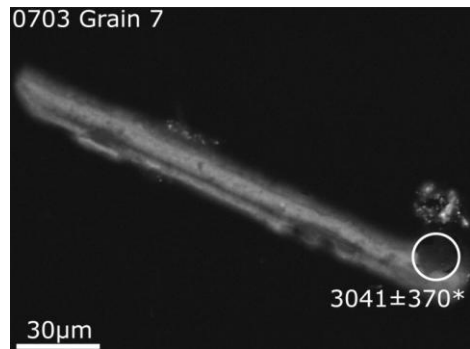
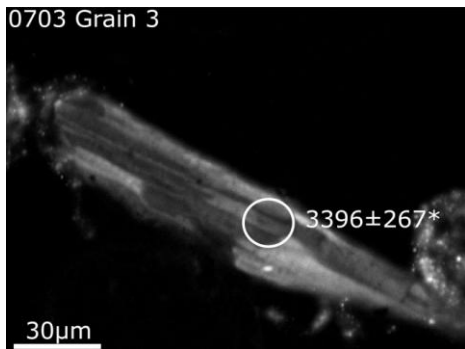
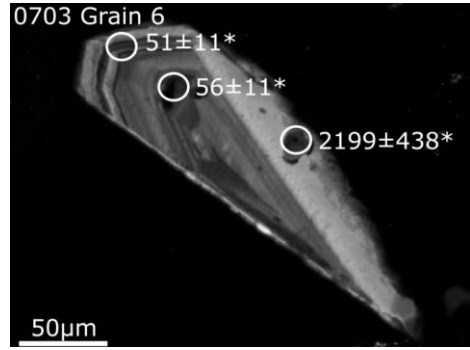
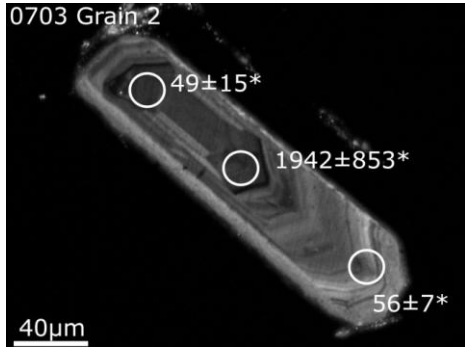
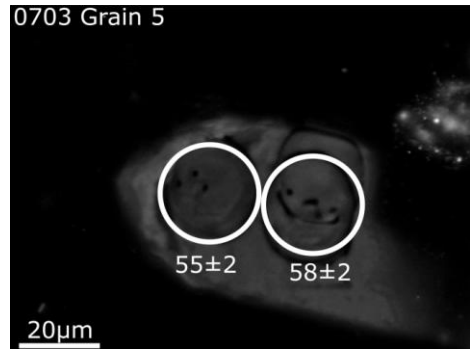
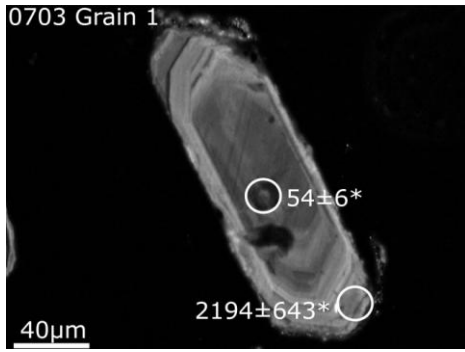


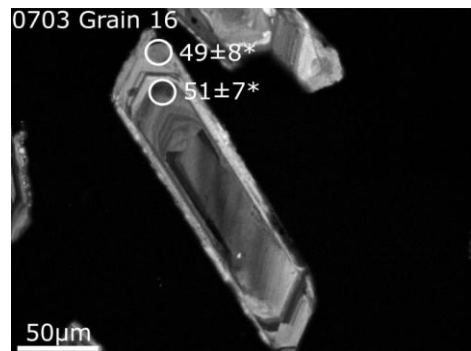
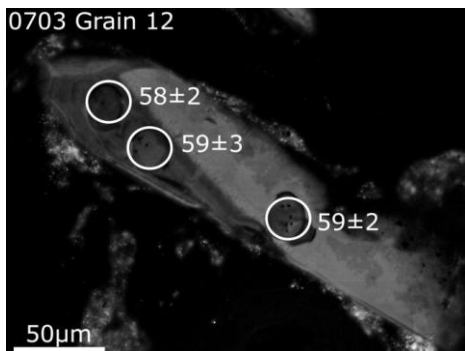
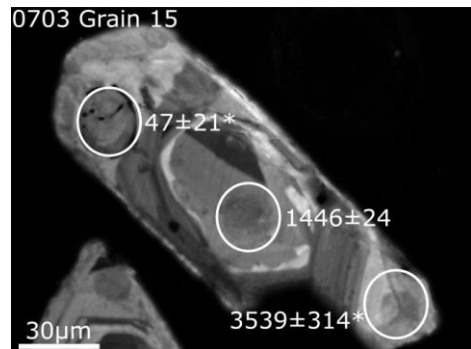
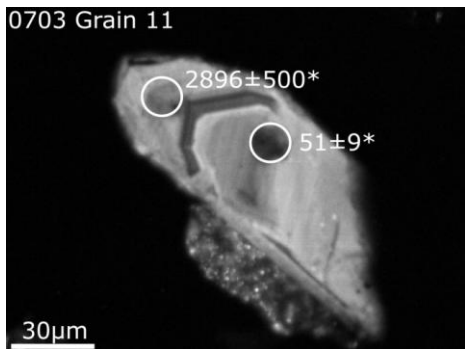
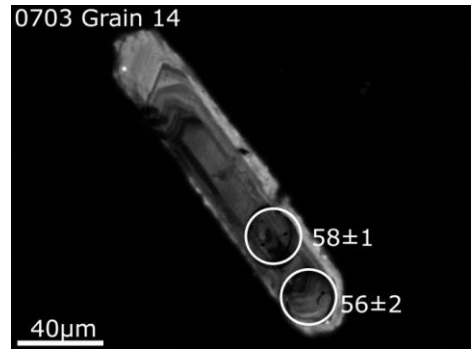
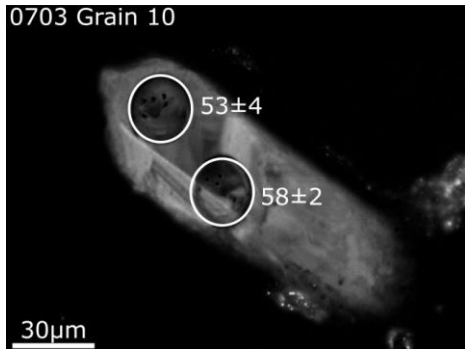
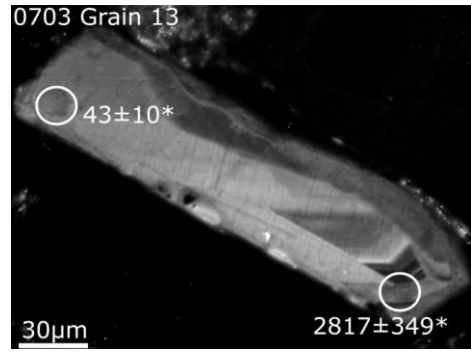
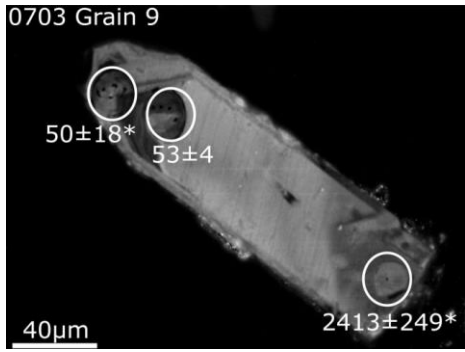


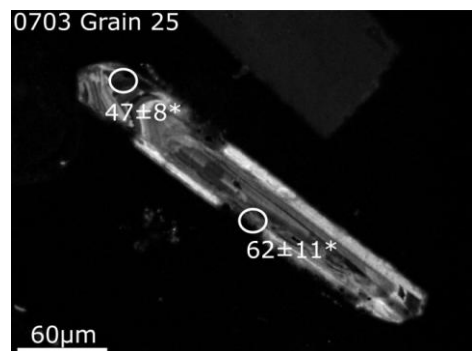
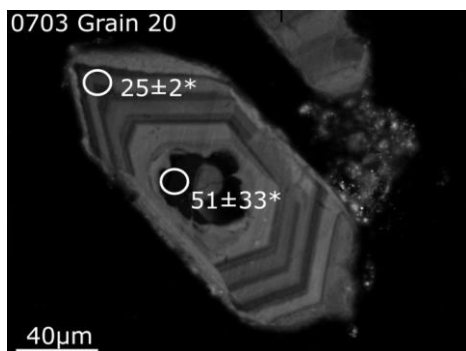
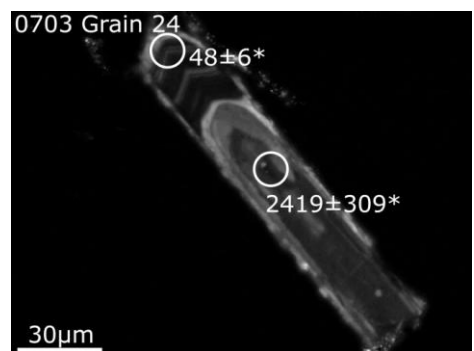
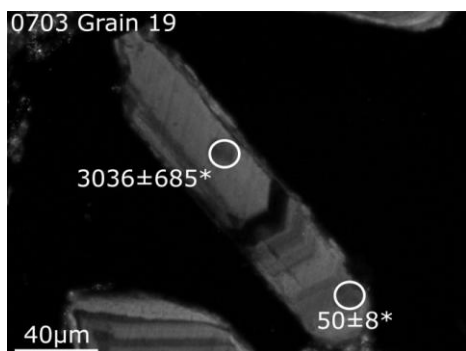
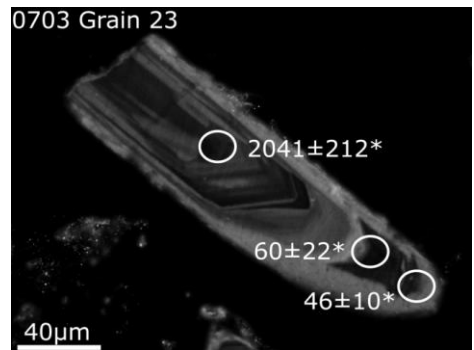
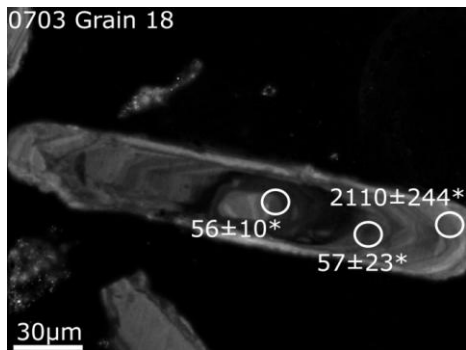
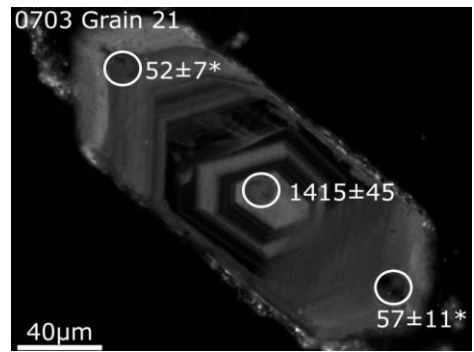
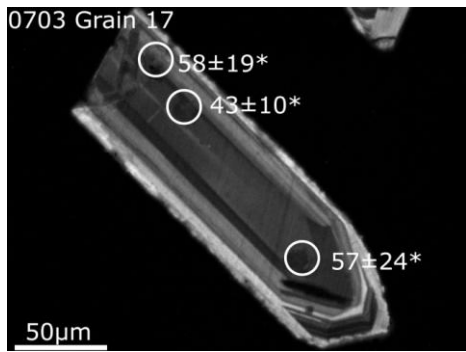


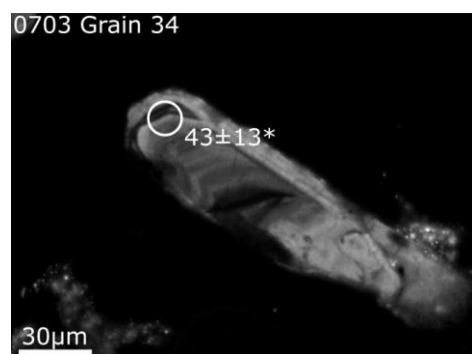
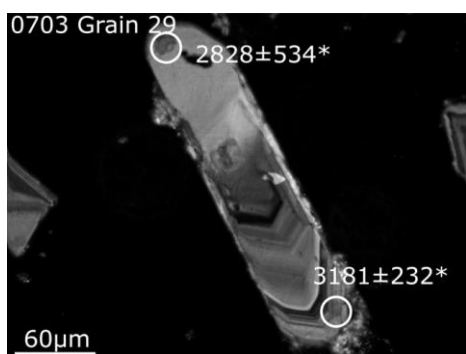
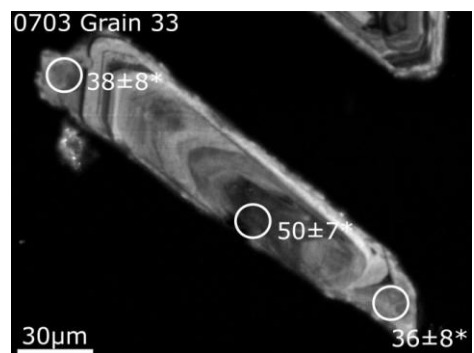
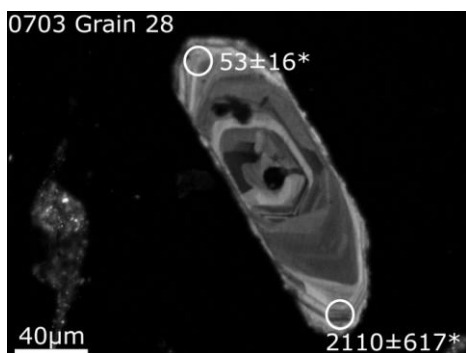
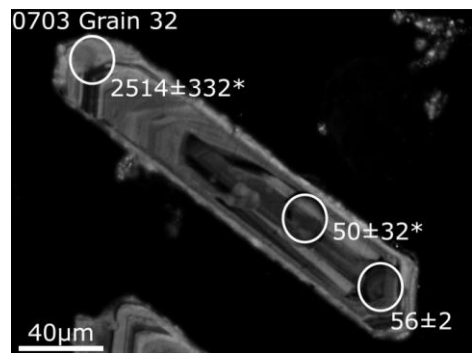
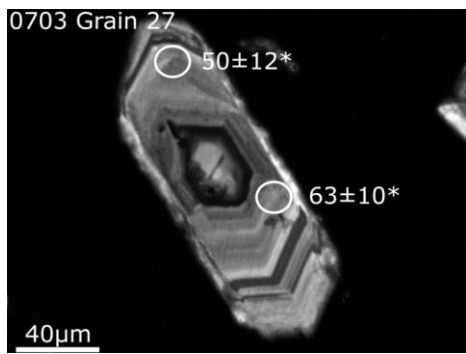
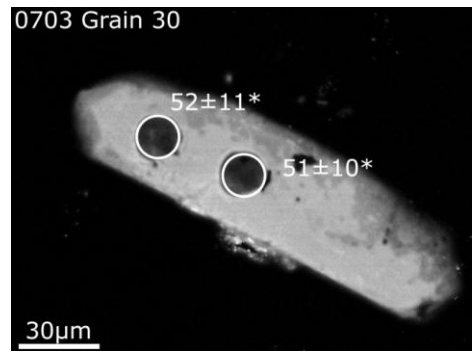
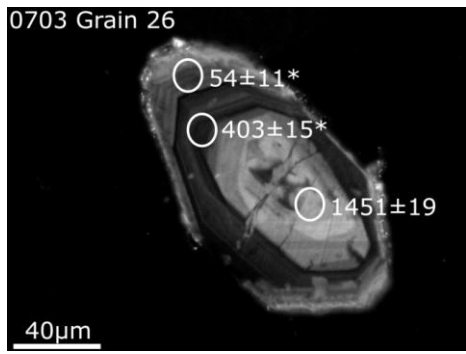


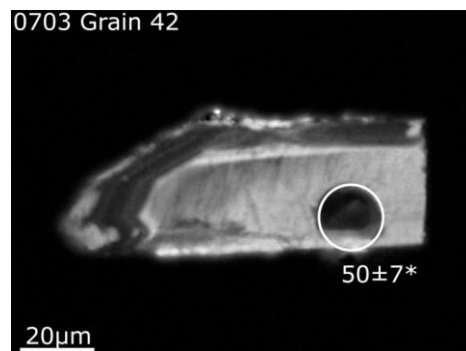
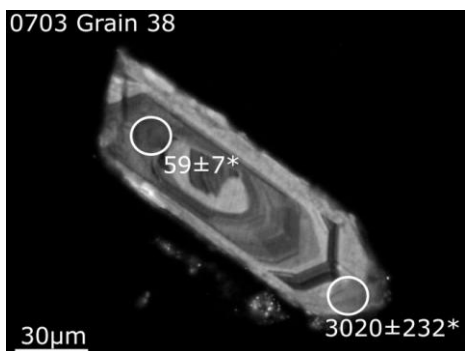
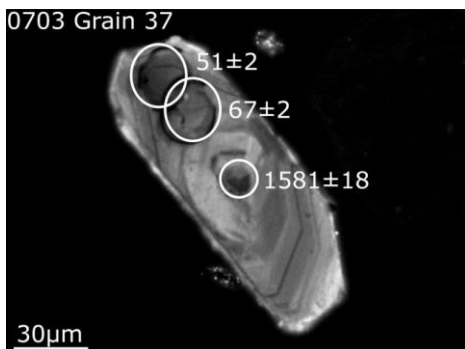
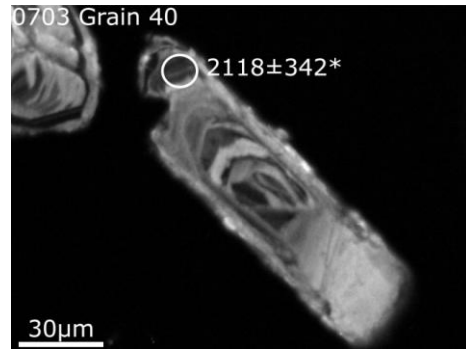
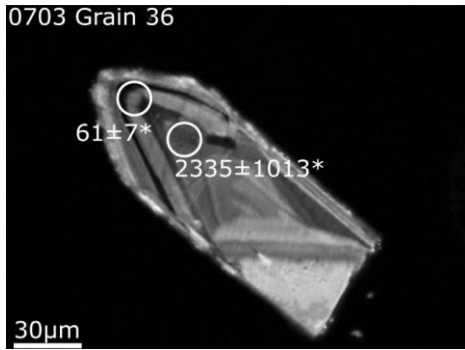
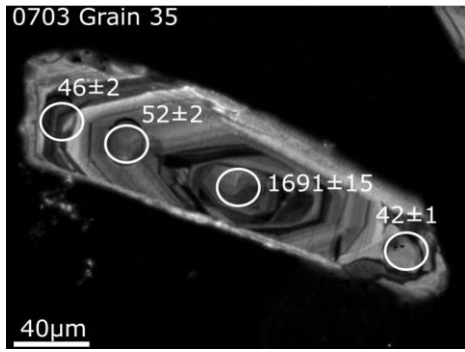


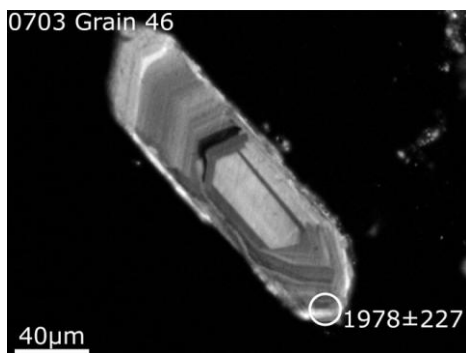
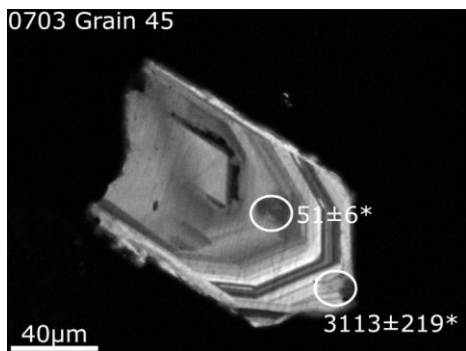
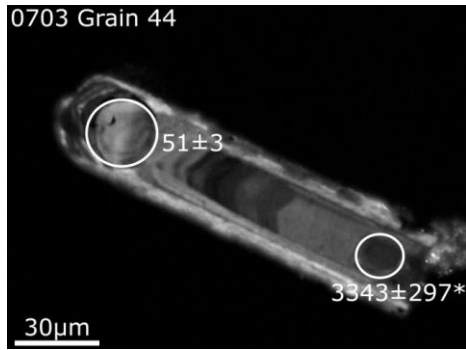
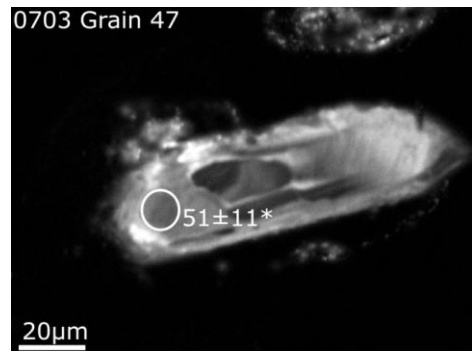
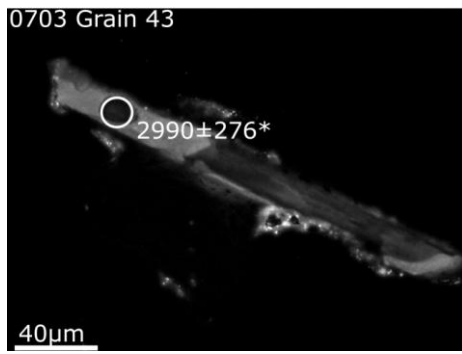




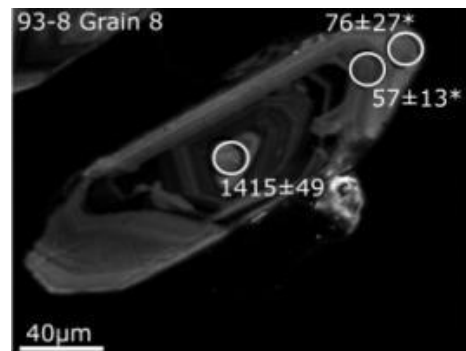
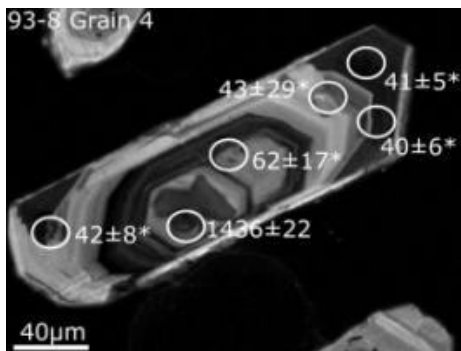
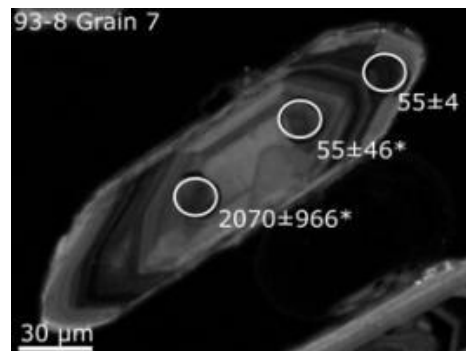
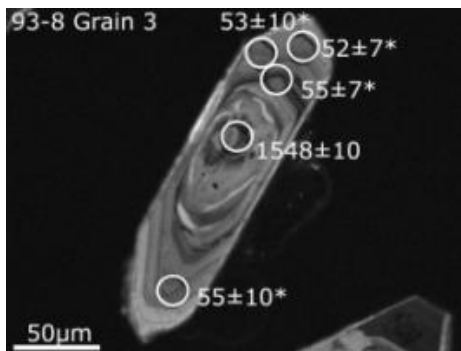
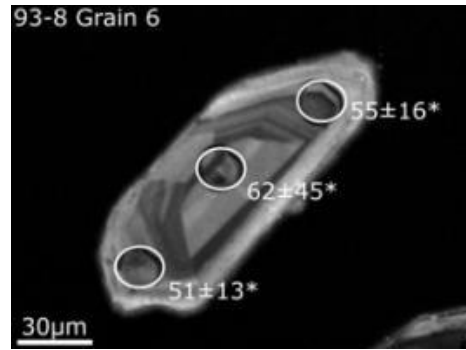
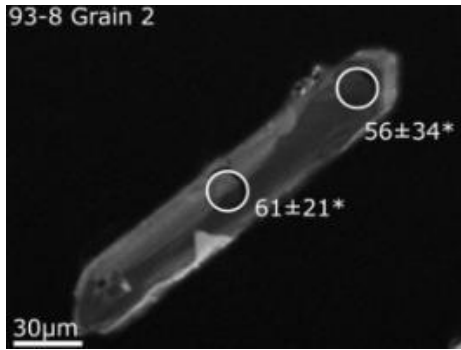
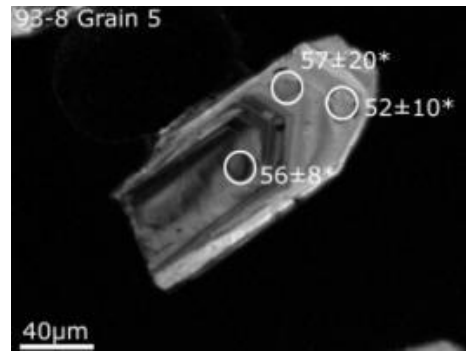
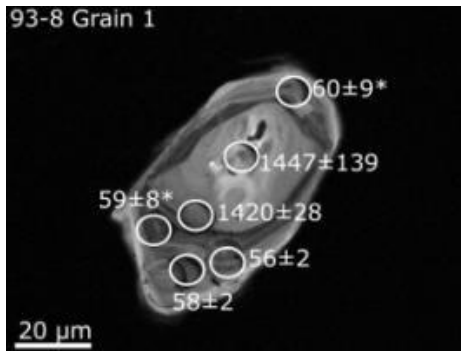


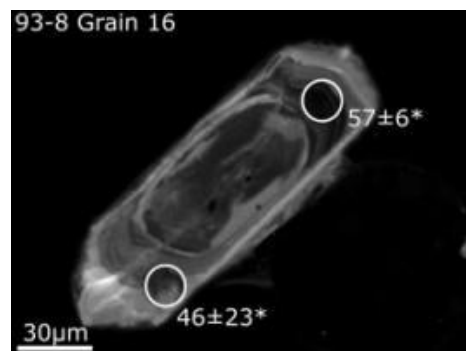
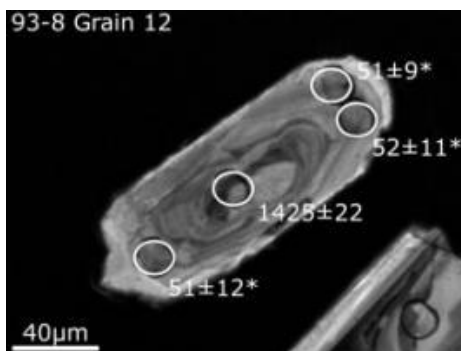
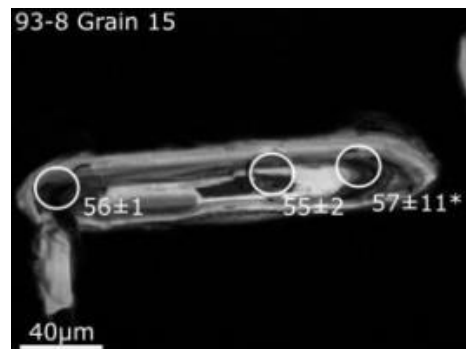
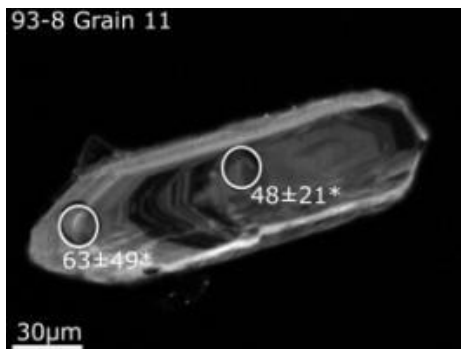
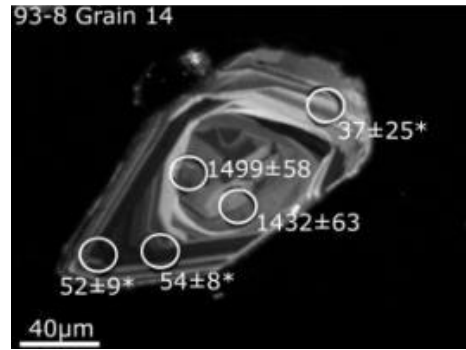
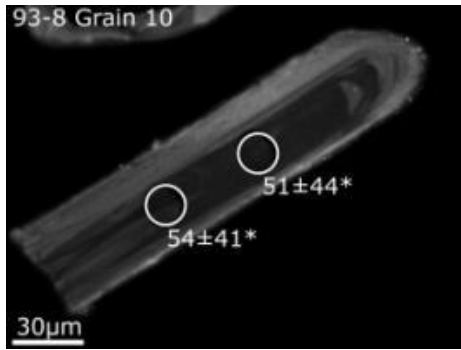
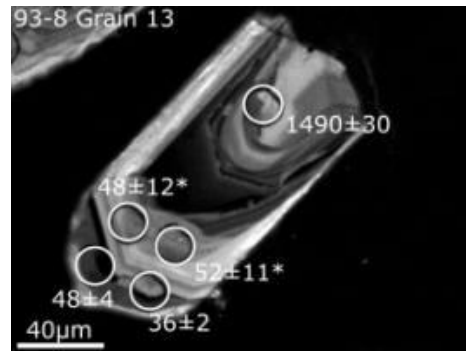
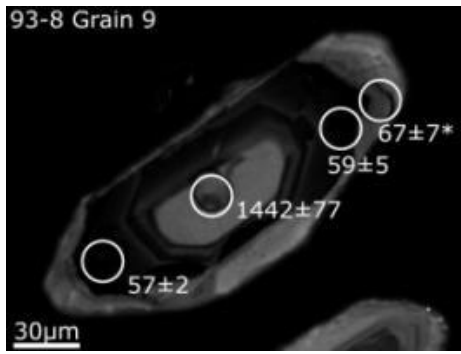


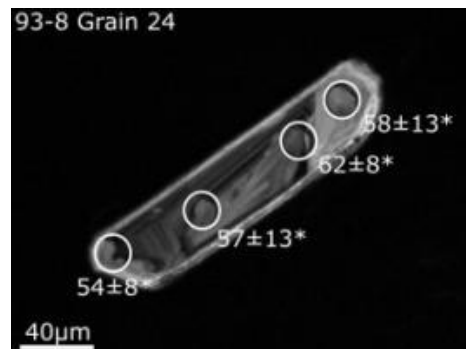
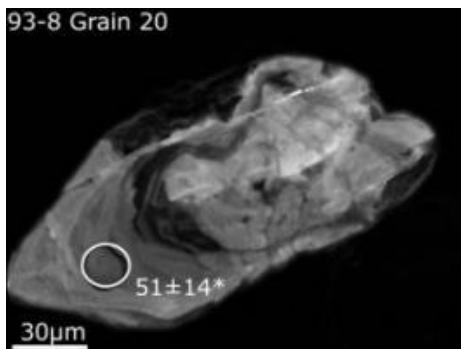
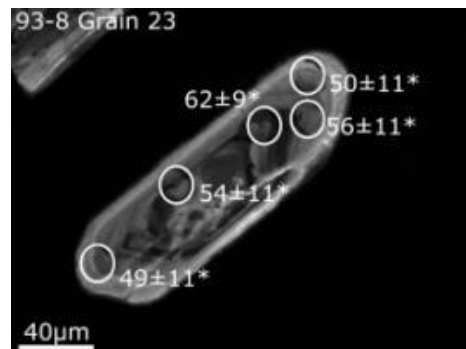
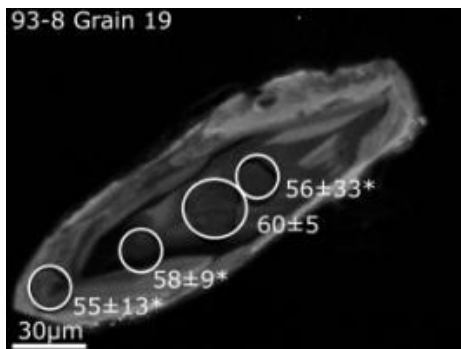
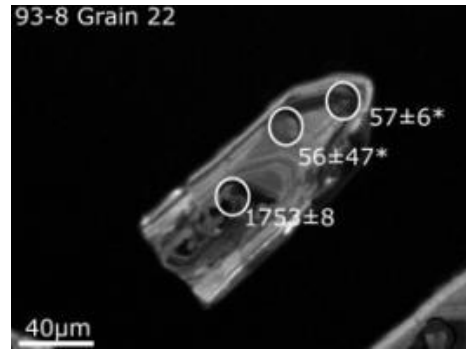
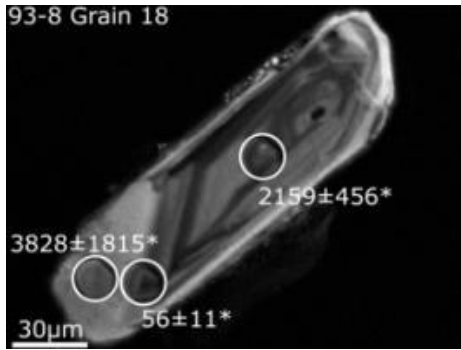
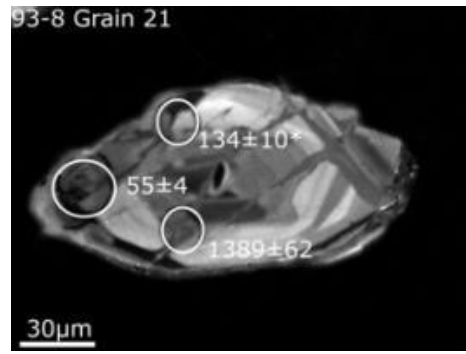
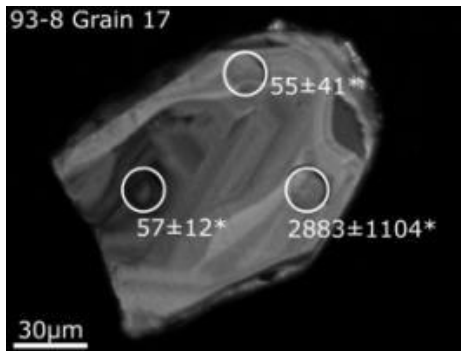


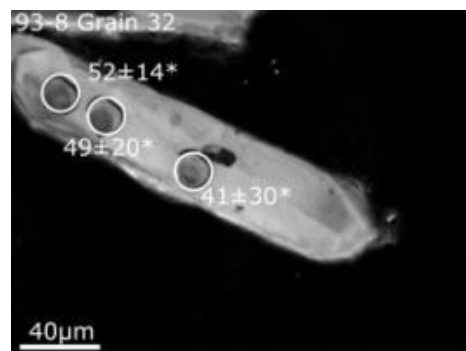
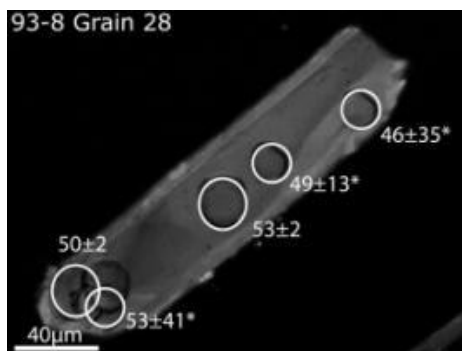
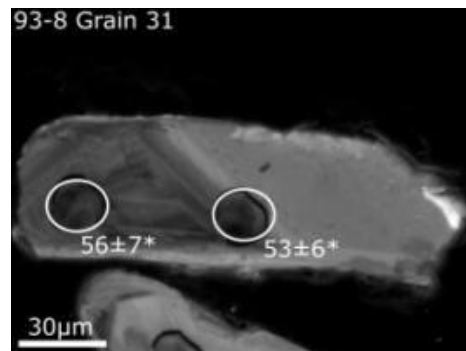
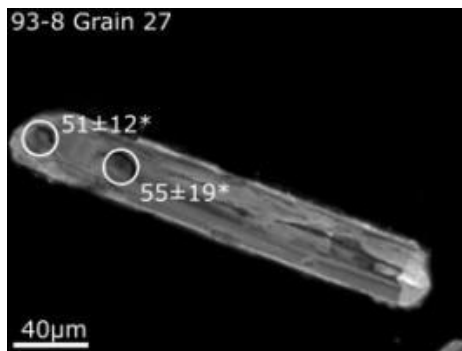
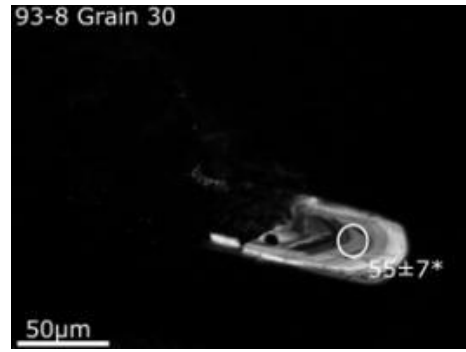
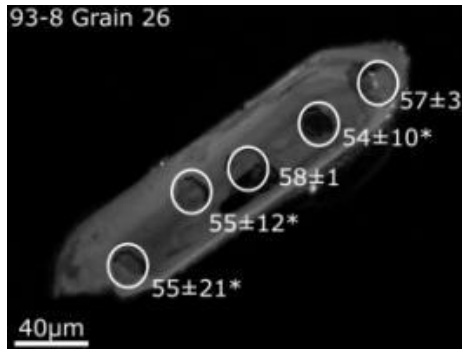
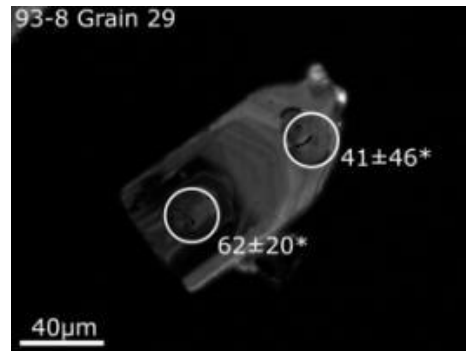
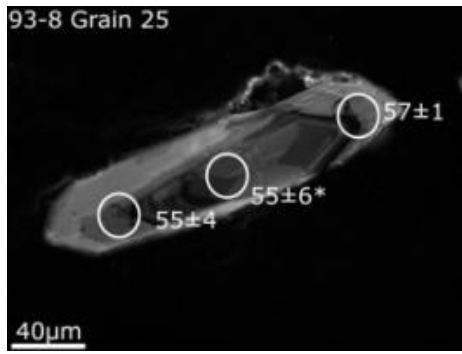


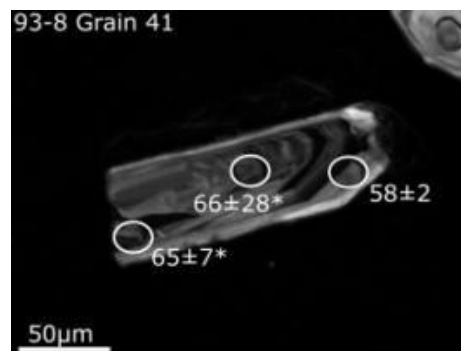
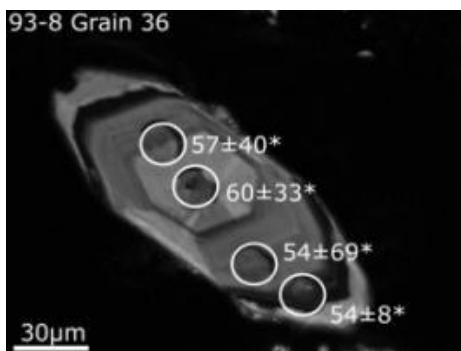
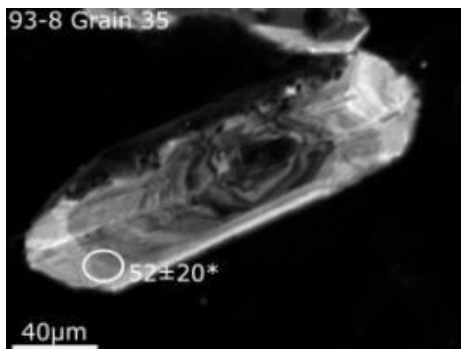
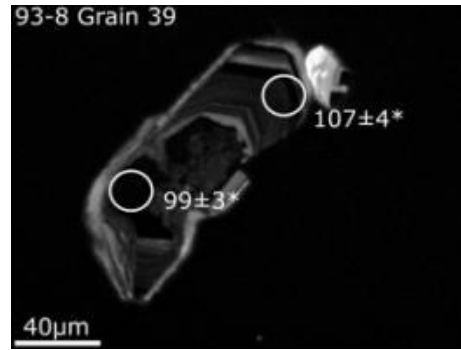
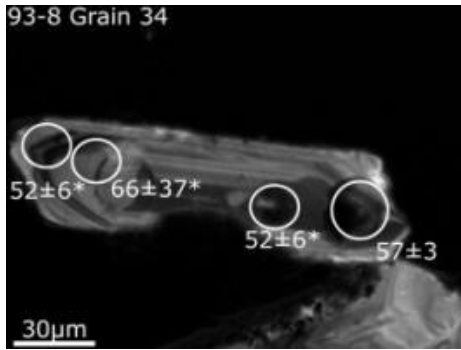
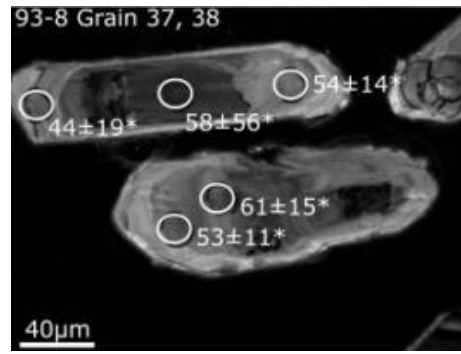
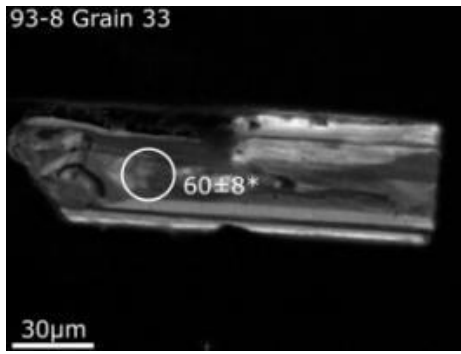


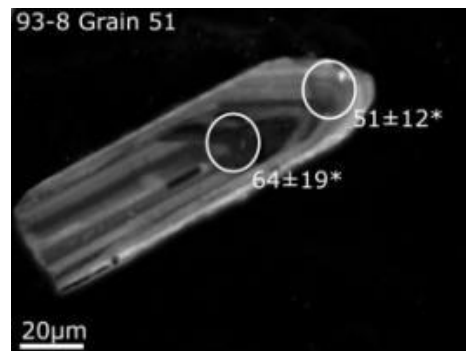
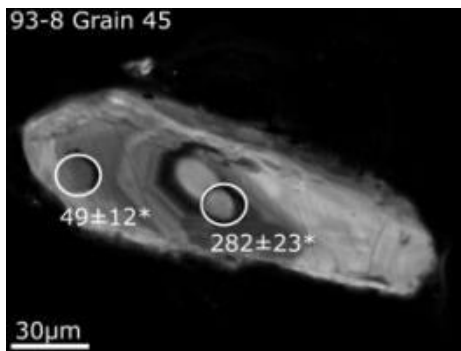
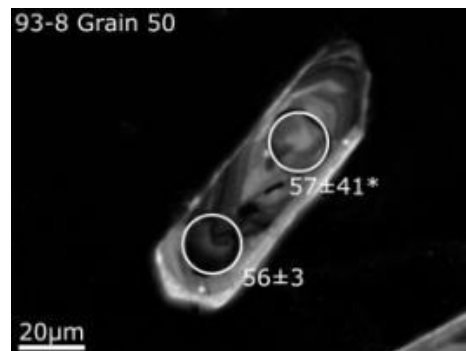
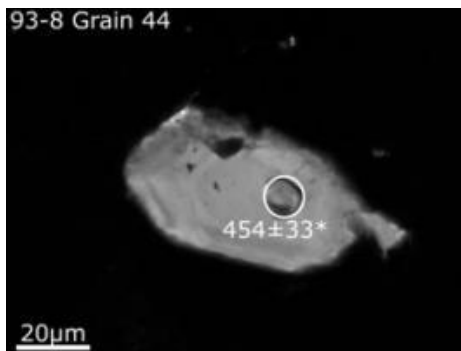
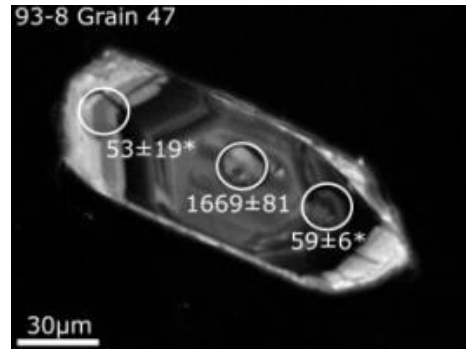
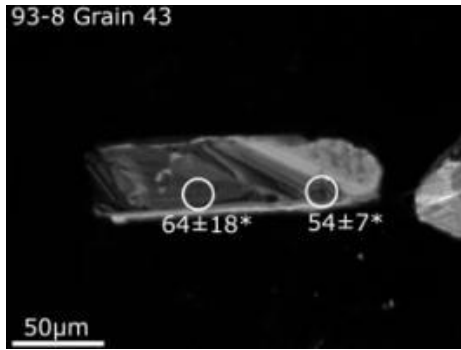
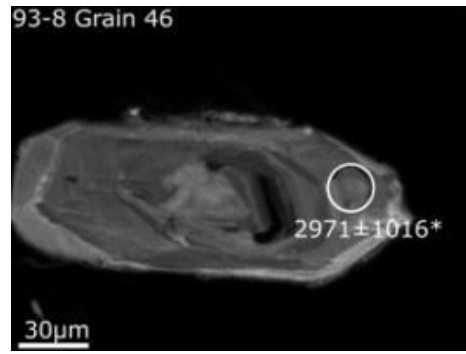
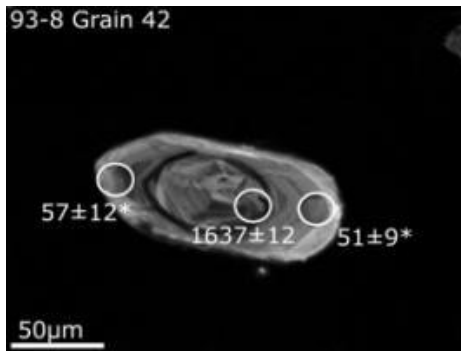


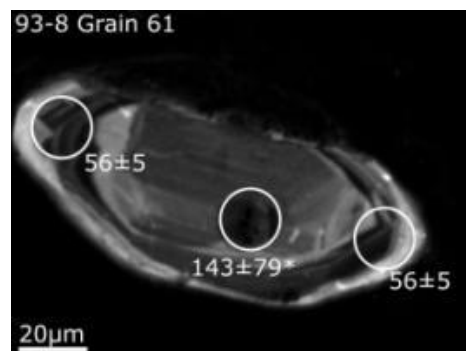
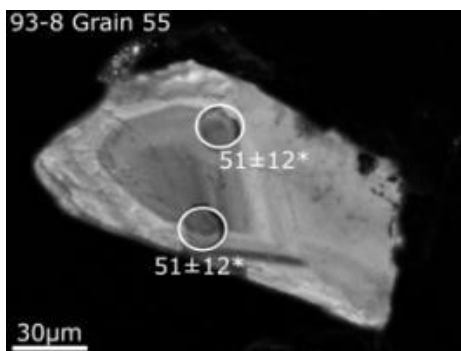
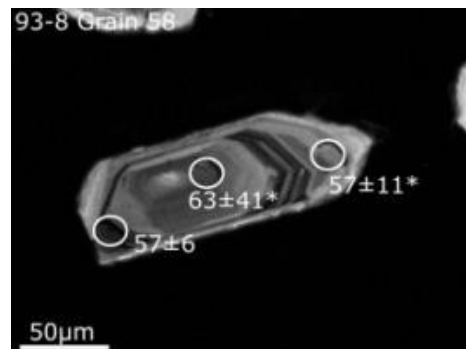
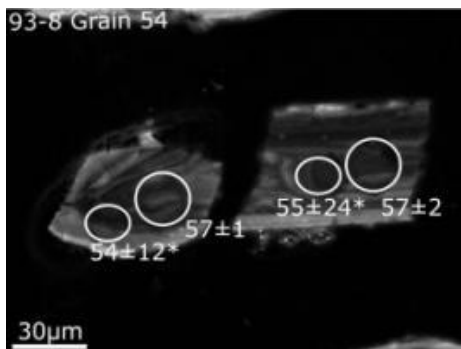
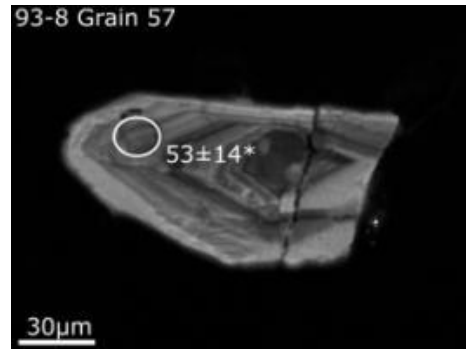
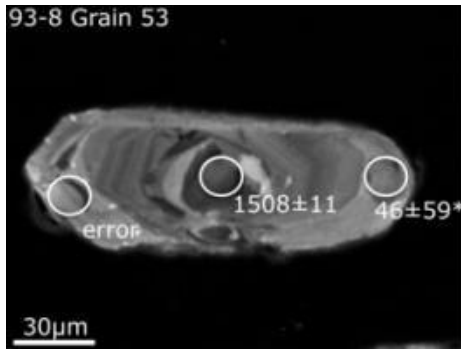
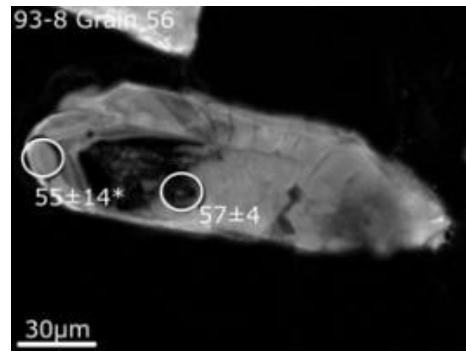
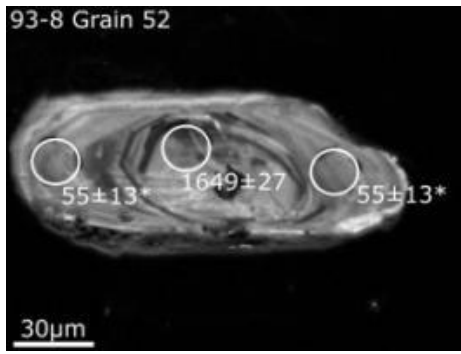


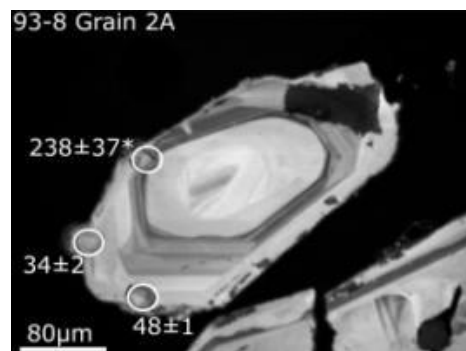
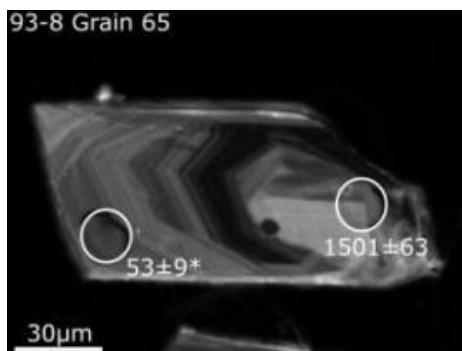
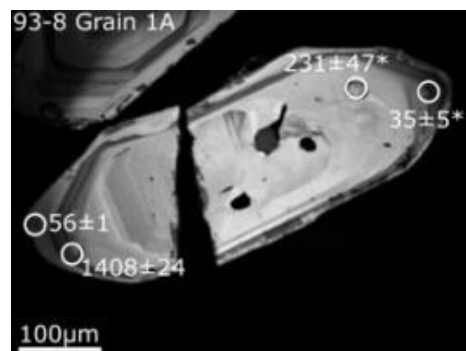
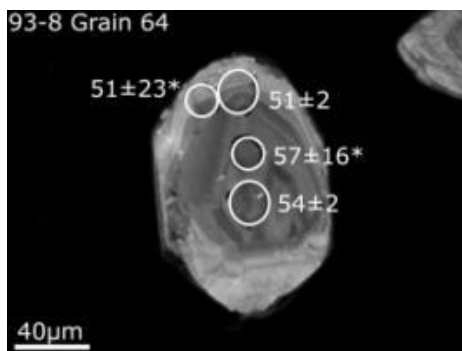
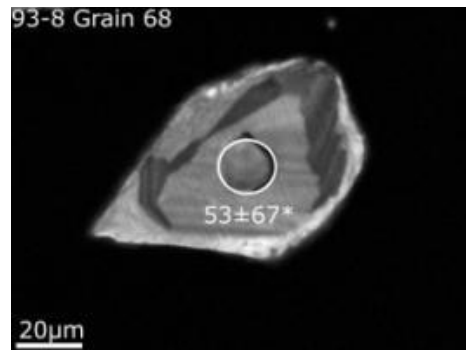
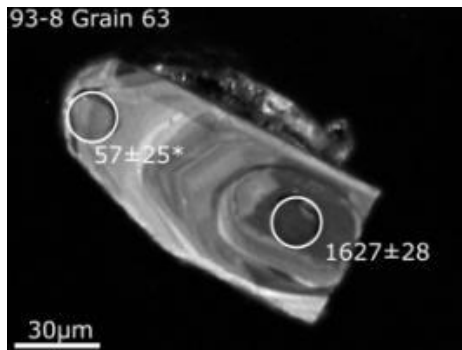
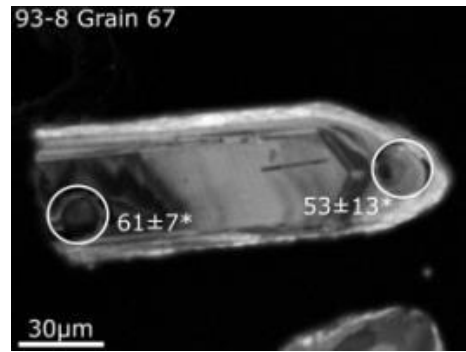
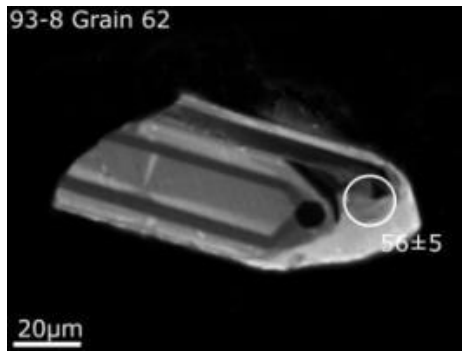




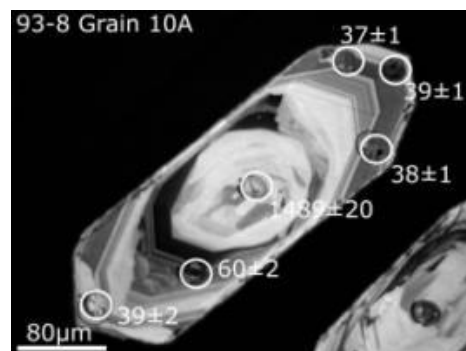
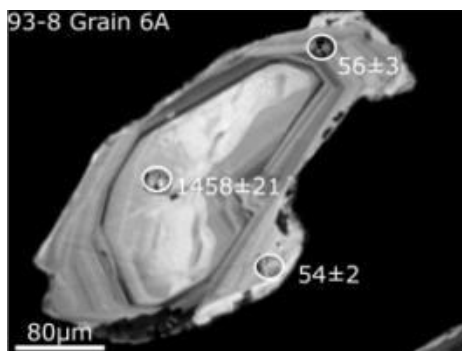
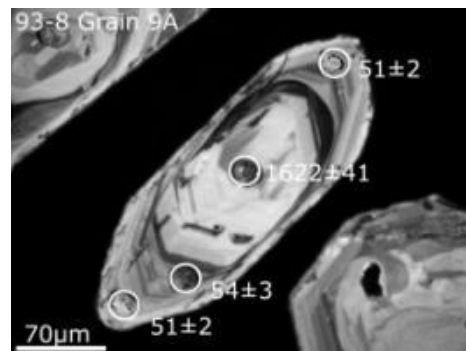
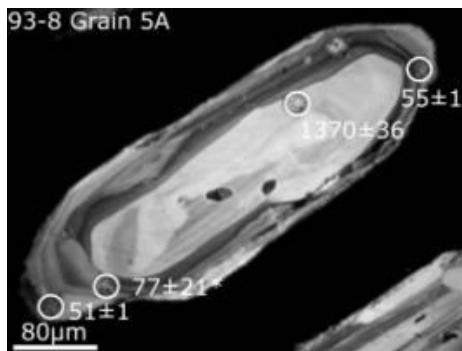
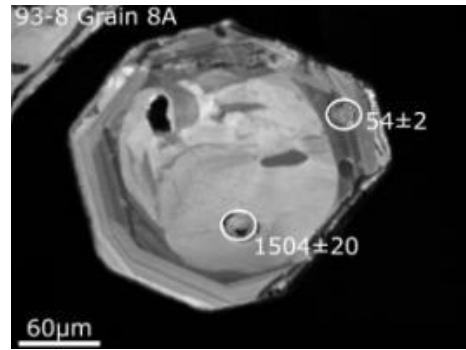
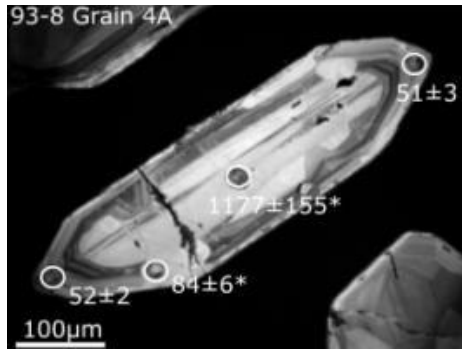
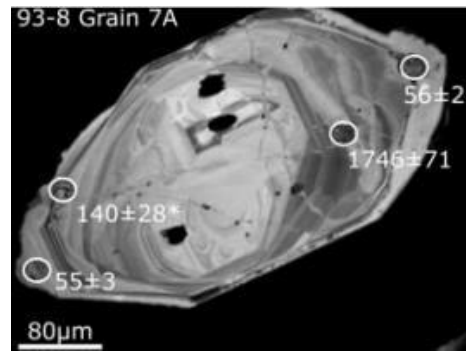
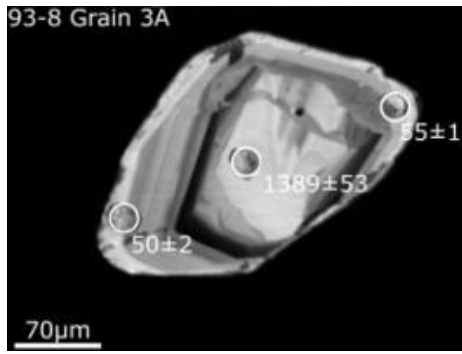


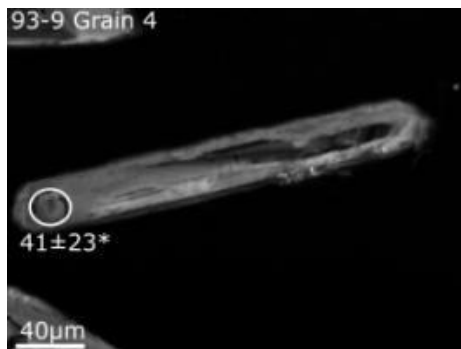
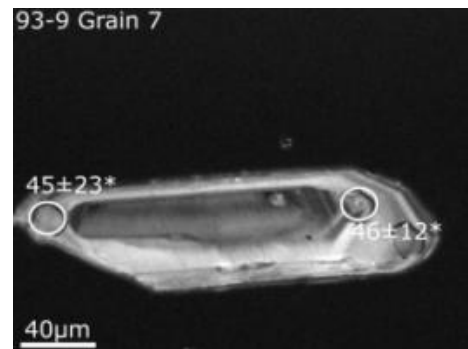
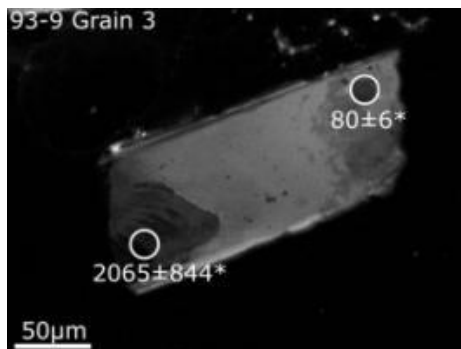
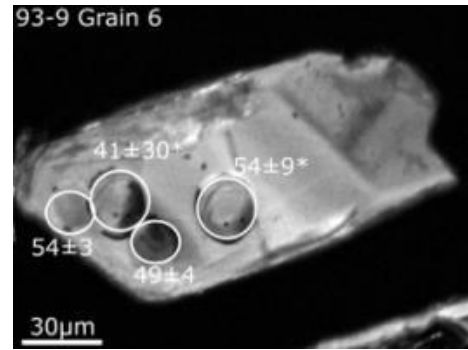
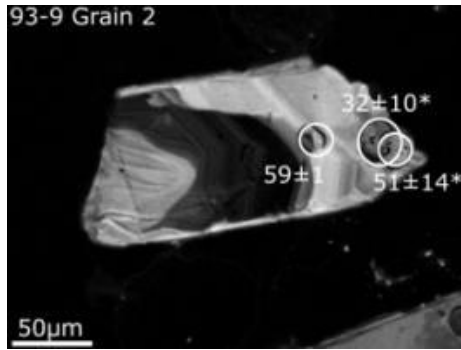
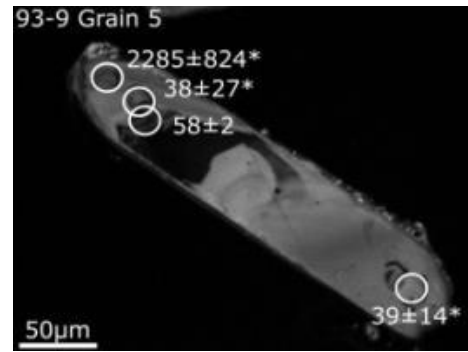
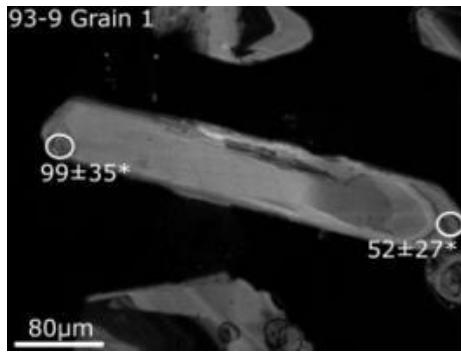


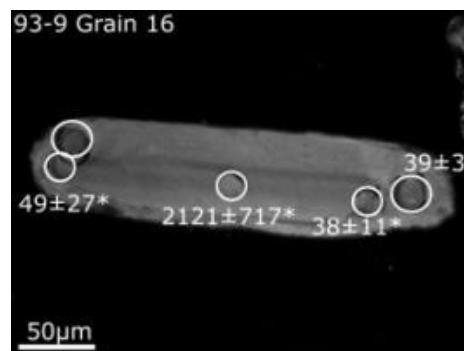
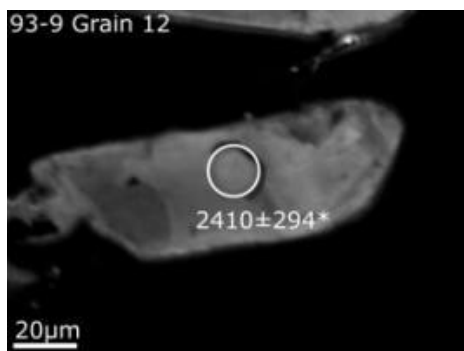
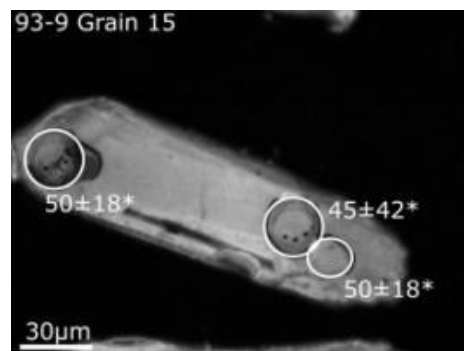
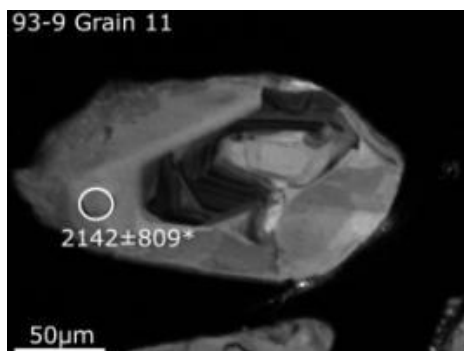
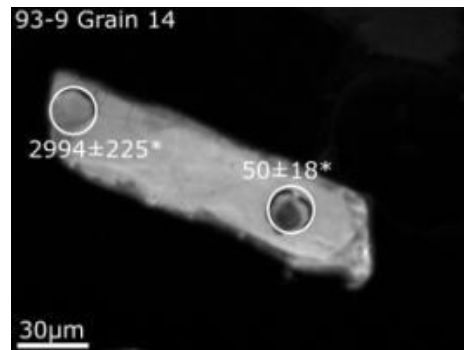
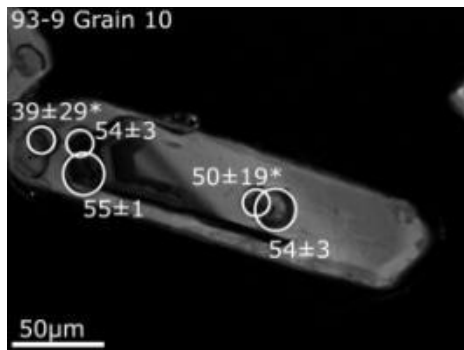
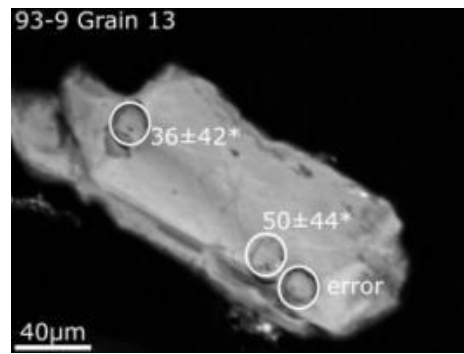
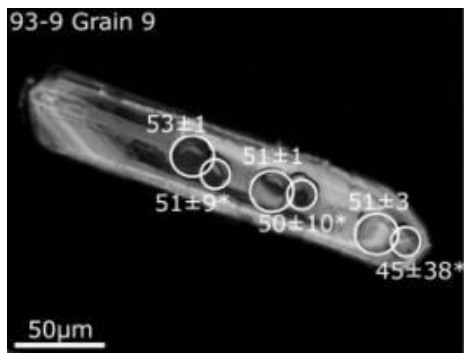


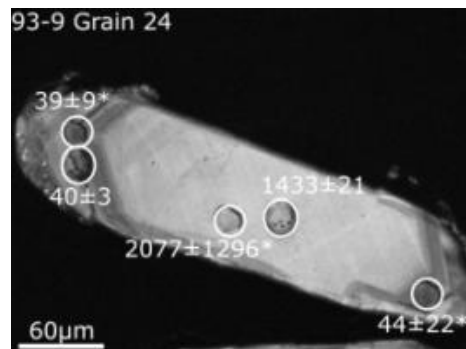
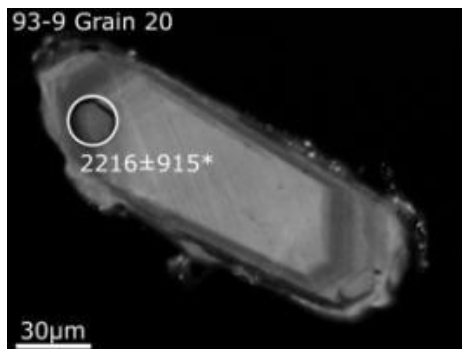
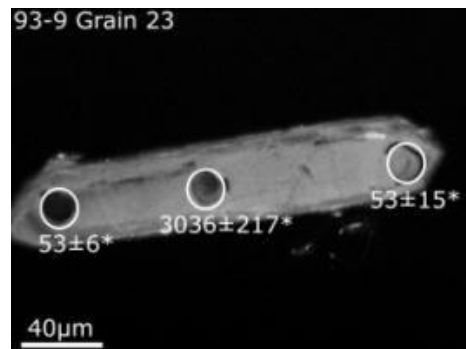
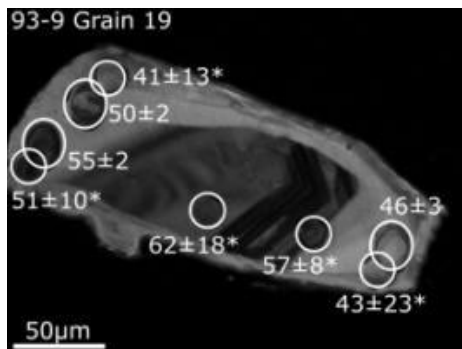
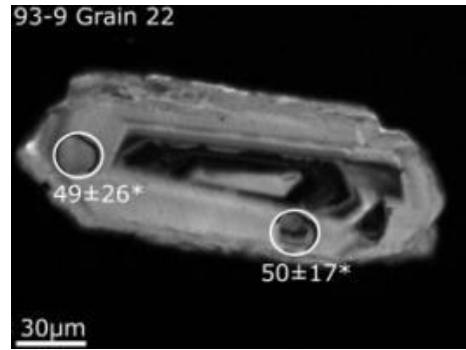
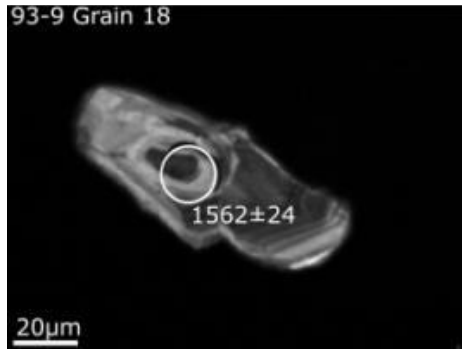
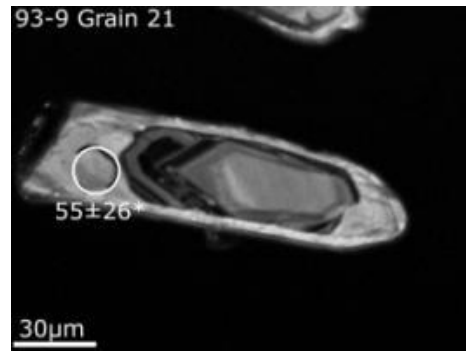
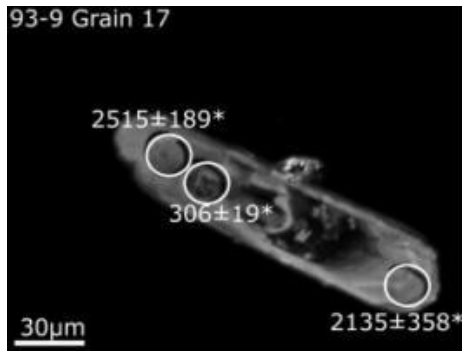


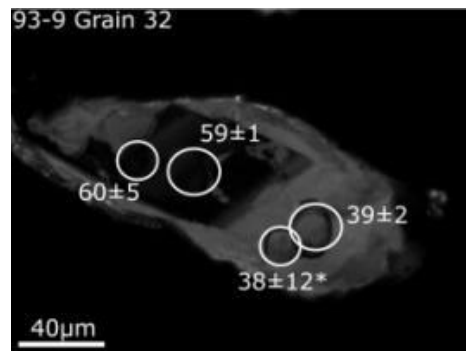
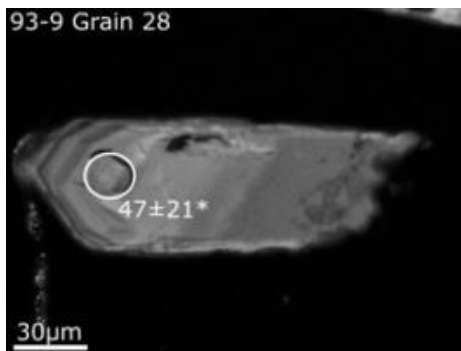
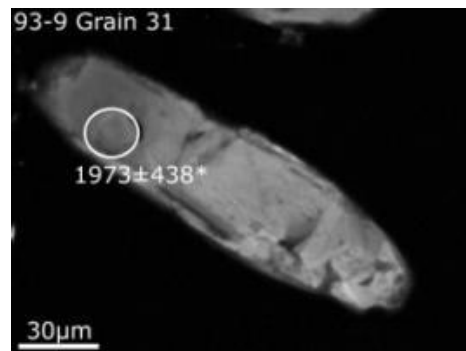
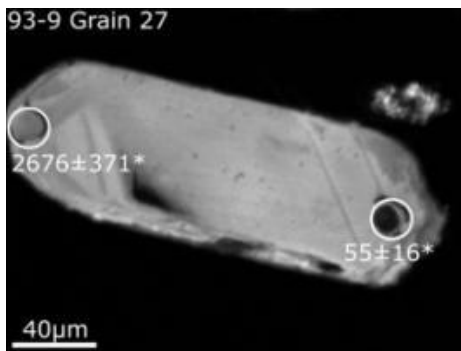
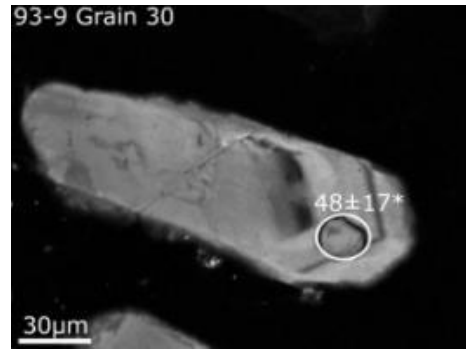
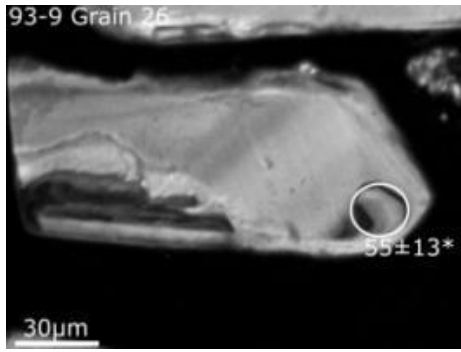
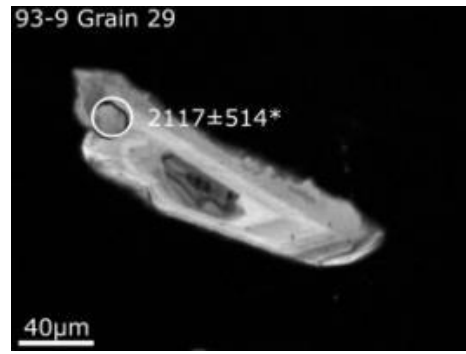
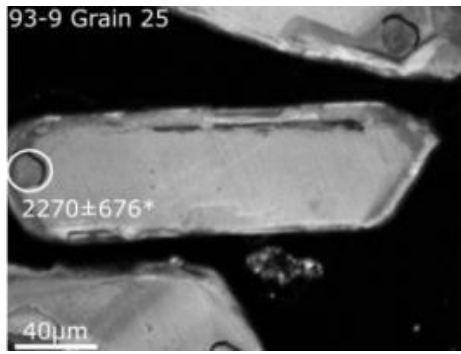


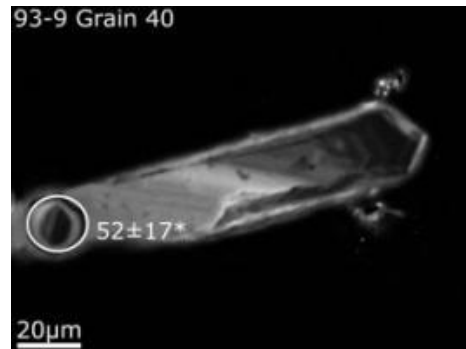
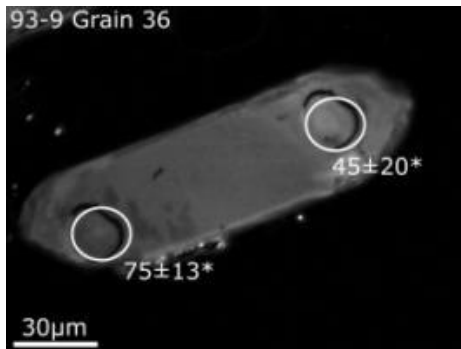
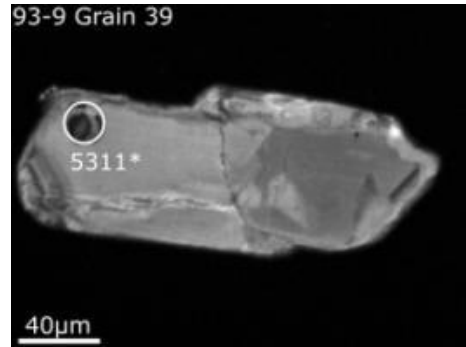
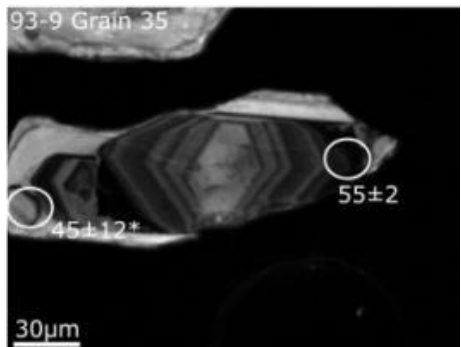
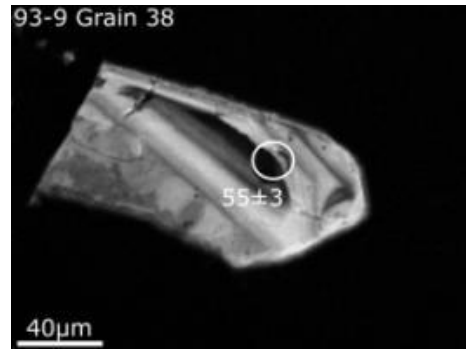
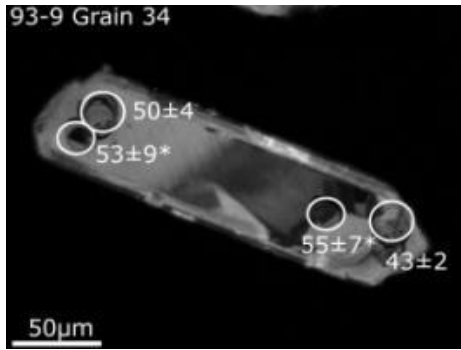
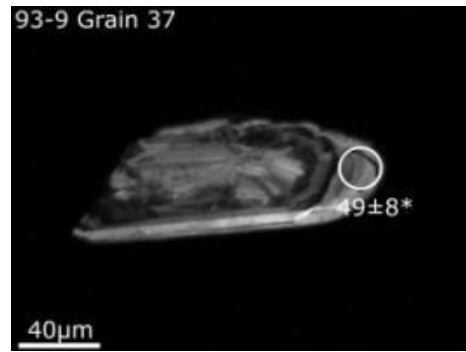
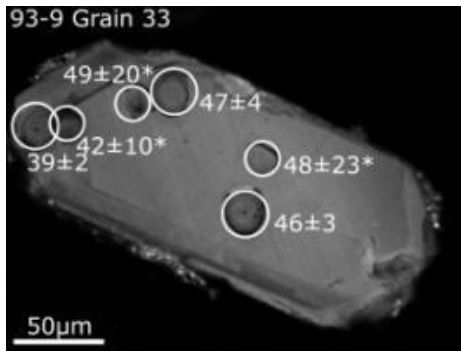


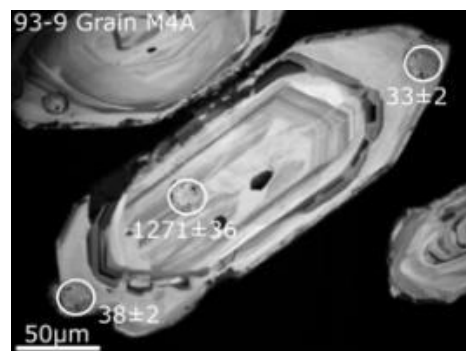
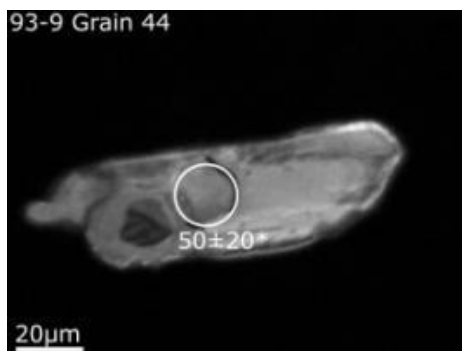
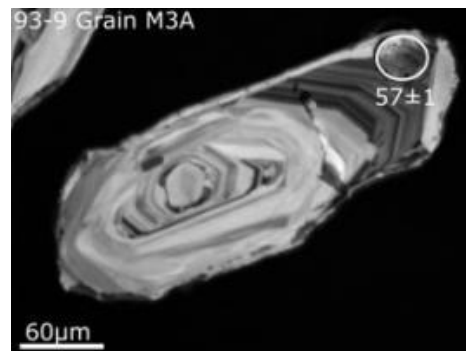
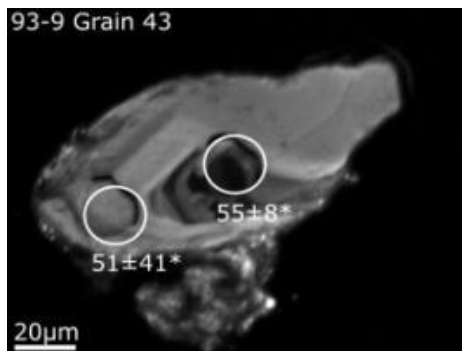
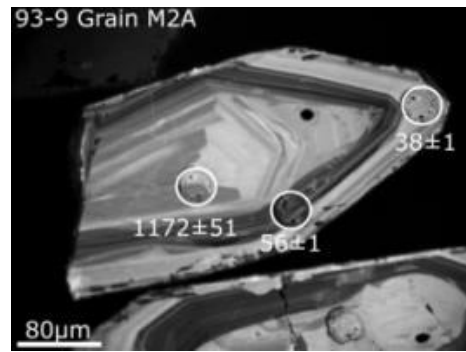
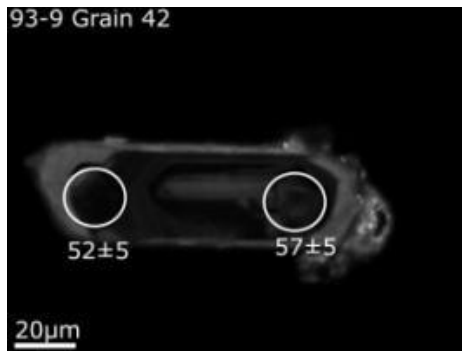
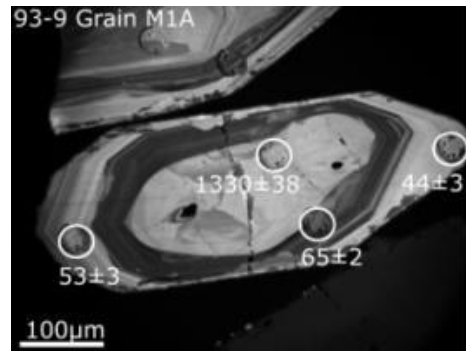
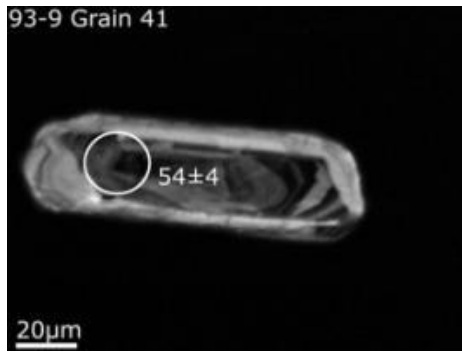


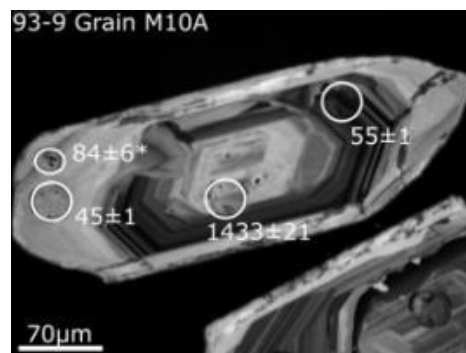
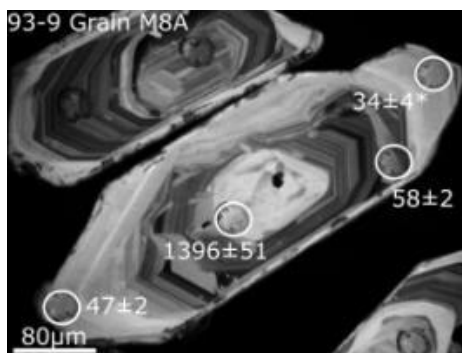
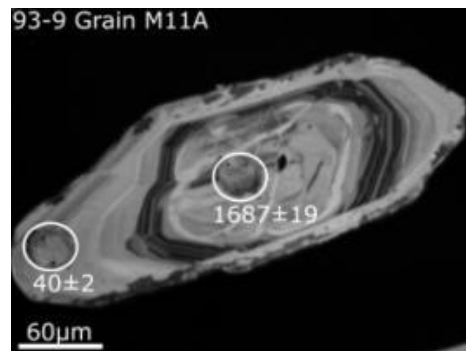
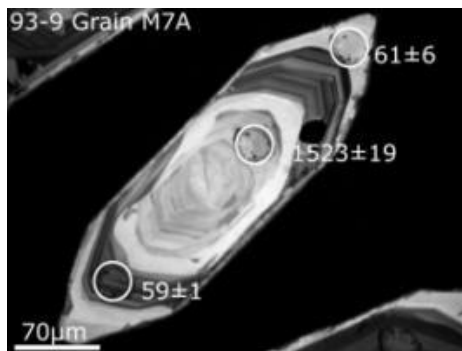
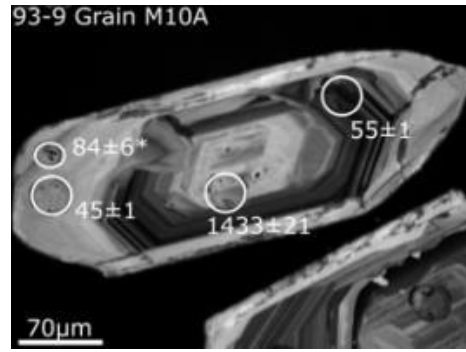
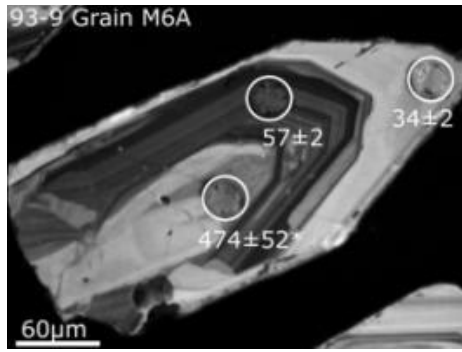
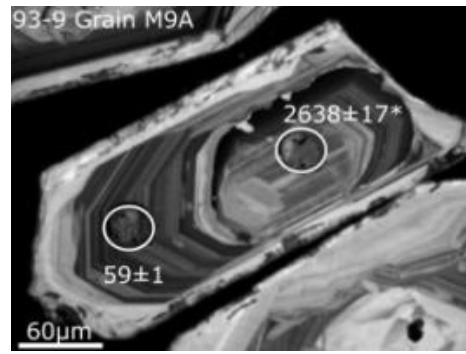
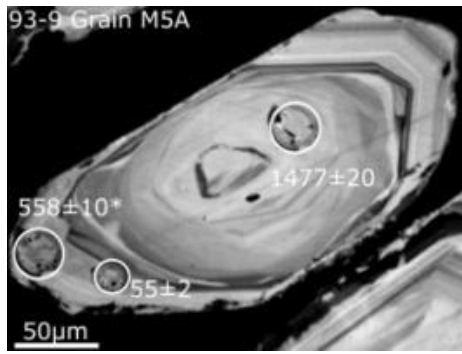




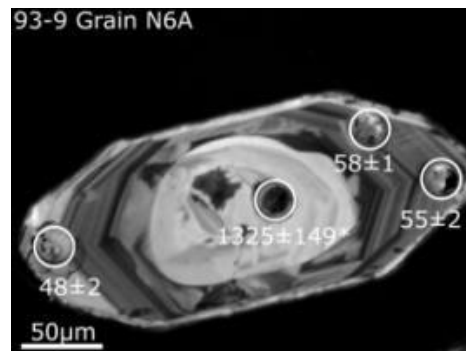
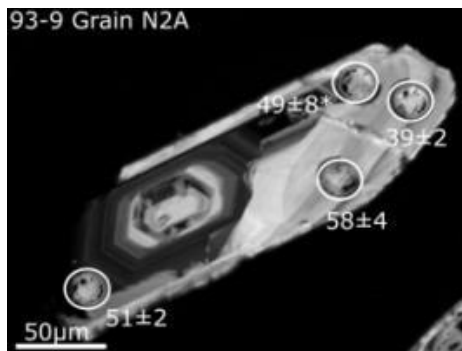
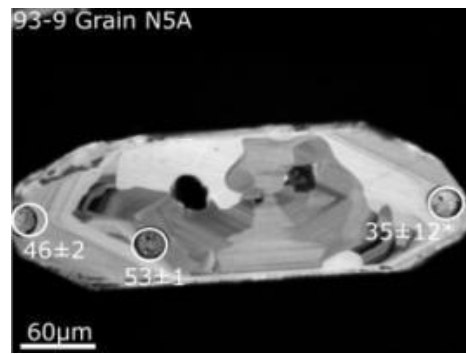
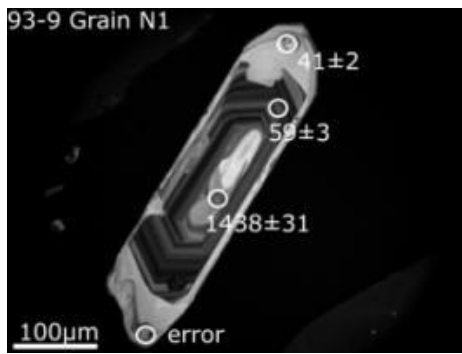
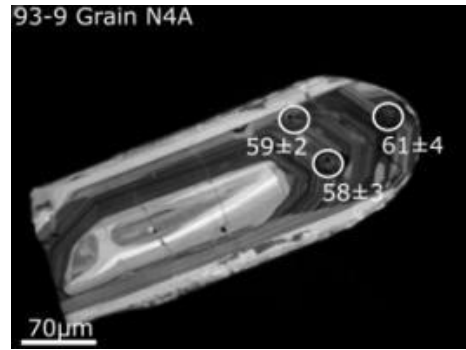
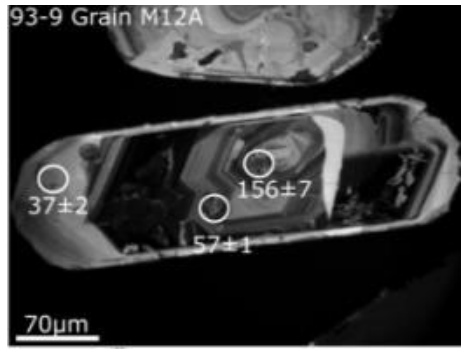
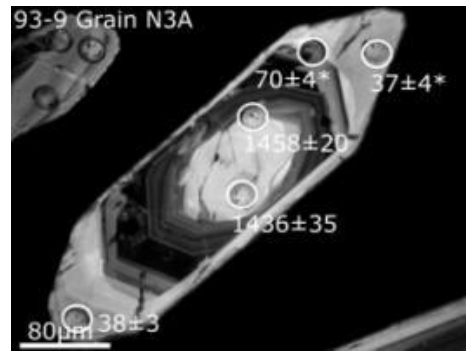
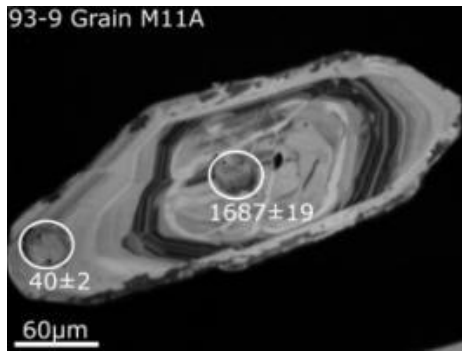


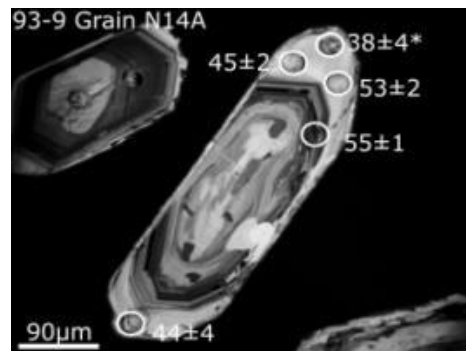
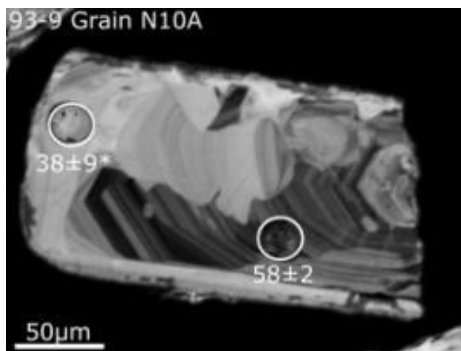
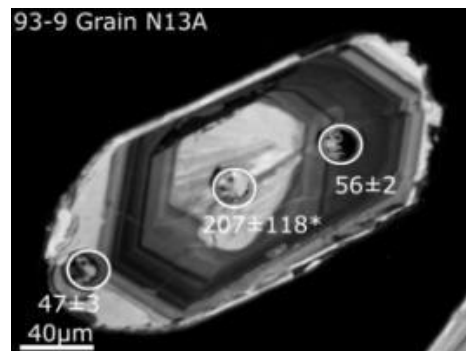
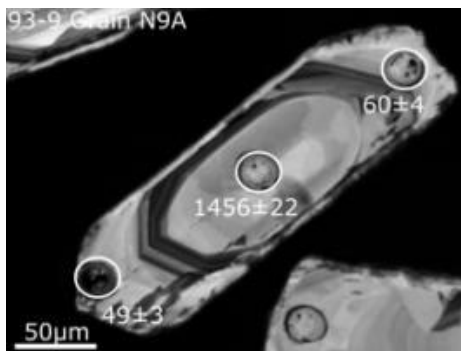
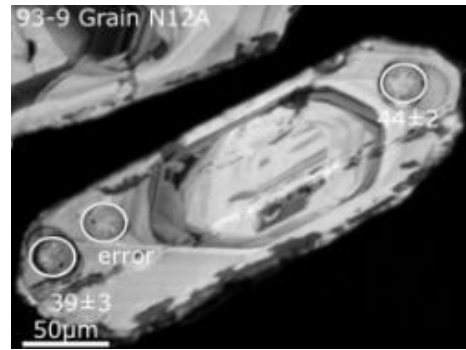
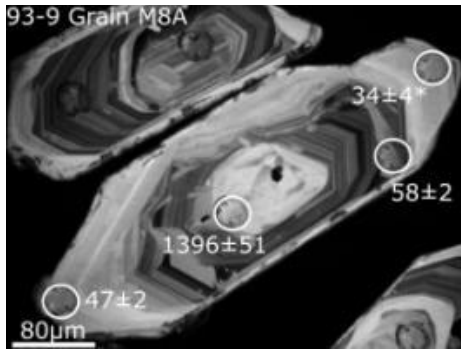
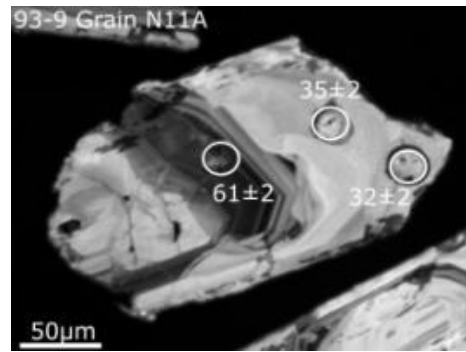
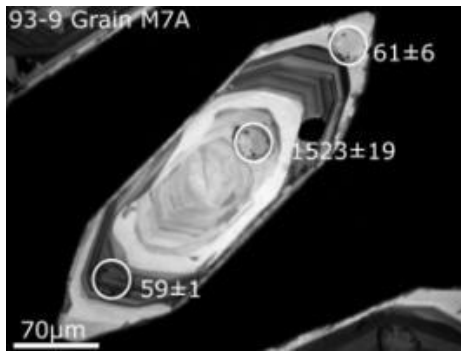


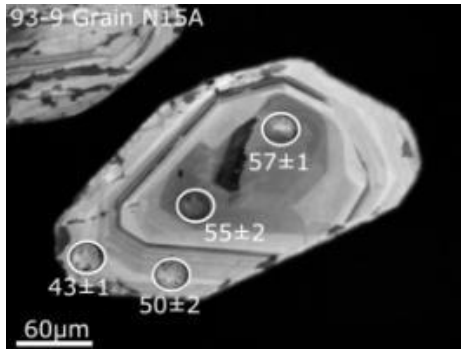












## **Appendix 1.3**

### **LA-ICPMS Zircon U/Pb Data**

| CAT 93-4      |       |       |         | Isotopic ratios |        |      |        |     |       |        | Apparent ages (Ma) |        |      |        |       |          |      |
|---------------|-------|-------|---------|-----------------|--------|------|--------|-----|-------|--------|--------------------|--------|------|--------|-------|----------|------|
| Analysis      | U     | 206Pb | 206Pb*  | ±               | 207Pb* | ±    | 206Pb* | ±   | error | 206Pb* | ±                  | 207Pb* | ±    | 206Pb* | ±     | Best age | ±    |
|               | (ppm) | 204Pb | 207Pb*  | (%)             | 235U*  | (%)  | 238U   | (%) | corr. | 238U*  | (Ma)               | 235U   | (Ma) | 207Pb* | (Ma)  | (Ma)     | (Ma) |
| CAT93-4-G1-1  | 3683  | 4647  | 20.4956 | 4.4             | 0.0577 | 6.2  | 0.0086 | 4.4 | 0.70  | 55.1   | 2.4                | 57.0   | 3.4  | 137.8  | 103.8 | 55.1     | 2.4  |
| CAT93-4-G2-1  | 4743  | 6686  | 20.2497 | 3.1             | 0.0611 | 4.6  | 0.0090 | 3.3 | 0.73  | 57.5   | 1.9                | 60.2   | 2.7  | 166.0  | 72.5  | 57.5     | 1.9  |
| CAT93-4-G2-2  | 6300  | 16383 | 20.2596 | 2.1             | 0.0603 | 3.9  | 0.0089 | 3.3 | 0.85  | 56.9   | 1.9                | 59.5   | 2.2  | 164.9  | 48.0  | 56.9     | 1.9  |
| CAT93-4-G3-1  | 5620  | 4225  | 20.7240 | 3.5             | 0.0590 | 5.1  | 0.0089 | 3.7 | 0.72  | 56.9   | 2.1                | 58.2   | 2.9  | 111.7  | 83.2  | 56.9     | 2.1  |
| CAT93-4-G4-1  | 1899  | 1070  | 22.3127 | 11.6            | 0.0526 | 13.1 | 0.0085 | 6.2 | 0.47  | 54.6   | 3.4                | 52.1   | 6.6  | -65.6  | 282.7 | 54.6     | 3.4  |
| CAT93-4-G4-2  | 1990  | 2478  | 19.9621 | 7.0             | 0.0621 | 10.5 | 0.0090 | 7.8 | 0.74  | 57.7   | 4.4                | 61.1   | 6.2  | 199.4  | 163.9 | 57.7     | 4.4  |
| CAT93-4-G5-1  | 2138  | 2130  | 22.0697 | 8.1             | 0.0553 | 10.2 | 0.0089 | 6.2 | 0.61  | 56.8   | 3.5                | 54.7   | 5.4  | -38.9  | 196.5 | 56.8     | 3.5  |
| CAT93-4-G7-1  | 6368  | 9521  | 20.6023 | 3.0             | 0.0587 | 4.4  | 0.0088 | 3.2 | 0.73  | 56.3   | 1.8                | 58.0   | 2.5  | 125.6  | 71.1  | 56.3     | 1.8  |
| CAT93-4-G8-2  | 2996  | 5290  | 20.1225 | 5.3             | 0.0573 | 7.1  | 0.0084 | 4.7 | 0.66  | 53.7   | 2.5                | 56.6   | 3.9  | 180.8  | 124.0 | 53.7     | 2.5  |
| CAT93-4-G9-1  | 4145  | 4069  | 22.0213 | 4.2             | 0.0527 | 5.9  | 0.0084 | 4.2 | 0.70  | 54.1   | 2.2                | 52.2   | 3.0  | -33.6  | 102.8 | 54.1     | 2.2  |
| CAT93-4-G10-1 | 4843  | 6688  | 20.1852 | 3.4             | 0.0600 | 4.9  | 0.0088 | 3.6 | 0.73  | 56.3   | 2.0                | 59.1   | 2.8  | 173.5  | 78.5  | 56.3     | 2.0  |
| CAT93-4-G11-1 | 3306  | 2879  | 20.2604 | 5.0             | 0.0601 | 6.7  | 0.0088 | 4.5 | 0.67  | 56.7   | 2.5                | 59.3   | 3.9  | 164.8  | 116.5 | 56.7     | 2.5  |
| CAT93-4-G11-2 | 2623  | 2266  | 20.6230 | 5.1             | 0.0578 | 7.3  | 0.0086 | 5.3 | 0.72  | 55.5   | 2.9                | 57.0   | 4.1  | 123.2  | 119.2 | 55.5     | 2.9  |
| CAT93-4-G12-1 | 1931  | 4994  | 18.3248 | 6.2             | 0.0677 | 8.9  | 0.0090 | 6.5 | 0.72  | 57.7   | 3.7                | 66.5   | 5.8  | 394.7  | 138.4 | 57.7     | 3.7  |
| CAT93-4-G12-2 | 3323  | 4775  | 20.0991 | 3.7             | 0.0655 | 5.8  | 0.0095 | 4.5 | 0.77  | 61.2   | 2.7                | 64.4   | 3.6  | 183.5  | 86.0  | 61.2     | 2.7  |
| CAT93-4-G13-1 | 1195  | 1538  | 18.6832 | 9.1             | 0.0721 | 12.7 | 0.0098 | 8.8 | 0.70  | 62.6   | 5.5                | 70.7   | 8.6  | 351.1  | 205.7 | 62.6     | 5.5  |
| CAT93-4-G14-1 | 2714  | 2772  | 20.1193 | 4.9             | 0.0615 | 7.3  | 0.0090 | 5.4 | 0.74  | 57.6   | 3.1                | 60.6   | 4.3  | 181.1  | 114.0 | 57.6     | 3.1  |
| CAT93-4-G14-2 | 3759  | 3736  | 19.5796 | 3.4             | 0.0697 | 5.3  | 0.0099 | 4.0 | 0.76  | 63.5   | 2.5                | 68.4   | 3.5  | 244.1  | 79.2  | 63.5     | 2.5  |
| CAT93-4-G15-1 | 1746  | 3201  | 18.1218 | 5.5             | 0.0711 | 8.6  | 0.0094 | 6.6 | 0.77  | 60.0   | 3.9                | 69.8   | 5.8  | 419.6  | 121.8 | 60.0     | 3.9  |
| CAT93-4-G16-1 | 4997  | 12538 | 20.5438 | 2.7             | 0.0580 | 4.6  | 0.0086 | 3.7 | 0.81  | 55.5   | 2.0                | 57.3   | 2.5  | 132.3  | 63.1  | 55.5     | 2.0  |
| CAT93-4-G16-2 | 2060  | 3577  | 18.1943 | 6.7             | 0.0655 | 9.3  | 0.0086 | 6.5 | 0.70  | 55.4   | 3.6                | 64.4   | 5.8  | 410.7  | 149.8 | 55.4     | 3.6  |
| CAT93-4-G17-1 | 1569  | 1068  | 21.7919 | 9.7             | 0.0546 | 12.3 | 0.0086 | 7.5 | 0.61  | 55.4   | 4.2                | 54.0   | 6.5  | -8.2   | 235.3 | 55.4     | 4.2  |
| CAT93-4-G18-1 | 4337  | 4269  | 20.4216 | 4.0             | 0.0576 | 5.7  | 0.0085 | 4.0 | 0.71  | 54.8   | 2.2                | 56.9   | 3.1  | 146.3  | 93.0  | 54.8     | 2.2  |
| CAT93-4-G18-2 | 6068  | 4638  | 20.8660 | 2.7             | 0.0581 | 4.2  | 0.0088 | 3.2 | 0.76  | 56.5   | 1.8                | 57.4   | 2.4  | 95.5   | 64.5  | 56.5     | 1.8  |
| CAT93-4-G19-1 | 4720  | 4415  | 20.0725 | 3.6             | 0.0577 | 5.4  | 0.0084 | 4.1 | 0.75  | 53.9   | 2.2                | 56.9   | 3.0  | 186.6  | 83.0  | 53.9     | 2.2  |
| CAT93-4-G21-1 | 8773  | 3377  | 18.7260 | 1.9             | 0.0672 | 3.4  | 0.0091 | 2.8 | 0.83  | 58.6   | 1.6                | 66.0   | 2.2  | 345.9  | 42.6  | 58.6     | 1.6  |
| CAT93-4-G21-2 | 4403  | 17000 | 20.7168 | 2.7             | 0.0605 | 4.8  | 0.0091 | 3.9 | 0.82  | 58.4   | 2.3                | 59.7   | 2.8  | 112.5  | 64.2  | 58.4     | 2.3  |
| CAT93-4-G6-1  | 1272  | 13519 | 9.5009  | 0.7             | 1.6381 | 2.3  | 0.1129 | 2.2 | 0.95  | 689.4  | 14.2               | 985.0  | 14.3 | 1718.7 | 12.5  | 1718.7   | 12.5 |

\*indicates the analysis was not included in the calculations for the mean age

| CAT0705        |       |       |         | Isotopic ratios |        |       |        |       |       | Apparent ages (Ma) |      |        |       |        |       |          |      |
|----------------|-------|-------|---------|-----------------|--------|-------|--------|-------|-------|--------------------|------|--------|-------|--------|-------|----------|------|
| Analysis       | U     | 206Pb | 206Pb*  | ±               | 207Pb* | ±     | 206Pb* | ±     | error | 206Pb*             | ±    | 207Pb* | ±     | 206Pb* | ±     | Best age | ±    |
|                | (ppm) | 204Pb | 207Pb*  | (%)             | 235U*  | (%)   | 238U   | (%)   | corr. | 238U*              | (Ma) | 235U   | (Ma)  | 207Pb* | (Ma)  | (Ma)     | (Ma) |
| CAT0705-G3-3   | 1452  | 1222  | 13.0480 | 6.8             | 0.0783 | 11.3  | 0.0074 | 9.0   | 0.80  | 47.6               | 4.3  | 76.5   | 8.3   | 1111.8 | 136.5 | 47.6     | 4.3  |
| CAT0705-G4-1   | 3884  | 3929  | 16.9794 | 3.8             | 0.0578 | 5.9   | 0.0071 | 4.4   | 0.76  | 45.7               | 2.0  | 57.0   | 3.3   | 563.2  | 83.8  | 45.7     | 2.0  |
| CAT0705-G6-2   | 2385  | 1290  | 12.2587 | 4.4             | 0.0802 | 7.6   | 0.0071 | 6.2   | 0.82  | 45.8               | 2.8  | 78.3   | 5.7   | 1235.3 | 86.3  | 45.8     | 2.8  |
| CAT0705-G6-3   | 2652  | 1452  | 17.3766 | 5.7             | 0.0541 | 9.0   | 0.0068 | 7.0   | 0.78  | 43.8               | 3.0  | 53.5   | 4.7   | 512.6  | 124.7 | 43.8     | 3.0  |
| CAT0705-G20-1  | 1173  | 701   | 14.8661 | 9.7             | 0.0664 | 13.4  | 0.0072 | 9.2   | 0.69  | 46.0               | 4.2  | 65.3   | 8.4   | 846.0  | 202.7 | 46.0     | 4.2  |
| CAT0705-G21-1  | 2526  | 922   | 14.9914 | 6.6             | 0.0657 | 9.2   | 0.0071 | 6.4   | 0.69  | 45.9               | 2.9  | 64.6   | 5.8   | 828.6  | 138.4 | 45.9     | 2.9  |
| CAT0705-G21-3  | 1504  | 1603  | 18.9435 | 9.3             | 0.0547 | 13.4  | 0.0075 | 9.6   | 0.72  | 48.3               | 4.6  | 54.1   | 7.0   | 319.7  | 211.6 | 48.3     | 4.6  |
| CAT0705-G27-1  | 2328  | 1823  | 18.0455 | 8.0             | 0.0518 | 10.3  | 0.0068 | 6.6   | 0.64  | 43.5               | 2.9  | 51.2   | 5.2   | 429.0  | 177.8 | 43.5     | 2.9  |
| CAT0705-G30-1  | 3007  | 2010  | 16.4749 | 4.3             | 0.0574 | 7.6   | 0.0069 | 6.2   | 0.82  | 44.1               | 2.7  | 56.7   | 4.2   | 628.5  | 93.5  | 44.1     | 2.7  |
| CAT0705-G33-1  | 1382  | 2125  | 15.1612 | 8.0             | 0.0670 | 11.4  | 0.0074 | 8.2   | 0.71  | 47.3               | 3.9  | 65.9   | 7.3   | 805.0  | 167.9 | 47.3     | 3.9  |
| CAT0705-G33-2  | 1925  | 2380  | 16.9019 | 5.1             | 0.0712 | 8.5   | 0.0087 | 6.9   | 0.80  | 56.0               | 3.8  | 69.8   | 5.8   | 573.2  | 110.7 | 56.0     | 3.8  |
| CAT0705-G34-1  | 1563  | 1456  | 14.4904 | 6.8             | 0.0631 | 11.7  | 0.0066 | 9.5   | 0.82  | 42.6               | 4.0  | 62.1   | 7.0   | 899.1  | 139.7 | 42.6     | 4.0  |
| CAT0705-G34-2  | 1467  | 9093  | 18.7693 | 6.9             | 0.0544 | 11.6  | 0.0074 | 9.3   | 0.80  | 47.5               | 4.4  | 53.7   | 6.1   | 340.6  | 157.3 | 47.5     | 4.4  |
| CAT0705-G35-1  | 2235  | 1559  | 13.1978 | 5.2             | 0.0716 | 8.4   | 0.0069 | 6.6   | 0.79  | 44.0               | 2.9  | 70.2   | 5.7   | 1089.0 | 104.6 | 44.0     | 2.9  |
| CAT0705-G36-1  | 1458  | 3309  | 13.7911 | 6.4             | 0.0707 | 11.2  | 0.0071 | 9.2   | 0.82  | 45.4               | 4.2  | 69.4   | 7.5   | 1000.3 | 130.6 | 45.4     | 4.2  |
| CAT0705-G1-3   | 1654  | 5951  | 20.5630 | 5.8             | 0.0610 | 8.7   | 0.0091 | 6.5   | 0.75  | 58.4               | 3.8  | 60.1   | 5.1   | 130.1  | 135.5 | 58.4     | 3.8  |
| CAT0705-G2-1*  | 1165  | 1293  | 14.0594 | 7.4             | 0.0712 | 13.1  | 0.0073 | 10.8  | 0.83  | 46.7               | 5.0  | 69.9   | 8.8   | 961.0  | 151.2 | 46.7     | 5.0  |
| CAT0705-G2-2*  | 1082  | 1265  | 13.9817 | 8.4             | 0.0690 | 13.7  | 0.0070 | 10.8  | 0.79  | 44.9               | 4.8  | 67.7   | 9.0   | 972.3  | 171.4 | 44.9     | 4.8  |
| CAT0705-G2-4*  | 48    | 258   | 13.0011 | 93.5            | 0.0911 | 151.4 | 0.0086 | 119.0 | 0.79  | 55.2               | 65.4 | 88.6   | 129.1 | 1119.0 | 183.8 | 55.2     | 65.4 |
| CAT0705-G3-1*  | 1085  | 8315  | 11.4928 | 1.3             | 0.7793 | 3.2   | 0.0650 | 2.9   | 0.91  | 405.7              | 11.5 | 585.1  | 14.2  | 1360.7 | 25.5  | 405.7    | 11.5 |
| CAT0705-G3-4*  | 546   | 1208  | 14.2141 | 15.6            | 0.0780 | 22.3  | 0.0080 | 16.0  | 0.71  | 51.6               | 8.2  | 76.3   | 16.4  | 938.6  | 322.0 | 51.6     | 8.2  |
| CAT0705-G5-1*  | 763   | 731   | 13.6793 | 11.0            | 0.0709 | 17.6  | 0.0070 | 13.8  | 0.78  | 45.2               | 6.2  | 69.5   | 11.9  | 1016.8 | 224.1 | 45.2     | 6.2  |
| CAT0705-G6-4*  | 67    | 168   | 10.1480 | 49.7            | 0.1249 | 93.7  | 0.0092 | 79.4  | 0.85  | 59.0               | 46.6 | 119.5  | 106.0 | 1596.7 | 996.2 | 59.0     | 46.6 |
| CAT0705-G7-1*  | 810   | 611   | 10.3766 | 9.4             | 0.0977 | 16.6  | 0.0074 | 13.7  | 0.83  | 47.2               | 6.4  | 94.7   | 15.0  | 1555.0 | 176.1 | 47.2     | 6.4  |
| CAT0705-G7-2*  | 885   | 1420  | 13.3911 | 7.2             | 0.0733 | 13.6  | 0.0071 | 11.5  | 0.85  | 45.8               | 5.2  | 71.9   | 9.4   | 1059.8 | 146.0 | 45.8     | 5.2  |
| CAT0705-G9-1*  | 892   | 451   | 11.2909 | 9.6             | 0.0867 | 15.2  | 0.0071 | 11.8  | 0.78  | 45.6               | 5.3  | 84.4   | 12.3  | 1394.8 | 184.3 | 45.6     | 5.3  |
| CAT0705-G10-1* | 67    | 87    | 2.1758  | 8.3             | 0.8906 | 42.1  | 0.0141 | 41.3  | 0.98  | 90.0               | 36.9 | 646.7  | 204.0 | 0.0    | 0.0   | 90.0     | 36.9 |
| CAT0705-G21-2* | 785   | 711   | 11.3834 | 10.1            | 0.0734 | 18.0  | 0.0061 | 14.9  | 0.83  | 38.9               | 5.8  | 71.9   | 12.5  | 1379.1 | 193.9 | 38.9     | 5.8  |

\*indicates the analysis was not included in the calculations for the mean age

| CAT0705, cont. |       |       |         | Isotopic ratios |        |      |        |      |       | Apparent ages (Ma) |       |        |      |        |       |          |      |
|----------------|-------|-------|---------|-----------------|--------|------|--------|------|-------|--------------------|-------|--------|------|--------|-------|----------|------|
| Analysis       | U     | 206Pb | 206Pb*  | ±               | 207Pb* | ±    | 206Pb* | ±    | error | 206Pb*             | ±     | 207Pb* | ±    | 206Pb* | ±     | Best age | ±    |
|                | (ppm) | 204Pb | 207Pb*  | (%)             | 235U*  | (%)  | 238U   | (%)  | corr. | 238U*              | (Ma)  | 235U   | (Ma) | 207Pb* | (Ma)  | (Ma)     | (Ma) |
| CAT0705-G22-1* | 136   | 457   | 10.1072 | 29.3            | 0.1357 | 54.8 | 0.0099 | 46.4 | 0.85  | 63.8               | 29.4  | 129.2  | 66.6 | 1604.2 | 558.7 | 63.8     | 29.4 |
| CAT0705-G23-1* | 761   | 896   | 11.6080 | 9.4             | 0.0874 | 17.6 | 0.0074 | 14.9 | 0.85  | 47.3               | 7.0   | 85.1   | 14.4 | 1341.5 | 182.1 | 47.3     | 7.0  |
| CAT0705-G24-1* | 968   | 967   | 12.5760 | 9.2             | 0.0836 | 14.7 | 0.0076 | 11.5 | 0.78  | 49.0               | 5.6   | 81.5   | 11.5 | 1185.0 | 181.4 | 49.0     | 5.6  |
| CAT0705-G25-1* | 409   | 540   | 9.3294  | 17.1            | 0.1079 | 26.9 | 0.0073 | 20.8 | 0.77  | 46.9               | 9.7   | 104.1  | 26.7 | 1752.1 | 315.6 | 46.9     | 9.7  |
| CAT0705-G25-2* | 1225  | 665   | 12.8509 | 9.0             | 0.0762 | 14.4 | 0.0071 | 11.3 | 0.78  | 45.6               | 5.1   | 74.6   | 10.4 | 1142.2 | 179.9 | 45.6     | 5.1  |
| CAT0705-G25-3* | 125   | 1078  | 10.5616 | 8.2             | 0.7623 | 17.0 | 0.0584 | 14.9 | 0.88  | 365.8              | 53.0  | 575.3  | 74.8 | 1521.8 | 154.0 | 365.8    | 53.0 |
| CAT0705-G26-1* | 747   | 819   | 14.5959 | 10.8            | 0.0716 | 18.1 | 0.0076 | 14.5 | 0.80  | 48.7               | 7.1   | 70.2   | 12.3 | 884.1  | 223.9 | 48.7     | 7.1  |
| CAT0705-G28-1* | 830   | 2104  | 15.1219 | 10.7            | 0.0640 | 17.3 | 0.0070 | 13.6 | 0.78  | 45.1               | 6.1   | 63.0   | 10.6 | 810.5  | 225.3 | 45.1     | 6.1  |
| CAT0705-G29-1* | 1071  | 780   | 10.0831 | 7.4             | 0.0941 | 14.0 | 0.0069 | 11.9 | 0.85  | 44.2               | 5.2   | 91.3   | 12.2 | 1608.7 | 137.7 | 44.2     | 5.2  |
| CAT0705-G31-1* | 1197  | 1007  | 10.6528 | 6.0             | 0.0967 | 12.4 | 0.0075 | 10.9 | 0.88  | 48.0               | 5.2   | 93.7   | 11.1 | 1505.5 | 113.7 | 48.0     | 5.2  |
| CAT0705-G35-2* | 820   | 895   | 11.6738 | 8.0             | 0.0905 | 17.6 | 0.0077 | 15.7 | 0.89  | 49.2               | 7.7   | 88.0   | 14.8 | 1330.5 | 154.5 | 49.2     | 7.7  |
| CAT0705-G36-2* | 400   | 1549  | 9.8837  | 11.0            | 0.1583 | 21.1 | 0.0113 | 18.0 | 0.85  | 72.7               | 13.0  | 149.2  | 29.3 | 1645.8 | 205.3 | 72.7     | 13.0 |
| CAT0705-G37-1* | 2099  | 4462  | 13.4078 | 2.6             | 0.1381 | 5.3  | 0.0134 | 4.6  | 0.87  | 86.0               | 3.9   | 131.3  | 6.5  | 1057.3 | 52.2  | 86.0     | 3.9  |
| CAT0705-G39-1* | 1183  | 594   | 8.9931  | 6.8             | 0.0992 | 13.9 | 0.0065 | 12.1 | 0.87  | 41.6               | 5.0   | 96.0   | 12.7 | 1819.0 | 123.2 | 41.6     | 5.0  |
| CAT0705-G39-2* | 522   | 717   | 15.3046 | 15.1            | 0.0745 | 20.5 | 0.0083 | 13.9 | 0.68  | 53.1               | 7.4   | 73.0   | 14.5 | 785.3  | 318.2 | 53.1     | 7.4  |
| CAT0705-G2-5   | 287   | 13552 | 11.4993 | 1.5             | 2.2748 | 4.7  | 0.1897 | 4.4  | 0.95  | 1119.9             | 45.6  | 1204.5 | 33.0 | 1359.6 | 28.3  | 1359.6   | 28.3 |
| CAT0705-G3-2   | 115   | 6589  | 11.3171 | 2.4             | 3.1713 | 8.8  | 0.2603 | 8.4  | 0.96  | 1491.4             | 112.2 | 1450.2 | 67.7 | 1390.3 | 46.1  | 1390.3   | 46.1 |
| CAT0705-G3-3   | 1452  | 1222  | 13.0480 | 6.8             | 0.0783 | 11.3 | 0.0074 | 9.0  | 0.80  | 47.6               | 4.3   | 76.5   | 8.3  | 1111.8 | 136.5 | 47.6     | 4.3  |
| CAT0705-G5-2   | 452   | 16654 | 11.0007 | 0.9             | 3.1733 | 3.6  | 0.2532 | 3.5  | 0.97  | 1454.9             | 45.3  | 1450.7 | 27.7 | 1444.6 | 17.0  | 1444.6   | 17.0 |
| CAT0705-G12-1  | 1270  | 57134 | 11.0279 | 0.5             | 2.3254 | 1.7  | 0.1860 | 1.6  | 0.95  | 1099.6             | 16.3  | 1220.1 | 12.0 | 1439.9 | 9.9   | 1439.9   | 9.9  |
| CAT0705-G20-2  | 176   | 3443  | 11.3771 | 2.9             | 1.6737 | 7.6  | 0.1381 | 7.0  | 0.92  | 834.0              | 54.7  | 998.6  | 48.2 | 1380.2 | 55.7  | 1380.2   | 55.7 |
| CAT0705-G21-4  | 238   | 15567 | 9.3672  | 1.1             | 5.0607 | 4.4  | 0.3438 | 4.2  | 0.97  | 1905.0             | 69.9  | 1829.6 | 37.0 | 1744.7 | 19.4  | 1744.7   | 19.4 |
| CAT0705-G23-2  | 147   | 8684  | 10.8897 | 1.9             | 3.1583 | 5.6  | 0.2494 | 5.3  | 0.94  | 1435.6             | 68.4  | 1447.0 | 43.6 | 1463.8 | 36.3  | 1463.8   | 36.3 |
| CAT0705-G23-3  | 485   | 14358 | 11.0461 | 1.3             | 1.4238 | 3.9  | 0.1141 | 3.6  | 0.94  | 696.3              | 24.1  | 899.0  | 23.1 | 1436.7 | 24.9  | 1436.7   | 24.9 |
| CAT0705-G32-1  | 1065  | 13675 | 10.9352 | 0.9             | 1.3849 | 2.4  | 0.1098 | 2.2  | 0.92  | 671.8              | 13.9  | 882.5  | 14.0 | 1455.9 | 17.7  | 1455.9   | 17.7 |
| CAT0705-G37-2  | 136   | 5595  | 10.9157 | 1.9             | 3.1055 | 6.6  | 0.2459 | 6.3  | 0.96  | 1417.1             | 80.4  | 1434.0 | 50.7 | 1459.3 | 36.1  | 1459.3   | 36.1 |
| CAT0705-G38-1  | 680   | 21793 | 10.9302 | 0.8             | 2.7052 | 2.5  | 0.2145 | 2.3  | 0.95  | 1252.5             | 26.6  | 1329.9 | 18.3 | 1456.8 | 15.2  | 1456.8   | 15.2 |
| CAT0705-G38-2  | 561   | 23339 | 10.9468 | 0.7             | 3.2488 | 2.9  | 0.2579 | 2.8  | 0.97  | 1479.3             | 37.1  | 1468.9 | 22.5 | 1453.9 | 13.8  | 1453.9   | 13.8 |

\*indicates the analysis was not included in the calculations for the mean age

| CAT0705, cont. |       |       |      |      | Isotopic ratios |      |        |       |        |       |       | Apparent ages (Ma) |      |        |       |        |        |          |        |
|----------------|-------|-------|------|------|-----------------|------|--------|-------|--------|-------|-------|--------------------|------|--------|-------|--------|--------|----------|--------|
| Analysis       | U     | 206Pb | U/Th | Th/U | 206Pb*          | ±    | 207Pb* | ±     | 206Pb* | ±     | error | 206Pb*             | ±    | 207Pb* | ±     | 206Pb* | ±      | Best age | ±      |
|                | (ppm) | 204Pb |      |      | 207Pb*          | (%)  | 235U*  | (%)   | 238U   | (%)   | corr. | 238U*              | (Ma) | 235U   | (Ma)  | 207Pb* | (Ma)   | (Ma)     | (Ma)   |
| CAT0705-G6-1*  | 786   | 488   | 1.8  | 0.6  | 6.8730          | 5.6  | 0.1609 | 14.7  | 0.0080 | 13.6  | 0.93  | 51.5               | 7.0  | 151.5  | 20.7  | 2293.7 | 95.6   | 2293.7   | 95.6   |
| CAT0705-G8-2*  | 187   | 397   | 1.2  | 0.8  | 6.8944          | 16.1 | 0.1729 | 32.6  | 0.0086 | 28.4  | 0.87  | 55.5               | 15.7 | 161.9  | 48.9  | 2288.3 | 278.3  | 2288.3   | 278.3  |
| CAT0705-G9-2*  | 443   | 191   | 7.5  | 0.1  | 5.6894          | 8.1  | 0.2168 | 19.5  | 0.0089 | 17.7  | 0.91  | 57.4               | 10.1 | 199.2  | 35.2  | 2613.3 | 135.4  | 2613.3   | 135.4  |
| CAT0705-G11-1* | 292   | 301   | 6.3  | 0.2  | 6.3301          | 10.7 | 0.1896 | 28.2  | 0.0087 | 26.1  | 0.93  | 55.9               | 14.5 | 176.3  | 45.6  | 2434.1 | 181.3  | 2434.1   | 181.3  |
| CAT0705-G14-1* | 51    | 108   | 3.2  | 0.3  | 2.5010          | 8.8  | 1.0363 | 43.3  | 0.0188 | 42.4  | 0.98  | 120.1              | 50.4 | 722.1  | 227.3 | 3908.5 | 1890.5 | 3908.5   | 1890.5 |
| CAT0705-G15-1* | 449   | 364   | 5.8  | 0.2  | 7.0402          | 9.2  | 0.1626 | 20.6  | 0.0083 | 18.4  | 0.89  | 53.3               | 9.8  | 153.0  | 29.2  | 2252.2 | 158.8  | 2252.2   | 158.8  |
| CAT0705-G15-2* | 158   | 410   | 2.6  | 0.4  | 7.3930          | 16.4 | 0.1502 | 45.2  | 0.0081 | 42.1  | 0.93  | 51.7               | 21.7 | 142.1  | 60.0  | 2167.4 | 287.2  | 2167.4   | 287.2  |
| CAT0705-G16-1* | 100   | 141   | 2.0  | 0.5  | 3.3849          | 11.0 | 0.4263 | 38.3  | 0.0105 | 36.7  | 0.96  | 67.1               | 24.5 | 360.6  | 116.9 | 3446.4 | 170.6  | 3446.4   | 170.6  |
| CAT0705-G16-2* | 42    | 87    | 1.6  | 0.6  | 4.8619          | 32.6 | 0.2704 | 134.8 | 0.0095 | 130.8 | 0.97  | 61.2               | 79.6 | 243.0  | 299.8 | 2871.8 | 546.5  | 2871.8   | 546.5  |
| CAT0705-G19-1* | 278   | 318   | 0.7  | 1.5  | 6.2745          | 11.2 | 0.1743 | 28.7  | 0.0079 | 26.4  | 0.92  | 50.9               | 13.4 | 163.2  | 43.3  | 2449.0 | 189.3  | 2449.0   | 189.3  |
| CAT0705-G19-2* | 179   | 241   | 1.1  | 0.9  | 7.9498          | 19.7 | 0.1342 | 42.8  | 0.0077 | 37.9  | 0.89  | 49.7               | 18.8 | 127.9  | 51.4  | 2039.9 | 352.6  | 2039.9   | 352.6  |
| CAT0705-G26-2* | 417   | 267   | 0.8  | 1.2  | 8.3547          | 13.2 | 0.1440 | 23.9  | 0.0087 | 19.9  | 0.83  | 56.0               | 11.1 | 136.6  | 30.6  | 1951.6 | 237.4  | 1951.6   | 237.4  |
| CAT0705-G37-3* | 831   | 532   | 17.5 | 0.1  | 6.8045          | 4.7  | 0.1791 | 11.9  | 0.0088 | 11.0  | 0.92  | 56.7               | 6.2  | 167.2  | 18.4  | 2310.9 | 79.9   | 2310.9   | 79.9   |

\*indicates the analysis was not included in the calculations for the mean age



| CAT0704        |       |       |          |       | Isotopic ratios |       |        |       |       | Apparent ages (Ma) |      |        |       |        |       |          |       |
|----------------|-------|-------|----------|-------|-----------------|-------|--------|-------|-------|--------------------|------|--------|-------|--------|-------|----------|-------|
| Analysis       | U     | 206Pb | 206Pb*   | ±     | 207Pb*          | ±     | 206Pb* | ±     | error | 206Pb*             | ±    | 207Pb* | ±     | 206Pb* | ±     | Best age | ±     |
|                | (ppm) | 204Pb | 207Pb*   | (%)   | 235U*           | (%)   | 238U   | (%)   | corr. | 238U*              | (Ma) | 235U   | (Ma)  | 207Pb* | (Ma)  | (Ma)     | (Ma)  |
| CAT0704-G1-2   | 2086  | 1171  | 17.1764  | 6.6   | 0.0568          | 10.5  | 0.0071 | 8.2   | 0.78  | 45.5               | 3.7  | 56.1   | 5.8   | 538.0  | 145.2 | 45.5     | 3.7   |
| CAT0704-G2-1   | 1622  | 1677  | 18.7530  | 8.8   | 0.0519          | 11.9  | 0.0071 | 8.1   | 0.68  | 45.4               | 3.7  | 51.4   | 6.0   | 342.6  | 198.9 | 45.4     | 3.7   |
| CAT0704-G2-2   | 1402  | 2484  | 18.2391  | 7.9   | 0.0510          | 12.4  | 0.0068 | 9.5   | 0.77  | 43.4               | 4.1  | 50.5   | 6.1   | 405.2  | 178.0 | 43.4     | 4.1   |
| CAT0704-G2-5   | 1397  | 1266  | 21.5681  | 12.5  | 0.0442          | 15.9  | 0.0069 | 9.8   | 0.62  | 44.4               | 4.3  | 43.9   | 6.8   | 16.6   | 300.7 | 44.4     | 4.3   |
| CAT0704-G10-1  | 1910  | 2347  | 18.2062  | 8.4   | 0.0506          | 11.9  | 0.0067 | 8.3   | 0.70  | 42.9               | 3.6  | 50.1   | 5.8   | 409.2  | 189.0 | 42.9     | 3.6   |
| CAT0704-G13-2  | 1271  | 2005  | 19.4948  | 11.3  | 0.0496          | 15.0  | 0.0070 | 9.9   | 0.66  | 45.1               | 4.4  | 49.2   | 7.2   | 254.1  | 260.6 | 45.1     | 4.4   |
| CAT0704-G13-3  | 1126  | 2057  | 19.2067  | 10.4  | 0.0513          | 14.3  | 0.0071 | 9.9   | 0.69  | 45.9               | 4.5  | 50.8   | 7.1   | 288.3  | 237.2 | 45.9     | 4.5   |
| CAT0704-G17-1  | 1891  | 1016  | 20.9092  | 10.1  | 0.0452          | 12.8  | 0.0069 | 7.9   | 0.62  | 44.0               | 3.4  | 44.9   | 5.6   | 90.6   | 238.8 | 44.0     | 3.4   |
| CAT0704-G18-2  | 3825  | 4406  | 21.4115  | 4.8   | 0.0459          | 7.0   | 0.0071 | 5.1   | 0.73  | 45.8               | 2.3  | 45.6   | 3.1   | 34.1   | 115.3 | 45.8     | 2.3   |
| CAT0704-G3-4   | 1321  | 28508 | 10.8727  | 0.6   | 2.2864          | 1.9   | 0.1803 | 1.8   | 0.95  | 1068.6             | 17.9 | 1208.1 | 13.5  | 1466.8 | 11.3  | 1466.8   | 11.3  |
| CAT0704-G8-2   | 328   | 14736 | 11.1871  | 1.2   | 2.7448          | 4.5   | 0.2227 | 4.3   | 0.97  | 1296.2             | 51.0 | 1340.7 | 33.5  | 1412.5 | 22.4  | 1412.5   | 22.4  |
| CAT0704-G17-2  | 563   | 12683 | 10.2706  | 0.9   | 2.6351          | 2.9   | 0.1963 | 2.8   | 0.95  | 1155.3             | 29.2 | 1310.5 | 21.4  | 1574.2 | 16.8  | 1574.2   | 16.8  |
| CAT0704-G11-1  | 1396  | 1459  | 21.1152  | 9.0   | 0.0612          | 12.7  | 0.0094 | 8.9   | 0.70  | 60.1               | 5.3  | 60.3   | 7.4   | 67.4   | 215.0 | 60.1     | 5.3   |
| CAT0704-G16-2* | 2062  | 2467  | 19.0386  | 7.2   | 0.0566          | 9.3   | 0.0078 | 5.9   | 0.63  | 50.2               | 2.9  | 55.9   | 5.0   | 308.3  | 163.8 | 50.2     | 2.9   |
| CAT0704-G19-3* | 1602  | 2120  | 19.6021  | 7.2   | 0.0599          | 10.6  | 0.0085 | 7.8   | 0.73  | 54.7               | 4.2  | 59.1   | 6.1   | 241.5  | 166.9 | 54.7     | 4.2   |
| CAT0704-G7-2*  | 1702  | 1545  | 22.4410  | 10.1  | 0.0520          | 12.8  | 0.0085 | 7.9   | 0.62  | 54.3               | 4.3  | 51.5   | 6.4   | -79.6  | 246.9 | 54.3     | 4.3   |
| CAT0704-G1-1*  | 201   | 176   | 12.2541  | 35.6  | 0.0790          | 55.5  | 0.0070 | 42.6  | 0.77  | 45.1               | 19.1 | 77.2   | 41.3  | 1236.0 | 722.1 | 45.1     | 19.1  |
| CAT0704-G1-3*  | 1201  | 1821  | 15.9374  | 10.1  | 0.0604          | 15.2  | 0.0070 | 11.4  | 0.75  | 44.8               | 5.1  | 59.5   | 8.8   | 699.6  | 215.3 | 44.8     | 5.1   |
| CAT0704-G1-4*  | 410   | 864   | 13.2509  | 26.0  | 0.0765          | 35.6  | 0.0074 | 24.3  | 0.68  | 47.2               | 11.4 | 74.9   | 25.7  | 1080.9 | 530.0 | 47.2     | 11.4  |
| CAT0704-G1-5*  | 714   | 288   | 411.0468 | 313.1 | 0.0062          | 313.2 | 0.0184 | 6.4   | 0.02  | 117.2              | 7.4  | 6.2    | 19.5  | 0.0    | 0.0   | 117.2    | 7.4   |
| CAT0704-G1-6*  | 164   | 287   | 10.5044  | 34.6  | 0.0966          | 53.9  | 0.0074 | 41.3  | 0.77  | 47.3               | 19.5 | 93.6   | 48.2  | 1532.0 | 672.1 | 47.3     | 19.5  |
| CAT0704-G2-3*  | 37    | 86    | 5.7309   | 53.1  | 0.2021          | 150.6 | 0.0084 | 141.0 | 0.94  | 53.9               | 75.7 | 186.9  | 262.9 | 2601.2 | 968.0 | 2601.2   | 968.0 |
| CAT0704-G2-4*  | 128   | 230   | 12.1025  | 45.3  | 0.0849          | 67.3  | 0.0075 | 49.8  | 0.74  | 47.9               | 23.7 | 82.8   | 53.5  | 1260.4 | 935.1 | 47.9     | 23.7  |
| CAT0704-G2-5*  | 1397  | 1266  | 21.5681  | 12.5  | 0.0442          | 15.9  | 0.0069 | 9.8   | 0.62  | 44.4               | 4.3  | 43.9   | 6.8   | 16.6   | 300.7 | 44.4     | 4.3   |
| CAT0704-G3-1*  | 431   | 947   | 19.0899  | 24.2  | 0.0520          | 33.0  | 0.0072 | 22.5  | 0.68  | 46.3               | 10.4 | 51.5   | 16.6  | 302.2  | 558.8 | 46.3     | 10.4  |
| CAT0704-G3-2*  | 135   | 572   | 9.8647   | 42.9  | 0.1147          | 58.9  | 0.0082 | 40.4  | 0.69  | 52.7               | 21.2 | 110.3  | 61.6  | 1649.4 | 836.1 | 52.7     | 21.2  |
| CAT0704-G3-3*  | 477   | 520   | 19.0683  | 24.0  | 0.0524          | 31.5  | 0.0072 | 20.4  | 0.65  | 46.6               | 9.5  | 51.9   | 15.9  | 304.8  | 553.7 | 46.6     | 9.5   |
| CAT0704-G4-1*  | 687   | 909   | 16.7568  | 14.8  | 0.0593          | 20.2  | 0.0072 | 13.8  | 0.68  | 46.3               | 6.4  | 58.5   | 11.5  | 591.9  | 321.8 | 46.3     | 6.4   |

\*indicates the analysis was not included in the calculations for the mean age

| CAT0704, cont. |       |       | Isotopic ratios |      |        |       |        |      |       | Apparent ages (Ma) |      |        |      |        |        |          |       |
|----------------|-------|-------|-----------------|------|--------|-------|--------|------|-------|--------------------|------|--------|------|--------|--------|----------|-------|
| Analysis       | U     | 206Pb | 206Pb*          | ±    | 207Pb* | ±     | 206Pb* | ±    | error | 206Pb*             | ±    | 207Pb* | ±    | 206Pb* | ±      | Best age | ±     |
|                | (ppm) | 204Pb | 207Pb*          | (%)  | 235U*  | (%)   | 238U   | (%)  | corr. | 238U*              | (Ma) | 235U   | (Ma) | 207Pb* | (Ma)   | (Ma)     | (Ma)  |
| CAT0704-G4-3*  | 338   | 488   | 18.1383         | 24.1 | 0.0548 | 35.7  | 0.0072 | 26.3 | 0.74  | 46.3               | 12.1 | 54.2   | 18.8 | 417.6  | 545.7  | 46.3     | 12.1  |
| CAT0704-G5-1*  | 253   | 434   | 13.1325         | 27.9 | 0.0760 | 46.2  | 0.0072 | 36.8 | 0.80  | 46.5               | 17.0 | 74.4   | 33.1 | 1098.9 | 569.3  | 46.5     | 17.0  |
| CAT0704-G6-1*  | 890   | 3993  | 15.4719         | 7.4  | 0.0818 | 12.9  | 0.0092 | 10.5 | 0.82  | 58.9               | 6.2  | 79.9   | 9.9  | 762.4  | 156.5  | 58.9     | 6.2   |
| CAT0704-G6-2*  | 165   | 450   | 12.3592         | 27.6 | 0.1174 | 43.6  | 0.0105 | 33.8 | 0.78  | 67.5               | 22.7 | 112.7  | 46.6 | 1219.3 | 552.4  | 67.5     | 22.7  |
| CAT0704-G8-1*  | 279   | 1118  | 10.8216         | 17.9 | 0.0954 | 36.1  | 0.0075 | 31.4 | 0.87  | 48.1               | 15.0 | 92.5   | 31.9 | 1475.8 | 341.9  | 48.1     | 15.0  |
| CAT0704-G9-1*  | 438   | 35981 | 12.6215         | 18.0 | 0.0771 | 26.6  | 0.0071 | 19.6 | 0.74  | 45.3               | 8.8  | 75.4   | 19.3 | 1177.9 | 359.3  | 45.3     | 8.8   |
| CAT0704-G9-2*  | 73    | 153   | 11.9593         | 62.7 | 0.0814 | 112.3 | 0.0071 | 93.1 | 0.83  | 45.3               | 42.1 | 79.4   | 86.0 | 1283.6 | 1375.7 | 45.3     | 42.1  |
| CAT0704-G9-3*  | 53    | 397   | 11.9030         | 70.9 | 0.0974 | 110.0 | 0.0084 | 84.2 | 0.77  | 54.0               | 45.3 | 94.4   | 99.5 | 1292.8 | 1626.2 | 54.0     | 45.3  |
| CAT0704-G10-2* | 932   | 1333  | 17.2499         | 11.0 | 0.0561 | 17.4  | 0.0070 | 13.5 | 0.78  | 45.1               | 6.1  | 55.4   | 9.4  | 528.7  | 240.8  | 45.1     | 6.1   |
| CAT0704-G10-3* | 509   | 573   | 15.0464         | 19.8 | 0.0671 | 27.2  | 0.0073 | 18.7 | 0.69  | 47.0               | 8.8  | 65.9   | 17.4 | 820.9  | 416.4  | 47.0     | 8.8   |
| CAT0704-G11-2* | 671   | 1197  | 13.7331         | 13.6 | 0.0874 | 19.8  | 0.0087 | 14.3 | 0.73  | 55.9               | 8.0  | 85.1   | 16.1 | 1008.8 | 277.4  | 55.9     | 8.0   |
| CAT0704-G12-1* | 768   | 1394  | 13.5255         | 11.3 | 0.0695 | 18.8  | 0.0068 | 15.0 | 0.80  | 43.8               | 6.6  | 68.2   | 12.4 | 1039.7 | 228.8  | 43.8     | 6.6   |
| CAT0704-G12-2* | 368   | 2536  | 11.5449         | 17.8 | 0.0860 | 27.7  | 0.0072 | 21.2 | 0.77  | 46.3               | 9.8  | 83.8   | 22.3 | 1352.0 | 346.2  | 46.3     | 9.8   |
| CAT0704-G14-1* | 1371  | 1950  | 14.4197         | 7.8  | 0.0651 | 13.9  | 0.0068 | 11.5 | 0.83  | 43.7               | 5.0  | 64.0   | 8.6  | 909.1  | 160.3  | 43.7     | 5.0   |
| CAT0704-G14-2* | 585   | 1191  | 12.9922         | 12.4 | 0.0756 | 21.3  | 0.0071 | 17.4 | 0.81  | 45.8               | 7.9  | 74.0   | 15.2 | 1120.4 | 247.7  | 45.8     | 7.9   |
| CAT0704-G14-3* | 405   | 4893  | 9.6660          | 2.7  | 0.7046 | 6.6   | 0.0494 | 6.1  | 0.92  | 310.8              | 18.4 | 541.5  | 27.8 | 1687.0 | 49.2   | 310.8    | 18.4  |
| CAT0704-G15-1* | 628   | 5435  | 11.0661         | 3.4  | 0.4055 | 7.1   | 0.0325 | 6.3  | 0.88  | 206.5              | 12.8 | 345.6  | 20.9 | 1433.3 | 64.1   | 206.5    | 12.8  |
| CAT0704-G18-1* | 519   | 460   | 15.4733         | 22.5 | 0.0632 | 31.6  | 0.0071 | 22.2 | 0.70  | 45.6               | 10.1 | 62.2   | 19.1 | 762.2  | 479.0  | 45.6     | 10.1  |
| CAT0704-G18-3* | 636   | 701   | 15.9006         | 19.6 | 0.0579 | 24.4  | 0.0067 | 14.6 | 0.60  | 42.9               | 6.2  | 57.1   | 13.6 | 704.5  | 420.2  | 42.9     | 6.2   |
| CAT0704-G19-1* | 301   | 267   | 11.5402         | 27.8 | 0.0913 | 37.1  | 0.0076 | 24.5 | 0.66  | 49.1               | 12.0 | 88.7   | 31.5 | 1352.8 | 546.7  | 49.1     | 12.0  |
| CAT0704-G19-2* | 177   | 123   | 21.0328         | 90.3 | 0.0480 | 96.0  | 0.0073 | 32.3 | 0.34  | 47.0               | 15.1 | 47.6   | 44.6 | 76.7   | 881.0  | 47.0     | 15.1  |
| CAT0704-G20-1* | 171   | 183   | 11.6443         | 43.2 | 0.0843 | 61.1  | 0.0071 | 43.2 | 0.71  | 45.7               | 19.7 | 82.1   | 48.2 | 1335.4 | 877.7  | 45.7     | 19.7  |
| CAT0704-G20-3* | 115   | 181   | 12.3677         | 55.0 | 0.1036 | 72.3  | 0.0093 | 47.0 | 0.65  | 59.6               | 27.9 | 100.1  | 69.0 | 1217.9 | 1178.2 | 59.6     | 27.9  |
| CAT0704-G7-1*  | 146   | 308   | 8.1941          | 22.9 | 0.1497 | 45.6  | 0.0089 | 39.4 | 0.86  | 57.1               | 22.4 | 141.7  | 60.3 | 1986.2 | 413.0  | 1986.2   | 413.0 |
| CAT0704-G8-3*  | 162   | 482   | 5.5161          | 14.5 | 0.2050 | 46.8  | 0.0082 | 44.5 | 0.95  | 52.6               | 23.4 | 189.3  | 81.1 | 2664.7 | 241.6  | 2664.7   | 241.6 |
| CAT0704-G13-1* | 190   | 297   | 7.4816          | 19.3 | 0.1393 | 39.8  | 0.0076 | 34.8 | 0.87  | 48.5               | 16.8 | 132.4  | 49.4 | 2146.6 | 340.2  | 2146.6   | 340.2 |

\*indicates the analysis was not included in the calculations for the mean age

| CAT0703       |       |        | Isotopic ratios |      |        |      |        |     |       | Apparent ages (Ma) |      |        |      |        |       |          |      |
|---------------|-------|--------|-----------------|------|--------|------|--------|-----|-------|--------------------|------|--------|------|--------|-------|----------|------|
| Analysis      | U     | 206Pb  | 206Pb*          | ±    | 207Pb* | ±    | 206Pb* | ±   | error | 206Pb*             | ±    | 207Pb* | ±    | 206Pb* | ±     | Best age | ±    |
|               | (ppm) | 204Pb  | 207Pb*          | (%)  | 235U*  | (%)  | 238U   | (%) | corr. | 238U*              | (Ma) | 235U   | (Ma) | 207Pb* | (Ma)  | (Ma)     | (Ma) |
| CAT0703-G14-2 | 1207  | 2987   | 21.0064         | 9.1  | 0.0587 | 12.0 | 0.0089 | 7.8 | 0.65  | 57.4               | 4.4  | 57.9   | 6.7  | 79.6   | 216.9 | 57.4     | 4.4  |
| CAT0703-G48-1 | 6076  | 4014   | 20.3279         | 3.2  | 0.0540 | 4.9  | 0.0080 | 3.7 | 0.75  | 51.1               | 1.9  | 53.4   | 2.5  | 157.0  | 74.8  | 51.1     | 1.9  |
| C0703G4-1     | 263   | 407    | 25.7775         | 34.7 | 0.0389 | 35.4 | 0.0073 | 6.8 | 0.19  | 46.7               | 3.2  | 38.7   | 13.4 | -430.7 | 934.2 | 46.7     | 3.2  |
| C0703G4-2     | 495   | 1364   | 23.0755         | 12.5 | 0.0549 | 13.1 | 0.0092 | 3.9 | 0.29  | 59.0               | 2.3  | 54.3   | 6.9  | -148.3 | 312.2 | 59.0     | 2.3  |
| C0703G5-1     | 709   | 1073   | 16.3190         | 5.5  | 0.0721 | 6.3  | 0.0085 | 3.2 | 0.51  | 54.8               | 1.8  | 70.7   | 4.3  | 649.0  | 117.2 | 54.8     | 1.8  |
| C0703G5-2     | 658   | 1014   | 16.6252         | 8.2  | 0.0744 | 8.8  | 0.0090 | 3.3 | 0.37  | 57.6               | 1.9  | 72.9   | 6.2  | 608.9  | 177.3 | 57.6     | 1.9  |
| C0703G9-2     | 244   | 1004   | 17.3332         | 13.9 | 0.0662 | 15.4 | 0.0083 | 6.6 | 0.43  | 53.4               | 3.5  | 65.1   | 9.7  | 518.1  | 307.5 | 53.4     | 3.5  |
| C0703G10-1    | 497   | 1489   | 16.7027         | 9.2  | 0.0751 | 10.0 | 0.0091 | 4.0 | 0.39  | 58.4               | 2.3  | 73.5   | 7.1  | 598.9  | 200.3 | 58.4     | 2.3  |
| C0703G10-2    | 431   | 2233   | 18.7900         | 10.0 | 0.0626 | 11.0 | 0.0085 | 4.5 | 0.41  | 54.8               | 2.4  | 61.7   | 6.6  | 338.2  | 227.4 | 54.8     | 2.4  |
| C0703G12-1    | 464   | 777    | 20.3540         | 13.9 | 0.0610 | 14.5 | 0.0090 | 4.0 | 0.28  | 57.8               | 2.3  | 60.2   | 8.5  | 154.0  | 327.1 | 57.8     | 2.3  |
| C0703G12-2    | 326   | 1405   | 22.5121         | 15.6 | 0.0560 | 16.4 | 0.0091 | 5.0 | 0.31  | 58.7               | 2.9  | 55.3   | 8.8  | -87.3  | 384.3 | 58.7     | 2.9  |
| C0703G12-3    | 640   | 1075   | 21.8704         | 10.2 | 0.0582 | 10.7 | 0.0092 | 3.3 | 0.30  | 59.3               | 1.9  | 57.5   | 6.0  | -16.9  | 247.7 | 59.3     | 1.9  |
| C0703G14-1    | 782   | 1461   | 20.1390         | 8.3  | 0.0595 | 8.8  | 0.0087 | 3.0 | 0.34  | 55.7               | 1.7  | 58.6   | 5.0  | 178.8  | 193.6 | 55.7     | 1.7  |
| C0703G14-2    | 1073  | 2149   | 20.9000         | 6.2  | 0.0593 | 6.7  | 0.0090 | 2.5 | 0.37  | 57.7               | 1.4  | 58.5   | 3.8  | 91.7   | 147.1 | 57.7     | 1.4  |
| C0703G35-1    | 632   | 811    | 24.5666         | 16.3 | 0.0400 | 16.8 | 0.0071 | 3.8 | 0.23  | 45.8               | 1.8  | 39.9   | 6.6  | -306.0 | 419.9 | 45.8     | 1.8  |
| C0703G35-2    | 832   | 1071   | 24.8676         | 12.4 | 0.0362 | 12.8 | 0.0065 | 3.4 | 0.27  | 42.0               | 1.4  | 36.2   | 4.6  | -337.2 | 319.9 | 42.0     | 1.4  |
| C0703G35-3    | 728   | 1541   | 23.9622         | 11.1 | 0.0467 | 11.6 | 0.0081 | 3.3 | 0.28  | 52.1               | 1.7  | 46.3   | 5.3  | -242.7 | 282.1 | 52.1     | 1.7  |
| C0703G37-1    | 863   | 4131   | 18.1622         | 5.6  | 0.0607 | 6.3  | 0.0080 | 3.0 | 0.47  | 51.4               | 1.5  | 59.9   | 3.7  | 414.6  | 124.4 | 51.4     | 1.5  |
| C0703G51-1    | 558   | 1186   | 16.3738         | 6.9  | 0.0692 | 7.9  | 0.0082 | 3.8 | 0.48  | 52.8               | 2.0  | 67.9   | 5.2  | 641.8  | 149.4 | 52.8     | 2.0  |
| C0703G44-1    | 373   | 708    | 17.4186         | 12.9 | 0.0623 | 13.8 | 0.0079 | 5.0 | 0.36  | 50.6               | 2.5  | 61.4   | 8.3  | 507.3  | 285.3 | 50.6     | 2.5  |
| C0703G41-1    | 609   | 3652   | 19.3248         | 7.3  | 0.0607 | 8.1  | 0.0085 | 3.5 | 0.43  | 54.6               | 1.9  | 59.9   | 4.7  | 274.2  | 167.1 | 54.6     | 1.9  |
| CAT0703-G15-2 | 304   | 17351  | 10.9955         | 1.2  | 3.1502 | 3.6  | 0.2512 | 3.3 | 0.94  | 1444.8             | 43.4 | 1445.1 | 27.6 | 1445.5 | 23.7  | 1445.5   | 23.7 |
| CAT0703-G26-3 | 320   | 18762  | 10.9641         | 1.0  | 2.9626 | 3.9  | 0.2356 | 3.8 | 0.97  | 1363.7             | 46.3 | 1398.1 | 29.6 | 1450.9 | 19.4  | 1450.9   | 19.4 |
| CAT0703-G35-4 | 361   | 127794 | 9.6435          | 0.8  | 4.3104 | 3.7  | 0.3015 | 3.6 | 0.98  | 1698.6             | 54.2 | 1695.4 | 30.6 | 1691.3 | 14.7  | 1691.3   | 14.7 |
| CAT0703-G37-3 | 426   | 14083  | 10.2332         | 0.9  | 3.4393 | 3.6  | 0.2553 | 3.4 | 0.97  | 1465.5             | 45.1 | 1513.4 | 28.1 | 1581.1 | 17.5  | 1581.1   | 17.5 |
| CAT0703-G41-2 | 262   | 19960  | 9.5310          | 1.2  | 4.2521 | 3.8  | 0.2939 | 3.6 | 0.95  | 1661.1             | 53.4 | 1684.1 | 31.6 | 1712.9 | 22.0  | 1712.9   | 22.0 |

\*indicates the analysis was not included in the calculations for the mean age

| CAT0703, cont. |       |       | Isotopic ratios |       |         |       |        |      |       | Apparent ages (Ma) |      |        |        |        |        |          |      |
|----------------|-------|-------|-----------------|-------|---------|-------|--------|------|-------|--------------------|------|--------|--------|--------|--------|----------|------|
| Analysis       | U     | 206Pb | 206Pb*          | ±     | 207Pb*  | ±     | 206Pb* | ±    | error | 206Pb*             | ±    | 207Pb* | ±      | 206Pb* | ±      | Best age | ±    |
|                | (ppm) | 204Pb | 207Pb*          | (%)   | 235U*   | (%)   | 238U   | (%)  | corr. | 238U*              | (Ma) | 235U   | (Ma)   | 207Pb* | (Ma)   | (Ma)     | (Ma) |
| CAT0703-G2-3*  | 765   | 664   | 19.6965         | 19.8  | 0.0610  | 23.8  | 0.0087 | 13.2 | 0.55  | 55.9               | 7.4  | 60.1   | 13.9   | 230.4  | 461.8  | 55.9     | 7.4  |
| CAT0703-G6-2*  | 442   | 338   | 17.4285         | 28.4  | 0.0624  | 35.5  | 0.0079 | 21.3 | 0.60  | 50.6               | 10.7 | 61.4   | 21.2   | 506.0  | 637.5  | 50.6     | 10.7 |
| CAT0703-G6-3*  | 322   | 268   | 20.3488         | 53.3  | 0.0595  | 57.0  | 0.0088 | 20.2 | 0.35  | 56.4               | 11.3 | 58.7   | 32.5   | 154.6  | 1337.6 | 56.4     | 11.3 |
| CAT0703-G9-1*  | 116   | 100   | 9.4576          | 44.9  | 0.1124  | 58.4  | 0.0077 | 37.4 | 0.64  | 49.5               | 18.4 | 108.1  | 60.0   | 1727.1 | 872.1  | 49.5     | 18.4 |
| CAT0703-G11-2* | 406   | 595   | 10.7411         | 15.0  | 0.1015  | 23.7  | 0.0079 | 18.3 | 0.77  | 50.8               | 9.3  | 98.2   | 22.2   | 1489.9 | 285.1  | 50.8     | 9.3  |
| CAT0703-G13-2* | 440   | 404   | 13.1184         | 22.4  | 0.0699  | 31.9  | 0.0066 | 22.7 | 0.71  | 42.7               | 9.6  | 68.6   | 21.1   | 1101.1 | 453.6  | 42.7     | 9.6  |
| CAT0703-G15-3* | 226   | 195   | 15.3871         | 43.7  | 0.0661  | 62.4  | 0.0074 | 44.6 | 0.71  | 47.4               | 21.0 | 65.0   | 39.3   | 774.0  | 964.6  | 47.4     | 21.0 |
| CAT0703-G16-1* | 653   | 375   | 9.3544          | 11.1  | 0.1114  | 20.1  | 0.0076 | 16.8 | 0.83  | 48.5               | 8.1  | 107.2  | 20.5   | 1747.2 | 204.4  | 48.5     | 8.1  |
| CAT0703-G16-2* | 773   | 1566  | 17.4457         | 16.0  | 0.0626  | 21.5  | 0.0079 | 14.3 | 0.67  | 50.9               | 7.3  | 61.7   | 12.9   | 503.9  | 354.9  | 50.9     | 7.3  |
| CAT0703-G17-1* | 159   | 232   | 13.7316         | 36.1  | 0.0914  | 48.2  | 0.0091 | 32.0 | 0.66  | 58.4               | 18.6 | 88.8   | 41.0   | 1009.1 | 756.5  | 58.4     | 18.6 |
| CAT0703-G17-2* | 480   | 245   | 10.1887         | 17.9  | 0.0903  | 30.2  | 0.0067 | 24.3 | 0.80  | 42.9               | 10.4 | 87.8   | 25.4   | 1589.2 | 337.6  | 42.9     | 10.4 |
| CAT0703-G17-3* | 142   | 367   | 15.0177         | 46.1  | 0.0810  | 63.1  | 0.0088 | 43.1 | 0.68  | 56.6               | 24.3 | 79.0   | 48.0   | 824.9  | 1016.8 | 56.6     | 24.3 |
| CAT0703-G18-2* | 158   | 389   | 12.2796         | 28.8  | 0.1004  | 47.4  | 0.0089 | 37.6 | 0.79  | 57.4               | 21.5 | 97.2   | 43.9   | 1232.0 | 576.7  | 57.4     | 21.5 |
| CAT0703-G18-3* | 518   | 367   | 10.8401         | 12.4  | 0.1116  | 21.2  | 0.0088 | 17.2 | 0.81  | 56.3               | 9.6  | 107.4  | 21.6   | 1472.5 | 235.8  | 56.3     | 9.6  |
| CAT0703-G19-2* | 609   | 214   | 12.7097         | 23.2  | 0.0852  | 27.9  | 0.0078 | 15.5 | 0.56  | 50.4               | 7.8  | 83.0   | 22.2   | 1164.1 | 464.9  | 50.4     | 7.8  |
| CAT0703-G20-1* | 106   | 138   | 27.3143         | 117.7 | 0.0398  | 134.6 | 0.0079 | 65.3 | 0.49  | 50.6               | 32.9 | 39.6   | 52.3   | -585.1 | 1740.6 | 50.6     | 32.9 |
| CAT0703-G20-2* | 2449  | 222   | -16.0883        | 456.7 | -0.0336 | 456.7 | 0.0039 | 5.9  | 0.01  | 25.2               | 1.5  | -34.7  | -162.5 | 0.0    | 1645.9 | 25.2     | 1.5  |
| CAT0703-G21-2* | 578   | 446   | 13.3342         | 17.3  | 0.0910  | 26.2  | 0.0088 | 19.7 | 0.75  | 56.5               | 11.1 | 88.5   | 22.2   | 1068.4 | 350.5  | 56.5     | 11.1 |
| CAT0703-G23-2* | 584   | 1487  | 17.5476         | 17.3  | 0.0560  | 28.0  | 0.0071 | 22.1 | 0.79  | 45.8               | 10.1 | 55.3   | 15.1   | 491.0  | 383.1  | 45.8     | 10.1 |
| CAT0703-G23-3* | 175   | 178   | 8.6243          | 25.2  | 0.1506  | 44.6  | 0.0094 | 36.9 | 0.83  | 60.4               | 22.2 | 142.5  | 59.4   | 1894.7 | 460.2  | 60.4     | 22.2 |
| CAT0703-G24-1* | 774   | 428   | 12.5543         | 13.5  | 0.0826  | 18.7  | 0.0075 | 13.0 | 0.69  | 48.3               | 6.2  | 80.6   | 14.5   | 1188.4 | 268.7  | 48.3     | 6.2  |
| CAT0703-G25-1* | 624   | 370   | 16.7831         | 23.8  | 0.0601  | 29.8  | 0.0073 | 17.9 | 0.60  | 47.0               | 8.4  | 59.3   | 17.1   | 588.5  | 522.1  | 47.0     | 8.4  |
| CAT0703-G25-2* | 291   | 449   | 12.1778         | 22.0  | 0.1092  | 28.6  | 0.0096 | 18.4 | 0.64  | 61.9               | 11.3 | 105.2  | 28.6   | 1248.3 | 435.4  | 61.9     | 11.3 |
| CAT0703-G26-1* | 492   | 445   | 28.0318         | 38.1  | 0.0411  | 43.4  | 0.0084 | 20.8 | 0.48  | 53.6               | 11.1 | 40.9   | 17.4   | -655.9 | 1079.2 | 53.6     | 11.1 |
| CAT0703-G26-2* | 672   | 12173 | 11.2280         | 1.9   | 0.7917  | 4.2   | 0.0645 | 3.7  | 0.89  | 402.7              | 14.5 | 592.1  | 18.7   | 1405.5 | 36.1   | 402.7    | 14.5 |
| CAT0703-G27-1* | 349   | 181   | 9.8194          | 25.0  | 0.1091  | 34.7  | 0.0078 | 24.1 | 0.69  | 49.9               | 12.0 | 105.1  | 34.7   | 1657.9 | 470.7  | 49.9     | 12.0 |

\*indicates the analysis was not included in the calculations for the mean age

| CAT0703, cont. |       |       | Isotopic ratios |       |        |       |        |      |       | Apparent ages (Ma) |      |        |       |         |        |          |       |
|----------------|-------|-------|-----------------|-------|--------|-------|--------|------|-------|--------------------|------|--------|-------|---------|--------|----------|-------|
| Analysis       | U     | 206Pb | 206Pb*          | ±     | 207Pb* | ±     | 206Pb* | ±    | error | 206Pb*             | ±    | 207Pb* | ±     | 206Pb*  | ±      | Best age | ±     |
|                | (ppm) | 204Pb | 207Pb*          | (%)   | 235U*  | (%)   | 238U   | (%)  | corr. | 238U*              | (Ma) | 235U   | (Ma)  | 207Pb*  | (Ma)   | (Ma)     | (Ma)  |
| CAT0703-G31-1* | 536   | 311   | 24.3911         | 51.1  | 0.0403 | 55.2  | 0.0071 | 20.8 | 0.38  | 45.8               | 9.5  | 40.1   | 21.7  | -287.7  | 1384.7 | 45.8     | 9.5   |
| CAT0703-G31-2* | 452   | 354   | 27.7047         | 46.9  | 0.0430 | 50.6  | 0.0086 | 19.1 | 0.38  | 55.5               | 10.6 | 42.8   | 21.2  | -623.8  | 1342.6 | 55.5     | 10.6  |
| CAT0703-G32-1* | 606   | 140   | 10.2295         | 17.5  | 0.1027 | 21.8  | 0.0076 | 12.9 | 0.59  | 48.9               | 6.3  | 99.2   | 20.6  | 1581.7  | 330.8  | 48.9     | 6.3   |
| CAT0703-G32-2* | 81    | 62    | 13.2483         | 130.3 | 0.0810 | 145.1 | 0.0078 | 64.0 | 0.44  | 50.0               | 31.9 | 79.1   | 110.9 | 1081.3  | 447.5  | 50.0     | 31.9  |
| CAT0703-G33-1* | 494   | 168   | 43.6721         | 125.7 | 0.0189 | 127.2 | 0.0060 | 19.5 | 0.15  | 38.4               | 7.5  | 19.0   | 23.9  | -2081.7 | 0.0    | 38.4     | 7.5   |
| CAT0703-G33-2* | 343   | 64    | 11.1394         | 67.5  | 0.0687 | 71.3  | 0.0055 | 23.2 | 0.33  | 35.7               | 8.3  | 67.5   | 46.6  | 1420.6  | 1492.5 | 35.7     | 8.3   |
| CAT0703-G33-3* | 703   | 221   | 29.7021         | 61.6  | 0.0358 | 63.0  | 0.0077 | 13.3 | 0.21  | 49.5               | 6.6  | 35.7   | 22.1  | -817.9  | 1917.0 | 49.5     | 6.6   |
| CAT0703-G34-1* | 382   | 137   | 161.9405        | 800.8 | 0.0057 | 801.4 | 0.0067 | 29.6 | 0.04  | 43.1               | 12.7 | 5.8    | 46.3  | 0.0     | 0.0    | 43.1     | 12.7  |
| CAT0703-G36-1* | 736   | 680   | 15.0557         | 15.3  | 0.0875 | 19.3  | 0.0096 | 11.8 | 0.61  | 61.3               | 7.2  | 85.2   | 15.8  | 819.6   | 322.4  | 61.3     | 7.2   |
| CAT0703-G38-2* | 616   | 407   | 18.7176         | 23.7  | 0.0673 | 26.4  | 0.0091 | 11.5 | 0.44  | 58.7               | 6.7  | 66.2   | 16.9  | 346.9   | 543.6  | 58.7     | 6.7   |
| CAT0703-G39-1* | 200   | 189   | 10.0280         | 37.6  | 0.0982 | 49.1  | 0.0071 | 31.6 | 0.64  | 45.9               | 14.4 | 95.1   | 44.6  | 1618.9  | 726.5  | 45.9     | 14.4  |
| CAT0703-G41-1* | 510   | 260   | 9.3209          | 17.6  | 0.1191 | 23.9  | 0.0081 | 16.1 | 0.67  | 51.7               | 8.3  | 114.3  | 25.8  | 1753.8  | 324.8  | 51.7     | 8.3   |
| CAT0703-G42-1* | 614   | 162   | 9.6900          | 17.9  | 0.1098 | 22.7  | 0.0077 | 14.0 | 0.61  | 49.5               | 6.9  | 105.8  | 22.8  | 1682.4  | 333.9  | 49.5     | 6.9   |
| CAT0703-G45-2* | 975   | 1852  | 19.9854         | 10.6  | 0.0547 | 15.6  | 0.0079 | 11.5 | 0.73  | 50.9               | 5.8  | 54.0   | 8.2   | 196.7   | 246.4  | 50.9     | 5.8   |
| CAT0703-G47-1* | 412   | 356   | 9.9692          | 15.7  | 0.1107 | 27.1  | 0.0080 | 22.0 | 0.81  | 51.4               | 11.3 | 106.6  | 27.4  | 1629.8  | 293.8  | 51.4     | 11.3  |
| CAT0703-G51-2* | 322   | 306   | 22.1048         | 41.0  | 0.0567 | 45.3  | 0.0091 | 19.3 | 0.43  | 58.3               | 11.2 | 56.0   | 24.7  | -42.8   | 1033.8 | 58.3     | 11.2  |
| CAT0703-G1-3*  | 203   | 93    | 7.2815          | 35.7  | 0.1231 | 54.1  | 0.0065 | 40.7 | 0.75  | 41.8               | 16.9 | 117.9  | 60.3  | 2193.8  | 643.0  | 2193.8   | 643.0 |
| CAT0703-G2-2*  | 67    | 149   | 8.4013          | 45.0  | 0.1492 | 80.4  | 0.0091 | 66.7 | 0.83  | 58.3               | 38.7 | 141.2  | 106.4 | 1941.7  | 853.4  | 1941.7   | 853.4 |
| CAT0703-G3-1*  | 81    | 84    | 3.4970          | 17.0  | 0.4364 | 56.1  | 0.0111 | 53.5 | 0.95  | 71.0               | 37.7 | 367.7  | 174.8 | 3395.8  | 266.5  | 3395.8   | 266.5 |
| CAT0703-G6-4*  | 290   | 93    | 7.2595          | 24.8  | 0.1473 | 33.3  | 0.0078 | 22.2 | 0.67  | 49.8               | 11.0 | 139.6  | 43.4  | 2199.1  | 437.7  | 2199.1   | 437.7 |
| CAT0703-G7-1*  | 244   | 35    | 4.3768          | 22.7  | 0.2285 | 30.3  | 0.0073 | 20.0 | 0.66  | 46.6               | 9.3  | 208.9  | 57.2  | 3041.4  | 369.8  | 3041.4   | 369.8 |
| CAT0703-G8-1*  | 388   | 132   | 6.7961          | 15.8  | 0.1743 | 25.2  | 0.0086 | 19.7 | 0.78  | 55.1               | 10.8 | 163.1  | 38.1  | 2313.0  | 273.5  | 2313.0   | 273.5 |
| CAT0703-G9-3*  | 572   | 136   | 6.4080          | 14.6  | 0.1401 | 20.4  | 0.0065 | 14.2 | 0.70  | 41.8               | 5.9  | 133.1  | 25.4  | 2413.3  | 249.3  | 2413.3   | 249.3 |
| CAT0703-G11-1* | 82    | 89    | 4.7912          | 30.0  | 0.2397 | 70.7  | 0.0083 | 64.0 | 0.91  | 53.5               | 34.1 | 218.2  | 139.6 | 2895.6  | 499.9  | 2895.6   | 499.9 |
| CAT0703-G13-1* | 213   | 112   | 5.0283          | 21.1  | 0.2103 | 35.6  | 0.0077 | 28.7 | 0.81  | 49.2               | 14.1 | 193.8  | 62.9  | 2817.0  | 348.7  | 2817.0   | 348.7 |
| CAT0703-G15-1* | 67    | 64    | 3.1926          | 20.1  | 0.3980 | 57.7  | 0.0092 | 54.1 | 0.94  | 59.1               | 31.9 | 340.2  | 168.4 | 3536.9  | 313.5  | 3536.9   | 313.5 |
| CAT0703-G18-1* | 302   | 262   | 7.6405          | 13.9  | 0.1540 | 32.5  | 0.0085 | 29.3 | 0.90  | 54.8               | 16.0 | 145.4  | 44.0  | 2109.8  | 244.4  | 2109.8   | 244.4 |

\*indicates the analysis was not included in the calculations for the mean age

| CAT0703, cont. |       |        | Isotopic ratios |      |        |      |        |      |       | Apparent ages (Ma) |      |        |       |        |        |          |        |
|----------------|-------|--------|-----------------|------|--------|------|--------|------|-------|--------------------|------|--------|-------|--------|--------|----------|--------|
| Analysis       | U     | 206Pb  | 206Pb*          | ±    | 207Pb* | ±    | 206Pb* | ±    | error | 206Pb*             | ±    | 207Pb* | ±     | 206Pb* | ±      | Best age | ±      |
|                | (ppm) | 204Pb  | 207Pb*          | (%)  | 235U*  | (%)  | 238U   | (%)  | corr. | 238U*              | (Ma) | 235U   | (Ma)  | 207Pb* | (Ma)   | (Ma)     | (Ma)   |
| CAT0703-G19-1* | 49    | 48     | 4.3918          | 40.6 | 0.2785 | 88.5 | 0.0089 | 78.7 | 0.89  | 56.9               | 44.6 | 249.4  | 198.3 | 3035.9 | 685.3  | 3035.9   | 685.3  |
| CAT0703-G22-1* | 184   | 165    | 6.6932          | 23.6 | 0.1519 | 49.0 | 0.0074 | 43.0 | 0.88  | 47.3               | 20.3 | 143.6  | 65.7  | 2339.1 | 409.8  | 2339.1   | 409.8  |
| CAT0703-G23-1* | 430   | 189    | 7.9443          | 12.0 | 0.1342 | 23.4 | 0.0077 | 20.1 | 0.86  | 49.7               | 9.9  | 127.9  | 28.1  | 2041.1 | 212.4  | 2041.1   | 212.4  |
| CAT0703-G24-2* | 157   | 182    | 6.3874          | 18.0 | 0.2185 | 42.5 | 0.0101 | 38.5 | 0.91  | 64.9               | 24.9 | 200.7  | 77.6  | 2418.8 | 309.0  | 2418.8   | 309.0  |
| CAT0703-G28-2* | 199   | 79     | 7.6420          | 34.0 | 0.1424 | 46.1 | 0.0079 | 31.0 | 0.67  | 50.7               | 15.7 | 135.1  | 58.3  | 2109.5 | 616.7  | 2109.5   | 616.7  |
| CAT0703-G29-1* | 154   | 75     | 4.0088          | 14.6 | 0.3110 | 35.0 | 0.0090 | 31.8 | 0.91  | 58.0               | 18.4 | 275.0  | 84.5  | 3181.3 | 232.1  | 3181.3   | 232.1  |
| CAT0703-G29-2* | 117   | 56     | 4.9940          | 31.8 | 0.2114 | 61.0 | 0.0077 | 52.1 | 0.85  | 49.2               | 25.5 | 194.8  | 108.5 | 2828.1 | 533.7  | 2828.1   | 533.7  |
| CAT0703-G31-3* | 284   | 64     | 6.8541          | 35.8 | 0.1400 | 42.0 | 0.0070 | 22.0 | 0.52  | 44.7               | 9.8  | 133.0  | 52.4  | 2298.4 | 637.4  | 2298.4   | 637.4  |
| CAT0703-G32-3* | 119   | 463    | 6.0389          | 19.5 | 0.2233 | 36.5 | 0.0098 | 30.9 | 0.85  | 62.8               | 19.3 | 204.7  | 67.9  | 2513.6 | 331.8  | 2513.6   | 331.8  |
| CAT0703-G35-4* | 361   | 127794 | 9.6435          | 0.8  | 4.3104 | 3.7  | 0.3015 | 3.6  | 0.98  | 1698.6             | 54.2 | 1695.4 | 30.6  | 1691.3 | 14.7   | 1691.3   | 14.7   |
| CAT0703-G36-2* | 71    | 89     | 6.7089          | 54.0 | 0.2034 | 77.3 | 0.0099 | 55.3 | 0.72  | 63.5               | 34.9 | 188.0  | 133.4 | 2335.1 | 1013.7 | 2335.1   | 1013.7 |
| CAT0703-G38-1* | 366   | 75     | 4.4345          | 14.4 | 0.2195 | 23.4 | 0.0071 | 18.5 | 0.79  | 45.4               | 8.4  | 201.5  | 42.8  | 3020.4 | 231.8  | 3020.4   | 231.8  |
| CAT0703-G40-1* | 463   | 149    | 7.6065          | 19.3 | 0.1493 | 24.5 | 0.0082 | 15.1 | 0.62  | 52.9               | 8.0  | 141.3  | 32.4  | 2117.6 | 342.2  | 2117.6   | 342.2  |
| CAT0703-G43-1* | 321   | 123    | 4.5200          | 10.9 | 0.2828 | 31.1 | 0.0093 | 29.1 | 0.94  | 59.5               | 17.2 | 252.9  | 69.7  | 2989.7 | 175.9  | 2989.7   | 175.9  |
| CAT0703-G44-2* | 65    | 75     | 3.6174          | 18.8 | 0.4415 | 52.8 | 0.0116 | 49.3 | 0.93  | 74.2               | 36.4 | 371.3  | 165.7 | 3343.0 | 296.9  | 3343.0   | 296.9  |
| CAT0703-G45-1* | 178   | 79     | 4.1847          | 13.7 | 0.2677 | 32.7 | 0.0081 | 29.7 | 0.91  | 52.2               | 15.4 | 240.8  | 70.1  | 3113.1 | 219.2  | 3113.1   | 219.2  |

\*indicates the analysis was not included in the calculations for the mean age

| CAT 93-8      |       |       | Isotopic ratios |      |        |      |        |     |       | Apparent ages (Ma) |      |        |      |        |       |          |      |
|---------------|-------|-------|-----------------|------|--------|------|--------|-----|-------|--------------------|------|--------|------|--------|-------|----------|------|
| Analysis      | U     | 206Pb | 206Pb*          | ±    | 207Pb* | ±    | 206Pb* | ±   | error | 206Pb*             | ±    | 207Pb* | ±    | 206Pb* | ±     | Best age | ±    |
|               | (ppm) | 204Pb | 207Pb*          | (%)  | 235U*  | (%)  | 238U   | (%) | corr. | 238U*              | (Ma) | 235U   | (Ma) | 207Pb* | (Ma)  | (Ma)     | (Ma) |
| CAT938G1-1    | 348   | 955   | 17.7260         | 7.9  | 0.0698 | 8.6  | 0.0090 | 3.4 | 0.40  | 57.6               | 2.0  | 68.5   | 5.7  | 468.7  | 174.1 | 57.6     | 2.0  |
| CAT938G1-3    | 521   | 1281  | 17.0666         | 4.7  | 0.0709 | 5.4  | 0.0088 | 2.7 | 0.50  | 56.3               | 1.5  | 69.5   | 3.6  | 552.0  | 102.1 | 56.3     | 1.5  |
| CAT93-8-G7-1  | 1597  | 3628  | 19.9387         | 5.6  | 0.0593 | 9.2  | 0.0086 | 7.3 | 0.79  | 55.0               | 4.0  | 58.5   | 5.2  | 202.1  | 130.0 | 55.0     | 4.0  |
| CAT93-8-G9-2  | 1484  | 4185  | 21.5107         | 7.8  | 0.0594 | 10.9 | 0.0093 | 7.6 | 0.70  | 59.4               | 4.5  | 58.6   | 6.2  | 23.0   | 186.5 | 59.4     | 4.5  |
| CAT93-8-G13-2 | 1701  | 5400  | 19.5484         | 8.4  | 0.0527 | 11.7 | 0.0075 | 8.1 | 0.69  | 48.0               | 3.9  | 52.2   | 6.0  | 247.8  | 194.3 | 48.0     | 3.9  |
| CAT938G15-R   | 1010  | 1631  | 16.2998         | 3.2  | 0.0737 | 3.7  | 0.0087 | 1.9 | 0.52  | 55.9               | 1.1  | 72.2   | 2.6  | 651.5  | 68.1  | 55.9     | 1.1  |
| CAT938G15-C   | 398   | 867   | 19.2316         | 7.2  | 0.0611 | 7.9  | 0.0085 | 3.2 | 0.41  | 54.7               | 1.8  | 60.2   | 4.6  | 285.3  | 164.7 | 54.7     | 1.8  |
| CAT938G19-C   | 77    | 468   | 25.8180         | 29.3 | 0.0504 | 30.5 | 0.0094 | 8.5 | 0.28  | 60.6               | 5.1  | 50.0   | 14.9 | -434.8 | 783.1 | 60.6     | 5.1  |
| CAT93-8-G21-1 | 1290  | 2145  | 20.7649         | 9.3  | 0.0571 | 12.2 | 0.0086 | 7.9 | 0.65  | 55.2               | 4.3  | 56.4   | 6.7  | 107.0  | 220.5 | 55.2     | 4.3  |
| CAT93-8-G25-2 | 1832  | 3796  | 22.1593         | 6.9  | 0.0533 | 10.0 | 0.0086 | 7.2 | 0.72  | 55.0               | 3.9  | 52.7   | 5.1  | -48.8  | 169.2 | 55.0     | 3.9  |
| CAT938G25-R   | 1006  | 1625  | 18.6842         | 4.1  | 0.0651 | 4.5  | 0.0088 | 1.9 | 0.42  | 56.6               | 1.1  | 64.0   | 2.8  | 350.9  | 91.8  | 56.6     | 1.1  |
| CAT938G26-1   | 154   | 679   | 18.5254         | 11.0 | 0.0656 | 12.3 | 0.0088 | 5.6 | 0.45  | 56.6               | 3.2  | 64.5   | 7.7  | 370.2  | 248.0 | 56.6     | 3.2  |
| CAT938G26-4   | 1113  | 3212  | 21.0074         | 3.4  | 0.0594 | 3.9  | 0.0090 | 1.8 | 0.46  | 58.1               | 1.0  | 58.6   | 2.2  | 79.5   | 81.8  | 58.1     | 1.0  |
| CAT938G28-R   | 319   | 3134  | 18.7485         | 7.5  | 0.0609 | 8.4  | 0.0083 | 3.8 | 0.45  | 53.2               | 2.0  | 60.0   | 4.9  | 343.2  | 169.6 | 53.2     | 2.0  |
| CAT938G28-C   | 445   | 1119  | 20.6135         | 9.1  | 0.0518 | 9.6  | 0.0077 | 3.2 | 0.33  | 49.7               | 1.6  | 51.3   | 4.8  | 124.3  | 214.6 | 49.7     | 1.6  |
| CAT938G34-1   | 154   | 1187  | 16.5227         | 13.1 | 0.0737 | 14.3 | 0.0088 | 5.7 | 0.40  | 56.7               | 3.2  | 72.3   | 10.0 | 622.3  | 282.8 | 56.7     | 3.2  |
| CAT93-8-G40-2 | 1180  | 4799  | 21.5255         | 9.9  | 0.0574 | 12.8 | 0.0090 | 8.2 | 0.64  | 57.5               | 4.7  | 56.7   | 7.1  | 21.4   | 237.6 | 57.5     | 4.7  |
| CAT93-8-G41-1 | 1640  | 9681  | 20.1261         | 7.2  | 0.0617 | 10.3 | 0.0090 | 7.3 | 0.71  | 57.8               | 4.2  | 60.8   | 6.1  | 180.3  | 168.4 | 57.8     | 4.2  |
| CAT93-8-G49-4 | 5851  | 9269  | 21.4649         | 3.1  | 0.0541 | 4.5  | 0.0084 | 3.2 | 0.72  | 54.1               | 1.7  | 53.5   | 2.3  | 28.1   | 74.3  | 54.1     | 1.7  |
| CAT93-8-G50-2 | 2300  | 1878  | 22.2287         | 9.3  | 0.0543 | 11.0 | 0.0087 | 5.9 | 0.54  | 56.1               | 3.3  | 53.6   | 5.8  | -56.4  | 226.8 | 56.1     | 3.3  |
| CAT938G54-2   | 605   | 2291  | 19.8976         | 5.5  | 0.0613 | 6.0  | 0.0089 | 2.5 | 0.42  | 56.8               | 1.4  | 60.4   | 3.5  | 206.9  | 127.4 | 56.8     | 1.4  |
| CAT938G54-3   | 263   | 854   | 22.4837         | 14.5 | 0.0546 | 15.0 | 0.0089 | 3.9 | 0.26  | 57.1               | 2.2  | 54.0   | 7.9  | -84.2  | 357.0 | 57.1     | 2.2  |
| CAT93-8-G56-2 | 1391  | 6511  | 20.0280         | 6.8  | 0.0609 | 10.2 | 0.0088 | 7.6 | 0.75  | 56.7               | 4.3  | 60.0   | 5.9  | 191.7  | 157.9 | 56.7     | 4.3  |
| CAT93-8-G58-2 | 933   | 1372  | 18.7433         | 10.5 | 0.0658 | 14.5 | 0.0089 | 9.9 | 0.69  | 57.4               | 5.7  | 64.7   | 9.1  | 343.8  | 239.2 | 57.4     | 5.7  |
| CAT938G59-1   | 784   | 1229  | 21.5084         | 6.3  | 0.0541 | 6.7  | 0.0084 | 2.2 | 0.33  | 54.2               | 1.2  | 53.5   | 3.5  | 23.3   | 151.7 | 54.2     | 1.2  |
| CAT938G59-2   | 383   | 926   | 22.1907         | 10.4 | 0.0565 | 10.9 | 0.0091 | 3.1 | 0.29  | 58.4               | 1.8  | 55.8   | 5.9  | -52.2  | 254.3 | 58.4     | 1.8  |
| CAT93-8-G61-1 | 1009  | 2957  | 19.9790         | 8.7  | 0.0598 | 13.1 | 0.0087 | 9.8 | 0.75  | 55.7               | 5.4  | 59.0   | 7.5  | 197.4  | 202.6 | 55.7     | 5.4  |
| CAT93-8-G61-3 | 1116  | 6534  | 18.2883         | 9.2  | 0.0653 | 13.5 | 0.0087 | 9.8 | 0.73  | 55.6               | 5.4  | 64.2   | 8.4  | 399.1  | 206.9 | 55.6     | 5.4  |

\*indicates the analysis was not included in the calculations for the mean age

| CAT 93-8, cont. |       | Isotopic ratios |         |      |        |      |        |     |       |        | Apparent ages (Ma) |        |      |         |        |          |      |
|-----------------|-------|-----------------|---------|------|--------|------|--------|-----|-------|--------|--------------------|--------|------|---------|--------|----------|------|
| Analysis        | U     | 206Pb           | 206Pb*  | ±    | 207Pb* | ±    | 206Pb* | ±   | error | 206Pb* | ±                  | 207Pb* | ±    | 206Pb*  | ±      | Best age | ±    |
|                 | (ppm) | 204Pb           | 207Pb*  | (%)  | 235U*  | (%)  | 238U   | (%) | corr. | 238U*  | (Ma)               | 235U   | (Ma) | 207Pb*  | (Ma)   | (Ma)     | (Ma) |
| CAT93-8-G62-1   | 1482  | 10755           | 20.8427 | 5.5  | 0.0576 | 10.3 | 0.0087 | 8.7 | 0.85  | 55.9   | 4.9                | 56.9   | 5.7  | 98.2    | 129.2  | 55.9     | 4.9  |
| CAT938G64-1     | 270   | 1305            | 18.3946 | 10.5 | 0.0593 | 11.3 | 0.0079 | 4.2 | 0.37  | 50.8   | 2.1                | 58.5   | 6.4  | 386.1   | 236.2  | 50.8     | 2.1  |
| CAT938G64-2     | 469   | 748             | 27.8120 | 13.0 | 0.0420 | 13.3 | 0.0085 | 2.9 | 0.22  | 54.3   | 1.6                | 41.7   | 5.4  | -634.3  | 356.2  | 54.3     | 1.6  |
| CAT938-1A       | 696   | 1326            | 16.4300 | 1.9  | 0.0468 | 6.9  | 0.0087 | 2.0 | 0.29  | 55.7   | 1.1                | 46.4   | 3.1  | -412.2  | 173.0  | 55.7     | 1.1  |
| CAT938-2        | 246   | 366             | 15.1100 | 8.6  | 0.0202 | 41.8 | 0.0075 | 2.9 | 0.07  | 48.4   | 1.4                | 20.3   | 8.4  | -2768.9 | 424.6  | 48.4     | 1.4  |
| CAT938-5        | 421   | 1038            | 17.1240 | 6.0  | 0.0372 | 11.2 | 0.0077 | 3.3 | 0.29  | 49.7   | 1.6                | 37.1   | 4.1  | -718.5  | 299.6  | 49.7     | 1.6  |
| CAT938-7        | 194   | 384             | 15.9210 | 7.7  | 0.0199 | 37.3 | 0.0079 | 6.3 | 0.17  | 50.8   | 3.2                | 20.1   | 7.4  | -3046.5 | 634.4  | 50.8     | 3.2  |
| CAT938-7A       | 670   | 1418            | 14.2440 | 5.8  | 0.0543 | 9.5  | 0.0083 | 4.6 | 0.48  | 53.4   | 2.4                | 53.7   | 5.0  | 67.2    | 198.5  | 53.4     | 2.4  |
| CAT938-9        | 852   | 1004            | 16.7420 | 2.8  | 0.0399 | 9.9  | 0.0081 | 4.0 | 0.40  | 52.2   | 2.1                | 39.7   | 3.9  | -663.4  | 251.7  | 52.2     | 2.1  |
| CAT938-10       | 360   | 612             | 15.1160 | 7.3  | 0.0362 | 19.4 | 0.0079 | 2.7 | 0.14  | 51.0   | 1.3                | 36.1   | 6.9  | -873.0  | 557.6  | 51.0     | 1.3  |
| CAT938-14       | 542   | 1168            | 16.5310 | 3.0  | 0.0436 | 8.0  | 0.0083 | 2.2 | 0.27  | 53.5   | 1.2                | 43.3   | 3.4  | -488.2  | 204.7  | 53.5     | 1.2  |
| CAT938-15       | 210   | 386             | 15.1520 | 6.3  | 0.0248 | 32.4 | 0.0085 | 5.4 | 0.17  | 54.6   | 2.9                | 24.9   | 8.0  | -2392.0 | 1348.6 | 54.6     | 2.9  |
| CAT938-27       | 418   | 680             | 15.7480 | 3.0  | 0.0398 | 14.0 | 0.0087 | 3.6 | 0.25  | 56.1   | 2.0                | 39.6   | 5.4  | -878.0  | 392.9  | 56.1     | 2.0  |
| CAT938-17       | 865   | 1384            | 16.3810 | 1.8  | 0.0462 | 6.5  | 0.0084 | 2.8 | 0.44  | 53.8   | 1.5                | 45.9   | 2.9  | -351.9  | 150.0  | 53.8     | 1.5  |
| CAT938-19       | 568   | 718             | 16.9860 | 4.8  | 0.0333 | 14.3 | 0.0080 | 3.7 | 0.26  | 51.3   | 1.9                | 33.2   | 4.7  | -1140.1 | 425.3  | 51.3     | 1.9  |
| CAT938-21       | 545   | 604             | 15.4480 | 16.4 | 0.0354 | 23.8 | 0.0081 | 2.0 | 0.08  | 52.1   | 1.0                | 35.4   | 8.3  | -992.7  | 710.0  | 52.1     | 1.0  |
| CAT93-8-G9-4    | 3856  | 3606            | 21.6157 | 5.1  | 0.0572 | 6.6  | 0.0090 | 4.2 | 0.63  | 57.6   | 2.4                | 56.5   | 3.7  | 11.3    | 123.8  | 57.6     | 2.4  |
| CAT938-25       | 3351  | 6744            | 16.6190 | 1.4  | 0.0587 | 3.5  | 0.0093 | 2.9 | 0.82  | 59.6   | 1.7                | 57.9   | 2.0  | -9.5    | 48.6   | 59.6     | 1.7  |
| CAT938-28       | 795   | 1644            | 16.8690 | 3.0  | 0.0471 | 6.5  | 0.0086 | 1.8 | 0.28  | 55.1   | 1.0                | 46.8   | 3.0  | -359.6  | 160.9  | 55.1     | 1.0  |
| J-938-2         | 277   | 2828            | 17.0760 | 3.9  | 0.0509 | 5.3  | 0.0085 | 2.1 | 0.39  | 54.9   | 1.1                | 50.4   | 2.6  | -159.2  | 120.5  | 54.9     | 1.1  |
| J-938-5         | 190   | 1658            | 16.6220 | 4.6  | 0.0495 | 9.3  | 0.0086 | 4.9 | 0.53  | 55.5   | 2.7                | 49.0   | 4.5  | -258.1  | 200.5  | 55.5     | 2.7  |
| J-938-7         | 228   | 2712            | 17.379  | 3.4  | 0.0489 | 7.1  | 0.0084 | 5.2 | 0.72  | 54.1   | 2.8                | 48.5   | 3.4  | -217.6  | 124.5  | 54.1     | 2.8  |
| J-938-8         | 252   | 1420            | 16.888  | 5.8  | 0.0315 | 9.1  | 0.0058 | 2.7 | 0.29  | 37.2   | 1.0                | 31.5   | 2.8  | -381.1  | 225.3  | 37.2     | 1.0  |
| CAT93-8-G13-1   | 4353  | 12910           | 21.3249 | 4.6  | 0.0365 | 6.9  | 0.0056 | 5.2 | 0.75  | 36.3   | 1.9                | 36.4   | 2.5  | 43.8    | 109.5  | 36.3     | 1.9  |
| CAT938-3        | 130   | 88              | 4.037   | 12.8 | 0.0515 | 31.8 | 0.0053 | 6.7 | 0.21  | 34.2   | 2.3                | 51.0   | 15.8 | 934.0   | 652.4  | 34.2     | 2.3  |

\*indicates the analysis was not included in the calculations for the mean age



| CAT 93-8, cont. |       | Isotopic ratios |         |       |         |        |         |       |       | Apparent ages (Ma) |      |        |       |         |        |          |      |
|-----------------|-------|-----------------|---------|-------|---------|--------|---------|-------|-------|--------------------|------|--------|-------|---------|--------|----------|------|
| Analysis        | U     | 206Pb           | 206Pb*  | ±     | 207Pb*  | ±      | 206Pb*  | ±     | error | 206Pb*             | ±    | 207Pb* | ±     | 206Pb*  | ±      | Best age | ±    |
|                 | (ppm) | 204Pb           | 207Pb*  | (%)   | 235U*   | (%)    | 238U    | (%)   | corr. | 238U*              | (Ma) | 235U   | (Ma)  | 207Pb*  | (Ma)   | (Ma)     | (Ma) |
| CAT938-22       | 1093  | 1642            | 16.6910 | 2.3   | 0.0339  | 10.3   | 0.0061  | 2.1   | 0.21  | 39.2               | 0.8  | 33.9   | 3.4   | -329.8  | 260.8  | 39.2     | 0.8  |
| CAT938-23       | 177   | 210             | 15.8700 | 6.9   | -0.0085 | 172.2  | 0.0061  | 5.6   | 0.03  | 39.4               | 2.2  | -8.7   | 15.0  | 0.0     | 0.0    | 39.4     | 2.2  |
| CAT938-24       | 689   | 844             | 16.2980 | 3.0   | 0.0284  | 9.5    | 0.0059  | 1.3   | 0.14  | 38.1               | 0.5  | 28.5   | 2.7   | -729.8  | 264.1  | 38.1     | 0.5  |
| J-938-3*        | 27    | 278             | 37.5353 | 29.62 | 0.0003  | 30.6   | 0.0131  | 7.6   | 0.25  | 83.8               | 6.3  | 0.4    | 0.1   | -1539.8 | 1011.1 | 83.8     | 6.3  |
| J-938-6*        | 91    | 1694            | 15.2419 | 7.491 | 0.1985  | 21.4   | 0.0219  | 20.1  | 0.94  | 139.9              | 27.8 | 183.8  | 36.1  | 793.9   | 157.3  | 139.9    | 27.8 |
| CAT938-11*      | 855   | 4682            | 2.12698 | 1.479 | 0.0964  | 30.7   | 0.01202 | 27.81 | 0.91  | 77.0               | 21.3 | 93.5   | 27.4  | 536.5   | 286.8  | 77.0     | 21.3 |
| CAT93-8-G1-2*   | 686   | 88286           | 18.9368 | 14.0  | 0.0672  | 19.5   | 0.0092  | 13.6  | 0.69  | 59.2               | 8.0  | 66.0   | 12.5  | 320.5   | 320.0  | 59.2     | 8.0  |
| CAT93-8-G1-6*   | 536   | 2026            | 15.9219 | 10.9  | 0.0805  | 18.4   | 0.0093  | 14.8  | 0.81  | 59.6               | 8.8  | 78.6   | 13.9  | 701.7   | 232.1  | 59.6     | 8.8  |
| CAT93-8-G2-1*   | 108   | 128             | 16.82   | 76.77 | 0.07    | 97.56  | 0.0088  | 60.2  | 0.62  | 56.3               | 33.7 | 70.5   | 66.5  | 583.5   | 2021.3 | 56       | 34   |
| CAT93-8-G2-2*   | 208   | 3656            | 12.96   | 18.22 | 0.10    | 39.31  | 0.0095  | 34.8  | 0.89  | 61.0               | 21.2 | 97.9   | 36.7  | 1125.7  | 366.1  | 61       | 21   |
| CAT93-8-G3-1*   | 561   | 979             | 20.45   | 18.35 | 0.05    | 23.16  | 0.0080  | 14.1  | 0.61  | 51.6               | 7.3  | 53.6   | 12.1  | 142.9   | 433.9  | 52       | 7    |
| CAT93-8-G3-2*   | 464   | 428             | 20.64   | 24.07 | 0.05    | 30.41  | 0.0082  | 18.6  | 0.61  | 52.7               | 9.8  | 54.2   | 16.1  | 121.8   | 574.3  | 53       | 10   |
| CAT93-8-G3-3*   | 587   | 2469            | 20.59   | 13.64 | 0.06    | 19.18  | 0.0086  | 13.5  | 0.70  | 55.0               | 7.4  | 56.7   | 10.6  | 126.8   | 322.3  | 55       | 7    |
| CAT93-8-G3-5*   | 460   | 950             | 19.17   | 22.86 | 0.06    | 29.30  | 0.0085  | 18.3  | 0.63  | 54.6               | 10.0 | 60.3   | 17.2  | 292.2   | 528.1  | 55       | 10   |
| CAT93-8-G4-1*   | 1036  | 1383            | 21.22   | 12.19 | 0.04    | 17.36  | 0.0064  | 12.4  | 0.71  | 41.4               | 5.1  | 41.6   | 7.1   | 56.0    | 291.6  | 41       | 5    |
| CAT93-8-G4-2*   | 873   | 1377            | 23.86   | 20.12 | 0.04    | 25.37  | 0.0062  | 15.5  | 0.61  | 39.8               | 6.1  | 35.7   | 8.9   | -232.2  | 511.5  | 40       | 6    |
| CAT93-8-G4-3*   | 113   | 568             | 13.09   | 59.32 | 0.07    | 89.99  | 0.0067  | 67.7  | 0.75  | 42.9               | 28.9 | 69.0   | 60.1  | 1105.3  | 1313.0 | 43       | 29   |
| CAT93-8-G4-5*   | 245   | 1533            | 18.03   | 28.18 | 0.07    | 39.03  | 0.0096  | 27.0  | 0.69  | 61.7               | 16.6 | 72.0   | 27.1  | 431.0   | 639.5  | 62       | 17   |
| CAT93-8-G4-6*   | 468   | 2728            | 15.60   | 20.21 | 0.06    | 27.52  | 0.0066  | 18.7  | 0.68  | 42.4               | 7.9  | 57.5   | 15.4  | 744.6   | 431.4  | 42       | 8    |
| CAT93-8-G5-1*   | 353   | 1020            | 16.76   | 20.61 | 0.07    | 27.84  | 0.0081  | 18.7  | 0.67  | 52.1               | 9.7  | 65.6   | 17.7  | 591.3   | 451.3  | 52       | 10   |
| CAT93-8-G5-2*   | 660   | 1391            | 22.60   | 14.08 | 0.05    | 20.49  | 0.0087  | 14.9  | 0.73  | 56.2               | 8.3  | 52.8   | 10.5  | -96.4   | 347.2  | 56       | 8    |
| CAT93-8-G5-3*   | 262   | 870             | 15.23   | 24.44 | 0.08    | 42.63  | 0.0089  | 34.9  | 0.82  | 57.3               | 19.9 | 78.9   | 32.4  | 795.2   | 519.8  | 57       | 20   |
| CAT93-8-G6-1*   | 230   | 535             | 19.94   | 34.03 | 0.06    | 44.44  | 0.0086  | 28.6  | 0.64  | 55.4               | 15.8 | 58.8   | 25.4  | 202.1   | 810.9  | 55       | 16   |
| CAT93-8-G6-2*   | 71    | 453             | 11.67   | 44.95 | 0.12    | 84.35  | 0.0098  | 71.4  | 0.85  | 62.6               | 44.5 | 110.8  | 88.8  | 1330.6  | 918.9  | 63       | 44   |
| CAT93-8-G6-3*   | 259   | 558             | 18.61   | 28.78 | 0.06    | 38.67  | 0.0080  | 25.8  | 0.67  | 51.4               | 13.2 | 58.6   | 22.0  | 360.3   | 661.6  | 51       | 13   |
| CAT93-8-G7-3*   | 61    | 166             | 15.31   | 78.57 | 0.08    | 115.34 | 0.0086  | 84.4  | 0.73  | 55.1               | 46.3 | 75.6   | 84.2  | 785.2   | 2040.8 | 55       | 46   |
| CAT93-8-G8-1*   | 65    | 58              | 1.86    | 7.87  | 0.87    | 36.20  | 0.0118  | 35.3  | 0.98  | 75.7               | 26.6 | 637.6  | 173.1 | 0.0     | 0.0    | 76       | 27   |
| CAT93-8-G8-2*   | 350   | 1042            | 18.82   | 23.06 | 0.06    | 32.34  | 0.0089  | 22.7  | 0.70  | 56.9               | 12.8 | 63.9   | 20.0  | 335.1   | 528.9  | 57       | 13   |

\*indicates the analysis was not included in the calculations for the mean age

| CAT 93-8, cont. |       | Isotopic ratios |        |        |        |        |        |      |       | Apparent ages (Ma) |      |        |       |         |         |          |      |
|-----------------|-------|-----------------|--------|--------|--------|--------|--------|------|-------|--------------------|------|--------|-------|---------|---------|----------|------|
| Analysis        | U     | 206Pb           | 206Pb* | ±      | 207Pb* | ±      | 206Pb* | ±    | error | 206Pb*             | ±    | 207Pb* | ±     | 206Pb*  | ±       | Best age | ±    |
|                 | (ppm) | 204Pb           | 207Pb* | (%)    | 235U*  | (%)    | 238U   | (%)  | corr. | 238U*              | (Ma) | 235U   | (Ma)  | 207Pb*  | (Ma)    | (Ma)     | (Ma) |
| CAT93-8-G9-1*   | 837   | 1377            | 20.19  | 11.02  | 0.07   | 15.61  | 0.0105 | 11.1 | 0.71  | 67.2               | 7.4  | 70.2   | 10.6  | 172.7   | 257.9   | 67       | 7    |
| CAT93-8-G10-1*  | 60    | 77              | -25.82 | 327.38 | -0.04  | 338.70 | 0.0080 | 86.8 | 0.26  | 51.1               | 44.2 | -44.1  | 153.8 | 0.0     | 1706.3  | 51       | 44   |
| CAT93-8-G10-2*  | 58    | 91              | 15.01  | 133.65 | 0.08   | 154.01 | 0.0085 | 76.5 | 0.50  | 54.4               | 41.5 | 76.2   | 113.5 | 826.6   | 658.5   | 54       | 41   |
| CAT93-8-G11-1*  | 167   | 144             | 15.54  | 86.06  | 0.07   | 96.61  | 0.0075 | 43.9 | 0.45  | 48.1               | 21.1 | 65.4   | 61.3  | 753.1   | 371.0   | 48       | 21   |
| CAT93-8-G11-2*  | 41    | 104             | 10.00  | 92.72  | 0.14   | 121.02 | 0.0099 | 77.8 | 0.64  | 63.8               | 49.3 | 130.4  | 149.2 | 1623.8  | #VALUE! | 64       | 49   |
| CAT93-8-G12-1*  | 516   | 254             | 43.59  | 120.10 | 0.03   | 121.31 | 0.0079 | 17.1 | 0.14  | 51.0               | 8.7  | 25.2   | 30.2  | -2074.9 | 0.0     | 51       | 9    |
| CAT93-8-G12-2*  | 444   | 361             | 46.10  | 117.06 | 0.02   | 118.80 | 0.0081 | 20.3 | 0.17  | 52.0               | 10.5 | 24.3   | 28.5  | -2294.3 | 0.0     | 52       | 10   |
| CAT93-8-G12-4*  | 392   | 4529            | 18.91  | 23.25  | 0.06   | 32.34  | 0.0081 | 22.5 | 0.70  | 51.7               | 11.6 | 58.0   | 18.2  | 324.1   | 534.4   | 52       | 12   |
| CAT93-8-G13-3*  | 242   | 149             | -30.66 | 149.00 | -0.03  | 151.07 | 0.0074 | 24.9 | 0.16  | 47.8               | 11.9 | -34.6  | -53.2 | 0.0     | 411.9   | 48       | 12   |
| CAT93-8-G13-4*  | 351   | 340             | 54.93  | 137.07 | 0.02   | 138.57 | 0.0082 | 20.3 | 0.15  | 52.4               | 10.6 | 20.6   | 28.3  | -3071.3 | 0.0     | 52       | 11   |
| CAT93-8-G14-1*  | 560   | 325             | 67.98  | 124.12 | 0.02   | 125.35 | 0.0081 | 17.5 | 0.14  | 52.1               | 9.1  | 16.6   | 20.6  | -4287.8 | 0.0     | 52       | 9    |
| CAT93-8-G14-2*  | 583   | 1059            | 23.41  | 25.35  | 0.05   | 29.62  | 0.0085 | 15.3 | 0.52  | 54.3               | 8.3  | 49.4   | 14.3  | -184.3  | 641.9   | 54       | 8    |
| CAT93-8-G14-5*  | 85    | 47              | -3.78  | 95.35  | -0.21  | 117.06 | 0.0058 | 67.9 | 0.58  | 37.1               | 25.1 | -240.3 | 328.4 | 0.0     | 0.0     | 37       | 25   |
| CAT93-8-G15-1*  | 366   | 396             | 30.22  | 61.85  | 0.04   | 65.03  | 0.0089 | 20.1 | 0.31  | 56.9               | 11.4 | 40.3   | 25.7  | -867.6  | 1947.4  | 57       | 11   |
| CAT93-8-G16-1*  | 918   | 752             | 26.62  | 22.28  | 0.05   | 24.58  | 0.0089 | 10.4 | 0.42  | 57.0               | 5.9  | 45.6   | 11.0  | -516.0  | 601.2   | 57       | 6    |
| CAT93-8-G16-2*  | 144   | 123             | 47.54  | 268.55 | 0.02   | 273.23 | 0.0072 | 50.4 | 0.18  | 46.4               | 23.3 | 21.1   | 57.0  | -2420.1 | 0.0     | 46       | 23   |
| CAT93-8-G17-1*  | 49    | 115             | 14.20  | 103.84 | 0.08   | 128.29 | 0.0086 | 75.3 | 0.59  | 54.9               | 41.2 | 81.0   | 100.2 | 940.0   | 372.9   | 55       | 41   |
| CAT93-8-G17-3*  | 306   | 769             | 22.84  | 32.70  | 0.05   | 39.07  | 0.0089 | 21.4 | 0.55  | 57.4               | 12.2 | 53.3   | 20.3  | -123.4  | 826.2   | 57       | 12   |
| CAT93-8-G18-2*  | 435   | 1030            | 24.77  | 24.91  | 0.05   | 31.39  | 0.0087 | 19.1 | 0.61  | 56.1               | 10.7 | 48.3   | 14.8  | -327.6  | 648.6   | 56       | 11   |
| CAT93-8-G19-1*  | 264   | 383             | 14.82  | 28.55  | 0.08   | 36.95  | 0.0086 | 23.5 | 0.63  | 55.4               | 12.9 | 78.4   | 27.9  | 851.8   | 605.1   | 55       | 13   |
| CAT93-8-G19-2*  | 513   | 552             | 22.18  | 27.02  | 0.06   | 31.59  | 0.0090 | 16.4 | 0.52  | 57.6               | 9.4  | 55.1   | 16.9  | -50.7   | 668.1   | 58       | 9    |
| CAT93-8-G19-3*  | 83    | 187             | 14.86  | 72.91  | 0.08   | 93.17  | 0.0088 | 58.0 | 0.62  | 56.2               | 32.5 | 79.4   | 71.2  | 846.7   | 1798.6  | 56       | 32   |
| CAT93-8-G20-1*  | 294   | 1091            | 15.88  | 23.29  | 0.07   | 35.45  | 0.0079 | 26.7 | 0.75  | 50.8               | 13.5 | 67.4   | 23.1  | 706.8   | 501.7   | 51       | 14   |
| CAT93-8-G21-3*  | 547   | 3977            | 12.86  | 4.34   | 0.22   | 9.16   | 0.0210 | 8.1  | 0.88  | 133.9              | 10.7 | 206.0  | 17.1  | 1140.7  | 86.3    | 134      | 11   |
| CAT93-8-G22-1*  | 594   | 7428            | 16.16  | 10.75  | 0.07   | 18.45  | 0.0088 | 15.0 | 0.81  | 56.4               | 8.4  | 73.3   | 13.1  | 669.4   | 230.8   | 56       | 8    |
| CAT93-8-G22-2*  | 59    | 133             | 12.73  | 65.61  | 0.11   | 97.15  | 0.0102 | 71.6 | 0.74  | 65.6               | 46.8 | 106.7  | 98.7  | 1160.7  | 1485.1  | 66       | 47   |

\*indicates the analysis was not included in the calculations for the mean age

| CAT 93-8, cont. |       |        | Isotopic ratios |        |        |        |         |       |         | Apparent ages (Ma) |       |         |        |         |        |          |      |
|-----------------|-------|--------|-----------------|--------|--------|--------|---------|-------|---------|--------------------|-------|---------|--------|---------|--------|----------|------|
| Analysis        | U     | 206Pb  | 206Pb*          | ±      | 207Pb* | ±      | 206Pb*  | ±     | error   | 206Pb*             | ±     | 207Pb*  | ±      | 206Pb*  | ±      | Best age | ±    |
|                 | (ppm) | 204Pb  | 207Pb*          | (%)    | 235U*  | (%)    | 238U    | (%)   | corr.   | 238U*              | (Ma)  | 235U    | (Ma)   | 207Pb*  | (Ma)   | (Ma)     | (Ma) |
| CAT93-8-G23-1*  | 416   | 637    | 14.51           | 16.53  | 0.07   | 26.75  | 0.0078  | 21.0  | 0.79    | 50.3               | 10.5  | 72.9    | 18.8   | 896.3   | 343.3  | 50       | 11   |
| CAT93-8-G23-2*  | 373   | 146951 | 17.91           | 13.28  | 0.07   | 23.74  | 0.0087  | 19.7  | 0.83    | 56.0               | 11.0  | 66.0    | 15.2   | 445.2   | 296.3  | 56       | 11   |
| CAT93-8-G23-3*  | 576   | 599960 | 21.44           | 13.96  | 0.06   | 19.81  | 0.0096  | 14.1  | 0.71    | 61.9               | 8.7   | 61.1    | 11.8   | 30.7    | 335.8  | 62       | 9    |
| CAT93-8-G23-4*  | 477   | 707    | 24.77           | 28.11  | 0.05   | 34.80  | 0.0084  | 20.5  | 0.59    | 53.9               | 11.0  | 46.4    | 15.8   | -327.6  | 734.6  | 54       | 11   |
| CAT93-8-G23-5*  | 341   | 859    | 23.70           | 30.19  | 0.04   | 37.26  | 0.0076  | 21.8  | 0.59    | 48.5               | 10.6  | 43.7    | 15.9   | -215.2  | 773.5  | 49       | 11   |
| CAT93-8-G24-1*  | 654   | 2297   | 17.28           | 12.98  | 0.07   | 19.75  | 0.0085  | 14.9  | 0.75    | 54.3               | 8.1   | 66.3    | 12.7   | 525.5   | 285.6  | 54       | 8    |
| CAT93-8-G24-2*  | 304   | 561    | 19.45           | 29.34  | 0.06   | 37.28  | 0.0090  | 23.0  | 0.62    | 57.9               | 13.3  | 63.0    | 22.8   | 259.6   | 687.2  | 58       | 13   |
| CAT93-8-G24-3*  | 482   | 4864   | 19.95           | 18.16  | 0.07   | 22.78  | 0.0096  | 13.7  | 0.60    | 61.7               | 8.4   | 65.4    | 14.4   | 200.2   | 424.9  | 62       | 8    |
| CAT93-8-G24-4*  | 368   | 4747   | 20.54           | 22.42  | 0.06   | 31.71  | 0.0089  | 22.4  | 0.71    | 57.0               | 12.7  | 58.8    | 18.1   | 132.8   | 532.9  | 57       | 13   |
| CAT93-8-G25-3*  | 873   | 10750  | 18.94           | 10.47  | 0.06   | 15.62  | 0.0086  | 11.6  | 0.74    | 55.0               | 6.3   | 61.5    | 9.3    | 319.8   | 238.5  | 55       | 6    |
| CAT93-8-G26-2*  | 573   | 130194 | 17.21           | 17.15  | 0.07   | 24.83  | 0.0085  | 18.0  | 0.72    | 54.4               | 9.7   | 66.7    | 16.0   | 533.7   | 378.1  | 54       | 10   |
| CAT93-8-G26-3*  | 168   | 632    | 14.05           | 30.62  | 0.08   | 49.42  | 0.0085  | 38.8  | 0.79    | 54.8               | 21.2  | 81.7    | 38.8   | 962.0   | 640.0  | 55       | 21   |
| CAT93-8-G26-5*  | 327   | 475    | 31.87           | 49.58  | 0.03   | 55.32  | 0.0078  | 24.5  | 0.44    | 50.3               | 12.3  | 33.8    | 18.4   | -1023.5 | 1557.0 | 50       | 12   |
| CAT93-8-G27-1*  | 144   | 369    | 14.09           | 41.32  | 0.08   | 54.00  | 0.0086  | 34.8  | 0.64    | 55.4               | 19.2  | 82.3    | 42.7   | 956.1   | 882.5  | 55       | 19   |
| CAT93-8-G27-2*  | 325   | 609    | 14.69           | 24.71  | 0.07   | 33.94  | 0.0079  | 23.3  | 0.69    | 50.6               | 11.7  | 72.4    | 23.7   | 870.2   | 519.6  | 51       | 12   |
| CAT93-8-G28-1*  | 72    | 481    | 11.17           | 60.60  | 0.10   | 98.47  | 0.0083  | 77.6  | 0.79    | 53.4               | 41.3  | 99.4    | 93.5   | 1416.0  | 1295.1 | 53       | 41   |
| CAT93-8-G28-2*  | 304   | 465    | 17.53           | 33.21  | 0.06   | 42.45  | 0.0076  | 26.4  | 0.62    | 49.0               | 12.9  | 59.2    | 24.4   | 493.0   | 751.4  | 49       | 13   |
| CAT93-8-G28-3*  | 68    | 354    | 9.71            | 43.16  | 0.10   | 87.21  | 0.0072  | 75.8  | 0.87    | 46.4               | 35.0  | 99.2    | 82.6   | 1678.5  | 839.7  | 46       | 35   |
| CAT93-8-G29-1*  | 57    | 56     | 35.65           | 370.53 | 0.02   | 387.30 | 0.0063  | 112.7 | 0.29    | 40.6               | 45.6  | 24.5    | 94.1   | -1370.4 | 0.0    | 41       | 46   |
| CAT93-8-G29-2*  | 184   | 1719   | 17.29           | 27.95  | 0.08   | 43.05  | 0.0097  | 32.7  | 0.76    | 62.2               | 20.3  | 75.6    | 31.4   | 523.2   | 624.2  | 62       | 20   |
| CAT93-8-G30-2*  | 642   | 20075  | 18.78           | 17.30  | 0.06   | 21.89  | 0.0085  | 13.4  | 0.61    | 54.8               | 7.3   | 61.7    | 13.1   | 339.1   | 394.4  | 55       | 7    |
| CAT93-8-G31-1*  | 601   | 1207   | 27.20           | 23.72  | 0.04   | 27.22  | 0.0086  | 13.3  | 0.49    | 55.5               | 7.4   | 43.6    | 11.6   | -573.4  | 648.6  | 55       | 7    |
| CAT93-8-G31-2*  | 699   | 8023   | 20.05           | 14.57  | 0.06   | 18.65  | 0.0083  | 11.6  | 0.62    | 53.2               | 6.2   | 56.2    | 10.2   | 189.0   | 340.7  | 53       | 6    |
| CAT93-8-G32-1*  | 279   | 1605   | 23.42           | 36.23  | 0.05   | 45.75  | 0.0080  | 27.9  | 0.61    | 51.5               | 14.3  | 46.9    | 21.0   | -184.7  | 931.3  | 52       | 14   |
| CAT93-8-G66-1*  | 388   | 603    | 25.63           | 33.51  | 0.05   | 38.39  | 0.0086  | 18.7  | 0.49    | 55.1               | 10.3  | 45.8    | 17.2   | -415.2  | 897.6  | 55       | 10   |
| CAT93-8-G68-1*  | 43    | 166    | 16.88           | 105.86 | 0.07   | 165.44 | 0.0082  | 127.1 | 0.77    | 52.8               | 66.9  | 66.0    | 106.2  | 576.5   | 643.9  | 53       | 67   |
| CAT938-1*       | 90    | 64     | -11.09          | 186.18 | -0.07  | 186.77 | 0.00536 | 14.91 | 0.07983 | 34.4916            | 5.129 | -70.089 | -136.3 | 0       | 853.9  | 34       | 5    |

\*indicates the analysis was not included in the calculations for the mean age

| CAT 93-8, cont. |       | Isotopic ratios |        |       |        |       |         |       |         | Apparent ages (Ma) |       |         |       |         |       |          |      |
|-----------------|-------|-----------------|--------|-------|--------|-------|---------|-------|---------|--------------------|-------|---------|-------|---------|-------|----------|------|
| Analysis        | U     | 206Pb           | 206Pb* | ±     | 207Pb* | ±     | 206Pb*  | ±     | error   | 206Pb*             | ±     | 207Pb*  | ±     | 206Pb*  | ±     | Best age | ±    |
|                 | (ppm) | 204Pb           | 207Pb* | (%)   | 235U*  | (%)   | 238U    | (%)   | corr.   | 238U*              | (Ma)  | 235U    | (Ma)  | 207Pb*  | (Ma)  | (Ma)     | (Ma) |
| CAT93-8-G1-5    | 31    | 2685            | 10.99  | 7.30  | 3.20   | 32.73 | 0.26    | 31.90 | 0.97    | 1466.12            | 419.0 | 1458.20 | 258.7 | 1446.67 | 139.3 | 1447     | 139  |
| CAT93-8-G3-4    | 883   | 83853           | 10.42  | 0.53  | 3.22   | 1.95  | 0.24    | 1.88  | 0.96    | 1403.10            | 23.7  | 1461.65 | 15.1  | 1547.79 | 9.9   | 1548     | 10   |
| CAT93-8-G4-4    | 502   | 33234           | 11.05  | 1.17  | 1.83   | 3.07  | 0.15    | 2.84  | 0.92    | 880.59             | 23.3  | 1055.01 | 20.1  | 1436.12 | 22.2  | 1436     | 22   |
| CAT93-8-G9-3    | 65    | 2830            | 11.02  | 4.04  | 2.96   | 15.30 | 0.24    | 14.75 | 0.96    | 1367.52            | 181.8 | 1396.69 | 116.6 | 1441.48 | 77.1  | 1441     | 77   |
| CAT93-8-G12-3   | 757   | 13451           | 11.12  | 1.14  | 1.74   | 2.85  | 0.14    | 2.61  | 0.92    | 846.62             | 20.7  | 1023.76 | 18.4  | 1424.66 | 21.9  | 1425     | 22   |
| CAT93-8-G13-5   | 238   | 20557           | 10.74  | 1.57  | 3.00   | 4.91  | 0.23    | 4.65  | 0.95    | 1353.12            | 56.7  | 1407.29 | 37.4  | 1490.29 | 29.7  | 1490     | 30   |
| CAT93-8-G14-3   | 90    | 4419            | 11.08  | 3.28  | 3.26   | 10.87 | 0.26    | 10.36 | 0.95    | 1498.57            | 138.6 | 1471.07 | 84.7  | 1431.59 | 62.7  | 1432     | 63   |
| CAT93-8-G14-4   | 128   | 2384            | 10.69  | 3.07  | 3.35   | 8.63  | 0.26    | 8.06  | 0.93    | 1488.67            | 107.2 | 1492.89 | 67.6  | 1498.86 | 58.1  | 1499     | 58   |
| CAT93-8-G18-3   | 85    | 633             | 7.43   | 25.67 | 0.17   | 56.94 | 0.01    | 50.82 | 0.89    | 60.05              | 30.4  | 162.65  | 85.8  | 2159.24 | 456.0 | 2159     | 456  |
| CAT93-8-G21-2   | 164   | 2666            | 11.33  | 3.24  | 1.54   | 8.49  | 0.13    | 7.85  | 0.92    | 769.01             | 56.9  | 947.40  | 52.4  | 1388.63 | 62.2  | 1389     | 62   |
| CAT93-8-G22-3   | 997   | 63722           | 9.32   | 0.43  | 4.17   | 1.80  | 0.28    | 1.75  | 0.97    | 1601.19            | 24.8  | 1667.95 | 14.7  | 1753.03 | 7.8   | 1753     | 8    |
| CAT938-1B       | 80    | 6034            | 11.21  | 1.23  | 2.88   | 2.41  | 0.23387 | 2.072 | 0.8601  | 1354.73            | 25.32 | 1375.56 | 18.2  | 1408.02 | 23.5  | 1408     | 24   |
| CAT938-4        | 373   | 1672            | 12.39  | 3.95  | 0.42   | 16.28 | 0.0377  | 15.79 | 0.97016 | 238.567            | 36.99 | 355.701 | 48.9  | 1214.2  | 77.7  | 1214     | 78   |
| CAT938-6        | 68    | 2944            | 11.32  | 2.78  | 2.93   | 3.54  | 0.24048 | 2.196 | 0.61946 | 1389.21            | 27.44 | 1389.21 | 26.8  | 1389.19 | 53.4  | 1389     | 53   |
| CAT938-12       | 67    | 3500            | 11.44  | 1.85  | 2.80   | 3.97  | 0.23188 | 3.515 | 0.88527 | 1344.36            | 42.66 | 1354.29 | 29.7  | 1369.99 | 35.5  | 1370     | 36   |
| CAT938-13       | 170   | 9940            | 10.93  | 1.13  | 2.89   | 3.05  | 0.22887 | 2.831 | 0.92906 | 1328.59            | 33.99 | 1378.86 | 23.0  | 1457.55 | 21.4  | 1458     | 21   |
| CAT938-16       | 1445  | 44242           | 9.36   | 3.89  | 2.52   | 15.06 | 0.17106 | 14.55 | 0.96606 | 1017.96            | 137   | 1277.6  | 109.9 | 1745.67 | 71.3  | 1746     | 71   |
| CAT938-18       | 308   | 11770           | 10.66  | 1.04  | 2.83   | 4.53  | 0.21863 | 4.41  | 0.97318 | 1274.62            | 51.01 | 1363.02 | 34.0  | 1504.44 | 19.7  | 1504     | 20   |
| CAT938-20       | 239   | 20606           | 10.01  | 2.22  | 4.17   | 7.35  | 0.30268 | 7.01  | 0.95346 | 1704.57            | 105   | 1667.85 | 60.3  | 1621.93 | 41.3  | 1622     | 41   |

\*indicates the analysis was not included in the calculations for the mean age

| CAT93-9       |       |       | Isotopic ratios |      |        |      |        |     |       | Apparent ages (Ma) |      |        |      |        |       |          |      |
|---------------|-------|-------|-----------------|------|--------|------|--------|-----|-------|--------------------|------|--------|------|--------|-------|----------|------|
| Analysis      | U     | 206Pb | 206Pb*          | ±    | 207Pb* | ±    | 206Pb* | ±   | error | 206Pb*             | ±    | 207Pb* | ±    | 206Pb* | ±     | Best age | ±    |
|               | (ppm) | 204Pb | 207Pb*          | (%)  | 235U*  | (%)  | 238U   | (%) | corr. | 238U*              | (Ma) | 235U   | (Ma) | 207Pb* | (Ma)  | (Ma)     | (Ma) |
| CAT93-9-G8-2  | 1571  | 1414  | 23.5777         | 13.9 | 0.0479 | 16.4 | 0.0082 | 8.7 | 0.53  | 52.6               | 4.5  | 47.5   | 7.6  | -201.9 | 350.5 | 52.6     | 4.5  |
| CAT93-9-G8-3  | 1256  | 1123  | 22.4235         | 16.7 | 0.0521 | 18.9 | 0.0085 | 8.9 | 0.47  | 54.4               | 4.8  | 51.6   | 9.5  | -77.7  | 410.3 | 54.4     | 4.8  |
| CAT93-9-G10-2 | 2149  | 6026  | 20.3280         | 6.2  | 0.0574 | 8.3  | 0.0085 | 5.5 | 0.67  | 54.4               | 3.0  | 56.7   | 4.6  | 157.0  | 145.5 | 54.4     | 3.0  |
| CAT93-9-G32-2 | 1246  | 2954  | 19.4981         | 9.4  | 0.0662 | 12.6 | 0.0094 | 8.4 | 0.67  | 60.1               | 5.0  | 65.1   | 7.9  | 253.7  | 215.7 | 60.1     | 5.0  |
| CAT93-9-G35-1 | 4855  | 7248  | 21.1095         | 3.6  | 0.0556 | 5.4  | 0.0085 | 4.1 | 0.75  | 54.6               | 2.2  | 54.9   | 2.9  | 68.0   | 85.0  | 54.6     | 2.2  |
| CAT93-9-G38-1 | 2960  | 4057  | 21.5149         | 5.5  | 0.0551 | 7.1  | 0.0086 | 4.6 | 0.64  | 55.1               | 2.5  | 54.4   | 3.8  | 22.5   | 131.2 | 55.1     | 2.5  |
| CAT93-9-G41-1 | 1826  | 2780  | 18.8145         | 8.0  | 0.0613 | 10.7 | 0.0084 | 7.0 | 0.66  | 53.7               | 3.8  | 60.4   | 6.3  | 335.2  | 182.6 | 53.7     | 3.8  |
| CAT93-9-G42-1 | 1190  | 2606  | 20.6134         | 9.5  | 0.0546 | 12.8 | 0.0082 | 8.6 | 0.67  | 52.4               | 4.5  | 54.0   | 6.7  | 124.3  | 224.9 | 52.4     | 4.5  |
| CAT93-9-G42-2 | 1277  | 3357  | 18.7560         | 8.2  | 0.0648 | 11.8 | 0.0088 | 8.6 | 0.72  | 56.6               | 4.8  | 63.8   | 7.3  | 342.3  | 185.5 | 56.6     | 4.8  |
| CAT939G2-2    | 1385  | 16510 | 19.8095         | 1.9  | 0.0644 | 2.5  | 0.0093 | 1.6 | 0.63  | 59.4               | 0.9  | 63.4   | 1.5  | 217.2  | 44.3  | 59.4     | 0.9  |
| CAT939G5-2    | 443   | 1180  | 21.3218         | 8.9  | 0.0582 | 9.4  | 0.0090 | 2.9 | 0.31  | 57.7               | 1.7  | 57.4   | 5.2  | 44.1   | 212.9 | 57.7     | 1.7  |
| CAT939G6-1    | 188   | 946   | 18.7121         | 14.6 | 0.0621 | 15.4 | 0.0084 | 5.0 | 0.32  | 54.1               | 2.7  | 61.2   | 9.2  | 347.6  | 332.0 | 54.1     | 2.7  |
| CAT939G6-2    | 120   | 689   | 17.7657         | 16.3 | 0.0597 | 17.9 | 0.0077 | 7.4 | 0.41  | 49.4               | 3.6  | 58.9   | 10.2 | 463.7  | 363.5 | 49.4     | 3.6  |
| CAT939G9-1    | 205   | 1481  | 18.1759         | 9.9  | 0.0607 | 11.1 | 0.0080 | 5.0 | 0.45  | 51.4               | 2.6  | 59.9   | 6.5  | 412.9  | 222.1 | 51.4     | 2.6  |
| CAT939G9-2    | 565   | 971   | 20.5385         | 7.5  | 0.0530 | 7.9  | 0.0079 | 2.7 | 0.34  | 50.7               | 1.4  | 52.5   | 4.1  | 132.9  | 175.7 | 50.7     | 1.4  |
| CAT939G9-3    | 547   | 1780  | 18.8749         | 6.1  | 0.0603 | 6.7  | 0.0083 | 2.7 | 0.41  | 53.0               | 1.4  | 59.5   | 3.8  | 327.9  | 138.2 | 53.0     | 1.4  |
| CAT939G10-2   | 1552  | 3127  | 18.6529         | 2.5  | 0.0629 | 2.9  | 0.0085 | 1.5 | 0.53  | 54.6               | 0.8  | 61.9   | 1.7  | 354.7  | 55.8  | 54.6     | 0.8  |
| CAT939G10-3   | 146   | 409   | 22.2991         | 23.2 | 0.0522 | 23.9 | 0.0084 | 5.8 | 0.24  | 54.2               | 3.1  | 51.6   | 12.0 | -64.1  | 573.3 | 54.2     | 3.1  |
| CAT939G19-1   | 166   | 500   | 19.2006         | 19.8 | 0.0511 | 20.7 | 0.0071 | 6.1 | 0.30  | 45.7               | 2.8  | 50.6   | 10.2 | 289.0  | 455.4 | 45.7     | 2.8  |
| CAT939G19-2   | 508   | 1223  | 21.8424         | 7.7  | 0.0539 | 8.2  | 0.0085 | 2.8 | 0.34  | 54.8               | 1.5  | 53.3   | 4.2  | -13.8  | 186.2 | 54.8     | 1.5  |
| CAT939G19-3   | 275   | 758   | 19.3347         | 11.8 | 0.0560 | 12.5 | 0.0079 | 4.1 | 0.33  | 50.4               | 2.1  | 55.3   | 6.8  | 273.0  | 272.4 | 50.4     | 2.1  |
| CAT939G24-1   | 186   | 1803  | 13.5118         | 10.3 | 0.0648 | 12.1 | 0.0064 | 6.3 | 0.52  | 40.8               | 2.6  | 63.8   | 7.5  | 1041.7 | 208.9 | 40.8     | 2.6  |
| CAT939G32-2   | 1958  | 10643 | 20.9662         | 1.7  | 0.0600 | 2.2  | 0.0091 | 1.3 | 0.60  | 58.6               | 0.8  | 59.2   | 1.3  | 84.2   | 41.4  | 58.6     | 0.8  |
| CAT939G33-2   | 103   | 348   | 17.1258         | 25.9 | 0.0586 | 27.1 | 0.0073 | 8.1 | 0.30  | 46.7               | 3.8  | 57.8   | 15.2 | 544.5  | 574.2 | 46.7     | 3.8  |
| CAT939G33-3   | 117   | 261   | 22.5853         | 34.2 | 0.0436 | 35.1 | 0.0071 | 7.5 | 0.21  | 45.9               | 3.4  | 43.3   | 14.9 | -95.3  | 862.4 | 45.9     | 3.4  |

\*indicates the analysis was not included in the calculations for the mean age

| CAT93-9, cont. |       | Isotopic ratios |         |      |         |       |        |     |       | Apparent ages (Ma) |      |        |        |         |        |          |      |
|----------------|-------|-----------------|---------|------|---------|-------|--------|-----|-------|--------------------|------|--------|--------|---------|--------|----------|------|
| Analysis       | U     | 206Pb           | 206Pb*  | ±    | 207Pb*  | ±     | 206Pb* | ±   | error | 206Pb*             | ±    | 207Pb* | ±      | 206Pb*  | ±      | Best age | ±    |
|                | (ppm) | 204Pb           | 207Pb*  | (%)  | 235U*   | (%)   | 238U   | (%) | corr. | 238U*              | (Ma) | 235U   | (Ma)   | 207Pb*  | (Ma)   | (Ma)     | (Ma) |
| CAT939G34-1    | 113   | 248             | 32.9678 | 53.0 | 0.0327  | 53.4  | 0.0078 | 7.1 | 0.13  | 50.2               | 3.6  | 32.7   | 17.2   | -1125.2 | 1715.2 | 50.2     | 3.6  |
| CAT939G34-2    | 201   | 740             | 14.5058 | 12.0 | 0.0642  | 13.3  | 0.0067 | 5.5 | 0.42  | 43.4               | 2.4  | 63.1   | 8.1    | 896.9   | 249.2  | 43.4     | 2.4  |
| CAT939N-1      | 145   | 206             | 15.2480 | 10.5 | -0.0082 | 177.4 | 0.0064 | 5.5 | 0.03  | 41.2               | 2.3  | -8.4   | -14.9  | 0.0     | 0.0    | 41.2     | 2.3  |
| CAT939N-2      | 2580  | 5100            | 17.0750 | 1.0  | 0.0572  | 5.1   | 0.0092 | 4.5 | 0.88  | 59.1               | 2.6  | 56.4   | 2.8    | -54.9   | 58.2   | 59.1     | 2.6  |
| CAT939N-8      | 3262  | 4390            | 16.4330 | 1.5  | 0.0511  | 4.9   | 0.0080 | 4.3 | 0.87  | 51.2               | 2.2  | 50.6   | 2.4    | 22.8    | 57.8   | 51.2     | 2.2  |
| CAT939N-9      | 1915  | 3506            | 16.8910 | 1.1  | 0.0587  | 6.9   | 0.0096 | 6.5 | 0.94  | 61.3               | 4.0  | 57.9   | 3.9    | -79.3   | 55.5   | 61.3     | 4.0  |
| CAT939N-10     | 1060  | 2148            | 16.7480 | 3.3  | 0.0530  | 7.6   | 0.0090 | 4.6 | 0.60  | 57.7               | 2.6  | 52.4   | 3.9    | -183.3  | 151.8  | 57.7     | 2.6  |
| CAT939N-12     | 122   | 448             | 14.5740 | 6.8  | 0.0279  | 36.7  | 0.0071 | 5.3 | 0.15  | 45.9               | 2.4  | 28.0   | 10.1   | -1331.9 | 1192.7 | 45.9     | 2.4  |
| CAT939N-14     | 667   | 1718            | 17.3130 | 2.1  | 0.0454  | 8.1   | 0.0083 | 2.6 | 0.32  | 53.3               | 1.4  | 45.0   | 3.6    | -374.9  | 198.5  | 53.3     | 1.4  |
| CAT939N-15     | 121   | 338             | 17.1960 | 17.8 | 0.0126  | 61.6  | 0.0090 | 6.2 | 0.10  | 57.7               | 3.6  | 12.7   | 7.8    | 0.0     | 800.5  | 57.7     | 3.6  |
| CAT939N-16     | 441   | 744             | 12.5200 | 23.7 | 0.0578  | 25.7  | 0.0086 | 3.3 | 0.13  | 55.1               | 1.8  | 57.1   | 14.2   | 142.9   | 605.5  | 55.1     | 1.8  |
| CAT939N-17     | 304   | 352             | 16.1460 | 6.5  | 0.0152  | 40.5  | 0.0074 | 4.0 | 0.10  | 47.5               | 1.9  | 15.3   | 6.2    | -4186.5 | 879.2  | 47.5     | 1.9  |
| CAT939N-19     | 195   | 180             | 13.8320 | 20.1 | -0.0115 | 323.2 | 0.0063 | 8.7 | 0.03  | 40.3               | 3.5  | -11.7  | -38.1  | 0.0     | 0.0    | 40.3     | 3.5  |
| CAT939N-22     | 149   | 300             | 12.3610 | 22.9 | 0.0260  | 50.5  | 0.0075 | 7.4 | 0.15  | 48.3               | 3.6  | 26.0   | 13.0   | -1754.4 | 1859.8 | 48.3     | 3.6  |
| CAT939N-23     | 111   | 102             | 3.8870  | 6.6  | 0.1096  | 16.2  | 0.0077 | 7.0 | 0.43  | 49.2               | 3.4  | 105.6  | 16.3   | 1694.5  | 272.1  | 49.2     | 3.4  |
| CAT939N-25     | 94    | 202             | 13.2850 | 31.5 | -0.0019 | 112.6 | 0.0068 | 9.0 | 0.08  | 43.6               | 3.9  | -1.9   | -2.2   | 0.0     | 1799.2 | 43.6     | 3.9  |
| CAT939N-27     | 2832  | 8562            | 16.9380 | 2.0  | 0.0555  | 3.0   | 0.0085 | 2.1 | 0.68  | 54.9               | 1.1  | 54.8   | 1.6    | 51.4    | 53.3   | 54.9     | 1.1  |
| CAT939N-28     | 152   | 178             | 15.0070 | 13.2 | -0.0179 | 307.7 | 0.0066 | 2.8 | 0.01  | 42.7               | 1.2  | -18.4  | -57.1  | 0.0     | 0.0    | 42.7     | 1.2  |
| CAT939N-29     | 1344  | 2550            | 16.8100 | 1.5  | 0.0536  | 5.4   | 0.0088 | 2.4 | 0.45  | 56.5               | 1.4  | 53.0   | 2.8    | -101.7  | 117.8  | 56.5     | 1.4  |
| CAT939N-30     | 173   | 520             | 12.4040 | 36.4 | 0.0430  | 43.0  | 0.0073 | 6.1 | 0.14  | 46.6               | 2.8  | 42.8   | 18.0   | -164.7  | 1102.8 | 46.6     | 2.8  |
| CAT939N-31     | 1155  | 1906            | 11.8540 | 51.3 | 0.0761  | 51.7  | 0.0087 | 4.3 | 0.08  | 55.9               | 2.4  | 74.5   | 37.1   | 720.4   | 1172.7 | 55.9     | 2.4  |
| CAT939N-32     | 216   | 256             | 16.5200 | 7.6  | -0.0005 | 102.6 | 0.0068 | 4.8 | 0.05  | 43.7               | 2.1  | -0.5   | -0.5   | 0.0     | 1061.6 | 43.7     | 2.1  |
| CAT939N-35     | 1140  | 2052            | 17.1360 | 2.3  | 0.0525  | 5.3   | 0.0090 | 2.7 | 0.51  | 57.7               | 1.5  | 52.0   | 2.7    | -206.3  | 113.5  | 57.7     | 1.5  |
| CAT939N-38     | 1804  | 1976            | 17.3250 | 2.1  | 0.0545  | 9.8   | 0.0095 | 2.8 | 0.29  | 60.9               | 1.7  | 53.9   | 5.1    | -248.2  | 237.3  | 60.9     | 1.7  |
| J-939-2        | 121   | 546             | 17.0760 | 3.9  | 0.0228  | 44.0  | 0.0070 | 3.3 | 0.08  | 45.1               | 1.5  | 22.9   | 10.0   | 45.1    | 1.5    | 45.1     | 1.5  |
| J-939-4        | 204   | 1132            | 9.2130  | 2.5  | 0.0417  | 17.8  | 0.0083 | 5.1 | 0.29  | 53.1               | 2.7  | -42.4  | -257.6 | 36.0    | 3.6    | 53.1     | 2.7  |
| J-939N-1       | 54    | 312             | 18.5930 | 11.6 | 0.0030  | 86.2  | 0.0069 | 4.1 | 0.05  | 44.5               | 1.8  | 3.1    | 2.6    | 44.5    | 1.8    | 44.5     | 1.8  |

\*indicates the analysis was not included in the calculations for the mean age

| CAT 93-9, cont. |       | Isotopic ratios |         |       |         |       |        |      |       | Apparent ages (Ma) |      |        |      |         |        |          |      |
|-----------------|-------|-----------------|---------|-------|---------|-------|--------|------|-------|--------------------|------|--------|------|---------|--------|----------|------|
| Analysis        | U     | 206Pb           | 206Pb*  | ±     | 207Pb*  | ±     | 206Pb* | ±    | error | 206Pb*             | ±    | 207Pb* | ±    | 206Pb*  | ±      | Best age | ±    |
|                 | (ppm) | 204Pb           | 207Pb*  | (%)   | 235U*   | (%)   | 238U   | (%)  | corr. | 238U*              | (Ma) | 235U   | (Ma) | 207Pb*  | (Ma)   | (Ma)     | (Ma) |
| J-939N-2        | 181   | 2096            | 17.2660 | 2.0   | 0.0519  | 6.3   | 0.0090 | 1.6  | 0.26  | 57.5               | 0.9  | 51.4   | 3.2  | 57.5    | 0.9    | 57.5     | 0.9  |
| J-939N-4        | 318   | 2740            | 15.0390 | 5.4   | 0.0637  | 9.4   | 0.0093 | 6.7  | 0.71  | 59.6               | 4.0  | 62.7   | 5.7  | 59.6    | 4.0    | 59.6     | 4.0  |
| J-939N-6        | 49    | 284             | 17.2860 | 11.9  | 0.0021  | 88.1  | 0.0064 | 3.6  | 0.04  | 41.3               | 1.5  | 2.1    | 1.9  | 41.3    | 1.5    | 41.3     | 1.5  |
| J-939N-7        | 120   | 712             | 17.2640 | 3.1   | 0.0318  | 19.2  | 0.0077 | 3.3  | 0.17  | 49.6               | 1.6  | 31.8   | 6.0  | 49.6    | 1.6    | 49.6     | 1.6  |
| J-939N-8        | 289   | 1170            | 17.2650 | 1.8   | 0.0433  | 19.4  | 0.0086 | 4.4  | 0.22  | 55.0               | 2.4  | 43.0   | 8.2  | 55.0    | 2.4    | 55.0     | 2.4  |
| J-939N-9        | 42    | 210             | 15.0580 | 7.8   | -0.0069 | 163.9 | 0.0069 | 3.6  | 0.02  | 44.5               | 1.6  | -7.0   | 11.6 | 44.5    | 1.6    | 44.5     | 1.6  |
| J-939N-10       | 309   | 2262            | 17.2710 | 1.6   | 0.0522  | 4.7   | 0.0091 | 3.5  | 0.75  | 58.5               | 2.1  | 51.7   | 2.4  | 58.5    | 2.1    | 58.5     | 2.1  |
| CAT939G16-2     | 119   | 1590            | 17.4621 | 14.2  | 0.0474  | 16.7  | 0.0060 | 8.8  | 0.53  | 38.6               | 3.4  | 47.0   | 7.7  | 501.8   | 313.4  | 38.6     | 3.4  |
| CAT939G32-1     | 274   | 1222            | 15.8221 | 7.6   | 0.0524  | 9.1   | 0.0060 | 5.1  | 0.56  | 38.7               | 2.0  | 51.9   | 4.6  | 715.0   | 161.6  | 38.7     | 2.0  |
| CAT939N-36      | 69    | 104             | 14.2400 | 23.2  | -0.0607 | 141.5 | 0.0054 | 6.9  | 0.05  | 34.9               | 2.4  | -63.5  | 93.1 | 0.0     | 1396.0 | 34.9     | 2.4  |
| CAT93-9-G19-2*  | 427   | 1251            | 18.3343 | 22.6  | 0.0592  | 29.8  | 0.0079 | 19.5 | 0.65  | 50.5               | 9.8  | 58.4   | 16.9 | 393.5   | 513.0  | 50.5     | 9.8  |
| CAT93-9-G19-3*  | 308   | 465             | 18.3458 | 39.2  | 0.0476  | 50.2  | 0.0063 | 31.3 | 0.62  | 40.7               | 12.7 | 47.3   | 23.2 | 392.1   | 912.6  | 40.7     | 12.7 |
| CAT93-9-G19-4*  | 179   | 645             | 19.4909 | 42.2  | 0.0680  | 51.5  | 0.0096 | 29.5 | 0.57  | 61.6               | 18.1 | 66.8   | 33.3 | 254.6   | 1012.3 | 61.6     | 18.1 |
| CAT93-9-G19-5*  | 710   | 6294            | 20.5563 | 13.5  | 0.0594  | 19.9  | 0.0089 | 14.6 | 0.73  | 56.8               | 8.3  | 58.6   | 11.3 | 130.8   | 319.7  | 56.8     | 8.3  |
| CAT93-9-G21-1*  | 123   | 459             | 12.6818 | 42.4  | 0.0924  | 64.0  | 0.0085 | 47.9 | 0.75  | 54.6               | 26.0 | 89.7   | 55.0 | 1168.4  | 881.1  | 54.6     | 26.0 |
| CAT93-9-G22-1*  | 111   | 3622            | 37.3963 | 140.0 | 0.0279  | 149.8 | 0.0076 | 53.2 | 0.36  | 48.6               | 25.8 | 27.9   | 41.3 | -1527.4 | 0.0    | 48.6     | 25.8 |
| CAT93-9-G22-2*  | 293   | 1037            | 15.9769 | 23.6  | 0.0671  | 40.7  | 0.0078 | 33.1 | 0.81  | 49.9               | 16.5 | 65.9   | 26.0 | 694.3   | 510.1  | 49.9     | 16.5 |
| CAT93-9-G23-1*  | 1196  | 13000           | 20.3560 | 10.0  | 0.0558  | 14.4  | 0.0082 | 10.3 | 0.72  | 52.9               | 5.4  | 55.2   | 7.7  | 153.8   | 235.0  | 52.9     | 5.4  |
| CAT93-9-G23-3*  | 260   | 830             | 15.0841 | 26.4  | 0.0748  | 38.3  | 0.0082 | 27.7 | 0.72  | 52.5               | 14.5 | 73.2   | 27.0 | 815.7   | 560.0  | 52.5     | 14.5 |
| CAT93-9-G24-1*  | 410   | 1164            | 15.7912 | 34.8  | 0.0532  | 41.6  | 0.0061 | 22.9 | 0.55  | 39.2               | 8.9  | 52.6   | 21.3 | 719.2   | 759.9  | 39.2     | 8.9  |
| CAT93-9-G24-3*  | 127   | 826             | 19.2903 | 67.6  | 0.0491  | 84.3  | 0.0069 | 50.4 | 0.60  | 44.2               | 22.2 | 48.7   | 40.1 | 278.3   | 1761.7 | 44.2     | 22.2 |
| CAT93-9-G26-1*  | 376   | 1734            | 16.4176 | 20.0  | 0.0725  | 30.3  | 0.0086 | 22.8 | 0.75  | 55.4               | 12.6 | 71.1   | 20.8 | 636.0   | 435.4  | 55.4     | 12.6 |
| CAT93-9-G27-2*  | 239   | 382             | 9.1162  | 17.1  | 0.1285  | 33.4  | 0.0085 | 28.7 | 0.86  | 54.5               | 15.6 | 122.8  | 38.7 | 1794.3  | 314.0  | 54.5     | 15.6 |
| CAT93-9-G28-1*  | 140   | 217             | 14.0688 | 45.3  | 0.0723  | 63.6  | 0.0074 | 44.6 | 0.70  | 47.4               | 21.0 | 70.9   | 43.6 | 959.7   | 977.3  | 47.4     | 21.0 |
| CAT93-9-G30-1*  | 132   | 2872            | 12.6752 | 42.0  | 0.0806  | 55.3  | 0.0074 | 36.0 | 0.65  | 47.6               | 17.1 | 78.7   | 41.9 | 1169.5  | 870.5  | 47.6     | 17.1 |
| CAT93-9-G32-1*  | 281   | 897             | 13.1822 | 25.2  | 0.0630  | 39.6  | 0.0060 | 30.5 | 0.77  | 38.7               | 11.8 | 62.0   | 23.8 | 1091.4  | 513.2  | 38.7     | 11.8 |
| CAT93-9-G33-1*  | 452   | 1031            | 25.1534 | 34.1  | 0.0361  | 41.0  | 0.0066 | 22.8 | 0.56  | 42.3               | 9.6  | 36.0   | 14.5 | -366.8  | 904.7  | 42.3     | 9.6  |
| CAT93-9-G33-2*  | 170   | 308             | 20.6003 | 41.7  | 0.0507  | 58.8  | 0.0076 | 41.4 | 0.71  | 48.6               | 20.1 | 50.2   | 28.8 | 125.8   | 1021.4 | 48.6     | 20.1 |
| CAT93-9-G33-3*  | 136   | 924             | 28.0136 | 76.8  | 0.0368  | 90.6  | 0.0075 | 48.1 | 0.53  | 48.1               | 23.0 | 36.7   | 32.7 | -654.1  | 2492.4 | 48.1     | 23.0 |
| CAT93-9-G34-1*  | 418   | 1283            | 29.0491 | 30.4  | 0.0391  | 34.6  | 0.0082 | 16.6 | 0.48  | 52.9               | 8.7  | 38.9   | 13.2 | -755.0  | 868.9  | 52.9     | 8.7  |
| CAT93-9-G34-3*  | 463   | 1109            | 20.1560 | 23.4  | 0.0587  | 27.0  | 0.0086 | 13.5 | 0.50  | 55.1               | 7.4  | 58.0   | 15.2 | 176.9   | 552.0  | 55.1     | 7.4  |

\*indicates the analysis was not included in the calculations for the mean age

| CAT 93-9, cont. |       | Isotopic ratios |         |       |        |       |        |      |       | Apparent ages (Ma) |      |        |      |         |        |          |      |
|-----------------|-------|-----------------|---------|-------|--------|-------|--------|------|-------|--------------------|------|--------|------|---------|--------|----------|------|
| Analysis        | U     | 206Pb           | 206Pb*  | ±     | 207Pb* | ±     | 206Pb* | ±    | error | 206Pb*             | ±    | 207Pb* | ±    | 206Pb*  | ±      | Best age | ±    |
|                 | (ppm) | 204Pb           | 207Pb*  | (%)   | 235U*  | (%)   | 238U   | (%)  | corr. | 238U*              | (Ma) | 235U   | (Ma) | 207Pb*  | (Ma)   | (Ma)     | (Ma) |
| CAT93-9-G35-2*  | 224   | 330             | 8.9434  | 18.7  | 0.1087 | 32.1  | 0.0071 | 26.0 | 0.81  | 45.3               | 11.8 | 104.8  | 31.9 | 1829.1  | 342.4  | 45.3     | 11.8 |
| CAT93-9-G36-1*  | 269   | 84              | 2.0724  | 2.9   | 0.7740 | 17.1  | 0.0116 | 16.8 | 0.99  | 74.6               | 12.5 | 582.1  | 75.8 | 0.0     | 0.0    | 74.6     | 12.5 |
| CAT93-9-G36-2*  | 150   | 140             | 14.4938 | 65.3  | 0.0659 | 79.8  | 0.0069 | 45.9 | 0.57  | 44.5               | 20.4 | 64.8   | 50.2 | 898.6   | 1529.4 | 44.5     | 20.4 |
| CAT93-9-G37-1*  | 458   | 346             | 13.4166 | 19.7  | 0.0779 | 26.3  | 0.0076 | 17.4 | 0.66  | 48.7               | 8.4  | 76.2   | 19.3 | 1056.0  | 400.3  | 48.7     | 8.4  |
| CAT93-9-G39-1*  | 428   | 924             | 16.1644 | 25.0  | 0.0700 | 32.5  | 0.0082 | 20.7 | 0.64  | 52.7               | 10.9 | 68.7   | 21.6 | 669.4   | 544.0  | 52.7     | 10.9 |
| CAT93-9-G40-1*  | 329   | 327             | 8.7924  | 17.4  | 0.1273 | 36.2  | 0.0081 | 31.7 | 0.88  | 52.1               | 16.5 | 121.7  | 41.5 | 1859.9  | 317.1  | 52.1     | 16.5 |
| CAT93-9-G43-1*  | 101   | 171             | 12.6056 | 55.7  | 0.0868 | 97.9  | 0.0079 | 80.6 | 0.82  | 50.9               | 40.9 | 84.5   | 79.5 | 1180.4  | 1202.5 | 50.9     | 40.9 |
| CAT93-9-G43-2*  | 734   | 1061            | 21.6325 | 17.9  | 0.0544 | 23.1  | 0.0085 | 14.7 | 0.63  | 54.8               | 8.0  | 53.8   | 12.1 | 9.4     | 433.0  | 54.8     | 8.0  |
| CAT93-9-G44-1*  | 207   | 217             | 8.8599  | 25.9  | 0.1205 | 45.7  | 0.0077 | 37.7 | 0.82  | 49.7               | 18.7 | 115.5  | 50.0 | 1846.1  | 477.7  | 49.7     | 18.7 |
| CAT93-9-G19-2*  | 427   | 1251            | 18.3343 | 22.6  | 0.0592 | 29.8  | 0.0079 | 19.5 | 0.65  | 50.5               | 9.8  | 58.4   | 16.9 | 393.5   | 513.0  | 50.5     | 9.8  |
| CAT93-9-G19-3*  | 308   | 465             | 18.3458 | 39.2  | 0.0476 | 50.2  | 0.0063 | 31.3 | 0.62  | 40.7               | 12.7 | 47.3   | 23.2 | 392.1   | 912.6  | 40.7     | 12.7 |
| CAT93-9-G19-4*  | 179   | 645             | 19.4909 | 42.2  | 0.0680 | 51.5  | 0.0096 | 29.5 | 0.57  | 61.6               | 18.1 | 66.8   | 33.3 | 254.6   | 1012.3 | 61.6     | 18.1 |
| CAT93-9-G19-5*  | 710   | 6294            | 20.5563 | 13.5  | 0.0594 | 19.9  | 0.0089 | 14.6 | 0.73  | 56.8               | 8.3  | 58.6   | 11.3 | 130.8   | 319.7  | 56.8     | 8.3  |
| CAT93-9-G21-1*  | 123   | 459             | 12.6818 | 42.4  | 0.0924 | 64.0  | 0.0085 | 47.9 | 0.75  | 54.6               | 26.0 | 89.7   | 55.0 | 1168.4  | 881.1  | 54.6     | 26.0 |
| CAT93-9-G22-1*  | 111   | 3622            | 37.3963 | 140.0 | 0.0279 | 149.8 | 0.0076 | 53.2 | 0.36  | 48.6               | 25.8 | 27.9   | 41.3 | -1527.4 | 0.0    | 48.6     | 25.8 |
| CAT93-9-G22-2*  | 293   | 1037            | 15.9769 | 23.6  | 0.0671 | 40.7  | 0.0078 | 33.1 | 0.81  | 49.9               | 16.5 | 65.9   | 26.0 | 694.3   | 510.1  | 49.9     | 16.5 |
| CAT93-9-G23-1*  | 1196  | 13000           | 20.3560 | 10.0  | 0.0558 | 14.4  | 0.0082 | 10.3 | 0.72  | 52.9               | 5.4  | 55.2   | 7.7  | 153.8   | 235.0  | 52.9     | 5.4  |
| CAT93-9-G23-3*  | 260   | 830             | 15.0841 | 26.4  | 0.0748 | 38.3  | 0.0082 | 27.7 | 0.72  | 52.5               | 14.5 | 73.2   | 27.0 | 815.7   | 560.0  | 52.5     | 14.5 |
| CAT93-9-G24-1*  | 410   | 1164            | 15.7912 | 34.8  | 0.0532 | 41.6  | 0.0061 | 22.9 | 0.55  | 39.2               | 8.9  | 52.6   | 21.3 | 719.2   | 759.9  | 39.2     | 8.9  |
| CAT93-9-G24-3*  | 127   | 826             | 19.2903 | 67.6  | 0.0491 | 84.3  | 0.0069 | 50.4 | 0.60  | 44.2               | 22.2 | 48.7   | 40.1 | 278.3   | 1761.7 | 44.2     | 22.2 |
| CAT93-9-G26-1*  | 376   | 1734            | 16.4176 | 20.0  | 0.0725 | 30.3  | 0.0086 | 22.8 | 0.75  | 55.4               | 12.6 | 71.1   | 20.8 | 636.0   | 435.4  | 55.4     | 12.6 |
| CAT93-9-G27-2*  | 239   | 382             | 9.1162  | 17.1  | 0.1285 | 33.4  | 0.0085 | 28.7 | 0.86  | 54.5               | 15.6 | 122.8  | 38.7 | 1794.3  | 314.0  | 54.5     | 15.6 |
| CAT93-9-G28-1*  | 140   | 217             | 14.0688 | 45.3  | 0.0723 | 63.6  | 0.0074 | 44.6 | 0.70  | 47.4               | 21.0 | 70.9   | 43.6 | 959.7   | 977.3  | 47.4     | 21.0 |
| CAT93-9-G30-1*  | 132   | 2872            | 12.6752 | 42.0  | 0.0806 | 55.3  | 0.0074 | 36.0 | 0.65  | 47.6               | 17.1 | 78.7   | 41.9 | 1169.5  | 870.5  | 47.6     | 17.1 |
| CAT93-9-G32-1*  | 281   | 897             | 13.1822 | 25.2  | 0.0630 | 39.6  | 0.0060 | 30.5 | 0.77  | 38.7               | 11.8 | 62.0   | 23.8 | 1091.4  | 513.2  | 38.7     | 11.8 |
| CAT93-9-G33-1*  | 452   | 1031            | 25.1534 | 34.1  | 0.0361 | 41.0  | 0.0066 | 22.8 | 0.56  | 42.3               | 9.6  | 36.0   | 14.5 | -366.8  | 904.7  | 42.3     | 9.6  |

\*indicates the analysis was not included in the calculations for the mean age



| CAT 93-9, cont. |       |       | Isotopic ratios |       |         |       |        |      |       | Apparent ages (Ma) |      |        |        |        |        |          |        |
|-----------------|-------|-------|-----------------|-------|---------|-------|--------|------|-------|--------------------|------|--------|--------|--------|--------|----------|--------|
| Analysis        | U     | 206Pb | 206Pb*          | ±     | 207Pb*  | ±     | 206Pb* | ±    | error | 206Pb*             | ±    | 207Pb* | ±      | 206Pb* | ±      | Best age | ±      |
|                 | (ppm) | 204Pb | 207Pb*          | (%)   | 235U*   | (%)   | 238U   | (%)  | corr. | 238U*              | (Ma) | 235U   | (Ma)   | 207Pb* | (Ma)   | (Ma)     | (Ma)   |
| CAT93-9-G33-2*  | 170   | 308   | 20.6003         | 41.7  | 0.0507  | 58.8  | 0.0076 | 41.4 | 0.71  | 48.6               | 20.1 | 50.2   | 28.8   | 125.8  | 1021.4 | 48.6     | 20.1   |
| CAT93-9-G33-3*  | 136   | 924   | 28.0136         | 76.8  | 0.0368  | 90.6  | 0.0075 | 48.1 | 0.53  | 48.1               | 23.0 | 36.7   | 32.7   | -654.1 | 2492.4 | 48.1     | 23.0   |
| CAT93-9-G34-1*  | 418   | 1283  | 29.0491         | 30.4  | 0.0391  | 34.6  | 0.0082 | 16.6 | 0.48  | 52.9               | 8.7  | 38.9   | 13.2   | -755.0 | 868.9  | 52.9     | 8.7    |
| CAT93-9-G34-3*  | 463   | 1109  | 20.1560         | 23.4  | 0.0587  | 27.0  | 0.0086 | 13.5 | 0.50  | 55.1               | 7.4  | 58.0   | 15.2   | 176.9  | 552.0  | 55.1     | 7.4    |
| CAT93-9-G35-2*  | 224   | 330   | 8.9434          | 18.7  | 0.1087  | 32.1  | 0.0071 | 26.0 | 0.81  | 45.3               | 11.8 | 104.8  | 31.9   | 1829.1 | 342.4  | 45.3     | 11.8   |
| CAT93-9-G36-1*  | 269   | 84    | 2.0724          | 2.9   | 0.7740  | 17.1  | 0.0116 | 16.8 | 0.99  | 74.6               | 12.5 | 582.1  | 75.8   | 0.0    | 0.0    | 74.6     | 12.5   |
| CAT93-9-G36-2*  | 150   | 140   | 14.4938         | 65.3  | 0.0659  | 79.8  | 0.0069 | 45.9 | 0.57  | 44.5               | 20.4 | 64.8   | 50.2   | 898.6  | 1529.4 | 44.5     | 20.4   |
| CAT93-9-G37-1*  | 458   | 346   | 13.4166         | 19.7  | 0.0779  | 26.3  | 0.0076 | 17.4 | 0.66  | 48.7               | 8.4  | 76.2   | 19.3   | 1056.0 | 400.3  | 48.7     | 8.4    |
| CAT93-9-G39-1*  | 428   | 924   | 16.1644         | 25.0  | 0.0700  | 32.5  | 0.0082 | 20.7 | 0.64  | 52.7               | 10.9 | 68.7   | 21.6   | 669.4  | 544.0  | 52.7     | 10.9   |
| CAT93-9-G40-1*  | 329   | 327   | 8.7924          | 17.4  | 0.1273  | 36.2  | 0.0081 | 31.7 | 0.88  | 52.1               | 16.5 | 121.7  | 41.5   | 1859.9 | 317.1  | 52.1     | 16.5   |
| CAT93-9-G43-1*  | 101   | 171   | 12.6056         | 55.7  | 0.0868  | 97.9  | 0.0079 | 80.6 | 0.82  | 50.9               | 40.9 | 84.5   | 79.5   | 1180.4 | 1202.5 | 50.9     | 40.9   |
| CAT93-9-G43-2*  | 734   | 1061  | 21.6325         | 17.9  | 0.0544  | 23.1  | 0.0085 | 14.7 | 0.63  | 54.8               | 8.0  | 53.8   | 12.1   | 9.4    | 433.0  | 54.8     | 8.0    |
| CAT93-9-G44-1*  | 207   | 217   | 8.8599          | 25.9  | 0.1205  | 45.7  | 0.0077 | 37.7 | 0.82  | 49.7               | 18.7 | 115.5  | 50.0   | 1846.1 | 477.7  | 49.7     | 18.7   |
| CAT93-9-G18-1   | 365   | 20807 | 10.3363         | 1.3   | 2.1429  | 3.4   | 0.1606 | 3.2  | 0.93  | 960.4              | 28.3 | 1162.8 | 23.7   | 1562.3 | 24.3   | 1562.3   | 24.3   |
| CAT93-9-G3-2*   | 60    | 257   | 7.8400          | 45.1  | 0.1562  | 81.9  | 0.0089 | 68.4 | 0.83  | 57.0               | 38.8 | 147.4  | 112.8  | 2064.5 | 843.6  | 2064.5   | 843.6  |
| CAT93-9-G5-1*   | 136   | 78    | 6.9096          | 45.1  | 0.1334  | 61.5  | 0.0067 | 41.9 | 0.68  | 42.9               | 17.9 | 127.1  | 73.6   | 2284.5 | 824.1  | 2284.5   | 824.1  |
| CAT93-9-G5-2    | 96    | 83    | -13.6757        | 143.5 | -0.0595 | 159.6 | 0.0059 | 70.0 | 0.44  | 37.9               | 26.5 | -62.3  | -102.9 | 0.0    | 1269.7 | 37.9     | 26.5   |
| CAT93-9-G8-4*   | 62    | 583   | 7.7954          | 60.7  | 0.1603  | 106.7 | 0.0091 | 87.7 | 0.82  | 58.2               | 50.8 | 151.0  | 150.7  | 2074.5 | 1203.8 | 2074.5   | 1203.8 |
| CAT93-9-G11-1*  | 83    | 1813  | 7.5032          | 43.8  | 0.1339  | 91.5  | 0.0073 | 80.4 | 0.88  | 46.8               | 37.5 | 127.6  | 110.2  | 2141.6 | 809.4  | 2141.6   | 809.4  |
| CAT93-9-G12-1*  | 242   | 338   | 6.4203          | 17.2  | 0.1530  | 32.4  | 0.0071 | 27.5 | 0.85  | 45.8               | 12.5 | 144.5  | 43.7   | 2410.1 | 294.2  | 2410.1   | 294.2  |
| CAT93-9-G14-1*  | 183   | 139   | 4.5091          | 13.9  | 0.2387  | 37.5  | 0.0078 | 34.9 | 0.93  | 50.1               | 17.4 | 217.3  | 73.6   | 2993.6 | 224.6  | 2993.6   | 224.6  |
| CAT93-9-G16-3*  | 67    | 480   | 7.5894          | 39.2  | 0.1346  | 78.5  | 0.0074 | 68.1 | 0.87  | 47.6               | 32.3 | 128.2  | 94.8   | 2121.6 | 717.2  | 2121.6   | 717.2  |
| CAT93-9-G17-3*  | 140   | 554   | 7.5299          | 20.2  | 0.1517  | 48.8  | 0.0083 | 44.4 | 0.91  | 53.2               | 23.5 | 143.4  | 65.3   | 2135.4 | 358.2  | 2135.4   | 358.2  |
| CAT93-9-G20-1*  | 65    | 193   | 7.1875          | 49.1  | 0.1355  | 104.9 | 0.0071 | 92.7 | 0.88  | 45.4               | 41.9 | 129.0  | 127.8  | 2216.4 | 915.3  | 2216.4   | 915.3  |
| CAT93-9-G23-2*  | 150   | 171   | 4.3912          | 13.5  | 0.2654  | 49.9  | 0.0085 | 48.0 | 0.96  | 54.3               | 26.0 | 239.0  | 106.7  | 3036.2 | 217.6  | 3036.2   | 217.6  |
| CAT93-9-G25-1*  | 95    | 2189  | 6.9670          | 37.7  | 0.1476  | 67.7  | 0.0075 | 56.3 | 0.83  | 47.9               | 26.9 | 139.8  | 88.7   | 2270.3 | 676.3  | 2270.3   | 676.3  |

\*indicates the analysis was not included in the calculations for the mean age

| CAT0701       |       | Isotopic ratios |         |     |        |      |        |      |       |        | Apparent ages (Ma) |        |       |        |      |          |      |
|---------------|-------|-----------------|---------|-----|--------|------|--------|------|-------|--------|--------------------|--------|-------|--------|------|----------|------|
| Analysis      | U     | 206Pb           | 206Pb*  | ±   | 207Pb* | ±    | 206Pb* | ±    | error | 206Pb* | ±                  | 207Pb* | ±     | 206Pb* | ±    | Best age | ±    |
|               | (ppm) | 204Pb           | 207Pb*  | (%) | 235U*  | (%)  | 238U   | (%)  | corr. | 238U*  | (Ma)               | 235U   | (Ma)  | 207Pb* | (Ma) | (Ma)     | (Ma) |
| CAT0701-G1-1  | 210   | 8329            | 10.8453 | 1.7 | 3.1135 | 6.2  | 0.2449 | 5.9  | 0.96  | 1412.1 | 75.2               | 1436.0 | 47.5  | 1471.6 | 32.6 | 1471.6   | 32.6 |
| CAT0701-G2-2  | 247   | 6425            | 11.0318 | 1.2 | 3.2966 | 5.4  | 0.2638 | 5.2  | 0.97  | 1509.0 | 70.6               | 1480.2 | 41.9  | 1439.2 | 22.8 | 1439.2   | 22.8 |
| CAT0701-G2-3  | 79    | 5821            | 11.1975 | 3.3 | 3.0777 | 13.0 | 0.2499 | 12.6 | 0.97  | 1438.2 | 161.9              | 1427.2 | 99.8  | 1410.7 | 63.1 | 1410.7   | 63.1 |
| CAT0701-G3-1  | 270   | 6270            | 10.9846 | 1.4 | 3.0938 | 5.6  | 0.2465 | 5.4  | 0.97  | 1420.3 | 68.6               | 1431.2 | 42.6  | 1447.3 | 26.2 | 1447.3   | 26.2 |
| CAT0701-G3-2  | 69    | 3167            | 10.5723 | 3.5 | 3.2626 | 13.3 | 0.2502 | 12.8 | 0.97  | 1439.3 | 165.1              | 1472.2 | 103.4 | 1519.8 | 65.4 | 1519.8   | 65.4 |
| CAT0701-G4-1  | 184   | 8135            | 10.9102 | 2.1 | 3.1731 | 6.1  | 0.2511 | 5.8  | 0.94  | 1444.0 | 74.7               | 1450.6 | 47.4  | 1460.3 | 39.4 | 1460.3   | 39.4 |
| CAT0701-G4-2  | 307   | 991011          | 10.9737 | 1.2 | 3.1568 | 4.2  | 0.2512 | 4.1  | 0.96  | 1444.9 | 52.6               | 1446.7 | 32.6  | 1449.2 | 21.9 | 1449.2   | 21.9 |
| CAT0701-G5-1  | 482   | 14664           | 10.7561 | 1.0 | 2.9675 | 3.1  | 0.2315 | 2.9  | 0.95  | 1342.3 | 35.3               | 1399.3 | 23.4  | 1487.3 | 19.0 | 1487.3   | 19.0 |
| CAT0701-G6-1  | 1471  | 20644           | 11.0070 | 0.6 | 1.6986 | 1.7  | 0.1356 | 1.6  | 0.93  | 819.7  | 12.3               | 1008.0 | 10.9  | 1443.5 | 11.7 | 1443.5   | 11.7 |
| CAT0701-G7-1  | 178   | 8222            | 10.8255 | 1.9 | 2.6147 | 6.8  | 0.2053 | 6.5  | 0.96  | 1203.7 | 71.8               | 1304.8 | 50.1  | 1475.1 | 36.0 | 1475.1   | 36.0 |
| CAT0701-G8-1  | 318   | 57788           | 11.0952 | 1.1 | 3.1092 | 4.2  | 0.2502 | 4.0  | 0.96  | 1439.5 | 52.0               | 1435.0 | 32.2  | 1428.3 | 21.9 | 1428.3   | 21.9 |
| CAT0701-G9-1  | 314   | 7592            | 11.1694 | 1.3 | 3.1569 | 4.5  | 0.2557 | 4.3  | 0.96  | 1468.0 | 56.0               | 1446.7 | 34.4  | 1415.5 | 25.1 | 1415.5   | 25.1 |
| CAT0701-G10-1 | 895   | 4894            | 10.4579 | 1.0 | 1.4515 | 2.4  | 0.1101 | 2.2  | 0.90  | 673.3  | 13.8               | 910.5  | 14.4  | 1540.3 | 19.3 | 1540.3   | 19.3 |
| CAT0701-G11-1 | 507   | 62018           | 10.8111 | 0.7 | 3.3511 | 2.8  | 0.2628 | 2.7  | 0.97  | 1503.9 | 36.4               | 1493.1 | 21.9  | 1477.6 | 13.5 | 1477.6   | 13.5 |
| CAT0701-G12-1 | 411   | 44646           | 10.8924 | 1.1 | 3.1395 | 3.8  | 0.2480 | 3.7  | 0.96  | 1428.3 | 46.8               | 1442.4 | 29.3  | 1463.4 | 20.4 | 1463.4   | 20.4 |
| CAT0701-G13-1 | 227   | 4991            | 11.2653 | 2.1 | 2.6589 | 6.4  | 0.2172 | 6.0  | 0.95  | 1267.3 | 69.2               | 1317.1 | 46.9  | 1399.1 | 39.3 | 1399.1   | 39.3 |
| CAT0701-G15-1 | 454   | 10074           | 10.9851 | 1.0 | 3.0073 | 3.4  | 0.2396 | 3.3  | 0.96  | 1384.6 | 41.1               | 1409.5 | 26.3  | 1447.3 | 18.9 | 1447.3   | 18.9 |
| CAT0701-G16-1 | 145   | 17043           | 10.8146 | 2.5 | 3.5924 | 8.7  | 0.2818 | 8.4  | 0.96  | 1600.3 | 118.9              | 1547.8 | 69.6  | 1477.0 | 47.0 | 1477.0   | 47.0 |
| CAT0701-G17-1 | 652   | 69160           | 10.7963 | 0.7 | 3.2067 | 2.4  | 0.2511 | 2.3  | 0.96  | 1444.1 | 30.1               | 1458.8 | 18.8  | 1480.2 | 13.4 | 1480.2   | 13.4 |
| CAT0701-G20-1 | 271   | 7618            | 11.0442 | 1.3 | 3.0143 | 4.3  | 0.2414 | 4.1  | 0.95  | 1394.2 | 51.8               | 1411.2 | 33.1  | 1437.0 | 25.7 | 1437.0   | 25.7 |
| CAT0701-G22-1 | 955   | 27615           | 10.9877 | 0.6 | 2.8846 | 1.9  | 0.2299 | 1.9  | 0.95  | 1333.8 | 22.4               | 1377.9 | 14.7  | 1446.8 | 11.4 | 1446.8   | 11.4 |
| CAT0701-G23-1 | 486   | 5994            | 11.3082 | 1.9 | 1.4107 | 4.3  | 0.1157 | 3.8  | 0.90  | 705.7  | 25.7               | 893.4  | 25.4  | 1391.9 | 35.8 | 1391.9   | 35.8 |
| CAT0701-G24-2 | 696   | 20339           | 11.0080 | 0.7 | 3.2183 | 2.1  | 0.2569 | 2.0  | 0.95  | 1474.2 | 26.3               | 1461.6 | 16.3  | 1443.3 | 12.8 | 1443.3   | 12.8 |
| CAT0701-G25-1 | 425   | 9336            | 11.0534 | 1.1 | 2.9856 | 3.3  | 0.2393 | 3.2  | 0.95  | 1383.3 | 39.3               | 1403.9 | 25.3  | 1435.4 | 20.1 | 1435.4   | 20.1 |
| CAT0701-G26-1 | 444   | 20120           | 10.9924 | 1.1 | 2.7141 | 3.6  | 0.2164 | 3.4  | 0.95  | 1262.7 | 39.2               | 1332.3 | 26.7  | 1446.0 | 21.1 | 1446.0   | 21.1 |
| CAT0701-G27-1 | 402   | 12936           | 11.0872 | 1.0 | 3.0834 | 3.6  | 0.2479 | 3.5  | 0.96  | 1427.8 | 44.8               | 1428.6 | 27.9  | 1429.6 | 18.6 | 1429.6   | 18.6 |

\*indicates the analysis was not included in the calculations for the mean age

| CAT 93-1 |         |       | Isotopic ratios |      |         |       |        |       | Sample Concordia |       |           |       |         | Best age |       |
|----------|---------|-------|-----------------|------|---------|-------|--------|-------|------------------|-------|-----------|-------|---------|----------|-------|
| Analysis | U       | Th    | 208 Pb          | 8-2% | 206Pb   | 6-8%  | 206 Pb | 6-7%  | 7/5 ratio        | ±(%)  | 6/8 ratio | ±(%)  | errcorr | 8/2 age  | ±(Ma) |
|          | (ppm)   | (ppm) | 232 Th          |      | 238 U   |       | 207 Pb |       |                  |       |           |       |         |          |       |
| 931-1    | 4.3907  | 1768  | 0.00186         | 5.21 | 0.02108 | 18.53 | 1.473  | 41.99 | -3.21            | 58.10 | -0.02     | 39.55 | 0.68    | 40.87    | 2.14  |
| 931-2    | 4.1029  | 1288  | 0.00194         | 3.87 | 0.01855 | 25.98 | 1.87   | 45.86 | -3.36            | 73.52 | -0.02     | 53.96 | 0.73    | 42.14    | 1.67  |
| 931-3    | 4.3084  | 1382  | 0.00201         | 3.14 | 0.02291 | 15.92 | 1.71   | 36.8  | -2.05            | 75.11 | -0.01     | 55.97 | 0.75    | 44.43    | 1.43  |
| 931-4    | 5.8953  | 2120  | 0.00193         | 3.3  | 0.01894 | 27.83 | 1.311  | 18.71 | -2.58            | 60.57 | -0.02     | 57.49 | 0.95    | 41.78    | 1.40  |
| 931-5    | 6.4462  | 1988  | 0.00198         | 2.46 | 0.01723 | 14.93 | 1.759  | 29.2  | -4.24            | 40.49 | -0.03     | 27.60 | 0.68    | 42.59    | 1.08  |
| 931-6    | 5.5418  | 1446  | 0.00196         | 2.46 | 0.02006 | 24.45 | 1.358  | 31.27 | -2.93            | 59.45 | -0.02     | 50.29 | 0.85    | 41.08    | 1.04  |
| 931-7    | 6.1173  | 2133  | 0.00187         | 1.67 | 0.01885 | 32.22 | 1.883  | 31.74 | -3.54            | 74.55 | -0.02     | 62.84 | 0.84    | 40.69    | 0.73  |
| 931-8    | 7.7864  | 2687  | 0.00188         | 1.4  | 0.0173  | 14.23 | 1.702  | 20.81 | -3.07            | 36.86 | -0.02     | 29.49 | 0.80    | 41.49    | 0.61  |
| 931-9    | 7.9673  | 2743  | 0.00186         | 1.3  | 0.01435 | 22.96 | 1.441  | 20.49 | -3.40            | 44.60 | -0.02     | 39.41 | 0.88    | 41.20    | 0.56  |
| 931-10   | 7.8193  | 2459  | 0.00185         | 1.33 | 0.01842 | 6.34  | 1.755  | 20.2  | -4.82            | 22.37 | -0.03     | 9.52  | 0.43    | 38.90    | 0.56  |
| 931-11   | 6.6189  | 2368  | 0.00193         | 1.07 | 0.01538 | 15.13 | 1.39   | 41.67 | -3.57            | 48.81 | -0.03     | 25.37 | 0.52    | 42.80    | 0.51  |
| 931-12   | 6.9067  | 1880  | 0.00195         | 1.54 | 0.02054 | 14.86 | 2.449  | 45.27 | -3.52            | 71.12 | -0.01     | 47.31 | 0.67    | 43.64    | 0.72  |
| 931-13   | 4.9498  | 1503  | 0.00199         | 1.45 | 0.01985 | 21.47 | 2.264  | 34.99 | -4.39            | 59.86 | -0.02     | 45.01 | 0.75    | 44.38    | 0.68  |
| 931-14   | 5.0731  | 1794  | 0.002           | 2.11 | 0.02215 | 12.58 | 2.119  | 58.08 | -3.64            | 69.94 | -0.02     | 35.01 | 0.50    | 45.44    | 0.99  |
| 931-15   | 7.1862  | 1790  | 0.002           | 2.9  | 0.01722 | 15.41 | 1.595  | 24.3  | -3.17            | 43.64 | -0.02     | 35.28 | 0.81    | 43.71    | 1.28  |
| 931-16   | 6.1831  | 1965  | 0.00197         | 1.65 | 0.02221 | 19.12 | 1.537  | 20.94 | -3.95            | 46.07 | -0.02     | 40.15 | 0.87    | 42.47    | 0.73  |
| 931-17   | 7.2684  | 2686  | 0.00192         | 1.82 | 0.01428 | 18.59 | 2.059  | 38.6  | -6.19            | 48.81 | -0.04     | 29.54 | 0.61    | 44.07    | 0.82  |
| 931-18   | 9.5378  | 2926  | 0.00194         | 1.69 | 0.01712 | 17.31 | 1.905  | 22.8  | -3.55            | 45.22 | -0.02     | 37.12 | 0.82    | 44.08    | 0.76  |
| 931-19   | 8.0331  | 2574  | 0.00194         | 1.94 | 0.01597 | 21.64 | 1.671  | 32.53 | -4.37            | 50.31 | -0.03     | 37.81 | 0.75    | 44.36    | 0.92  |
| 931-20   | 6.7916  | 1925  | 0.00196         | 2.64 | 0.01978 | 24.77 | 1.862  | 32.38 | -5.64            | 53.55 | -0.03     | 41.70 | 0.78    | 42.40    | 1.19  |
| 931-21   | 10.7136 | 3534  | 0.00191         | 1    | 0.01416 | 12.5  | 1.727  | 36.39 | -3.93            | 42.75 | -0.02     | 22.13 | 0.52    | 43.10    | 0.45  |
| 931-22   | 11.6262 | 3411  | 0.00188         | 1.08 | 0.01565 | 13.27 | 1.767  | 6.67  | -4.42            | 25.12 | -0.03     | 23.85 | 0.95    | 42.35    | 0.47  |
| 931-23   | 10.6889 | 2871  | 0.00194         | 1.73 | 0.01423 | 9.7   | 1.987  | 18.45 | -4.21            | 25.64 | -0.02     | 17.45 | 0.68    | 44.26    | 0.78  |
| 931-24   | 8.3044  | 2523  | 0.00194         | 3.81 | 0.01389 | 19.54 | 1.879  | 50.02 | -4.02            | 61.02 | -0.02     | 34.18 | 0.56    | 44.23    | 1.72  |
| 931-25   | 10.9356 | 3502  | 0.00186         | 2.23 | 0.01436 | 12.89 | 1.588  | 18.65 | -3.84            | 31.99 | -0.03     | 25.72 | 0.80    | 42.26    | 0.97  |
| 931-26   | 9.9982  | 3282  | 0.0018          | 3.4  | 0.01577 | 12.76 | 1.765  | 26.32 | -4.42            | 34.70 | -0.03     | 22.29 | 0.64    | 40.31    | 1.37  |
| 931-27   | 11.4207 | 3693  | 0.00185         | 2.71 | 0.01574 | 8.94  | 1.795  | 16.06 | -4.45            | 23.72 | -0.03     | 17.18 | 0.72    | 41.75    | 1.15  |

## **Appendix 1.4**

### **Statistical Discussion of Zircon Populations from the Gibbon Mountain and Seven**

#### **Falls sills**

The zircons from the Gibbon Mountain and Seven Falls sills yielded  $^{238}\text{U}/^{206}\text{Pb}$  ages less than 40 Ma. Zircon less than 40 Ma were not found in the other sills. The younger zircons are interpreted to represent a distinct period of zircon growth and indicate multiple age components are present.

Cumulative probability plots and histograms for the Gibbon Mountain and Seven Falls samples are shown below to illustrate the number of age components within these sills. The cumulative probability distribution is obtained by summing the probability distributions of a suite of data with normally-distributed errors [Ludwig, 2000]. The relative misfit represents how the relative improvement in the data fit relates to the number of components [Sambridge and Compston, 1994]. If the number of age components increases it is predicted that the misfit would decrease.

The probability density plot for the Gibbon Mountain sill illustrates that the zircon analyses are separated into two age components at  $38 \pm 1$  Ma and  $54 \pm 1$  Ma. The relative misfit of the Gibbon Mountain analyses is low and increases if three age components are calculated. If there is no reduction in misfit, when the number of components is increased then only two distinct age components exist [Sambridge and Compston, 1994].

The probability density plot for the Seven Falls sill illustrates that the zircon analyses are separated into three age components at  $38 \pm 1$  Ma,  $46 \pm 1$  Ma, and  $57 \pm 1$  Ma. Regardless of the number of components in Seven Falls the relative misfit remains high.

## **Appendix 2.1**

### **$^{40}\text{Ar}/^{39}\text{Ar}$ Data from the Wilderness suite sills**

## BIOTITE AND MUSCOVITE SAMPLES

**CAT 93-4**

**Muscovite**

**J factor: 0.00188004**

**%err in J: 0.23**

| Temp<br>° C | Dwell<br>Time<br>(Min) | <sup>37</sup> Ar/ <sup>39</sup> Ar | <sup>36</sup> Ar/ <sup>39</sup> Ar | <sup>39</sup> Ar<br>(mols) | Cumulative<br><sup>39</sup> Ar released | % <sup>40</sup> Ar* | <sup>40</sup> Ar*/ <sup>39</sup> Ar | Age<br>(Ma) | %error | 39/40    | 39/40er  | 36/40    | 36/40er  |
|-------------|------------------------|------------------------------------|------------------------------------|----------------------------|---|---------------------|-------------------------------------|-------------|--------|----------|----------|----------|----------|
| 500         | 12                     | 1.82E-01                           | 1.04E-01                           | 1.03E-16                   | 0.0026                                  | 17.98               | 6.75E+00                            | 22.7        | 4.21   | 2.68E-02 | 3.62E-04 | 2.78E-03 | 8.67E-05 |
| 600         | 12                     | 1.89E-02                           | 3.09E-02                           | 2.67E-16                   | 0.0092                                  | 50.12               | 9.18E+00                            | 30.9        | 1.68   | 5.46E-02 | 7.63E-04 | 1.69E-03 | 6.24E-05 |
| 720         | 12                     | 5.05E-03                           | 1.75E-02                           | 1.41E-15                   | 0.0441                                  | 63.32               | 8.92E+00                            | 30.0        | 0.79   | 7.10E-02 | 8.63E-04 | 1.24E-03 | 2.41E-05 |
| 820         | 12                     | 7.00E-03                           | 1.41E-02                           | 2.82E-15                   | 0.1139                                  | 68.38               | 9.03E+00                            | 30.4        | 0.71   | 7.57E-02 | 9.14E-04 | 1.07E-03 | 1.68E-05 |
| 900         | 12                     | 7.74E-04                           | 5.88E-03                           | 1.15E-14                   | 0.3988                                  | 85.54               | 1.03E+01                            | 34.5        | 0.59   | 8.32E-02 | 1.01E-03 | 4.90E-04 | 3.65E-06 |
| 950         | 12                     | 5.31E-03                           | 3.69E-03                           | 3.73E-15                   | 0.4909                                  | 91.29               | 1.14E+01                            | 38.3        | 0.57   | 7.99E-02 | 9.69E-04 | 2.95E-04 | 5.75E-06 |
| 1000        | 12                     | 5.57E-04                           | 4.60E-03                           | 3.21E-15                   | 0.5703                                  | 90.23               | 1.25E+01                            | 42.1        | 0.64   | 7.19E-02 | 8.92E-04 | 3.31E-04 | 1.37E-05 |
| 1050        | 12                     | 2.93E-04                           | 2.84E-03                           | 9.47E-15                   | 0.8046                                  | 93.6                | 1.23E+01                            | 41.2        | 0.54   | 7.62E-02 | 9.21E-04 | 2.17E-04 | 3.87E-06 |
| 1090        | 12                     | 2.26E-04                           | 8.88E-04                           | 7.70E-15                   | 0.9949                                  | 97.9                | 1.22E+01                            | 41.0        | 0.51   | 8.01E-02 | 9.65E-04 | 7.11E-05 | 4.21E-06 |
| 1150        | 12                     | 3.64E-02                           | 8.43E-03                           | 1.58E-16                   | 0.9989                                  | 81.63               | 1.11E+01                            | 37.2        | 2.36   | 7.37E-02 | 1.64E-03 | 6.22E-04 | 7.94E-05 |
| 1250        | 12                     | 4.00E-01                           | 7.12E-02                           | 3.20E-17                   | 0.9996                                  | 43.53               | 1.63E+01                            | 54.3        | 5.27   | 2.69E-02 | 6.94E-04 | 1.91E-03 | 1.86E-04 |
| 1350        | 12                     | 5.18E-01                           | 3.31E-01                           | 1.44E-17                   | 1                                       | 9.56                | 1.05E+01                            | 35.2        | 32.87  | 9.25E-03 | 3.15E-04 | 3.06E-03 | 2.79E-04 |

**CAT 0705**  
**Muscovite**  
**J factor: 0.00013895**  
**%err in J: 0.45**

| Temp<br>° C | Dwell<br>Time<br>(Min) | <sup>37</sup> Ar/ <sup>39</sup> Ar | <sup>36</sup> Ar/ <sup>39</sup> Ar | <sup>39</sup> Ar<br>(mols) | Cumulative<br><sup>39</sup> Ar released | % <sup>40</sup> Ar* | <sup>40</sup> Ar*/ <sup>39</sup> Ar | Age<br>(Ma) | %error | 39/40    | 39/40er  | 36/40    | 36/40er  |
|-------------|------------------------|------------------------------------|------------------------------------|----------------------------|---|---------------------|-------------------------------------|-------------|--------|----------|----------|----------|----------|
| 500         | 12                     | 6.18E-03                           | 1.19E+00                           | 4.99E-18                   | 0.004                                   | 18.39               | 79.388                              | 19.79       | 19.13  | 2.33E-03 | 8.65E-05 | 2.76E-03 | 1.50E-04 |
| 620         | 12                     | 4.95E-02                           | 4.51E-01                           | 1.58E-17                   | 0.0167                                  | 45.76               | 112.628                             | 28.02       | 5.27   | 4.07E-03 | 1.09E-04 | 1.84E-03 | 7.01E-05 |
| 720         | 12                     | 2.16E-02                           | 2.66E-01                           | 4.94E-17                   | 0.0565                                  | 58.73               | 111.843                             | 27.82       | 1.37   | 5.26E-03 | 7.12E-05 | 1.40E-03 | 2.38E-05 |
| 800         | 12                     | 2.09E-03                           | 2.31E-01                           | 1.88E-16                   | 0.2076                                  | 61.11               | 107.557                             | 26.76       | 1.66   | 5.69E-03 | 8.47E-05 | 1.32E-03 | 2.22E-05 |
| 860         | 12                     | 1.70E-03                           | 6.90E-02                           | 3.67E-16                   | 0.5025                                  | 83.65               | 104.45                              | 26          | 0.86   | 8.02E-03 | 1.02E-04 | 5.53E-04 | 9.50E-06 |
| 910         | 12                     | 2.36E-03                           | 5.05E-02                           | 2.11E-16                   | 0.6726                                  | 87.7                | 106.536                             | 26.51       | 1.11   | 8.24E-03 | 1.18E-04 | 4.16E-04 | 1.51E-05 |
| 970         | 12                     | 6.67E-03                           | 1.20E-01                           | 1.27E-16                   | 0.7746                                  | 75.15               | 107.203                             | 26.68       | 1.45   | 7.02E-03 | 1.07E-04 | 8.41E-04 | 1.60E-05 |
| 1040        | 12                     | 4.07E-02                           | 1.31E-01                           | 1.61E-16                   | 0.904                                   | 73.01               | 105.127                             | 26.16       | 1.17   | 6.95E-03 | 9.51E-05 | 9.13E-04 | 1.62E-05 |
| 1120        | 12                     | 4.44E-03                           | 8.54E-02                           | 1.08E-16                   | 0.9909                                  | 81.05               | 108.073                             | 26.89       | 1.38   | 7.51E-03 | 1.16E-04 | 6.41E-04 | 2.38E-05 |
| 1250        | 12                     | 1.03E-01                           | 6.23E-01                           | 1.13E-17                   | 1                                       | 37.53               | 110.86                              | 27.58       | 9.42   | 3.39E-03 | 1.27E-04 | 2.11E-03 | 8.33E-05 |



**CAT 93-1**  
**Muscovite**  
**J factor: 0.00013765**  
**%err in J: 0.6**

| Temp<br>° C | Dwell<br>Time<br>(Min) | <sup>37</sup> Ar/ <sup>39</sup> Ar | <sup>36</sup> Ar/ <sup>39</sup> Ar | <sup>39</sup> Ar<br>(mols) | Cumulative<br><sup>39</sup> Ar released | % <sup>40</sup> Ar* | <sup>40</sup> Ar*/ <sup>39</sup> Ar | Age<br>(Ma) | %error | 39/40    | 39/40er  | 36/40    | 36/40er  |
|-------------|------------------------|------------------------------------|------------------------------------|----------------------------|---|---------------------|-------------------------------------|-------------|--------|----------|----------|----------|----------|
| 500         | 12                     | 1.25E-01                           | 3.23E+00                           | 4.73E-18                   | 0.002                                   | 17.47               | 2.03E+02                            | 49.67       | 44.4   | 8.65E-04 | 6.89E-05 | 2.79E-03 | 1.11E-04 |
| 600         | 12                     | 9.82E-02                           | 6.17E-01                           | 7.71E-18                   | 0.0052                                  | 43.71               | 1.42E+02                            | 34.88       | 12.99  | 3.09E-03 | 1.80E-04 | 1.91E-03 | 1.42E-04 |
| 725         | 12                     | 1.07E-02                           | 4.21E-01                           | 5.07E-17                   | 0.0262                                  | 48.14               | 1.16E+02                            | 28.46       | 3.1    | 4.17E-03 | 7.71E-05 | 1.76E-03 | 3.16E-05 |
| 800         | 12                     | 1.27E-02                           | 1.29E-01                           | 3.72E-16                   | 0.1805                                  | 73.37               | 1.05E+02                            | 25.94       | 0.88   | 6.98E-03 | 8.48E-05 | 9.01E-04 | 2.21E-05 |
| 875         | 12                     | 9.00E-04                           | 2.83E-02                           | 1.03E-15                   | 0.6082                                  | 92.57               | 1.04E+02                            | 25.69       | 0.76   | 8.89E-03 | 1.07E-04 | 2.51E-04 | 4.59E-06 |
| 925         | 12                     | 3.31E-04                           | 1.70E-02                           | 2.91E-16                   | 0.7289                                  | 95.54               | 1.08E+02                            | 26.49       | 0.83   | 8.89E-03 | 1.11E-04 | 1.51E-04 | 1.33E-05 |
| 975         | 12                     | 5.09E-03                           | 4.91E-02                           | 1.44E-16                   | 0.7886                                  | 87.67               | 1.03E+02                            | 25.43       | 1.37   | 8.51E-03 | 1.33E-04 | 4.17E-04 | 2.41E-05 |
| 1050        | 12                     | 4.30E-03                           | 3.36E-02                           | 2.99E-16                   | 0.9124                                  | 91.33               | 1.05E+02                            | 25.8        | 0.83   | 8.73E-03 | 1.08E-04 | 2.93E-04 | 1.13E-05 |
| 1130        | 12                     | 1.18E-02                           | 8.46E-03                           | 1.88E-16                   | 0.9904                                  | 97.58               | 1.01E+02                            | 24.87       | 0.97   | 9.68E-03 | 1.30E-04 | 8.19E-05 | 2.99E-05 |
| 1250        | 12                     | 5.45E-01                           | 1.57E-02                           | 2.30E-17                   | 1                                       | 94.49               | 7.98E+01                            | 19.71       | 2.58   | 1.19E-02 | 3.12E-04 | 1.87E-04 | 1.61E-04 |

**CAT 0703**  
**Biotite**  
**J factor: 0.00013818**  
**%err in J: 0.49**

| Temp<br>° C | Dwell<br>Time<br>(Min) | <sup>37</sup> Ar/ <sup>39</sup> Ar | <sup>36</sup> Ar/ <sup>39</sup> Ar | <sup>39</sup> Ar<br>(mols) | Cumulative<br><sup>39</sup> Ar released | % <sup>40</sup> Ar* | <sup>40</sup> Ar*/ <sup>39</sup> Ar | Age<br>(Ma) | %error | 39/40    | 39/40er  | 36/40    | 36/40er  |
|-------------|------------------------|------------------------------------|------------------------------------|----------------------------|---|---------------------|-------------------------------------|-------------|--------|----------|----------|----------|----------|
| 500         | 12                     | 5.76E-02                           | 1.50E+00                           | 1.73E-17                   | 0.0092                                  | 4.8                 | 2.28E+01                            | 5.67        | 53.66  | 2.14E-03 | 6.11E-05 | 3.22E-03 | 7.09E-05 |
| 580         | 12                     | 4.91E-03                           | 3.81E-01                           | 6.49E-17                   | 0.0437                                  | 42.76               | 8.43E+01                            | 20.89       | 2.64   | 5.08E-03 | 8.02E-05 | 1.94E-03 | 4.44E-05 |
| 660         | 12                     | 1.58E-03                           | 9.39E-02                           | 2.41E-16                   | 0.1717                                  | 78.26               | 9.99E+01                            | 24.74       | 1.14   | 7.84E-03 | 1.08E-04 | 7.36E-04 | 1.64E-05 |
| 720         | 12                     | 4.22E-03                           | 2.64E-02                           | 3.66E-16                   | 0.3663                                  | 92.83               | 1.01E+02                            | 25.06       | 0.77   | 9.18E-03 | 1.14E-04 | 2.43E-04 | 6.92E-06 |
| 780         | 12                     | 6.21E-03                           | 1.95E-02                           | 3.35E-16                   | 0.5443                                  | 94.66               | 1.02E+02                            | 25.25       | 0.96   | 9.29E-03 | 1.27E-04 | 1.81E-04 | 6.07E-06 |
| 860         | 12                     | 1.35E-02                           | 5.79E-02                           | 1.25E-16                   | 0.6105                                  | 85.35               | 9.97E+01                            | 24.69       | 1.04   | 8.56E-03 | 1.17E-04 | 4.96E-04 | 1.53E-05 |
| 950         | 12                     | 7.17E-03                           | 6.22E-02                           | 1.18E-16                   | 0.6731                                  | 84.39               | 9.95E+01                            | 24.64       | 1.07   | 8.49E-03 | 1.17E-04 | 5.28E-04 | 1.61E-05 |
| 1050        | 12                     | 3.06E-03                           | 2.74E-02                           | 4.05E-16                   | 0.8883                                  | 92.61               | 1.02E+02                            | 25.17       | 1.01   | 9.12E-03 | 1.27E-04 | 2.50E-04 | 8.58E-06 |
| 1150        | 12                     | 4.13E-03                           | 6.79E-02                           | 1.76E-16                   | 0.982                                   | 83.36               | 1.01E+02                            | 24.92       | 0.95   | 8.29E-03 | 1.09E-04 | 5.63E-04 | 1.68E-05 |
| 1250        | 12                     | 4.70E-02                           | 2.21E-01                           | 3.39E-17                   | 1                                       | 60.19               | 9.91E+01                            | 24.52       | 2.45   | 6.08E-03 | 1.12E-04 | 1.35E-03 | 4.43E-05 |

**CAT 93-8**  
**Muscovite**  
**J factor: 0.00013164**  
**%err in J: 0.5**

| Temp °<br>C | Dwell<br>Time<br>(Min) | <sup>37</sup> Ar/ <sup>39</sup> Ar | <sup>36</sup> Ar/ <sup>39</sup> Ar | <sup>39</sup> Ar<br>(mols) | Cumulative<br><sup>39</sup> Ar released | % <sup>40</sup> Ar* | <sup>40</sup> Ar*/ <sup>39</sup> Ar | Age<br>(Ma) | %error | 39/40    | 39/40er  | 36/40    | 36/40er  |
|-------------|------------------------|------------------------------------|------------------------------------|----------------------------|---|---------------------|-------------------------------------|-------------|--------|----------|----------|----------|----------|
| 500         | 12                     | 6.89E+01                           | 7.25E-01                           | 1.05E-17                   | 0.0034                                  | 17.7                | 55.222                              | 13.07       | 7.89   | 3.84E-03 | 7.45E-05 | 2.79E-03 | 1.78E-04 |
| 610         | 12                     | 7.06E+01                           | 2.27E-01                           | 3.16E-17                   | 0.0136                                  | 60.05               | 112.638                             | 26.55       | 3.82   | 5.97E-03 | 1.59E-04 | 1.35E-03 | 8.13E-05 |
| 730         | 12                     | 9.86E+00                           | 1.55E-01                           | 1.61E-16                   | 0.0655                                  | 69.88               | 108.088                             | 25.49       | 1.29   | 6.59E-03 | 9.23E-05 | 1.02E-03 | 2.28E-05 |
| 840         | 12                     | 6.43E-01                           | 6.41E-02                           | 1.45E-15                   | 0.5317                                  | 84.25               | 101.886                             | 24.04       | 0.85   | 8.31E-03 | 1.05E-04 | 5.33E-04 | 6.07E-06 |
| 900         | 12                     | 4.53E+00                           | 2.32E-02                           | 4.92E-16                   | 0.6902                                  | 93.73               | 103.405                             | 24.39       | 0.84   | 9.16E-03 | 1.18E-04 | 2.12E-04 | 6.69E-06 |
| 980         | 12                     | 8.35E+00                           | 7.57E-02                           | 2.43E-16                   | 0.7684                                  | 81.63               | 101.077                             | 23.85       | 1.05   | 8.21E-03 | 1.11E-04 | 6.22E-04 | 1.42E-05 |
| 1060        | 12                     | 3.20E-01                           | 2.51E-02                           | 6.84E-16                   | 0.9888                                  | 93.11               | 100.611                             | 23.74       | 0.91   | 9.29E-03 | 1.23E-04 | 2.33E-04 | 7.83E-06 |
| 1140        | 12                     | 1.44E+01                           | 3.32E-02                           | 2.71E-17                   | 0.9975                                  | 90.77               | 99.094                              | 23.38       | 5.35   | 9.40E-03 | 4.75E-04 | 3.12E-04 | 8.14E-05 |
| 1250        | 12                     | 2.53E+01                           | 6.36E-02                           | 6.22E-18                   | 0.9995                                  | 84.52               | 107.021                             | 25.24       | 7.17   | 8.24E-03 | 5.09E-04 | 5.24E-04 | 2.38E-04 |
| 1350        | 12                     | 1.88E+02                           | 1.59E+00                           | 1.46E-18                   | 1                                       | 18.61               | 144.612                             | 34.02       | 76.67  | 1.73E-03 | 2.86E-04 | 2.75E-03 | 4.88E-04 |

**CAT 93-9**

**Biotite**

**J factor: 0.00013789**

**%err in J: 0.53**

| Temp<br>° C | Dwell<br>Time<br>(Min) | <sup>37</sup> Ar/ <sup>39</sup> Ar | <sup>36</sup> Ar/ <sup>39</sup> Ar | <sup>39</sup> Ar<br>(mols) | Cumulative<br><sup>39</sup> Ar released | % <sup>40</sup> Ar* | <sup>40</sup> Ar*/ <sup>39</sup> Ar | Age<br>(Ma) | %erro<br>r | 39/40    | 39/40er  | 36/40    | 36/40er  |
|-------------|------------------------|------------------------------------|------------------------------------|----------------------------|---|---------------------|-------------------------------------|-------------|------------|----------|----------|----------|----------|
| 500         | 12                     | 3.08E-01                           | 1.43E+00                           | 6.04E-18                   | 0.0058                                  | 3.43                | 1.54E+01                            | 3.82        | 209.83     | 2.29E-03 | 1.70E-04 | 3.27E-03 | 8.79E-05 |
| 610         | 12                     | 4.71E-02                           | 1.60E-01                           | 6.65E-17                   | 0.0697                                  | 65.66               | 9.05E+01                            | 22.36       | 2.24       | 7.27E-03 | 1.32E-04 | 1.16E-03 | 3.35E-05 |
| 710         | 12                     | 5.92E-03                           | 2.08E-02                           | 2.99E-16                   | 0.3576                                  | 94.28               | 1.01E+02                            | 24.97       | 0.76       | 9.33E-03 | 1.15E-04 | 1.94E-04 | 9.43E-06 |
| 780         | 12                     | 8.45E-03                           | 1.14E-02                           | 2.41E-16                   | 0.5893                                  | 96.67               | 9.79E+01                            | 24.18       | 0.91       | 9.88E-03 | 1.31E-04 | 1.13E-04 | 7.20E-06 |
| 850         | 12                     | 2.44E-02                           | 1.87E-02                           | 6.68E-17                   | 0.6535                                  | 94.54               | 9.56E+01                            | 23.63       | 1.73       | 9.90E-03 | 1.91E-04 | 1.85E-04 | 3.19E-05 |
| 950         | 12                     | 1.54E-03                           | 1.50E-02                           | 1.13E-16                   | 0.7619                                  | 95.53               | 9.51E+01                            | 23.5        | 1.5        | 1.01E-02 | 1.76E-04 | 1.51E-04 | 1.43E-05 |
| 1050        | 12                     | 1.01E-03                           | 1.36E-02                           | 1.14E-16                   | 0.8712                                  | 95.83               | 9.24E+01                            | 22.84       | 1.08       | 1.04E-02 | 1.49E-04 | 1.41E-04 | 1.84E-05 |
| 1130        | 12                     | 5.28E-04                           | 1.09E-03                           | 1.13E-16                   | 0.9795                                  | 99.67               | 9.63E+01                            | 23.81       | 1.12       | 1.04E-02 | 1.54E-04 | 1.13E-05 | 1.99E-05 |
| 1250        | 12                     | 2.13E-02                           | 1.61E-03                           | 2.13E-17                   | 1                                       | 99.51               | 9.68E+01                            | 23.92       | 3.35       | 1.03E-02 | 3.59E-04 | 1.66E-05 | 7.12E-05 |

POTASSIUM FELDSPARS

CAT 93-4

Potassium Feldspar

J factor: 0.00013671

%err in J: 0.59

| Temp<br>° C | Dwell<br>Time<br>(Min) | <sup>37</sup> Ar/ <sup>39</sup> Ar | <sup>36</sup> Ar/ <sup>39</sup> Ar | <sup>39</sup> Ar<br>(mols) | Cumulative<br><sup>39</sup> Ar released | % <sup>40</sup> Ar* | <sup>40</sup> Ar*/ <sup>39</sup> Ar | Age<br>(Ma) | %error | 39/40    | 39/40er  | 36/40    | 36/40er  |
|-------------|------------------------|------------------------------------|------------------------------------|----------------------------|---|---------------------|-------------------------------------|-------------|--------|----------|----------|----------|----------|
| 350         | 12                     | 1.19E+00                           | 1.93E+01                           | 8.29E-18                   | 0.0013                                  | 0.87                | 5.77E+01                            | 14.18       | 226.21 | 1.74E-04 | 4.40E-06 | 3.36E-03 | 2.96E-05 |
| 350         | 42                     | 2.75E-01                           | 2.19E+01                           | 8.26E-18                   | 0.0026                                  | 1.52                | 1.09E+02                            | 26.55       | 177.89 | 1.52E-04 | 4.80E-06 | 3.33E-03 | 3.17E-05 |
| 400         | 12                     | 6.69E-01                           | 5.93E+00                           | 4.72E-18                   | 0.0033                                  | 18.05               | 3.89E+02                            | 93.45       | 35.1   | 4.68E-04 | 3.10E-05 | 2.77E-03 | 3.52E-05 |
| 400         | 40                     | 4.30E-01                           | 2.64E+00                           | 1.96E-17                   | 0.0064                                  | 7.45                | 6.39E+01                            | 15.69       | 15.08  | 1.19E-03 | 1.90E-05 | 3.13E-03 | 4.14E-05 |
| 450         | 12                     | 8.19E-02                           | 7.47E-01                           | 2.10E-17                   | 0.0097                                  | 41.36               | 1.56E+02                            | 38.1        | 3.29   | 2.66E-03 | 4.67E-05 | 1.98E-03 | 3.27E-05 |
| 450         | 40                     | 9.55E-02                           | 3.63E-01                           | 5.04E-17                   | 0.0177                                  | 45.8                | 9.10E+01                            | 22.3        | 3.28   | 5.05E-03 | 9.40E-05 | 1.83E-03 | 3.15E-05 |
| 500         | 12                     | 1.48E-01                           | 7.60E-03                           | 4.63E-17                   | 0.025                                   | 98.82               | 1.88E+02                            | 45.88       | 2.5    | 5.25E-03 | 1.40E-04 | 3.99E-05 | 2.06E-05 |
| 500         | 40                     | 6.69E+00                           | 8.24E-02                           | 1.10E-16                   | 0.0423                                  | 79.55               | 9.58E+01                            | 23.48       | 1.35   | 8.40E-03 | 1.25E-04 | 6.92E-04 | 2.54E-05 |
| 550         | 12                     | 6.01E+00                           | 1.07E-01                           | 7.14E-17                   | 0.0535                                  | 78.17               | 1.15E+02                            | 28.05       | 1.62   | 6.89E-03 | 1.13E-04 | 7.39E-04 | 2.52E-05 |
| 550         | 40                     | 3.47E+01                           | 3.28E-02                           | 8.94E-17                   | 0.0676                                  | 90.99               | 1.03E+02                            | 25.3        | 1.31   | 9.30E-03 | 1.46E-04 | 3.05E-04 | 3.40E-05 |
| 600         | 12                     | 1.24E+01                           | 6.42E-02                           | 6.90E-17                   | 0.0785                                  | 84.6                | 1.06E+02                            | 26.03       | 1.51   | 8.12E-03 | 1.33E-04 | 5.21E-04 | 3.34E-05 |
| 600         | 40                     | 2.99E-02                           | 3.57E-02                           | 1.11E-16                   | 0.0959                                  | 90.13               | 9.64E+01                            | 23.61       | 1.66   | 9.37E-03 | 1.68E-04 | 3.34E-04 | 2.12E-05 |
| 650         | 12                     | 6.98E-02                           | 2.80E-02                           | 8.88E-17                   | 0.1099                                  | 92.19               | 9.76E+01                            | 23.92       | 1.18   | 9.46E-03 | 1.38E-04 | 2.65E-04 | 2.15E-05 |
| 650         | 40                     | 1.63E+01                           | 1.98E-02                           | 8.88E-17                   | 0.1367                                  | 94.36               | 1.01E+02                            | 24.64       | 0.98   | 9.63E-03 | 1.30E-04 | 1.91E-04 | 7.32E-06 |
| 700         | 12                     | 8.91E-02                           | 2.40E-02                           | 1.70E-16                   | 0.1529                                  | 92.94               | 9.36E+01                            | 22.94       | 0.87   | 9.94E-03 | 1.26E-04 | 2.39E-04 | 1.46E-05 |
| 760         | 12                     | 3.36E+00                           | 1.45E-02                           | 1.03E-16                   | 0.194                                   | 95.76               | 9.74E+01                            | 23.87       | 0.9    | 9.89E-03 | 1.28E-04 | 1.44E-04 | 1.53E-05 |
| 820         | 12                     | 4.20E-02                           | 1.29E-02                           | 2.61E-16                   | 0.2283                                  | 96.21               | 9.68E+01                            | 23.71       | 1.03   | 9.96E-03 | 1.38E-04 | 1.28E-04 | 9.85E-06 |
| 880         | 12                     | 4.44E-02                           | 2.54E-02                           | 2.18E-16                   | 0.2626                                  | 92.81               | 9.69E+01                            | 23.74       | 0.95   | 9.59E-03 | 1.26E-04 | 2.43E-04 | 7.83E-06 |
| 940         | 12                     | 5.78E-02                           | 2.77E-02                           | 2.18E-16                   | 0.2946                                  | 92.3                | 9.80E+01                            | 24.01       | 0.98   | 9.43E-03 | 1.26E-04 | 2.61E-04 | 6.20E-06 |
| 1000        | 12                     | 7.60E-03                           | 1.90E-02                           | 2.04E-16                   | 0.3368                                  | 94.7                | 1.01E+02                            | 24.62       | 1.14   | 9.44E-03 | 1.37E-04 | 1.79E-04 | 1.20E-05 |
| 1000        | 40                     | 1.05E-02                           | 2.41E-02                           | 2.68E-16                   | 0.3857                                  | 93.51               | 1.03E+02                            | 25.14       | 0.94   | 9.12E-03 | 1.20E-04 | 2.20E-04 | 8.82E-06 |
| 1060        | 12                     | 2.80E-02                           | 3.40E-02                           | 3.10E-16                   | 0.4196                                  | 91.18               | 1.04E+02                            | 25.49       | 1.2    | 8.77E-03 | 1.29E-04 | 2.98E-04 | 1.47E-05 |
| 1060        | 40                     | 2.24E-02                           | 3.61E-02                           | 2.16E-16                   | 0.4748                                  | 90.86               | 1.06E+02                            | 26.01       | 0.94   | 8.56E-03 | 1.12E-04 | 3.09E-04 | 7.24E-06 |

|      |    |          |          |          |        |       |          |       |      |          |          |          |          |
|------|----|----------|----------|----------|--------|-------|----------|-------|------|----------|----------|----------|----------|
| 1120 | 12 | 5.24E-02 | 7.72E-02 | 3.50E-16 | 0.5048 | 82.91 | 1.11E+02 | 27.13 | 1.02 | 7.49E-03 | 9.84E-05 | 5.78E-04 | 9.87E-06 |
| 1120 | 40 | 2.64E-02 | 6.47E-02 | 1.91E-16 | 0.5749 | 85.29 | 1.11E+02 | 27.15 | 0.95 | 7.70E-03 | 9.90E-05 | 4.98E-04 | 8.77E-06 |
| 1180 | 12 | 1.87E-02 | 9.00E-02 | 4.46E-16 | 0.6814 | 80.8  | 1.12E+02 | 27.43 | 0.92 | 7.22E-03 | 9.05E-05 | 6.50E-04 | 4.49E-06 |
| 1180 | 40 | 1.43E-02 | 9.32E-02 | 6.77E-16 | 0.8349 | 80.24 | 1.12E+02 | 27.4  | 0.94 | 7.18E-03 | 9.08E-05 | 6.69E-04 | 6.67E-06 |
| 1210 | 12 | 2.09E-02 | 1.11E-01 | 9.75E-16 | 0.8826 | 77.4  | 1.12E+02 | 27.5  | 1.2  | 6.90E-03 | 9.53E-05 | 7.65E-04 | 1.33E-05 |
| 1250 | 12 | 1.02E-03 | 1.32E-01 | 3.03E-16 | 0.9564 | 74.73 | 1.16E+02 | 28.28 | 1.06 | 6.48E-03 | 8.42E-05 | 8.55E-04 | 8.02E-06 |
| 1300 | 12 | 4.09E-02 | 1.31E-01 | 4.69E-16 | 0.974  | 75.09 | 1.17E+02 | 28.59 | 1.59 | 6.44E-03 | 1.02E-04 | 8.43E-04 | 2.29E-05 |
| 1400 | 12 | 1.85E-01 | 1.10E-01 | 1.12E-16 | 0.9964 | 77.05 | 1.09E+02 | 26.66 | 1.07 | 7.09E-03 | 9.31E-05 | 7.77E-04 | 1.45E-05 |
| 1500 | 12 | 8.87E-01 | 1.18E+00 | 1.42E-16 | 1      | 26.53 | 1.27E+02 | 31.03 | 3.94 | 2.10E-03 | 3.22E-05 | 2.49E-03 | 4.85E-05 |

**CAT 0705**

**Potassium Feldspar**

**J factor:0.00013895**

**%err in J: 0.45**

| Tem<br>p ° C | Dwell<br>Time<br>(Min) | <sup>37</sup> Ar/ <sup>39</sup> Ar | <sup>36</sup> Ar/ <sup>39</sup> Ar | <sup>39</sup> Ar<br>(mols) | Cumulative<br><sup>39</sup> Ar released | % <sup>40</sup> Ar* | <sup>40</sup> Ar*/ <sup>39</sup> Ar | Age<br>(Ma) | %erro<br>r | 39/40    | 39/40er  | 36/40    | 36/40er  |
|--------------|------------------------|------------------------------------|------------------------------------|----------------------------|---|---------------------|-------------------------------------|-------------|------------|----------|----------|----------|----------|
| 350          | 12                     | 5.62E+01                           | 1.81E+00                           | 5.27E-18                   | 0.0047                                  | 29.35               | 2.38E+02                            | 58.62       | 9.18       | 1.32E-03 | 4.00E-05 | 2.39E-03 | 1.14E-04 |
| 350          | 40                     | 3.33E-01                           | 1.28E+00                           | 2.36E-18                   | 0.0069                                  | 22.96               | 1.14E+02                            | 28.26       | 13.07      | 2.03E-03 | 6.58E-05 | 2.61E-03 | 2.91E-04 |
| 425          | 12                     | 9.71E-01                           | 2.63E-01                           | 9.84E-18                   | 0.0157                                  | 64.09               | 1.40E+02                            | 34.66       | 7.65       | 4.62E-03 | 2.34E-04 | 1.22E-03 | 9.00E-05 |
| 425          | 40                     | 4.88E+00                           | 1.30E-01                           | 1.51E-17                   | 0.0294                                  | 71.75               | 9.84E+01                            | 24.5        | 5.3        | 7.37E-03 | 2.94E-04 | 9.56E-04 | 1.40E-04 |
| 500          | 12                     | 1.12E+01                           | 5.50E-02                           | 4.35E-17                   | 0.0686                                  | 86.88               | 1.10E+02                            | 27.28       | 1.78       | 8.08E-03 | 1.53E-04 | 4.44E-04 | 2.43E-05 |
| 500          | 40                     | 7.96E+00                           | 5.35E-02                           | 4.21E-17                   | 0.1065                                  | 86.03               | 9.89E+01                            | 24.63       | 1.99       | 8.83E-03 | 1.79E-04 | 4.73E-04 | 7.54E-05 |
| 575          | 12                     | 1.29E+00                           | 3.18E-02                           | 9.23E-17                   | 0.1897                                  | 91.28               | 9.89E+01                            | 24.63       | 1.36       | 9.27E-03 | 1.51E-04 | 2.95E-04 | 2.24E-05 |
| 650          | 12                     | 1.95E+00                           | 1.54E-02                           | 1.78E-16                   | 0.3499                                  | 95.74               | 1.03E+02                            | 25.65       | 1.04       | 9.34E-03 | 1.34E-04 | 1.44E-04 | 6.42E-06 |
| 725          | 12                     | 9.54E-02                           | 2.31E-02                           | 1.70E-16                   | 0.5026                                  | 93.91               | 1.06E+02                            | 26.27       | 1.02       | 8.92E-03 | 1.26E-04 | 2.06E-04 | 1.55E-05 |
| 800          | 12                     | 7.14E+00                           | 4.28E-02                           | 7.81E-17                   | 0.573                                   | 89.02               | 1.04E+02                            | 25.88       | 1.05       | 8.68E-03 | 1.22E-04 | 3.72E-04 | 2.00E-05 |
| 875          | 12                     | 1.54E+00                           | 7.25E-02                           | 5.58E-17                   | 0.6232                                  | 82.57               | 1.02E+02                            | 25.39       | 2.37       | 8.14E-03 | 1.82E-04 | 5.90E-04 | 2.27E-05 |
| 925          | 12                     | 1.56E+01                           | 3.50E-02                           | 4.69E-17                   | 0.6655                                  | 90.86               | 1.06E+02                            | 26.27       | 2.39       | 8.84E-03 | 2.16E-04 | 3.09E-04 | 5.27E-05 |
| 1000         | 12                     | 8.83E-02                           | 9.85E-02                           | 1.23E-16                   | 0.7764                                  | 79.93               | 1.16E+02                            | 28.91       | 1.03       | 6.90E-03 | 9.25E-05 | 6.79E-04 | 2.90E-05 |
| 1000         | 40                     | 6.54E-01                           | 1.66E-01                           | 1.23E-16                   | 0.8856                                  | 70.28               | 1.17E+02                            | 28.99       | 2.42       | 6.06E-03 | 1.23E-04 | 1.01E-03 | 2.88E-05 |
| 1060         | 12                     | 5.53E-01                           | 9.07E-02                           | 1.21E-16                   | 0.9338                                  | 82.44               | 1.26E+02                            | 31.39       | 2.01       | 6.55E-03 | 1.30E-04 | 5.94E-04 | 4.59E-05 |
| 1060         | 40                     | 8.44E-01                           | 4.46E-01                           | 5.35E-17                   | 0.9696                                  | 49.17               | 1.28E+02                            | 31.85       | 1.52       | 3.86E-03 | 5.13E-05 | 1.72E-03 | 5.36E-05 |
| 1120         | 12                     | 5.72E+00                           | 3.01E-01                           | 3.97E-17                   | 0.9782                                  | 67.38               | 1.86E+02                            | 45.91       | 5.17       | 3.67E-03 | 1.36E-04 | 1.10E-03 | 8.82E-05 |
| 1200         | 12                     | 3.46E-01                           | 4.13E-01                           | 9.52E-18                   | 0.9883                                  | 56.57               | 1.60E+02                            | 39.6        | 4.73       | 3.56E-03 | 1.04E-04 | 1.47E-03 | 1.16E-04 |
| 1350         | 12                     | 1.33E+01                           | 8.50E-01                           | 1.13E-17                   | 1                                       | 35.36               | 1.41E+02                            | 34.97       | 9.13       | 2.57E-03 | 8.95E-05 | 2.19E-03 | 8.70E-05 |

**CAT 0704**

**Potassium Feldspar**

**J factor: 0.00011663**

**%err in J: 0.35**

| Temp<br>° C | Dwell<br>Time<br>(Min) | <sup>37</sup> Ar/ <sup>39</sup> Ar | <sup>36</sup> Ar/ <sup>39</sup> Ar | <sup>39</sup> Ar<br>(mols) | Cumulative<br><sup>39</sup> Ar released | % <sup>40</sup> Ar* | <sup>40</sup> Ar*/ <sup>39</sup> Ar | Age<br>(Ma) | %error | 39/40    | 39/40er  | 36/40    | 36/40er  |
|-------------|------------------------|------------------------------------|------------------------------------|----------------------------|---|---------------------|-------------------------------------|-------------|--------|----------|----------|----------|----------|
| 450         | 12                     | 1.61E+00                           | 7.79E+00                           | 7.22E-18                   | 0.0017                                  | 23.86               | 7.28E+02                            | 147.04      | 11.29  | 3.31E-04 | 1.00E-05 | 2.58E-03 | 3.39E-05 |
| 500         | 12                     | 9.25E-01                           | 1.31E+00                           | 1.80E-17                   | 0.0058                                  | 35.04               | 2.11E+02                            | 43.75       | 3.3    | 1.68E-03 | 2.70E-05 | 2.20E-03 | 3.55E-05 |
| 560         | 12                     | 2.06E-01                           | 3.22E-01                           | 4.95E-17                   | 0.0172                                  | 60.93               | 1.49E+02                            | 31.08       | 2.27   | 4.10E-03 | 7.27E-05 | 1.32E-03 | 1.81E-05 |
| 630         | 12                     | 9.49E-02                           | 1.19E-01                           | 9.99E-17                   | 0.0403                                  | 79                  | 1.32E+02                            | 27.58       | 1.02   | 6.00E-03 | 8.10E-05 | 7.11E-04 | 9.49E-06 |
| 700         | 12                     | 2.92E-01                           | 5.14E-02                           | 1.68E-16                   | 0.0791                                  | 89.37               | 1.28E+02                            | 26.7        | 0.87   | 7.01E-03 | 9.28E-05 | 3.60E-04 | 1.18E-05 |
| 770         | 12                     | 7.48E-02                           | 1.56E-02                           | 2.88E-16                   | 0.1454                                  | 96.4                | 1.24E+02                            | 25.93       | 0.64   | 7.78E-03 | 9.57E-05 | 1.22E-04 | 5.43E-06 |
| 840         | 12                     | 1.02E-01                           | 6.87E-03                           | 3.14E-16                   | 0.2177                                  | 98.37               | 1.23E+02                            | 25.7        | 0.77   | 8.01E-03 | 1.05E-04 | 5.50E-05 | 2.36E-06 |
| 900         | 20                     | 6.98E-02                           | 8.35E-03                           | 4.05E-16                   | 0.311                                   | 98.02               | 1.22E+02                            | 25.56       | 0.63   | 8.03E-03 | 9.88E-05 | 6.70E-05 | 4.06E-06 |
| 960         | 20                     | 4.04E-02                           | 1.09E-02                           | 3.03E-16                   | 0.3808                                  | 97.48               | 1.25E+02                            | 26.13       | 0.7    | 7.81E-03 | 9.87E-05 | 8.52E-05 | 3.76E-06 |
| 1020        | 20                     | 1.39E-01                           | 2.24E-02                           | 2.20E-16                   | 0.4316                                  | 94.97               | 1.25E+02                            | 26.14       | 0.85   | 7.61E-03 | 1.02E-04 | 1.70E-04 | 5.00E-06 |
| 1080        | 20                     | 5.08E-02                           | 3.41E-02                           | 2.12E-16                   | 0.4803                                  | 92.75               | 1.29E+02                            | 26.97       | 0.81   | 7.19E-03 | 9.41E-05 | 2.45E-04 | 5.24E-06 |
| 1150        | 12                     | 3.66E-03                           | 4.11E-02                           | 4.47E-16                   | 0.5834                                  | 91.68               | 1.34E+02                            | 28.03       | 0.73   | 6.84E-03 | 8.64E-05 | 2.81E-04 | 6.75E-06 |
| 1210        | 12                     | 2.41E-04                           | 6.80E-02                           | 1.10E-15                   | 0.8357                                  | 86.98               | 1.35E+02                            | 28.1        | 0.62   | 6.48E-03 | 7.78E-05 | 4.41E-04 | 2.86E-06 |
| 1270        | 12                     | 5.63E-04                           | 7.08E-02                           | 1.10E-15                   | 0.9375                                  | 86.65               | 1.36E+02                            | 28.42       | 0.82   | 6.38E-03 | 8.24E-05 | 4.52E-04 | 5.18E-06 |
| 1350        | 12                     | 9.95E-02                           | 9.98E-02                           | 4.42E-16                   | 0.9622                                  | 82.25               | 1.37E+02                            | 28.6        | 1.17   | 6.02E-03 | 8.71E-05 | 6.01E-04 | 1.53E-05 |
| 1500        | 12                     | 1.23E-02                           | 2.21E-01                           | 1.07E-16                   | 1                                       | 67.97               | 1.39E+02                            | 28.94       | 0.88   | 4.92E-03 | 6.12E-05 | 1.08E-03 | 1.71E-05 |



**CAT 93-1**  
**Potassium Feldspar**  
**J factor: 0.00011474**  
**%err in J: 0.26**

| Temp<br>° C | Dwell<br>Time<br>(Min) | <sup>37</sup> Ar/ <sup>39</sup> Ar | <sup>36</sup> Ar/ <sup>39</sup> Ar | <sup>39</sup> Ar<br>(mols) | Cumulative<br><sup>39</sup> Ar released | % <sup>40</sup> Ar* | <sup>40</sup> Ar*/ <sup>39</sup> Ar | Age<br>(Ma) | %error | 39/40    | 39/40er  | 36/40    | 36/40er  |
|-------------|------------------------|------------------------------------|------------------------------------|----------------------------|---|---------------------|-------------------------------------|-------------|--------|----------|----------|----------|----------|
| 450         | 12                     | 3.92E-01                           | 8.22E+00                           | 1.02E-17                   | 0.0024                                  | 51.95               | 2.64E+03                            | 476.7       | 4.31   | 1.98E-04 | 5.51E-06 | 1.63E-03 | 1.33E-05 |
| 500         | 12                     | 3.65E-01                           | 1.28E+00                           | 1.44E-17                   | 0.0058                                  | 52.55               | 4.21E+02                            | 85.1        | 3.44   | 1.25E-03 | 2.70E-05 | 1.61E-03 | 2.74E-05 |
| 570         | 12                     | 9.92E-02                           | 6.52E-01                           | 4.32E-17                   | 0.0161                                  | 60.21               | 2.93E+02                            | 59.6        | 1.06   | 2.06E-03 | 2.65E-05 | 1.35E-03 | 1.24E-05 |
| 640         | 12                     | 6.62E-02                           | 2.41E-01                           | 8.48E-17                   | 0.0362                                  | 68.64               | 1.56E+02                            | 32.01       | 1.09   | 4.41E-03 | 5.89E-05 | 1.06E-03 | 1.61E-05 |
| 720         | 12                     | 9.23E-02                           | 9.39E-02                           | 1.95E-16                   | 0.0823                                  | 82.69               | 1.33E+02                            | 27.3        | 0.72   | 6.24E-03 | 7.77E-05 | 5.86E-04 | 9.60E-06 |
| 800         | 12                     | 2.35E-03                           | 3.82E-02                           | 3.00E-16                   | 0.1535                                  | 91.7                | 1.25E+02                            | 25.68       | 0.79   | 7.35E-03 | 9.66E-05 | 2.81E-04 | 4.79E-06 |
| 880         | 12                     | 8.00E-03                           | 2.08E-02                           | 3.49E-16                   | 0.2361                                  | 95.19               | 1.22E+02                            | 25.1        | 0.6    | 7.81E-03 | 9.62E-05 | 1.63E-04 | 4.81E-06 |
| 960         | 20                     | 4.30E-03                           | 2.84E-02                           | 2.99E-16                   | 0.3069                                  | 93.6                | 1.23E+02                            | 25.24       | 1.33   | 7.64E-03 | 1.27E-04 | 2.17E-04 | 9.23E-06 |
| 1060        | 20                     | 1.92E-03                           | 6.16E-02                           | 3.09E-16                   | 0.3802                                  | 87.28               | 1.25E+02                            | 25.71       | 0.65   | 6.99E-03 | 8.61E-05 | 4.31E-04 | 6.67E-06 |
| 1160        | 12                     | 3.76E-02                           | 1.17E-01                           | 4.64E-16                   | 0.4902                                  | 79.69               | 1.36E+02                            | 28.01       | 0.76   | 5.86E-03 | 7.35E-05 | 6.87E-04 | 7.15E-06 |
| 1250        | 12                     | 8.06E-03                           | 7.48E-02                           | 1.62E-15                   | 0.874                                   | 85.91               | 1.35E+02                            | 27.75       | 0.6    | 6.37E-03 | 7.72E-05 | 4.77E-04 | 3.93E-06 |
| 1310        | 12                     | 4.28E-02                           | 5.78E-02                           | 2.53E-16                   | 0.9339                                  | 88.85               | 1.36E+02                            | 28          | 0.72   | 6.53E-03 | 8.27E-05 | 3.77E-04 | 7.59E-06 |
| 1400        | 12                     | 1.12E-02                           | 4.71E-02                           | 2.04E-16                   | 0.9823                                  | 90.52               | 1.33E+02                            | 27.35       | 0.77   | 6.81E-03 | 8.84E-05 | 3.21E-04 | 9.20E-06 |
| 1500        | 12                     | 1.51E-01                           | 2.22E-02                           | 2.04E-16                   | 1                                       | 95.23               | 1.31E+02                            | 26.96       | 1.26   | 7.27E-03 | 1.18E-04 | 1.62E-04 | 3.27E-05 |

**CAT 0703**  
**Potassium Feldspar**  
**J factor: 0.00013718**  
**%err in J: 0.56**

| Temp<br>° C | Dwell<br>Time<br>(Min) | <sup>37</sup> Ar/ <sup>39</sup> Ar | <sup>36</sup> Ar/ <sup>39</sup> Ar | <sup>39</sup> Ar<br>(mols) | Cumulative<br><sup>39</sup> Ar released | % <sup>40</sup> Ar* | <sup>40</sup> Ar*/ <sup>39</sup> Ar | Age<br>(Ma) | %error | 39/40    | 39/40er  | 36/40    | 36/40er  |
|-------------|------------------------|------------------------------------|------------------------------------|----------------------------|---|---------------------|-------------------------------------|-------------|--------|----------|----------|----------|----------|
| 350         | 12                     | 4.60E+01                           | 5.52E+00                           | 5.10E-18                   | 0.0017                                  | 45.02               | 1.39E+03                            | 315.59      | 12.14  | 3.37E-04 | 2.05E-05 | 1.86E-03 | 2.96E-05 |
| 350         | 40                     | 2.03E+01                           | 2.81E+00                           | 2.96E-18                   | 0.0026                                  | 22.22               | 2.45E+02                            | 59.65       | 23.22  | 9.37E-04 | 5.10E-05 | 2.63E-03 | 6.78E-05 |
| 400         | 12                     | 1.13E+02                           | 3.14E+00                           | 1.05E-17                   | 0.0061                                  | 47.21               | 9.17E+02                            | 213.78      | 4.96   | 5.69E-04 | 1.56E-05 | 1.79E-03 | 3.36E-05 |
| 400         | 40                     | 2.33E+01                           | 3.34E-01                           | 1.58E-17                   | 0.0112                                  | 52.35               | 1.13E+02                            | 27.66       | 5.05   | 4.83E-03 | 1.41E-04 | 1.61E-03 | 4.45E-05 |
| 450         | 12                     | 4.10E+00                           | 1.12E+00                           | 2.15E-17                   | 0.0182                                  | 46.04               | 2.85E+02                            | 69.07       | 5.8    | 1.63E-03 | 4.80E-05 | 1.83E-03 | 3.89E-05 |
| 450         | 40                     | 1.49E+01                           | 6.43E-02                           | 3.21E-17                   | 0.0287                                  | 83.26               | 9.70E+01                            | 23.84       | 1.54   | 8.82E-03 | 1.45E-04 | 5.67E-04 | 4.70E-05 |
| 500         | 12                     | 5.12E+00                           | 2.75E-01                           | 7.04E-17                   | 0.0518                                  | 63.98               | 1.46E+02                            | 35.76       | 2.83   | 4.43E-03 | 9.38E-05 | 1.22E-03 | 2.60E-05 |
| 500         | 40                     | 9.40E-01                           | 1.39E-02                           | 6.46E-17                   | 0.0729                                  | 95.85               | 9.52E+01                            | 23.4        | 2.35   | 1.01E-02 | 2.50E-04 | 1.41E-04 | 3.81E-05 |
| 550         | 12                     | 1.62E+00                           | 2.91E-02                           | 5.54E-17                   | 0.091                                   | 92.13               | 1.01E+02                            | 24.84       | 2.31   | 9.16E-03 | 2.17E-04 | 2.66E-04 | 2.24E-05 |
| 550         | 40                     | 9.70E-01                           | 1.06E-02                           | 1.10E-16                   | 0.127                                   | 96.9                | 9.79E+01                            | 24.07       | 1.56   | 9.93E-03 | 1.80E-04 | 1.05E-04 | 1.24E-05 |
| 610         | 12                     | 1.59E+00                           | 3.75E-02                           | 1.17E-16                   | 0.1654                                  | 89.95               | 9.96E+01                            | 24.49       | 0.98   | 9.08E-03 | 1.21E-04 | 3.40E-04 | 1.28E-05 |
| 670         | 12                     | 3.01E-01                           | 2.10E-02                           | 1.73E-16                   | 0.2219                                  | 94.15               | 1.00E+02                            | 24.64       | 1.02   | 9.42E-03 | 1.30E-04 | 1.98E-04 | 1.23E-05 |
| 710         | 12                     | 6.48E-01                           | 1.21E-02                           | 1.35E-16                   | 0.2659                                  | 96.6                | 1.01E+02                            | 24.91       | 0.98   | 9.56E-03 | 1.31E-04 | 1.15E-04 | 8.29E-06 |
| 750         | 12                     | 7.38E+00                           | 8.47E-03                           | 1.35E-16                   | 0.297                                   | 97.46               | 9.73E+01                            | 23.93       | 1.08   | 1.02E-02 | 1.46E-04 | 8.60E-05 | 1.29E-05 |
| 800         | 12                     | 5.94E-01                           | 1.28E-02                           | 9.51E-17                   | 0.3325                                  | 96.29               | 9.83E+01                            | 24.17       | 1.88   | 9.83E-03 | 2.04E-04 | 1.26E-04 | 1.32E-05 |
| 850         | 12                     | 3.59E+00                           | 1.85E-02                           | 1.08E-16                   | 0.3638                                  | 94.89               | 1.02E+02                            | 25.06       | 1.37   | 9.38E-03 | 1.54E-04 | 1.73E-04 | 1.38E-05 |
| 910         | 12                     | 3.05E+00                           | 1.55E-02                           | 9.59E-17                   | 0.4065                                  | 95.48               | 9.72E+01                            | 23.9        | 1.25   | 9.90E-03 | 1.54E-04 | 1.53E-04 | 8.64E-06 |
| 950         | 12                     | 1.17E+00                           | 2.76E-02                           | 1.30E-16                   | 0.4422                                  | 92.77               | 1.05E+02                            | 25.86       | 1.21   | 8.85E-03 | 1.33E-04 | 2.45E-04 | 1.63E-05 |
| 1000        | 12                     | 1.10E+00                           | 4.35E-02                           | 1.09E-16                   | 0.498                                   | 89.37               | 1.09E+02                            | 26.66       | 1.24   | 8.27E-03 | 1.24E-04 | 3.60E-04 | 8.71E-06 |
| 1030        | 12                     | 1.97E-01                           | 8.87E-02                           | 1.70E-16                   | 0.5743                                  | 81.41               | 1.15E+02                            | 28.27       | 0.88   | 7.10E-03 | 8.87E-05 | 6.29E-04 | 1.77E-05 |
| 1060        | 12                     | 1.70E+00                           | 9.87E-02                           | 2.34E-16                   | 0.6984                                  | 79.15               | 1.11E+02                            | 27.35       | 1.04   | 7.15E-03 | 9.43E-05 | 7.06E-04 | 1.11E-05 |
| 1080        | 12                     | 1.74E+00                           | 1.05E-01                           | 3.79E-16                   | 0.8194                                  | 77.98               | 1.11E+02                            | 27.15       | 1.78   | 7.09E-03 | 1.23E-04 | 7.45E-04 | 1.20E-05 |
| 1080        | 40                     | 1.50E-01                           | 1.08E-01                           | 3.70E-16                   | 0.9558                                  | 77.56               | 1.11E+02                            | 27.29       | 1.22   | 7.01E-03 | 9.82E-05 | 7.59E-04 | 1.63E-05 |

|       |       |          |          |          |        |       |          |       |      |          |          |          |          |
|-------|-------|----------|----------|----------|--------|-------|----------|-------|------|----------|----------|----------|----------|
| 1100  | 12    | 1.35E+01 | 9.73E-02 | 4.17E-16 | 0.9652 | 81.06 | 1.26E+02 | 30.86 | 2.02 | 6.59E-03 | 1.28E-04 | 6.41E-04 | 5.46E-05 |
| error | error | 0.00E+00 | 0.00E+00 | 2.87E-17 | 0.9652 | 0     | 0.00E+00 | 0     | 0    | 0.00E+00 | 0.00E+00 | 0.00E+00 | 0.00E+00 |
| 1180  | 12    | 7.06E+00 | 8.94E-02 | 0.00E+00 | 0.9834 | 78.41 | 9.73E+01 | 23.91 | 1.41 | 8.18E-03 | 1.24E-04 | 7.31E-04 | 1.98E-05 |
| 1250  | 12    | 1.02E+01 | 1.32E-01 | 5.59E-17 | 0.9889 | 75.69 | 1.24E+02 | 30.34 | 3.54 | 6.23E-03 | 1.81E-04 | 8.23E-04 | 1.09E-04 |
| 1350  | 12    | 9.32E+00 | 2.30E-01 | 1.66E-17 | 0.9929 | 62.88 | 1.17E+02 | 28.71 | 3.67 | 5.47E-03 | 1.41E-04 | 1.26E-03 | 1.29E-04 |
| 1500  | 12    | 1.03E+01 | 9.17E-01 | 1.24E-17 | 1      | 28.86 | 1.13E+02 | 27.65 | 2.9  | 2.63E-03 | 3.67E-05 | 2.41E-03 | 7.12E-05 |

### CAT 93-8

#### Potassium Feldspar

J factor: 0.00013292

%err in J: 0.61

| Temp<br>° C | Dwell<br>Time<br>(Min) | <sup>37</sup> Ar/ <sup>39</sup> Ar | <sup>36</sup> Ar/ <sup>39</sup> Ar | <sup>39</sup> Ar<br>(mols) | Cumulative<br><sup>39</sup> Ar released | % <sup>40</sup> Ar* | <sup>40</sup> Ar*/ <sup>39</sup> Ar | Age<br>(Ma) | %error | 39/40    | 39/40er  | 36/40    | 36/40er  |
|-------------|------------------------|------------------------------------|------------------------------------|----------------------------|---|---------------------|-------------------------------------|-------------|--------|----------|----------|----------|----------|
| 450         | 12                     | 9.42E+01                           | 1.89E+00                           | 2.81E-17                   | 0.0079                                  | 45.95               | 5.21E+02                            | 120.79      | 3.44   | 9.70E-04 | 1.93E-05 | 1.83E-03 | 1.65E-05 |
| 500         | 12                     | 3.88E+01                           | 4.31E-01                           | 3.83E-17                   | 0.0186                                  | 52.11               | 1.47E+02                            | 34.9        | 3.81   | 3.76E-03 | 8.69E-05 | 1.62E-03 | 4.86E-05 |
| 600         | 12                     | 2.66E+01                           | 1.56E-01                           | 1.52E-16                   | 0.0614                                  | 74.24               | 1.38E+02                            | 32.78       | 1.11   | 5.60E-03 | 7.41E-05 | 8.72E-04 | 2.24E-05 |
| 700         | 12                     | 3.56E+00                           | 6.28E-02                           | 2.77E-16                   | 0.1392                                  | 83.75               | 9.65E+01                            | 22.99       | 0.93   | 8.76E-03 | 1.11E-04 | 5.50E-04 | 1.23E-05 |
| 780         | 12                     | 8.27E+00                           | 1.46E-02                           | 3.31E-16                   | 0.2321                                  | 95.62               | 9.54E+01                            | 22.73       | 0.88   | 1.02E-02 | 1.30E-04 | 1.48E-04 | 4.60E-06 |
| 880         | 12                     | 4.26E+00                           | 1.71E-02                           | 3.58E-16                   | 0.3325                                  | 94.99               | 9.69E+01                            | 23.08       | 0.98   | 9.91E-03 | 1.33E-04 | 1.70E-04 | 4.68E-06 |
| 980         | 12                     | 4.37E+00                           | 2.63E-02                           | 2.68E-16                   | 0.4077                                  | 92.37               | 9.50E+01                            | 22.65       | 1.24   | 9.82E-03 | 1.48E-04 | 2.58E-04 | 5.38E-06 |
| 1080        | 12                     | 8.73E+00                           | 4.76E-02                           | 3.19E-16                   | 0.4972                                  | 87.35               | 9.89E+01                            | 23.57       | 0.84   | 8.99E-03 | 1.10E-04 | 4.28E-04 | 1.00E-05 |
| 1180        | 12                     | 2.60E+00                           | 1.01E-01                           | 8.81E-16                   | 0.7445                                  | 78.35               | 1.09E+02                            | 26          | 0.95   | 7.24E-03 | 9.09E-05 | 7.33E-04 | 1.17E-05 |
| 1240        | 12                     | 4.93E+00                           | 5.70E-02                           | 7.09E-16                   | 0.9436                                  | 87.28               | 1.17E+02                            | 27.82       | 0.82   | 7.55E-03 | 9.18E-05 | 4.31E-04 | 4.61E-06 |
| 1290        | 12                     | 3.47E+01                           | 6.56E-02                           | 8.09E-17                   | 0.9663                                  | 85.39               | 1.20E+02                            | 28.43       | 1.19   | 7.54E-03 | 1.08E-04 | 4.95E-04 | 2.06E-05 |
| 1350        | 12                     | 9.43E+00                           | 4.95E-02                           | 9.17E-17                   | 0.9921                                  | 88.57               | 1.15E+02                            | 27.43       | 1.22   | 7.82E-03 | 1.14E-04 | 3.87E-04 | 2.25E-05 |
| 1500        | 12                     | 1.27E+01                           | 1.01E-01                           | 2.83E-17                   | 1                                       | 79.67               | 1.19E+02                            | 28.4        | 4.42   | 6.83E-03 | 1.14E-04 | 6.88E-04 | 4.98E-05 |

**CAT 93-9**  
**Potassium Feldspar**  
**J factor: 0.00013303**  
**%err in J: 0.61**

| Temp<br>° C | Dwell<br>Time<br>(Min) | <sup>37</sup> Ar/ <sup>39</sup> Ar | <sup>36</sup> Ar/ <sup>39</sup> Ar | <sup>39</sup> Ar<br>(mols) | Cumulative<br><sup>39</sup> Ar released | % <sup>40</sup> Ar* | <sup>40</sup> Ar*/ <sup>39</sup> Ar | Age<br>(Ma) | %error | 39/40    | 39/40er  | 36/40    | 36/40er  |
|-------------|------------------------|------------------------------------|------------------------------------|----------------------------|---|---------------------|-------------------------------------|-------------|--------|----------|----------|----------|----------|
| 500         | 12                     | 3.66E+01                           | 1.86E+00                           | 3.40E-17                   | 0.0082                                  | 36.92               | 3.36E+02                            | 78.96       | 5.52   | 1.15E-03 | 2.74E-05 | 2.14E-03 | 2.75E-05 |
| 580         | 12                     | 1.14E+02                           | 3.08E-01                           | 7.41E-17                   | 0.0261                                  | 56.12               | 1.38E+02                            | 32.75       | 1.54   | 4.83E-03 | 6.82E-05 | 1.49E-03 | 2.86E-05 |
| 670         | 12                     | 1.67E+01                           | 9.05E-02                           | 2.17E-16                   | 0.0784                                  | 79.35               | 1.06E+02                            | 25.23       | 1.19   | 7.73E-03 | 1.07E-04 | 6.99E-04 | 2.01E-05 |
| 770         | 12                     | 3.01E+01                           | 1.84E-01                           | 4.59E-17                   | 0.0895                                  | 94.74               | 1.01E+03                            | 227.14      | 0.82   | 9.67E-04 | 1.22E-05 | 1.78E-04 | 4.84E-06 |
| 860         | 12                     | 6.87E+00                           | 1.82E-02                           | 7.31E-16                   | 0.2662                                  | 94.57               | 9.49E+01                            | 22.66       | 0.86   | 1.01E-02 | 1.27E-04 | 1.84E-04 | 4.65E-06 |
| 920         | 12                     | 1.73E+01                           | 9.61E-03                           | 6.08E-16                   | 0.4132                                  | 97.16               | 1.00E+02                            | 23.89       | 0.82   | 1.00E-02 | 1.24E-04 | 9.62E-05 | 5.06E-06 |
| 990         | 12                     | 2.77E-01                           | 1.93E-02                           | 3.39E-16                   | 0.495                                   | 94.49               | 9.82E+01                            | 23.43       | 0.88   | 9.66E-03 | 1.22E-04 | 1.86E-04 | 6.31E-06 |
| 1080        | 12                     | 8.46E-01                           | 8.38E-02                           | 2.61E-16                   | 0.5581                                  | 80.02               | 9.97E+01                            | 23.79       | 1.16   | 8.07E-03 | 1.11E-04 | 6.76E-04 | 1.15E-05 |
| 1180        | 12                     | 1.31E+00                           | 1.66E-01                           | 7.98E-16                   | 0.7509                                  | 68.57               | 1.08E+02                            | 25.63       | 1.15   | 6.43E-03 | 8.38E-05 | 1.06E-03 | 9.44E-06 |
| 1240        | 12                     | 7.51E-01                           | 8.50E-02                           | 7.13E-16                   | 0.9231                                  | 81.38               | 1.10E+02                            | 26.3        | 1.01   | 7.42E-03 | 9.64E-05 | 6.30E-04 | 6.73E-06 |
| 1300        | 12                     | 1.43E+01                           | 1.37E-01                           | 1.16E-16                   | 0.9511                                  | 74.18               | 1.19E+02                            | 28.31       | 1.74   | 6.40E-03 | 1.07E-04 | 8.74E-04 | 1.61E-05 |
| 1400        | 12                     | 5.71E+00                           | 9.58E-02                           | 1.26E-16                   | 0.9815                                  | 79.89               | 1.14E+02                            | 27.17       | 1.16   | 7.10E-03 | 9.74E-05 | 6.80E-04 | 1.14E-05 |
| 1500        | 12                     | 3.13E+01                           | 1.53E-01                           | 7.68E-17                   | 1                                       | 71.08               | 1.17E+02                            | 27.85       | 1.42   | 6.40E-03 | 9.34E-05 | 9.79E-04 | 2.83E-05 |

## VITA

NAME OF AUTHOR: Jessica J. Terrien

PLACE OF BIRTH: Greenville, Michigan

DATE OF BIRTH: 05/13/1979

### GRADUATE AND UNDERGRADUATE SCHOOLS ATTENDED:

Augustana College, Rock Island, Illinois

University of Missouri—Rolla

### DEGREES AWARDED:

A.B., 2001 Augustana College, Rock Island, Illinois

M.S., 2003, University of Missouri—Rolla